

AFRL-PR-WP-TR-1998-2096

**DEVELOPMENT OF LARGE LI-
ION BATTERIES FOR
AIRCRAFT AND SPACECRAFT
APPLICATIONS**



**Gregg Bruce
Lynn Marcoux**

**Blue Star Advanced Technology Corporation
1155 West 15th Street
North Vancouver, B.C.
Canada V7P 1M7**

JUNE 1998

FINAL REPORT FOR PERIOD 1 JULY 1996 – 31 DECEMBER 1997

Approved for public release; distribution unlimited

19990617 050

**PROPULSION DIRECTORATE
AIR FORCE RESEARCH LABORATORY
AIR FORCE MATERIEL COMMAND
WRIGHT-PATTERSON AIR FORCE BASE, OH 45433-7251**

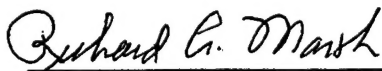
DTIC QUALITY INSPECTED 4

NOTICE

USING GOVERNMENT DRAWINGS, SPECIFICATIONS, OR OTHER DATA INCLUDED IN THIS DOCUMENT FOR ANY PURPOSE OTHER THAN GOVERNMENT PROCUREMENT DOES NOT IN ANY WAY OBLIGATE THE US GOVERNMENT. THE FACT THAT THE GOVERNMENT FORMULATED OR SUPPLIED THE DRAWINGS, SPECIFICATIONS, OR OTHER DATA DOES NOT LICENSE THE HOLDER OR ANY OTHER PERSON OR CORPORATION; OR CONVEY ANY RIGHTS OR PERMISSION TO MANUFACTURE, USE, OR SELL ANY PATENTED INVENTION THAT MAY RELATE TO THEM.

THIS REPORT IS RELEASABLE TO THE NATIONAL TECHNICAL INFORMATION SERVICE (NTIS). AT NTIS, IT WILL BE AVAILABLE TO THE GENERAL PUBLIC, INCLUDING FOREIGN NATIONS.

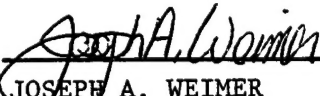
THIS TECHNICAL REPORT HAS BEEN REVIEWED AND IS APPROVED FOR PUBLICATION.



RICHARD A. MARSH
Task Scientist
AFRL/PRPB
Air Force Research Laboratory
Wright-Patterson AFB OH 45433-7251



RICHARD A. MARSH
Chief, Battery Branch
AFRL/PRPB
Air Force Research Laboratory
Wright-Patterson AFB OH 45433-7251



JOSEPH A. WEIMER
Acting Chief
Power Division
Propulsion Directorate

Do not return copies of this report unless contractual obligations or notice on a specific document requires its return.

REPORT DOCUMENTATION PAGE			Form Approved OMB No. 0704-0188	
<small>Public reporting burden for this collection of information is estimated to average 1 hour per response, including the time for reviewing instructions, searching existing data sources, gathering and maintaining the data needed, and completing and reviewing the collection of information. Send comments regarding this burden estimate or any other aspect of this collection of information, including suggestions for reducing this burden, to Washington Headquarters Services, Directorate for Information Operations and Reports, 1215 Jefferson Davis Highway, Suite 1204, Arlington, VA 22202-4302, and to the Office of Management and Budget, Paperwork Reduction Project (0704-0188), Washington, DC 20503.</small>				
1. AGENCY USE ONLY (Leave blank)		2. REPORT DATE June 1998	3. REPORT TYPE AND DATES COVERED Final Report 1 July 1996 - 1 December 1997	
4. TITLE AND SUBTITLE Development of Large Li-Ion Batteries for Aircraft and Spacecraft Applications			5. FUNDING NUMBERS C: F33615-91-C-2167 PE: 62203F PR: 3145 TA: 22 WU: 9A	
6. AUTHOR(S) Gregg Bruce Lynn Marcoux				
7. PERFORMING ORGANIZATION NAME(S) AND ADDRESS(ES) Blue Star Advanced Technology Corporation 1155 West 15th Street North Vancouver, B.C. Canada V7P 1M7			8. PERFORMING ORGANIZATION REPORT NUMBER	
9. SPONSORING/MONITORING AGENCY NAME(S) AND ADDRESS(ES) Propulsion Directorate Air Force Research Laboratory Air Force Materiel Command Wright-Patterson Air Force Base, OH 45433-7251 POC: R. A. Marsh, AFRL/PRPB, 937-255-7770			10. SPONSORING/MONITORING AGENCY REPORT NUMBER AFRL-PR-WP-TR-1998-2096	
11. SUPPLEMENTARY NOTES				
12a. DISTRIBUTION AVAILABILITY STATEMENT Approved for public release; distribution unlimited			12b. DISTRIBUTION CODE	
13. ABSTRACT (Maximum 200 words) This program was initially focussed on the development of very large rechargeable Li/SO ₂ cells for use as a survival power source in missile silos. With the diminishment in the strategic value of these missile systems came a redirection of the program towards smaller cell sizes. Concurrent was a chemical direction which changed the emphasis of the program from the rechargeable Li/SO ₂ chemistry to that of the family of cell chemistries which are collectively referred to as lithium ion. These cells are based on a metal oxide cathode, a carbon-lithium intercalation anode and an electrolyte solution consisting of a mixture of organic solvents and a soluble Li salt. These systems moved to the forefront of advanced battery technology in the early 1990s because they clearly offered significant improvements in cycle life, cell safety and energy density/specific energy. More recently, it became clear that spacecraft batteries based on large (20 to 100-Ah) Li ion cells would offer a significant reduction in spacecraft power subsystem mass and the USAF Phillips Laboratory joined Wright Laboratory and Canada's DND in the sponsorship of this program.				
14. SUBJECT TERMS Lithium-Ion Cell, Electrochemistry, Rechargeable			15. NUMBER OF PAGES 123	
			16. PRICE CODE	
17. SECURITY CLASSIFICATION OF REPORT UNCLASSIFIED	18. SECURITY CLASSIFICATION OF THIS PAGE UNCLASSIFIED	19. SECURITY CLASSIFICATION OF ABSTRACT UNCLASSIFIED	20. LIMITATION OF ABSTRACT SAR	

Table of Contents

	Page
1.0 Introduction and Summary	1
1.1 Introduction	1
1.2 Summary	1
2.0 Technical Progress	2
2.1 Task 1.0. Cell Component Development (In C Cells)	2
2.1.1 Task 1.1 Improve Energy Density/Specific Energy of the Li/C _x Anode ..	2
2.1.2 Task 1.2 Develop LiCoO ₂ and LiNiO ₂ Cathodes	9
2.1.3 Task 1.3 Evaluate and Improve Li _x Mn _y O _z Cathode Materials	14
2.1.4 Task 1.4 Evaluate and Improve Electrolyte Performance	16
2.1.5 Task 1.5 Status Cells	29
2.2 Task 2.0. Evaluate Cell Fabrication Techniques	34
2.2.1 Task 2.1 Improve Electrode Fabrication Process	34
2.2.2 Task 2.2 Evaluate Alternative Electrode Configurations	35
2.3 Task 3.0 20-Ah Prismatic Cell Development	42
2.4 Task 4.0 20-Ah Cylindrical Cell Development	50
2.5 Task 5.0 25-Ah Design II Cell Development	65
2.6 Task 6.0 45-Ah Cylindrical Cell Development	72
2.7 Task 7.0 DD Cell Development	91
2.8 Task 8.0 Cell Safety	102
3.0 Conclusions	114

List of Figures

	Page
Figure 1. Effect of particle size on reversible capacity in Lonza KS graphite samples	3
Figure 2. Lithium intercalation into graphite as a function of graphite electrode density	4
Figure 3. Negative electrode performance with various graphites.	5
Figure 4. Capacity versus cycle for Lk-702 and MCMB negative electrodes.	6
Figure 5. Petroleum coke cells tested at three different end of charge voltage limits.	7
Figure 6. Hard carbon C cells tested at three different end of charge voltage limits.	8
Figure 7. Capacity versus cycle number for LK-702 and petroleum coke.	8
Figure 8. Comparison of LiCoO ₂ C cell performance from different suppliers.	10
Figure 9. Capacity as a function of discharge rate for cells containing LiCoO ₂ or LiNiO ₂ positive electrodes.	11
Figure 10. Capacity as a function of discharge rate at 0 °C for cells using LiCoO ₂ or LiNiO ₂ positive electrodes.	12
Figure 11. Comparison of LiNi _{0.82} Co _{0.18} O ₂ positive electrode cells made from material supplied by Seimi, FMC and Westaim.	13
Figure 12. Capacity as a function of cycle number for LiNi _{0.82} Co _{0.18} O ₂ supplied by several companies and compared to LiCoO ₂	13
Figure 13. Charge voltage dependence for LiNi _{0.82} Co _{0.18} O ₂ positive electrode cells.	14
Figure 14. Performance of LiMn ₂ O ₄ supplied by several different companies.	15
Figure 15. Performance of LiMn ₂ O ₄ supplied by several different companies, 1998.	16
Figure 16. Conductivity versus temperature for three selected electrolytes.	19
Figure 17. Melting Point Determination of EC/DMC/EMC 1M LiPF ₆ using Environmental Chamber.	22
Figure 18. Pulse discharge resistance for C cells using three different electrolytes.	24
Figure 19. Capacity versus temperature for C cells using three different electrolytes.	25
Figure 20. Capacity at -30 °C for three C cell battery packs using two different low temperature electrolytes.	26
Figure 21. Capacity of three DD cell battery packs at -30 °C.	27
Figure 22. Cell capacity after exposure to ultra-low temperatures 1M LiPF ₆ EC/EMC 1:3.	29
Figure 23. Generation III Status Cells cycle life data, C/2 rate.	31
Figure 24. Generation IV Status Cells cycle life data, C/2 rate.	33
Figure 25. Generations III, IV and V at 90% dod.	34
Figure 26. Model of pseudo-elliptical wound element.	36
Figure 27. Packing efficiency as a function of the geometry of the pseudo-elliptical wound element.	36
Figure 28. General assembly drawing of 10-Ah prismatic cell.	37
Figure 29. Cycle life of 10-Ah prismatic cell.	38
Figure 30. Pulse discharge resistance as a function of cycle number for the 10-Ah prismatic cell.	39

List of Figures (Continued)

	Page
Figure 31. Contribution to total charge capacity of the constant current and constant charge portions of the charge half-cycle.	40
Figure 32. Charge-discharge for 10-Ah prismatic cell LiCoO_2 versus graphite.	41
Figure 33. Charge-discharge voltage for 10-Ah prismatic cell negative electrode versus case. .	41
Figure 34. Charge-discharge voltage for 10-Ah prismatic cell positive electrode versus case. .	42
Figure 35. General assembly drawing of 20-Ah prismatic cell.	43
Figure 36. Capacity versus cycle number for 20-Ah prismatic cells filled with different electrolyte mass.	44
Figure 37. Cycle life for cell P010 at C5 to 100% dod.	48
Figure 38. Rate capability of 20-Ah prismatic cell at room temperature and 100% dod.	49
Figure 39. Capacity versus log rate for 20-Ah prismatic cell at room temperature and 100% dod.	49
Figure 40. General assembly of 20-Ah cylindrical cell Design I.	51
Figure 41. Capacity versus cycle number for cell C034 at the C/2 rate to 100% dod.	55
Figure 42. Capacity versus cycle number for cell C039 at the C/5 rate to 100% dod.	56
Figure 43. Capacity versus cycle number for cell C036 at the C/10 rate to 100% dod.	57
Figure 44. Cycle life performance of MCMB and LK-702 to 100% dod.	57
Figure 45. Rate performance of 20-Ah at room temperature at 100% dod.	58
Figure 46. Rate capability at room temperature, 100% dod, capacity versus log rate.	59
Figure 47. Rate capability at 0 °C, 100% dod.	59
Figure 48. Rate comparison between 20-Ah prismatic and 20-Ah Design I cylindrical cell. .	60
Figure 49. Temperature and power plot versus cycle number for 20-Ah Design I cylindrical cell.	61
Figure 50. Pressure and temperature profiles of 20-Ah cylindrical cell during first charge half-cycle.	62
Figure 51. Cell pressure of 20-Ah Design I cylindrical cell during cell testing.	63
Figure 52. Accelerated LEO testing with 20-Ah cylindrical Design I cell, capacity versus cycle number.	64
Figure 53. Accelerated LEO testing with 20-Ah cylindrical Design I cell, end of discharge voltage versus cycle number.	64
Figure 54. General assembly drawing of 25-Ah Design II cylindrical cell.	66
Figure 55. Comparison of rate performance between Design I and Design II cylindrical cells. .	68
Figure 56. Cycle life testing, 25-Ah cell at C/5 to 100% dod.	70
Figure 57. Cycle life testing, 25-Ah cell at C/2 to 100% dod.	70
Figure 58. General assembly drawing for 45-Ah cylindrical cell.	72
Figure 59. Cell temperature during the first charge cycle at two different rates for 45-Ah cylindrical cells.	76
Figure 60. Pulse discharge resistance as a function of cell size.	77
Figure 61. Effect of separate voltage leads on cell voltage during cycling for 45-Ah cylindrical cell.	78

List of Figures (Continued)

	Page
Figure 62. Effect of separate voltage leads on cell capacity during cycling for 45-Ah cylindrical cell.	78
Figure 63. Current versus time during charging of 45-Ah cells with separate and combined voltage leads.	79
Figure 64. Cell cycling performance of 45-Ah cell at the C/2 rate to 100% dod.	83
Figure 65. Cell cycling performance of 45-Ah cell at the C/5 rate to 100% dod.	83
Figure 66. Coulombic charging of 45-Ah cell, capacity versus cycle number.	84
Figure 67. Coulombic charging of 45-Ah cell, charge time versus cycle number.	85
Figure 68. Coulombic charging of 45-Ah cell, capacity versus cycle number.	86
Figure 69. Coulombic charging of 45-Ah cell, charge time versus cycle number.	86
Figure 70. Rate performance of 45-Ah cylindrical cell.	87
Figure 71. Cell temperature during high rate pulse testing.	89
Figure 72. Cell cycling performance of $\text{LiNi}_x\text{Co}_{1-x}\text{O}_2$ 45-Ah cell at the C/5 rate to 100% dod. .	90
Figure 73. Cell cycling performance of $\text{LiNi}_x\text{Co}_{1-x}\text{O}_2$ 45-Ah cell at the C/2 rate to 100% dod. .	90
Figure 74. Cell cycling performance of LiCoO_2 and $\text{LiNi}_x\text{Co}_{1-x}\text{O}_2$ 45-Ah cells at 100% dod. .	91
Figure 75. General assembly drawing of a DD cell.	92
Figure 76. Cell cycling performance of DD cell at the C/2 rate to 100% dod.	95
Figure 77. Cell cycling performance of a DD cell at the C/2 rate at 100% dod tested by the US Army.	96
Figure 78. Low temperature testing of a DD cell by the US Army.	96
Figure 79. Testing of a DD cell at 55 °C and room temperature by the US Army.	97
Figure 80. Rate performance of DD cell.	97
Figure 81. Cell cycling performance of a DD cell with a $\text{LiNi}_x\text{Co}_{1-x}\text{O}_2$ positive electrode at the C/2 rate at 100% dod.	98
Figure 82. Cell cycling performance of a DD cell with a $\text{LiNi}_x\text{Co}_{1-x}\text{O}_2$ or a LiCoO_2 positive electrode at the C/2 rate at 100% dod.	99
Figure 83. Coulombic charging of LiMn_2O_4 DD cell at the C/5 rate, capacity versus cycle number.	100
Figure 84. Coulombic charging of LiMn_2O_4 DD cell at the C/5 rate, total charge time.	101
Figure 85. Coulombic charging of LiCoO_2 DD cell at the C/5 rate, capacity versus cycle number.	101
Figure 86. Coulombic charging of LiCoO_2 DD cell at the C/5 rate, total charge time.	102
Figure 87. Short-circuit test of 20-Ah Design I cell.	103
Figure 88. Short-circuit test of Design II 25-Ah cell.	104
Figure 89. Over-discharge of Design I 20-Ah cylindrical cell.	105
Figure 90. Subsequent charge of over-discharged Design I 20-Ah cell.	106
Figure 91. Overcharge to 100% of Design I 20-Ah cell.	107
Figure 92. Cell cycling performance of Design I 20-Ah cell after 100% overcharge.	107

List of Figures (Continued)

	Page
Figure 93. Overcharge to 200% of Design I 20-Ah cell.	108
Figure 94. Oven test of Design I 20-Ah cylindrical cell.	109
Figure 95. Oven test with Design I 20-Ah cell with voltage sensors.	110
Figure 96. Oven test with DD cell using Celgard® 2500 and with voltage sensors.	110
Figure 97. Oven test with discharged Design I 20-Ah cell.	111
Figure 98. Crush test of Design II 25-Ah cell.	112
Figure 99. Crush test of 45-Ah cell.	113

List of Tables

	Page
Table 1. Abbreviations and Melting points of selected solvents for Lithium ion electrolytes.	17
Table 2. Selected Electrolyte Candidates with solvent system listed on a volume basis.	17
Table 3. Conductivity versus Temperature for the selected electrolyte systems.	18
Table 4. Melting Points of Electrolytes using the Environmental Chamber method.	21
Table 5. Thermal expansion and contraction of electrolytes heated to 50 °C or frozen in liquid nitrogen.	23
Table 6. Discharge performance of C cells after ultra-low temperature tests.	28
Table 7. Status Cells general characteristics.	30
Table 8. Performance characteristics of Generation I Status Cell.	30
Table 9. Performance characteristics of Generation III Status Cells.	31
Table 10. Performance data for Generation I to V Status Cells.	32
Table 11. Cell cycling history for 10-Ah wound prismatic cell.	39
Table 12. Performance characteristics of first iteration of 20-Ah prismatic cell.	43
Table 13. Cell mass analysis of 20-Ah prismatic cell.	45
Table 14. Cell capacity, mass and cell performance data for 20-Ah prismatic cells.	46
Table 15. Cell mass, performance and cycle life of 20-Ah prismatic cells still under test.	47
Table 16. Projected performance versus measured performance for design changes to 20-Ah prismatic cell.	50
Table 17. Cell mass, capacity and performance of 20-Ah Design I delivered cells.	52
Table 18. Cell mass analysis of 20-Ah Design I cylindrical cell.	53
Table 19. Cell capacity, mass and cycle life of 20-Ah Design I cylindrical cell.	54
Table 20. Cell mass, capacity and performance of 25-Ah Design II cylindrical deliverable cells.	67
Table 21. Comparison of electrode characteristics of Design I and Design II cells.	67
Table 22. Cell mass analysis of 25-Ah Design II cell.	69
Table 23. Cell performance for 45-Ah cylindrical cells.	73
Table 24. Drying temperature and negative electrode expansion.	74
Table 25. 45-Ah cell performance with different negative electrode drying temperatures. ...	75
Table 26. Cell mass, capacity and performance for delivered 45-Ah cylindrical cells.	80
Table 27. Mass analysis for 45-Ah cylindrical cell.	81
Table 28. Comparison of Mass Analysis for the various cell sizes.	82
Table 29. Cell performance for 45-Ah cylindrical cells.	82
Table 30. High rate pulse testing for Design II 25-Ah and 45-Ah cell.	88
Table 31. Cell mass, capacity and performance of delivered DD cells.	93
Table 32. Cell mass analysis of DD cells.	94
Table 33. Program goals and achievements.	115

1.0 Introduction and Summary

This is the final Submittal of CDRL Item A003, Final Progress Report for Contract F33615-91-C-2167 and covers the period 01 July 1996 to 31 December 1997.

1.1 Introduction

This program was initially focussed on the development of very large rechargeable Li/SO₂ cells for use as a survival power source in missile silos. With the diminishment in the strategic value of these missile systems came a diminishment in program funding and a redirection of the program towards smaller cell sizes which would be applicable to several generic USAF needs. Concurrent with this program redirection was a chemical redirection which changed the emphasis of the program from the rechargeable Li/SO₂ chemistry to that of the family of cell chemistries which are collectively referred to as lithium ion. These cells are based on a metal oxide cathode, a carbon-lithium intercalation anode and an electrolyte solution consisting of a mixture of organic solvents and a soluble Li salt. These systems moved to the forefront of advanced battery technology in the early 1990s because they clearly offered significant improvements in cycle life, cell safety and energy density/specific energy.

More recently, it became clear that spacecraft batteries based on large (20 to 100-Ah) Li ion cells would offer a significant reduction in spacecraft power subsystem mass and the USAF Phillips Laboratory joined Wright Laboratory and Canada's DND in the sponsorship of this program. Full funding was restored in early 1996 which corresponds to the start date for this report.

Progress in these areas is discussed in detail in Section 2.0 of this report.

1.2 Summary

The highlight of this program was the delivery of hardware samples of lithium ion cells. The work carried out under this program resulted in BATC delivering lithium ion cells to the USAF for evaluation. The deliverables were 10, 20-Ah cells in May 1997, 12, DD cells and 12, 25-Ah cells in May 1998.

2.0 Technical Progress

Progress in these areas is discussed below.

2.1 Task 1.0. Cell Component Development (In C Cells)

This task is divided into sub-tasks directed towards the development of various specific cell components including lithium-carbon intercalation anodes, nickel and cobalt oxide cathodes, and in the longer term, the manganese oxide cathode system. Due to the environmental requirements of these cells, electrolyte evaluation was also done. Most of the component evaluation was done in hermetically sealed C cells. This format was chosen because it requires a smaller amount of materials and less time than a larger cell size. After initial tests with lithium half cells it was determined that the lithium ion cells are easier to handle than ones with metallic lithium.

2.1.1 Task 1.1. Improve Energy Density/Specific Energy of the of the Li/C_x Anode

The evolution of the lithium-carbon intercalation anode may be viewed from the standpoint of the atomic structure of the underlying carbon substrate. Simplistically, the evolution progresses from coke to graphite to a new class of highly disordered carbons sometimes referred to as "hard carbons". In this context, this program is situated on a plateau between the graphite and hard carbon stage. Graphite electrode technology is sufficiently mature at BlueStar to permit the construction of cells exhibiting good performance: almost a thousand cells of this type have been assembled. Studies to improve the performance of the graphite anodes and to evaluate various candidate carbons, including the newer "hard carbons", were carried out.

Initial testing on carbon negative electrodes examined the relationship between particle size and reversible capacity. Due to the importance of specific energy for the aircraft and spacecraft applications most work concentrated on graphite rather than petroleum coke due to the higher capacity of the former (372 versus 186 mAh/g). The first work on graphite was done on the KS series of synthetic graphites supplied by Lonza Timus. The samples tested were KS6, KS10, KS15, KS44 and KS75; the only variation is the size of the particles. For example KS6 has an average particle size of 6 microns. The results of the tests in lithium half cells are shown in Figure 1. Some interesting conclusions can be drawn from Figure 1. The best material for reversible capacity is KS15. The reversible capacity of KS44 and KS15 are almost identical, so either material can be used in a lithium ion cell. KS75, with the largest particle size, had very poor reversible capacity. Possibly the particle size is so large that all of the active material cannot be utilized and so the capacity is very poor. KS6 also had poor reversible capacity, possibly due to the relatively larger portion of exposed surface area becoming inactive by the formation of the passivating layer or SEI (solid electrolyte interface) on the carbon surface.

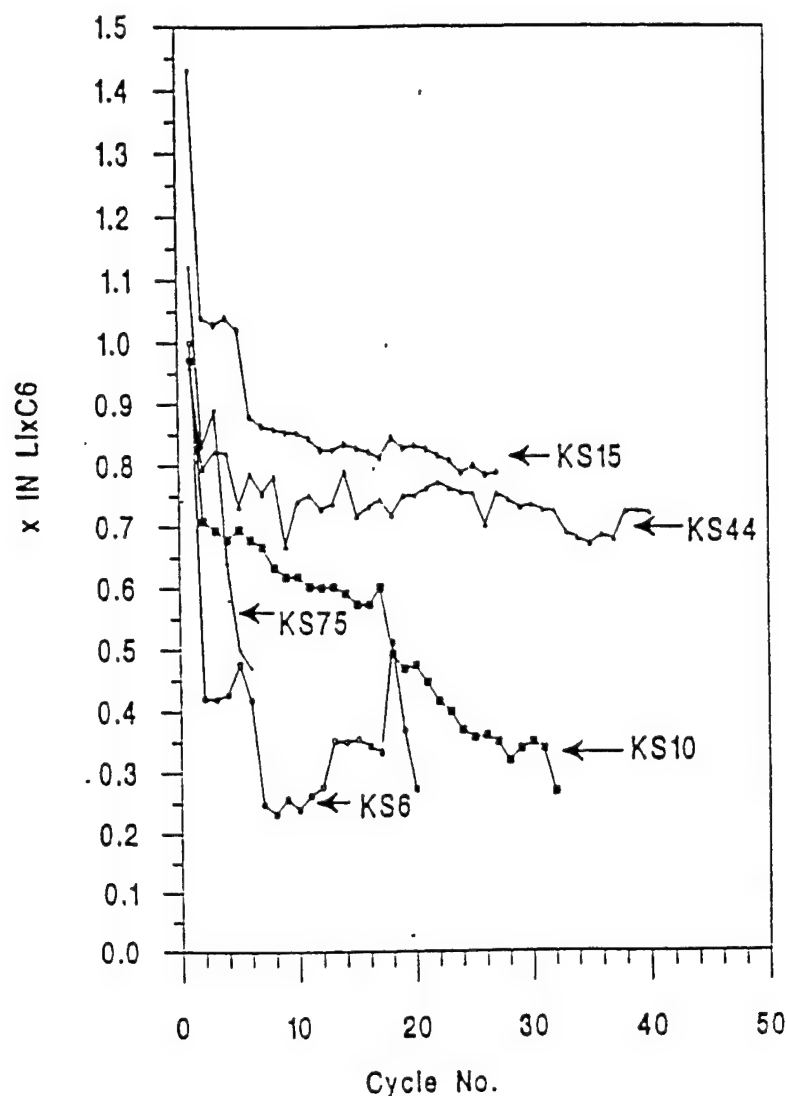


Figure 1. Effect of particle size on reversible capacity in Lonza KS graphite samples.

Another parameter tested was the effect of negative electrode density as a function of reversible capacity. Three different electrodes were prepared by hand methods and tested as lithium half-cells. The density of the negative electrodes tested was 0.61, 1.31 and 1.60 g/cm³. The results are shown in Figure 2. The capacity of the 1.60 g/cm³ electrode starts off substantially higher than that of the other electrodes, but soon levels off to an equivalent capacity for all three electrodes. Since a negative electrode density of 1.60 g/cm³ does not result in any performance problems, maximum negative electrode density will ensure maximum specific energy.

After the initial KS15 graphite studies, Lonza developed a new SFG graphite series for lithium ion applications. The new graphite was identical to the KS series except the SFG series was higher purity. Therefore, SFG15 became the new baseline for material evaluation during the initial stages of the lithium ion work.

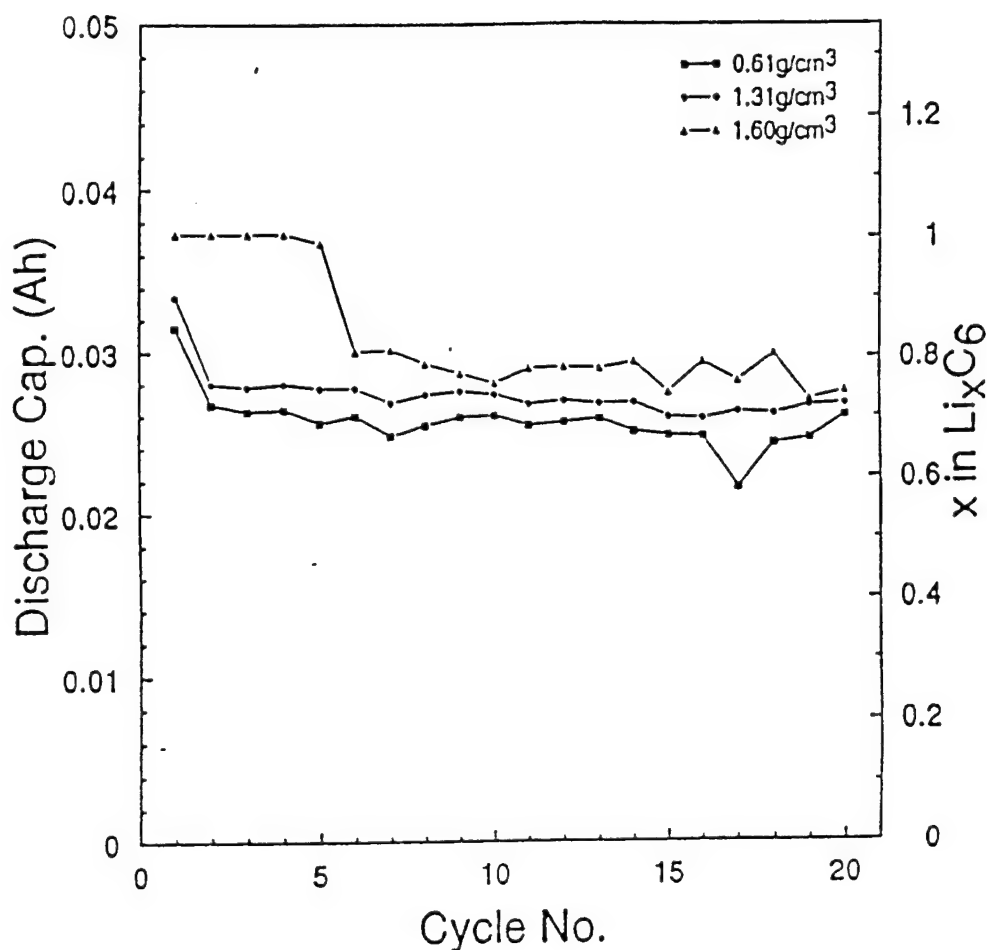


Figure 2. Lithium intercalation into graphite as a function of graphite electrode density.

As the production of lithium ion increased the carbon manufacturers were spurred to increase performance of negative electrode materials. Several new samples of graphite were obtained from suppliers for testing. One company, Nippon Carbon, supplied two samples: LK-702 and LK-201. During the manufacture of the electrodes it was noted that the adhesion for both materials was superior to the SFG and KS graphite. When the coating and press rolling equipment was used as opposed to the spraying technique previously used, the superior adhesion was evident during electrode processing. Electrodes with SFG15 coating experienced coating peeling off the foil during calendering. However, electrodes with Nippon Carbon coating suffered no peeling during calendering; these electrodes, prepared using the coating and press rolling equipment, had good adhesion and the desired density.

The performance of the Nippon carbons compared to SFG15 is shown in Figure 3. Of the three, K-201 had the poorest performance. A comparison of the other samples (SFG15 and LK-702) is more difficult. After 400 cycles the difference between two samples of LK-702 is very slight. After 400 cycles at 100% dod the SFG15 is not as good as the LK-702. Several of the cells were subjected to destructive physical analysis (DPA) after 100 cycles. The DPA revealed that the negative electrodes made with LK-702 and LK-201 showed superior adhesion when compared to SFG15.

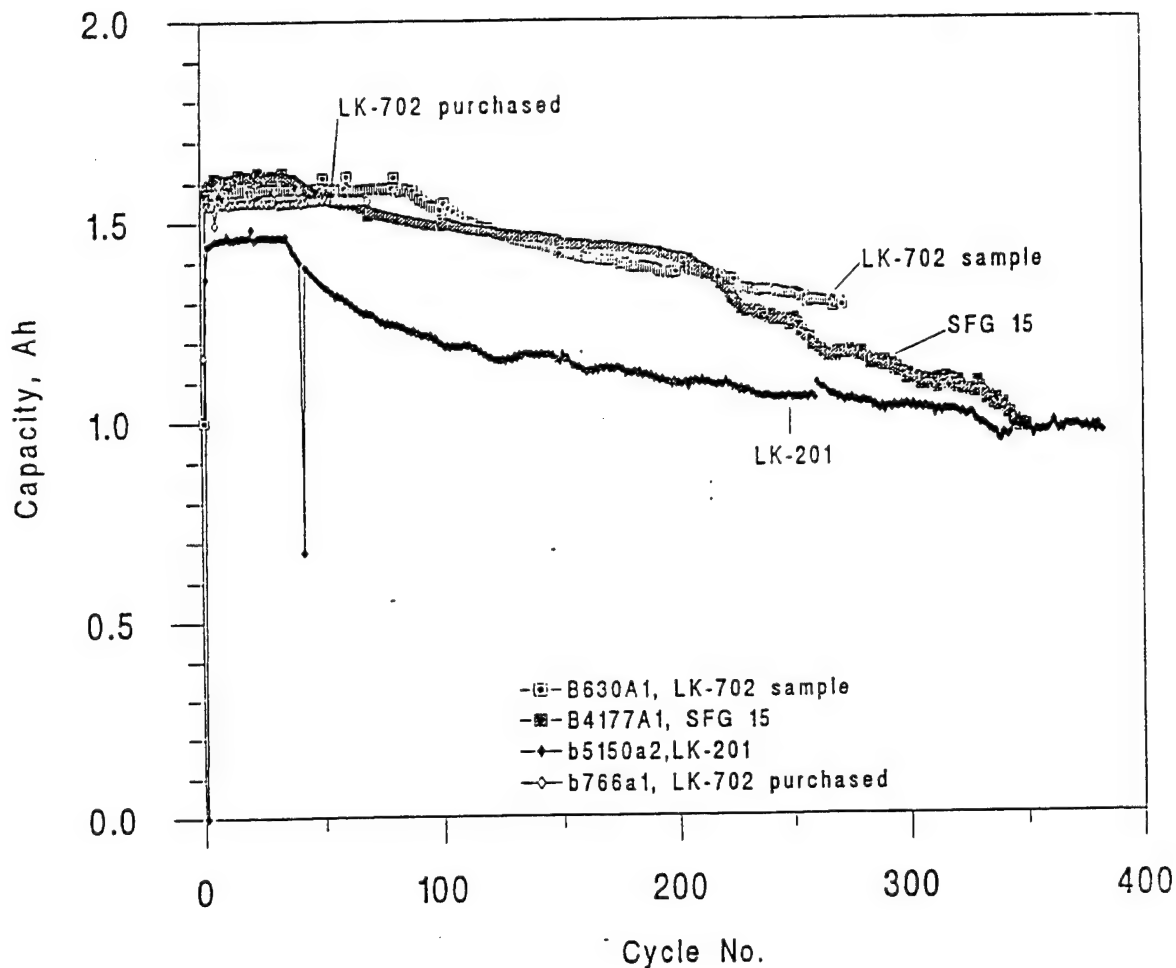


Figure 3. Negative electrode performance with various graphites.

As illustrated above, one of the overriding considerations in lithium ion technology is processing. With use of the coater and the semi-automatic press roller, negative electrodes of much higher density could be fabricated from mesophase carbon micro beads (MCMB) than from previously tested carbons including LK-702. This result was identical to the processing issue first encountered with SFG15 versus LK-702. Greater density of the negative electrode can lead to an enhanced cell capacity of 20% in a C cell configuration. Cell cycling data comparing MCMB to a similar cell with a LK-702 negative electrode is shown in Figure 4. This graph of capacity versus cycle number shows that the MCMB cell has 15% higher capacity than the LK-702 cell after 150 cycles at 100% dod. However, the capacity of the MCMB cell crosses over the capacity of the LK-702 cell after several hundred cycles, indicating that MCMB cannot maintain superior performance for the entire life of the cell.

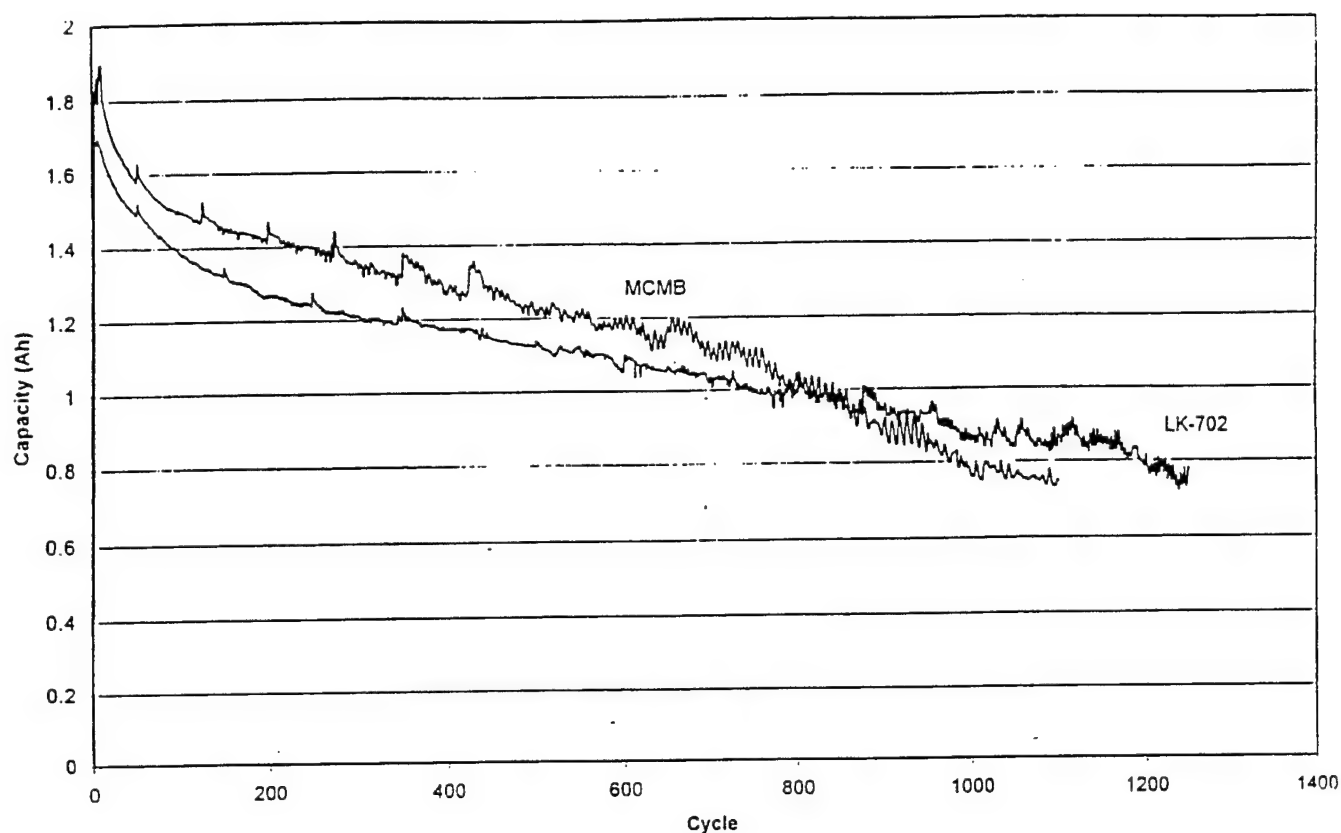


Figure 4. Capacity versus cycle for Lk-702 and MCMB negative electrodes.

Another issue with the negative electrodes made from MCMB is slitting. All of the C cell electrodes prepared are slit by hand. The positive electrodes were slit using a pair of scissors while the LK-702 negative electrodes were slit using an exacto-knife. However, MCMB negative electrodes were very difficult to slit, even with scissors. Disadvantages of MCMB electrodes include extreme difficulty of slitting, the resulting high incidence of internal short-circuits and the greater fade in capacity after extended cycling. Therefore, BATC was influenced to use LK-702 as the negative electrode material for the deliverable cells.

Cycle life is of great importance when supplying cells for spacecraft and aircraft applications. Orbiting satellites require up to 30,000 reliable cycles. Capacity fade versus cycle number must also be considered, since the capacity at 30,000 is more important than the capacity at cycle 500.

All of the negative electrode materials discussed so far are highly ordered synthetic graphite. Two other candidate materials for negative electrodes are petroleum coke and hard carbon. Neither of these materials is as highly ordered as graphite. Petroleum coke is a soft carbon which will become graphatized when heated to 2200 °C. The disordered nature of petroleum coke allows lithium intercalation without structural expansion. "Pinned" graphene sheets restrict realignment from ABAB to AAAA upon lithium intercalation. Therefore the system is far less dynamic than graphite and should have better adhesion during cycling. One disadvantage is that the capacity,

186 mAh/g, is half that of graphite.

Hard carbon is another class of carbon materials capable of lithium intercalation. This carbon is different from other disordered carbons, such as petroleum coke, because no amount of heating will cause graphitisation. The turbostatic disorder results in neither expansion or contraction during intercalation. Another advantage is that, at a rated capacity of 600 mAh/g, it has the highest capacity of all the carbons tested.

In the latter stages of the program, petroleum coke and hard carbon were tested at two different voltage limits. The results are shown in Figures 5 and 6. Petroleum coke performed as expected at 4.1 and 4.2V: the capacity is lower than both graphite and hard carbon at these voltage limits. However, petroleum coke experiences little capacity fade compared to graphite and hard carbon as illustrated in Figure 7. The capacity fade for a 4.1V cut-off is less than for a 4.2V cut-off. From cycle 11 to 150, the capacity fade for the 4.1V end point was 8.8% compared to 14.5% for the 4.2V end point. These numbers may seem quite high but the initial cycles have a higher rate of capacity fade than subsequent cycles. The hard carbon results are very disappointing; the capacity is only slightly higher than a similar graphite cell and has a greater capacity fade at both 4.1 and 4.2V end points.

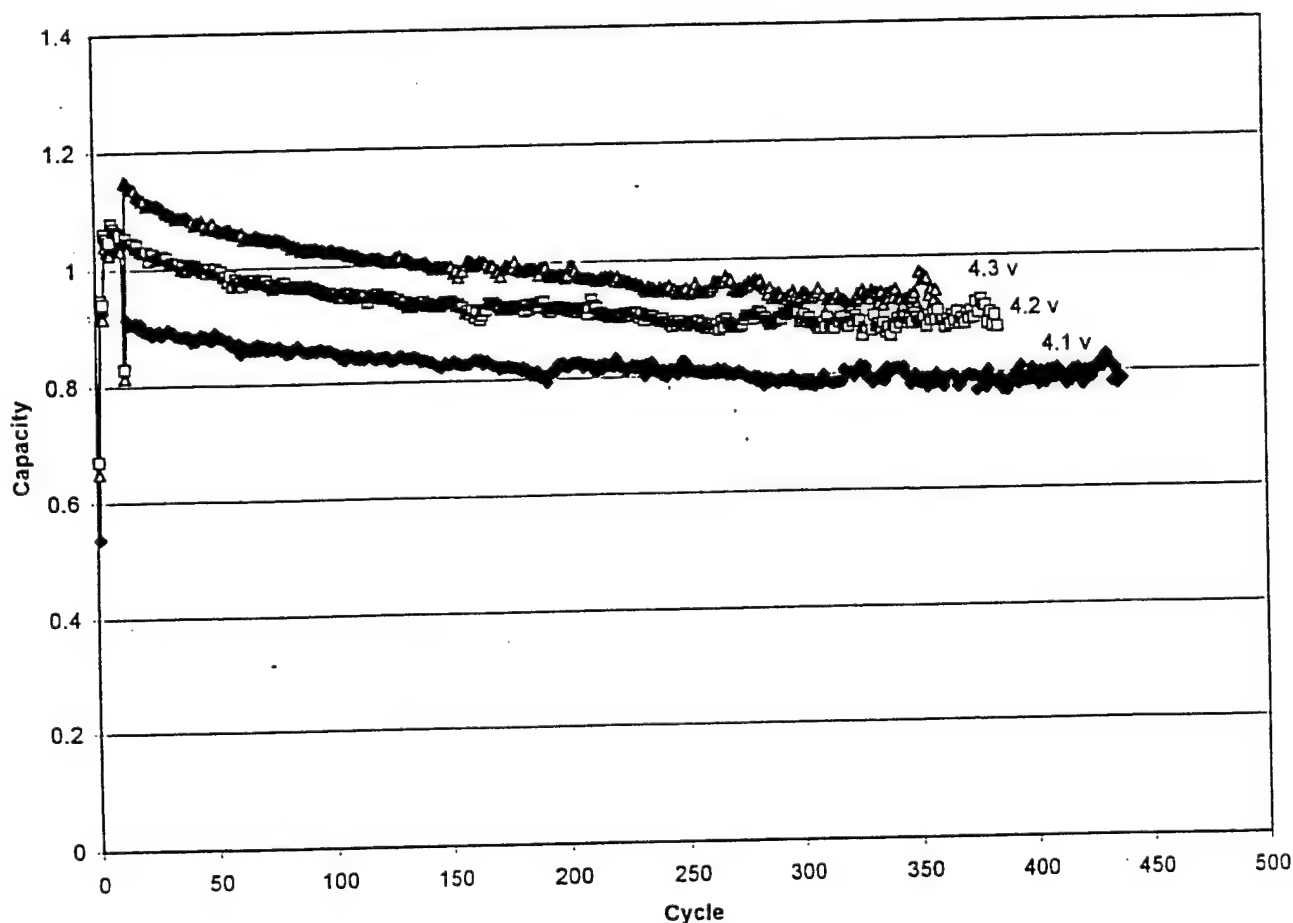


Figure 5. Petroleum coke cells tested at three different end of charge voltage limits.

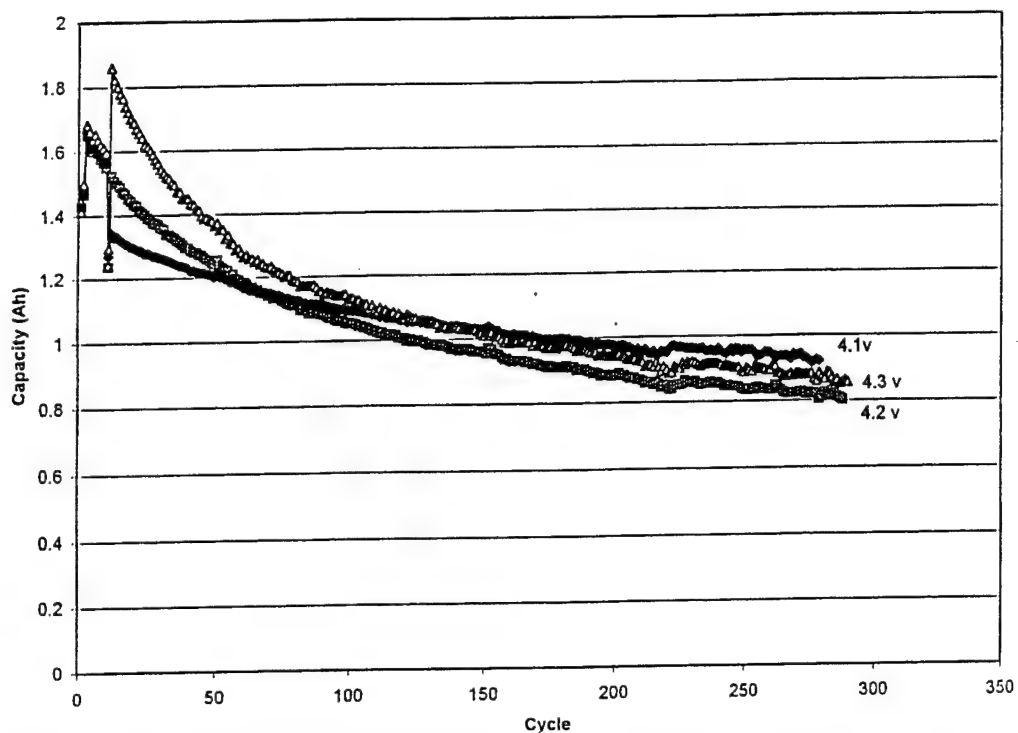


Figure 6. Hard carbon C cells tested at three different end of charge voltage limits.

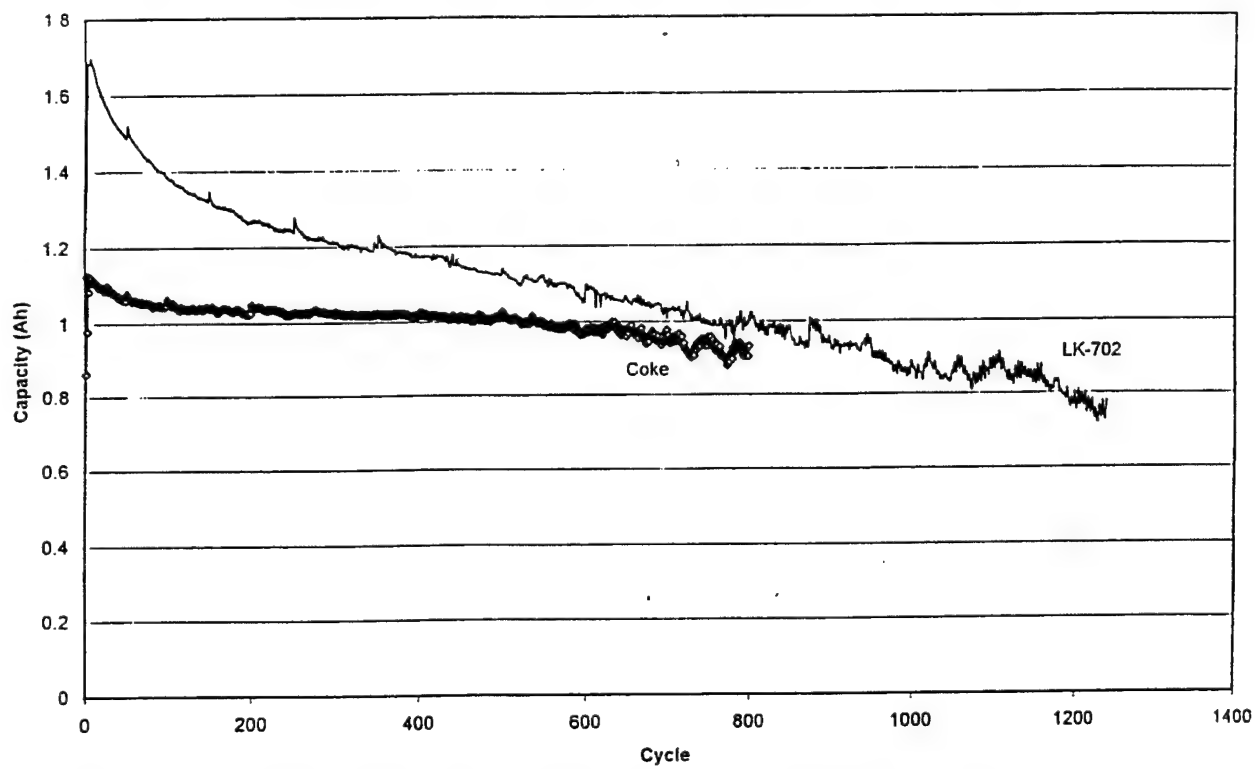


Figure 7. Capacity versus cycle number for LK-702 and petroleum coke.

After extensive testing and evaluation of candidate materials for negative electrodes, LK-702, a highly ordered synthetic graphite was selected. During testing, three critical issues arose and will be addressed in the future. The first is processing. This was observed during the change from hand made electrodes to electrodes made with bench scale processing equipment. Coater prepared SFG15 electrodes were not as dense as hand made electrodes. Since the performance of LK-702 was similar to SFG15 and the electrode density was higher using semi-automated techniques, LK-702 became the negative electrode material of choice. Since negative electrodes made from MCMB had higher density than electrodes made from LK-702, cell capacity increased by 10-15%. This trend also occurred with SFG15 versus LK-702. However, a different processing issue appeared with MCMB, slitting of the electrodes was extremely difficult. Due to the slitting difficulty and the resulting large number of internal high resistance short circuits MCMB, did not replace LK-702.

The second issue concerning negative electrode is capacity not only of the material but more importantly capacity of the finished cell. These are related but distinct due to the density of the electrode. The capacity of candidate materials increases from petroleum coke to graphite to hard carbon. Due to the difficulty in obtaining a high density negative electrode from hard carbon the capacity of that cell was not significantly greater than LK-702. However the capacity difference between cells made from petroleum coke (1.0 Ah) and LK-702 (1.6 Ah) is quite large.

The third issue for negative electrodes is capacity fade. An observation of the data suggests that the higher the initial electrode capacity the faster the capacity fade. This project concentrated on processing of graphite electrodes and more work with petroleum coke and hard carbon is required to prove or disprove the observed trend.

2.1.2 Task 1.2. Develop LiCoO_2 and LiNiO_2 Cathodes

The technology involving these general cathode chemistries is sufficiently mature that both are being used in the small commercial lithium ion batteries presently produced for consumer-type portable electronic devices. The industry believes that the next generation of these batteries will feature lithiated manganese oxide cathodes. Presently under development this cathode chemistry offers cost and environmental advantages. BATC has found this material exhibits neither the specific energy/energy density nor cycle life of equivalent cells constructed with either nickel or cobalt oxide.

Work in this area started with hand made electrodes and a variety of formulations to ensure electrical contact with the current collector. After several attempts the best formulation for adhesion was 91% LiCoO_2 , 3% KS6, 3% Super P, 3% Kynar 2801 (10% in NMP), 1185 g NMP and 0.001" Al foil alloy 1145. The graphite KS6 was mixed with an amorphous carbon, Super P, to give electrodes with better density than when carbon was used alone, and to provide superior adhesion than when graphite was used alone.

Initial work involved LiCoO_2 , since this cobalt system was widely used commercially. To locate a suitable supplier, samples were obtained from many sources, including FMC, Cyprus, JEC, Hall Metal Oxides and Honjo Chemical. Electrodes were prepared by hand and assembled into C cells. Results for most of the cells are shown in Figure 8. Despite inconsistencies in manual methods, it

is obvious that the LiCoO_2 supplied by Honjo Chemical gave the best capacity and best performance after extended cycling.

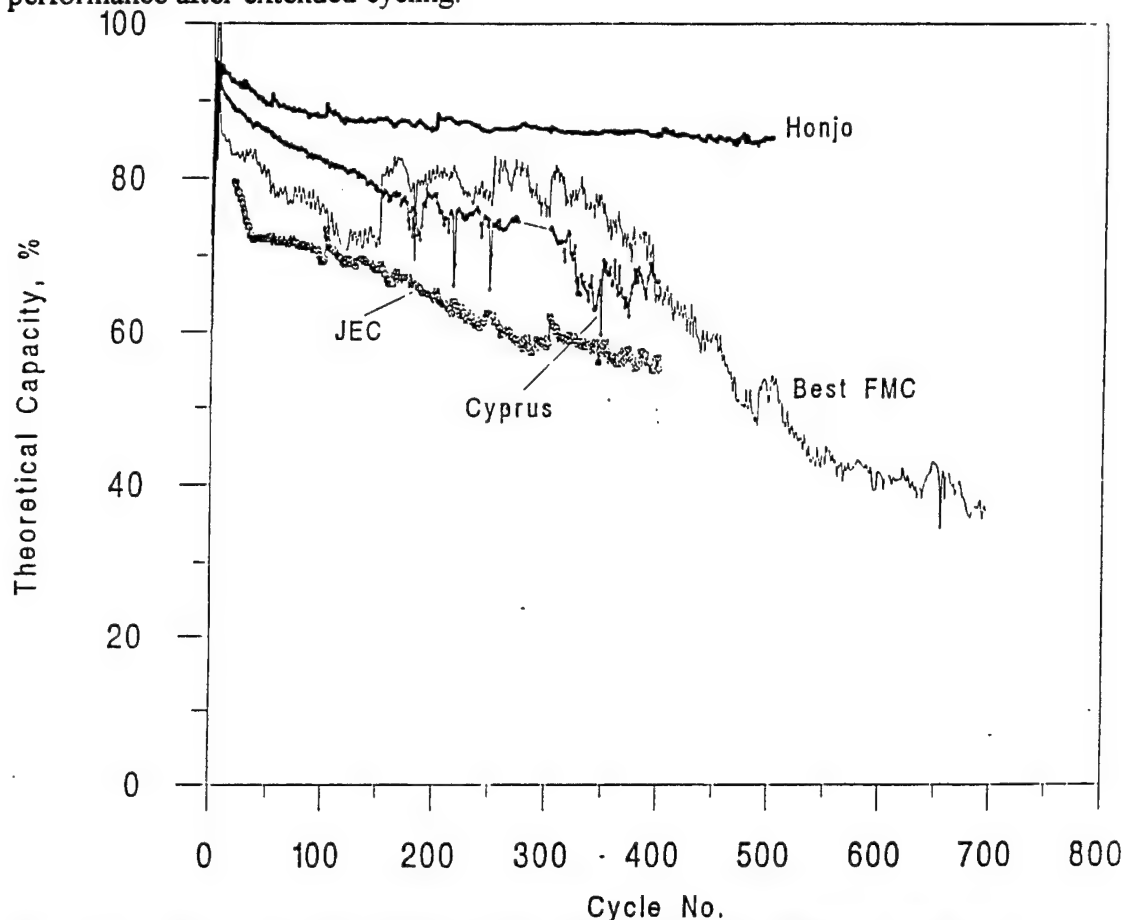


Figure 8. Comparison of LiCoO_2 C cell performance from different suppliers.

Another problem encountered was inconsistencies between lot numbers of LiCoO_2 from the same supplier; but the LiCoO_2 from Honjo Chemical showed very little lot to lot variation.

The first commercial lithium ion cells featured a LiCoO_2 positive electrode. As interest in this field increased, the desire for better performance than your competitor led several companies to investigate LiNiO_2 as an alternative to LiCoO_2 . One advantage of nickel is the higher energy compared to cobalt: the capacity of LiNiO_2 is 180 mAh/g as opposed to 140 mAh/g for LiCoO_2 . Since a LiNiO_2 positive electrode could result in higher specific energy and energy density, several different samples of LiNiO_2 were obtained. Problems occurred during preparation of all LiNiO_2 slurries. Ten to 20 minutes after preparation the slurry would gel, rendering electrode preparation impossible. Perhaps unreacted LiOH in the sample caused polymerization of the N-methylpyrrolidinone (NMP). Therefore, the samples were washed with distilled H_2O until the pH of the supernatant was neutral. After the material was washed no gelling of the LiNiO_2 slurries was observed.

The trade-off between LiCoO_2 and LiNiO_2 started with a study of rate capability. The electrolyte was 1M LiPF_6 ethylene carbonate/diethyl carbonate (EC:DEC) 1:1. All cells were charged at C/2 and the discharge rates varied from C/2 to 2C. All capacities reported were the average of 4

cycles. The results of this test comparison are shown in Figure 9.

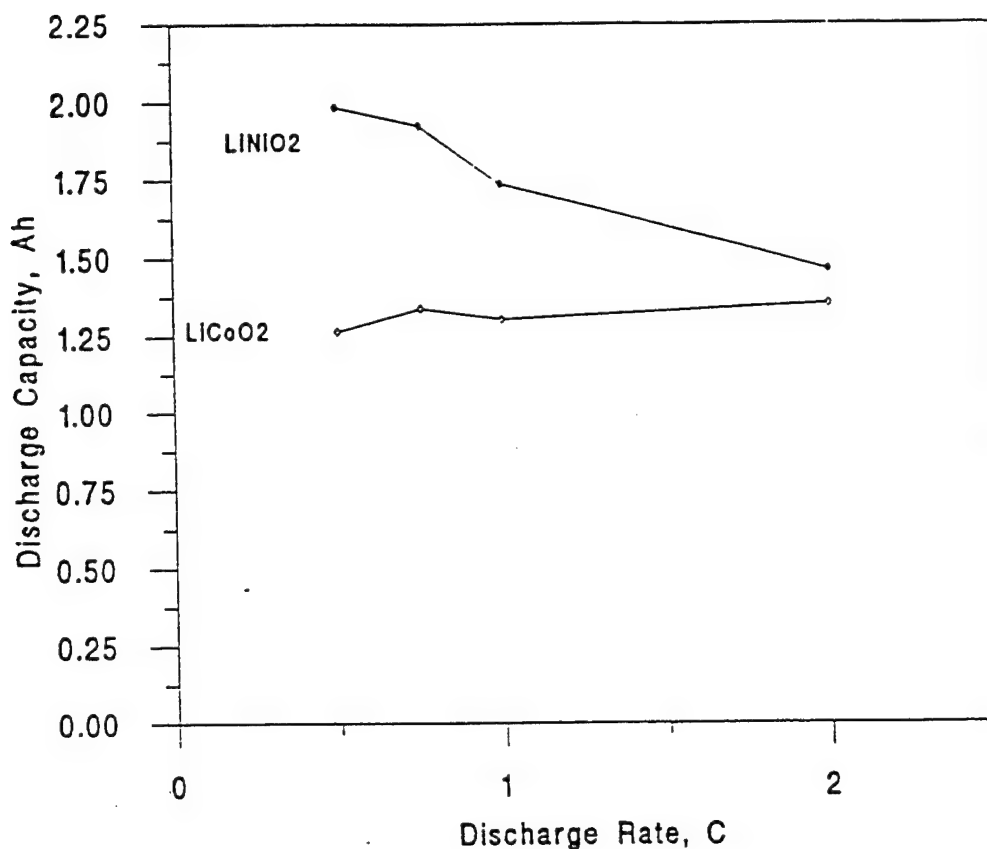


Figure 9. Capacity as a function of discharge rate for cells containing LiCoO₂ or LiNiO₂ positive electrodes.

Figure 9 shows that the capacity of the nickel system is higher at low rates, and is generally more rate dependent than the LiCoO₂ system. The capacities essentially converge at the 2C rate. The low capacity of the LiCoO₂ versus the LiNiO₂ is exaggerated since the cells featured hand made electrodes and BATC routinely produces LiCoO₂ C cells with higher capacity.

Low temperature performance of the two materials was examined. The key to low temperature performance is charge acceptance. Tests were done at 0°C and the cells were charged to 4.1V and discharged to 3.0V. Cells were charged and discharged at 0°C which gives a realistic capacity as opposed to charging at room temperature and then discharging at low temperature. Under the test conditions the LiCoO₂ cells exhibited approximately 33% more capacity than the LiNiO₂ cells. The capacity of both systems is reduced at this temperature with the LiCoO₂ delivering 80% of room temperature capacity, and the LiNiO₂ delivering 40%. When the test was carried out at -20°C the nickel system delivered no capacity while a small amount was delivered by the cobalt system. Low temperature performance will be further addressed in a section on electrolyte.

The cycle life of the nickel and cobalt systems was compared next. The results for these tests are shown in Figure 10. As can be seen from these results, the capacity of the cobalt system is closer to the nickel system. For tests carried out at 85% dod, the data illustrates that at BATC the

nickel system is inferior to the cobalt system. Therefore, it was decided that the baseline technology would use LiCoO_2 supplied by Honjo. This decision has proven to be correct since recently the LiNiO_2 system has been abandoned by the rechargeable battery community due to safety issues.

Recently a cobalt-doped nickel oxide has become available and several companies have planned production. BATC obtained samples from three different suppliers, FMC, Westaim and Seimi. The composition of these samples is approximately 18% cobalt doping of the nickel sites. The capacity of the material is 175 mAh/g. Initially, the samples were prepared by hand methods and evaluated. The results from these tests with an end of charge voltage cut-off of 4.1 V, are shown in Figure 11. The data suggested that the Seimi material was superior. Therefore, a larger sample of Seimi $\text{LiNi}_{0.82}\text{Co}_{0.18}\text{O}_2$ was purchased and ran on the coater. The results from this run along with the other samples of $\text{LiNi}_{0.82}\text{Co}_{0.18}\text{O}_2$ and a sample of LiCoO_2 are shown in Figure 12.

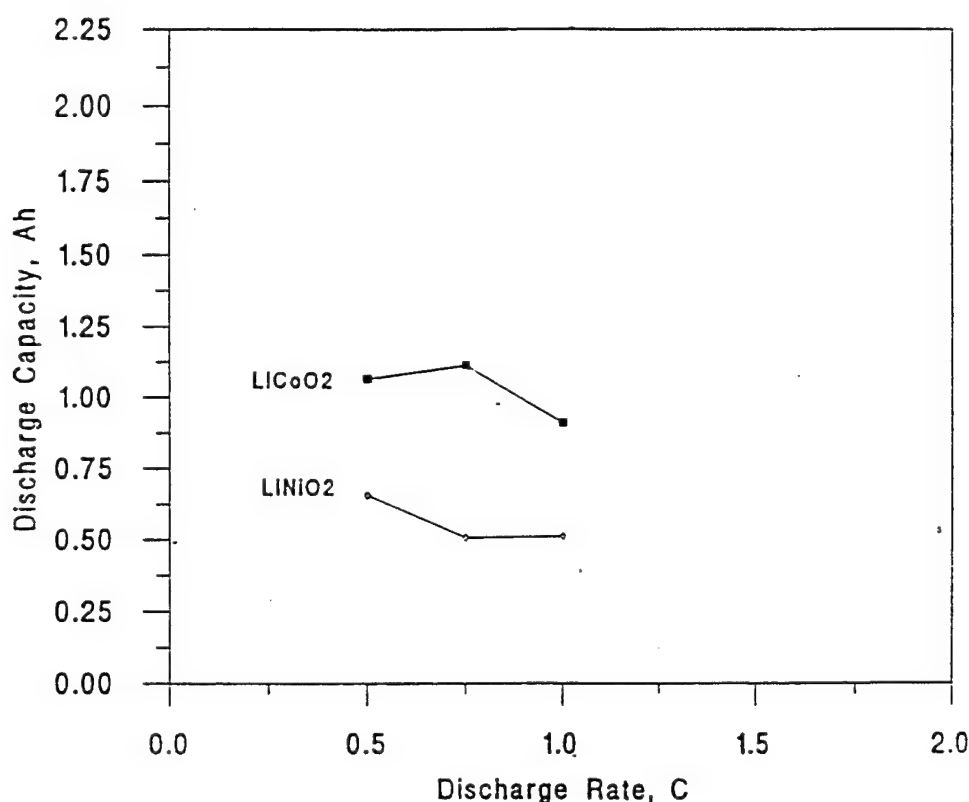


Figure 10. Capacity as a function of discharge rate at 0 °C for cells using LiCoO_2 or LiNiO_2 positive electrodes.

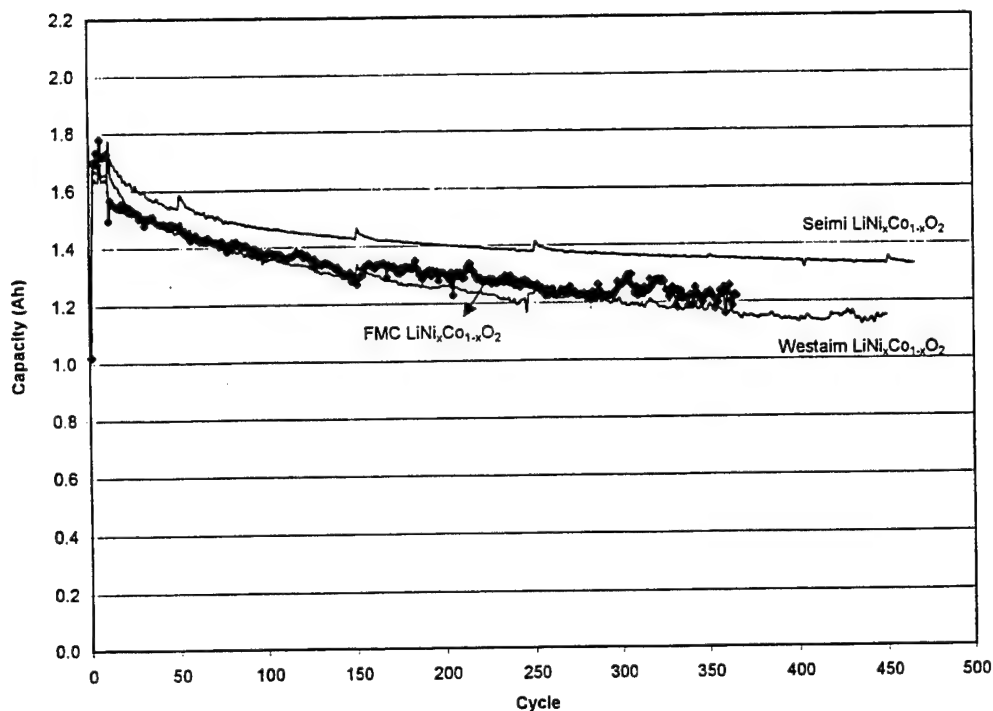


Figure 11. Comparison of $\text{LiNi}_{0.82}\text{Co}_{0.18}\text{O}_2$ positive electrode cells made from material supplied by Seimi, FMC and Westaim.

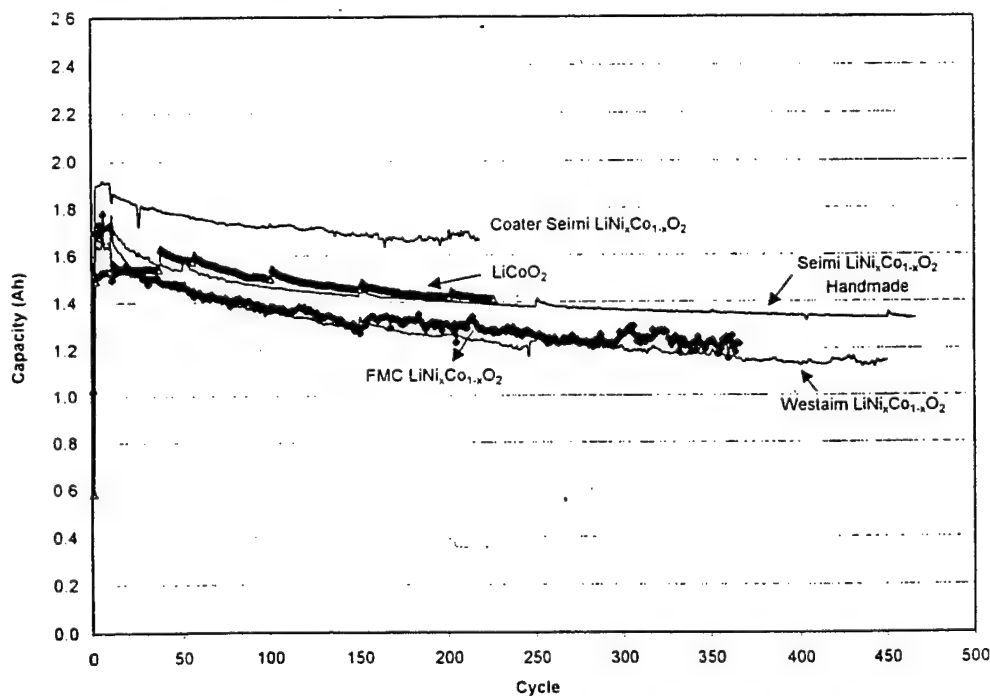


Figure 12. Capacity as a function of cycle number for $\text{LiNi}_{0.82}\text{Co}_{0.18}\text{O}_2$ supplied by several companies and compared to LiCoO_2 .

Two conclusions can be drawn from Figure 12. The capacity difference between the hand-made and machine-made Seimi $\text{LiNi}_{0.82}\text{Co}_{0.20}\text{O}_2$ is quite dramatic. Also, $\text{LiNi}_{0.82}\text{Co}_{0.20}\text{O}_2$ cells have a higher capacity than LiCoO_2 cells. Next, charge voltage dependence of the $\text{LiNi}_{0.82}\text{Co}_{0.20}\text{O}_2$ supplied by Seimi. The cells were charged to different end of charge voltages (4.1 and 4.2V) and discharged to 3.0V. The results are shown in Figure 13.

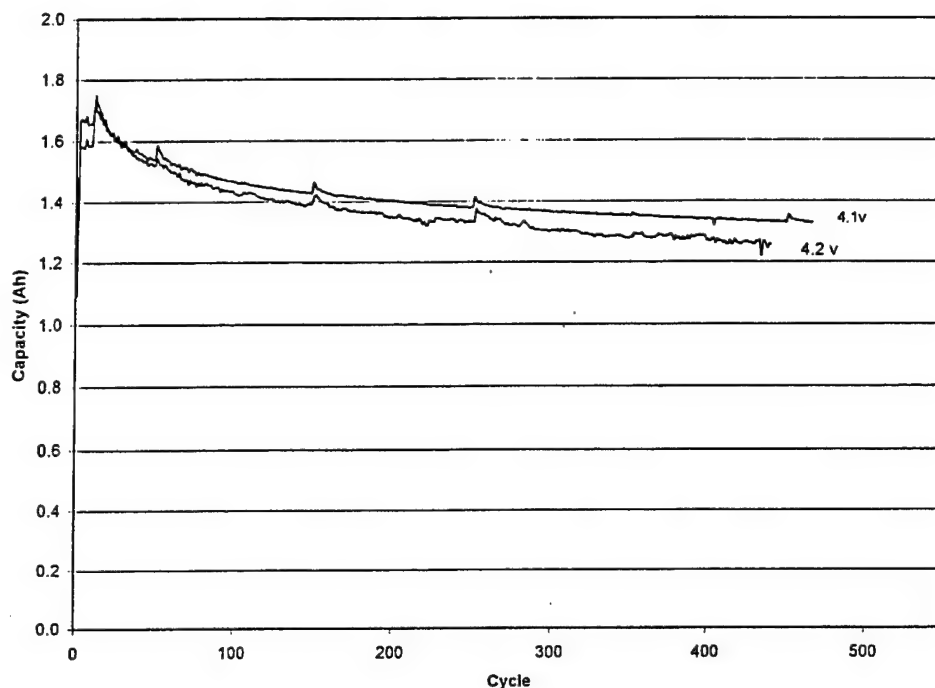


Figure 13. Charge voltage dependence for $\text{LiNi}_{0.82}\text{Co}_{0.18}\text{O}_2$ positive electrode cells.

It is apparent that the cycle life of the cells charged to 4.1V is greater than those charged to 4.2V. Two issues are still outstanding with $\text{LiNi}_{0.82}\text{Co}_{0.20}\text{O}_2$ supplied by Seimi. The first is that the material, like LiNiO_2 , has to be washed to remove impurities before slurry preparation. Second, the finished electrodes have a tendency to flake at the edges. New binders and varying binder concentration tests are underway.

2.1.3 Task 1.3. Evaluate and Improve $\text{Li}_x\text{Mn}_y\text{O}_z$ Cathode Materials

As noted above, the lithiated manganese oxide cathodes are viewed by the industry as the most likely materials to find their way into the next generation of commercial lithium ion cells. The objective of this task is to pursue the development of these materials in order to identify materials and processes which will make lower cost, high-performance large cells for aircraft and spacecraft applications possible.

The work in this area was initiated at the beginning of the program. LiMn_2O_4 was prepared by BATC and materials were obtained from several industrial sources. A disadvantage of the manganese system is an inherently lower capacity than the other metal oxides used in Li ion technology. The capacity of the material is quoted as 120 mAh/g. In practice the capacity is closer to 110 mAh/g. The advantages of LiMn_2O_4 include cost, tolerance to over-charge and safety. The issue of cost is over stated since the cost for LiMn_2O_4 is mostly due to processing and

not the cost of the starting material. Test results using samples from Cyprus, Kerr McGee and BATC are shown in Figure 14.

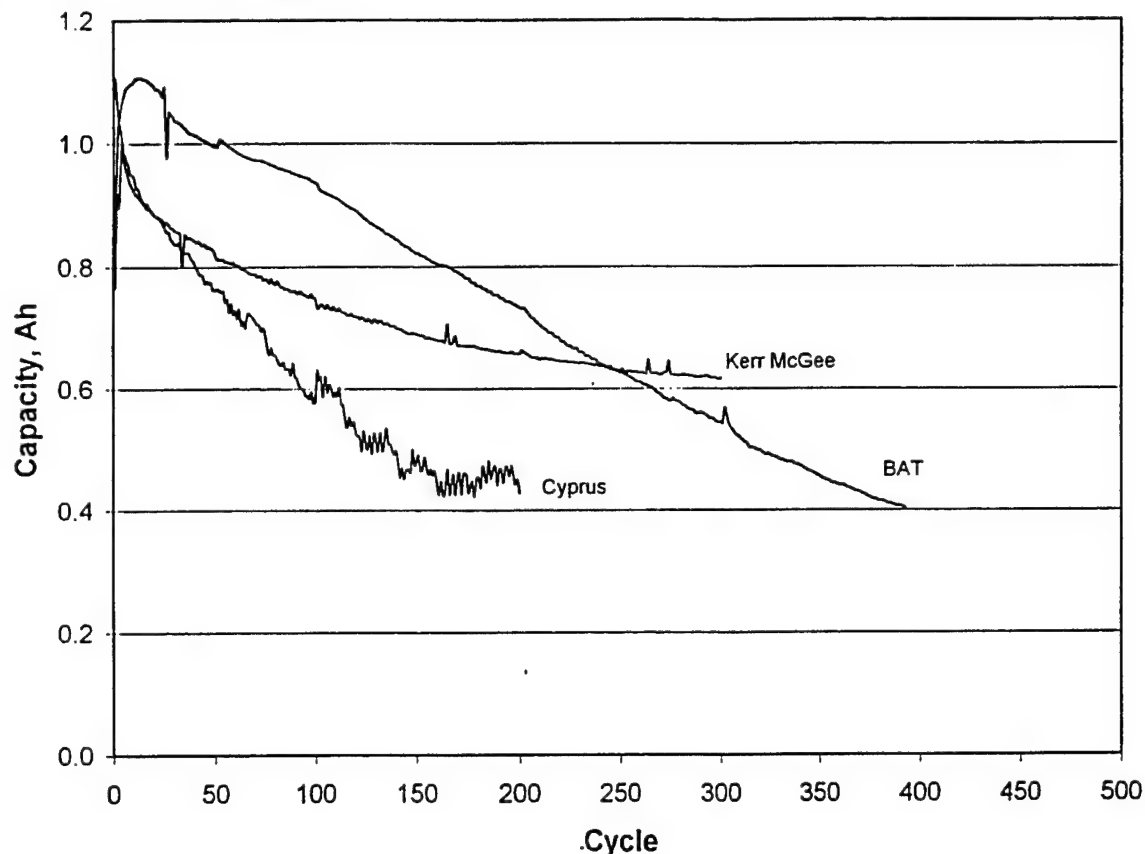


Figure 14. Performance of LiMn_2O_4 supplied by several different companies.

The capacity fade and cell capacity obtained from these samples of LiMn_2O_4 is inferior to that of the other metal oxide positive electrode materials. Of concern with the spacecraft and aircraft applications is specific energy, and these LiMn_2O_4 results spurred a decision to baseline the technology with the cobalt oxide. The relative performance of the materials supplied by Kerr McGee and Cyprus compared to that synthesised at BATC shows that the development of the materials by the industrial suppliers was in the initial stages.

Due to the possibility of a large pay-off in the electric vehicle market, suppliers of manganese oxides have been continually optimizing the performance of the manganese powders for lithium ion applications. Since the technology was continually evolving, samples were periodically tested. Recently, samples were obtained from two different suppliers, MaxPower and Riedel-de-Haen. The results from these materials, processed by semi-automated methods, are shown in Figure 15. Part of the difference in capacity can be attributed to the automated equipment versus hand methods. More striking is the reduced capacity fade of the new materials compared to the previously tested materials. After 500 cycles the sample from MaxPower still has over 70% of the initial capacity.

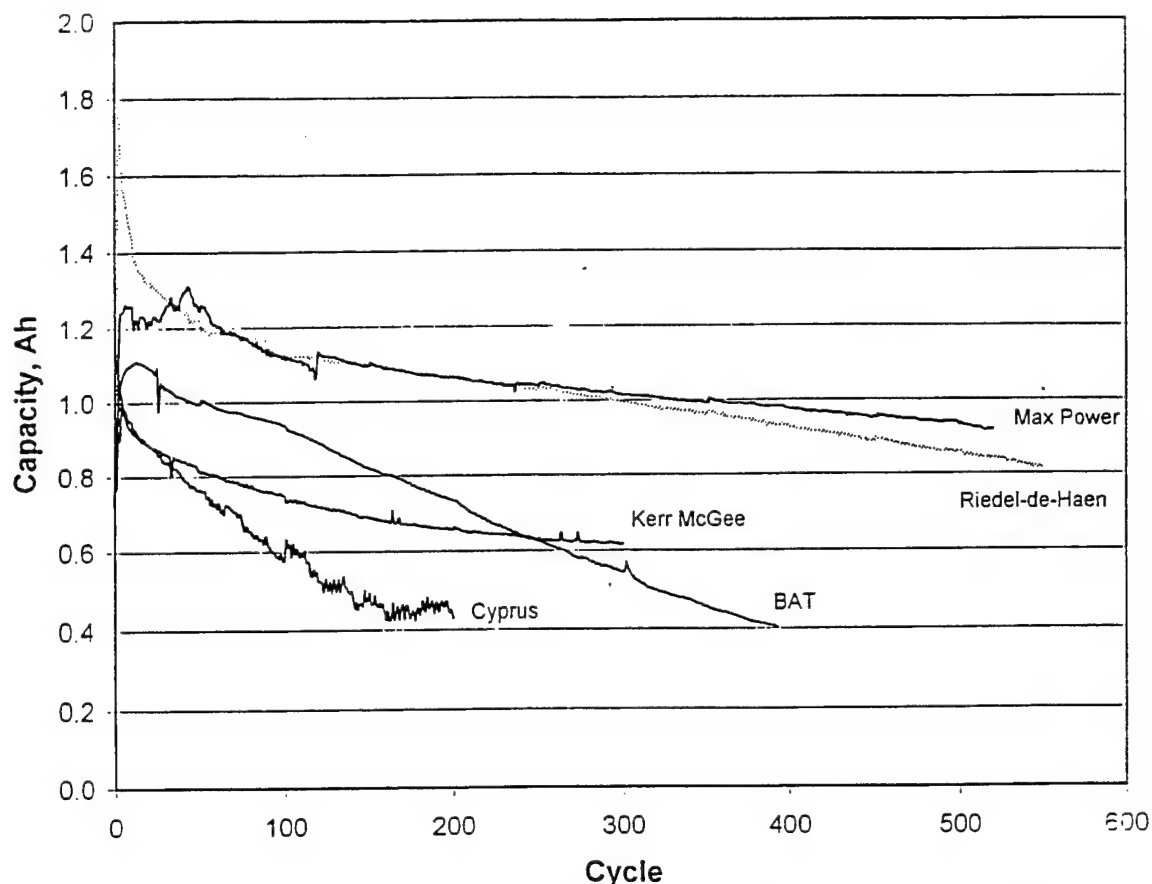


Figure 15. Performance of LiMn_2O_4 supplied by several different companies, 1998.

2.1.4 Task 1.4. Evaluate and Improve Electrolyte Performance

Significant improvement in low temperature performance of lithium ion batteries is required for this weight saving technology to be fully operational for spacecraft and aircraft applications. With the lithium ion technology, this can be achieved with relatively minor variations in the molecular structure of the organic solvent component of the electrolyte.

The first commercial lithium ion battery developed by Sony in the early 1990's used an electrolyte composed of 1M LiPF_6 in propylene carbonate (PC) and diethyl carbonate (DEC). With the gradual shift from a petroleum coke to a graphite negative electrode PC has been replaced with ethylene carbonate (EC).

Recently, work has been centered on electrolytes with improved low temperature performance. The literature reveals two approaches, one being the use of additives or new solvents as they become available (e.g. ethyl methyl carbonate), and the second being a shift to ternary from binary systems. A list of possible solvents and their abbreviations is given in Table 1, and a list of the selected electrolyte mixtures tested at BATC is given in Table 2.

Table 1. Abbreviations and Melting points of selected solvents for Lithium ion electrolytes.

Solvent	Abbreviation	Melting Point (°C)
ethylene carbonate	EC	38
diethyl carbonate	DEC	- 43
dimethyl carbonate	DMC	2 to 4
ethyl methyl carbonate	EMC	- 55
methyl acetate	MA	- 98
ethyl acetate	EA	- 84

Table 2. Selected Electrolyte Candidates with solvent system listed on a volume basis.

Electrolyte (1M LiPF ₆)	Solvent Ratio	Literature Source
EC/EMC	1:3	Reference 1
EC/DEC	1:1	BATC
EC/DMC/DEC	1:1:1	Reference 2
EC/DMC/EMC	1:1:1	BATC
EC/DEC/EMC	1:1:1	Reference 1
EC/DMC/MA	40:45:15	Reference 3
EC/DMC/EA	40:45:15	Reference 3
EC/EMC/MA	40:45:15	BATC
EC/EMC/EA	40:45:15	BATC

1. E.J. Plichta, Proceedings of The First Hawaii Battery Conference, January 5-7, 1998.
2. M.C. Smart, C.-K Huang, B.V. Ratnakumar, S. Surampudi, Proceedings of the Thirty Second Intersociety Energy Conversion Engineering Conference, July 27 -August 1, 1997
3. S.T. Mayer, H.C. Yoon, C. Bragg, J.H. Lee, The Thirteenth International Seminar on Primary and Secondary Battery Technology and Application, March 4-7, 1996, Boca Raton, Florida.

The temperature limitations of the lithium ion battery system are predominately due to the properties of the organic electrolyte systems. One parameter which must be optimized is the conductivity of the electrolyte as a function of temperature. The ability of the cell to operate at low temperature is dependent on the conductivity of the electrolyte. The conductivity of all the electrolyte candidates listed in Table 2 were determined, and the results are shown in Table 3. For the electrolyte EC/DEC 1:1 1M LiPF₆, no values for -25 °C and -35 °C were obtained. The conductivity was measured at -22 °C, and the electrolyte froze before a reading could be taken at -35 °C.

Table 3. Conductivity versus Temperature for the selected electrolyte systems.

Electrolyte 1M LiPF ₆	Conductivity at Selected Temperature (mS/cm)					
	-35 °C	-25 °C	-15 °C	-5 °C	5 °C	15 °C
EC/EMC 1:3	1.5	2.35	3.45	4.75	6.1	7.75
EC/DEC 1:1	-	-	2.3	3.60	5.05	6.75
EC/DEC/DMC 1:1:1	1.45	2.45	3.60	5.05	6.65	8.25
EC/DMC/EMC 1:1:1	1.55	2.70	4.05	5.60	7.20	9.00
EC/DEC/EMC 1:1:1	0.90	1.80	2.95	4.10	5.45	7.1
EC/DMC/MA 40:45:15	0.75	2.35	4.85	7.35	9.60	11.90
EC/DMC/EA 40:45:15	0.70	2.15	4.40	6.50	8.70	11.20
EC/EMC/MA 40:45:15	1.00	2.80	4.50	6.20	7.90	9.70
EC/EMC/EA 40:45:15	1.85	2.80	4.60	6.20	7.40	9.25

Based on the data two electrolytes were selected for comparison to the electrolyte currently in use at BATC. The compositions selected for further evaluation were 1M LiPF₆ in EC/EMC 1:3 and 1M LiPF₆ in EC:DMC:DEC 1:1:1. The electrolyte currently used at BATC is 1M LiPF₆ in EC:DEC 1:1. The conductivity for the three electrolytes is shown in Figure 16.

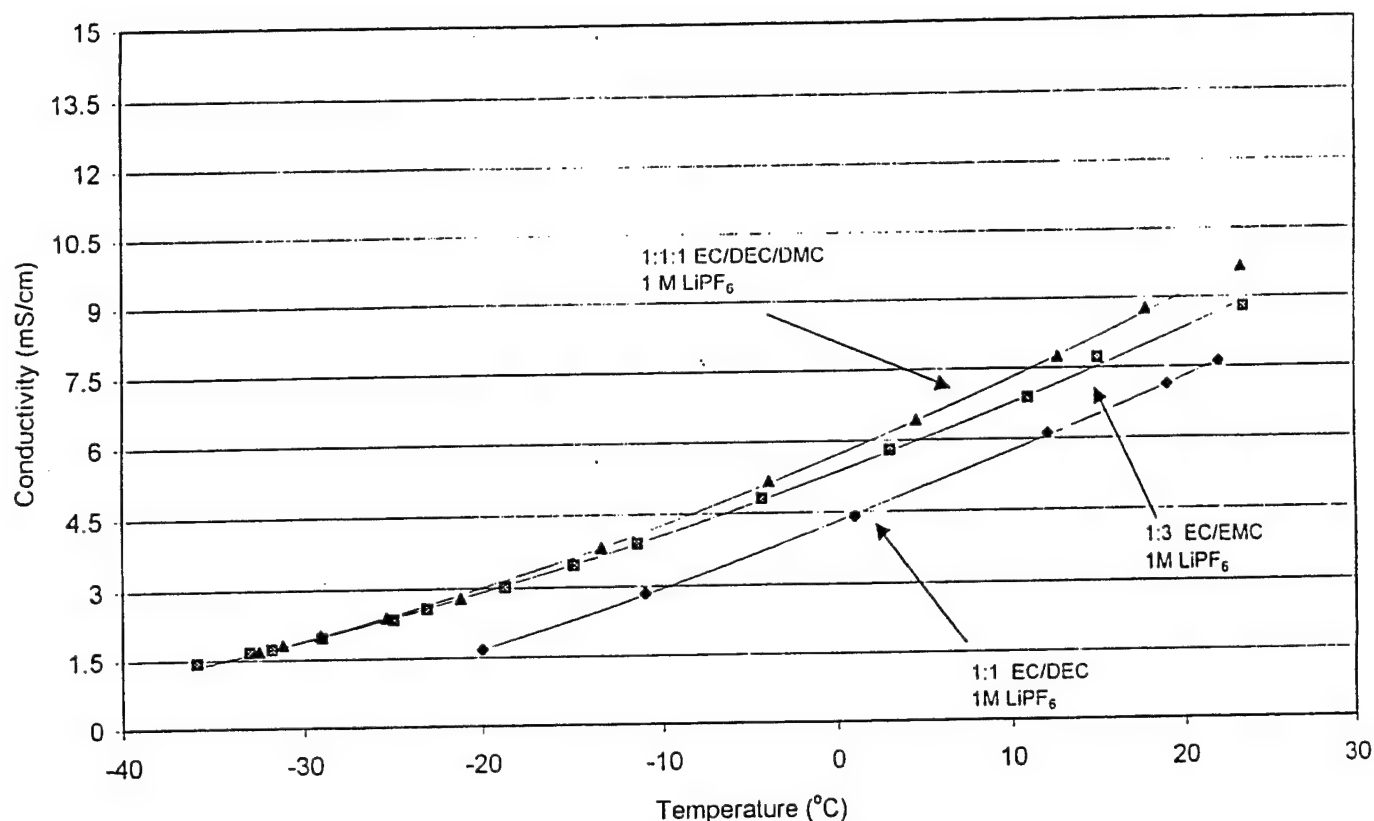


Figure 16. Conductivity versus temperature for three selected electrolytes.

A comparison between 1M LiPF₆ EC/DEC 1:1 and 1M LiPF₆ EC/EMC 1:3, the two binary electrolytes, showed superior conductivity of the latter. One other electrolyte, 1M LiPF₆ EC/DEC 1:3 was prepared to determine the reason for the enhanced conductivity of the EC/EMC electrolyte. The conductivity of the EC/DEC 1:3 electrolyte was the lowest of the binary group at room temperature but surpassed EC/DEC 1:1 at low temperature. Therefore, the enhanced conductivity of the 1M LiPF₆ EC/EMC 1:3 electrolyte was due two factors. The first being the substitution of EMC for DEC, and secondly the reduction of the concentration of EC.

One of the ternary electrolytes with higher conductivity was 1M LiPF₆ EC/DMC/EMC 1:1:1. The low temperature performance of this electrolyte is equivalent to or better than the other two selected electrolytes at low temperature and superior at temperatures below -30 °C. Once again when DEC is replaced, in this case with DMC, conductivity increased. When EMC was replaced with DMC conductivity also increases.

With the addition of methyl acetate or ethyl acetate, the room temperature conductivity of the DMC electrolytes is greatly enhanced while that of the EMC electrolytes is slightly enhanced. The conductivity of the DMC based electrolytes is superior to the EMC based electrolytes at room temperature. However, there is a crossover between -10 and -20 °C where the EMC based electrolytes have better low temperature conductivity. The ethyl acetate electrolytes have better low temperature conductivity but inferior high temperature conductivity compared to the methyl acetate electrolytes.

Another very important parameter for low temperature performance is the freezing point of the electrolyte. Freezing of the electrolyte significantly reduces conductivity, may lead to irreversible precipitation of the electrolyte salt, and may result in damage to the electrode structure. To determine the freezing point of the electrolyte mixtures, two separate methods were used and the results compared to a third method. The first method used was freezing a Pasteur pipette filled with the electrolyte in liquid nitrogen and then warming the sample slowly, monitoring the temperature with a thermocouple. To determine the validity of this method, initial tests were carried out using solvent standards and comparing the results to literature values. The experimental results showed excellent correlation with literature values.

However, when the same technique was used for a complex organic mixture with dissolved LiPF_6 , the results became less defined. In some cases an inflection point was noted and in other cases no change in slope was observed for the warming curve. Therefore, another method was required to determine the electrolyte phase transition temperature. Instead of trying to determine the melting point, as with the pipette method, it was decided to determine the freezing point. This method involved freezing the electrolyte at a slower rate so a clearly defined value could be observed. Samples of the electrolytes were placed into sample vials with thermocouples and the temperature lowered to $-60\text{ }^\circ\text{C}$ in an environmental chamber. Several samples of pure solvents were tested and the results confirmed the validity of the technique (acetonitrile $-44\text{ }^\circ\text{C}$, ethyl methyl carbonate $-55\text{ }^\circ\text{C}$, 1-methyl-2-pyrrolidinone, $-23.3\text{ }^\circ\text{C}$). The results for the electrolytes are shown in Table 4 and Figure 17. The resulting temperature curves were initially thought to exhibit supercooling. However, this is probably not the case since the curves are the result of the system being complex.

Table 4. Melting Points of Electrolytes using the Environmental Chamber method.

Electrolyte	Test Runs			Average
EC/EMC 1:3 1M LiPF ₆	frozen but point inconclusive	frozen but point inconclusive	did not freeze at -50 °C	freezing point near -60 °C
EC/DEC 1M LiPF ₆	-25.7 °C	-29.0 °C	-30.9 °C	-28.5 °C
EC/DEC/DMC 1M LiPF ₆	-47.2 °C	-48.1 °C	-49.7 °C	-48.3 °C
EC/DMC/EMC 1M LiPF ₆	-49.2 °C	-47.3 °C	-48.1 °C	-48.2 °C
EC/DEC/EMC 1M LiPF ₆	frozen but point inconclusive	did not freeze, small amount of precipitate	did not freeze, small amount of precipitate	precipitate noted at -40 °C freezing point near -60°C
EC/DMC/MA 1M LiPF ₆ 40:45:15	-29.7 °C	-32.0 °C	-27.5 °C	-29.7 °C
EC/DMC/EA 1M LiPF ₆ 40:45:15	-29.1 °C	-30.1 °C	-29.2 °C	-29.5 °C
EC/EMC/MA 1M LiPF ₆ 40:45:15	-47.7 °C	-48.1 °C	-48.8 °C	-48.2 °C
EC/EMC/EA 1M LiPF ₆ 40:45:15	-47.3 °C	-51.8 °C	-48.5 °C	-48.5 °C

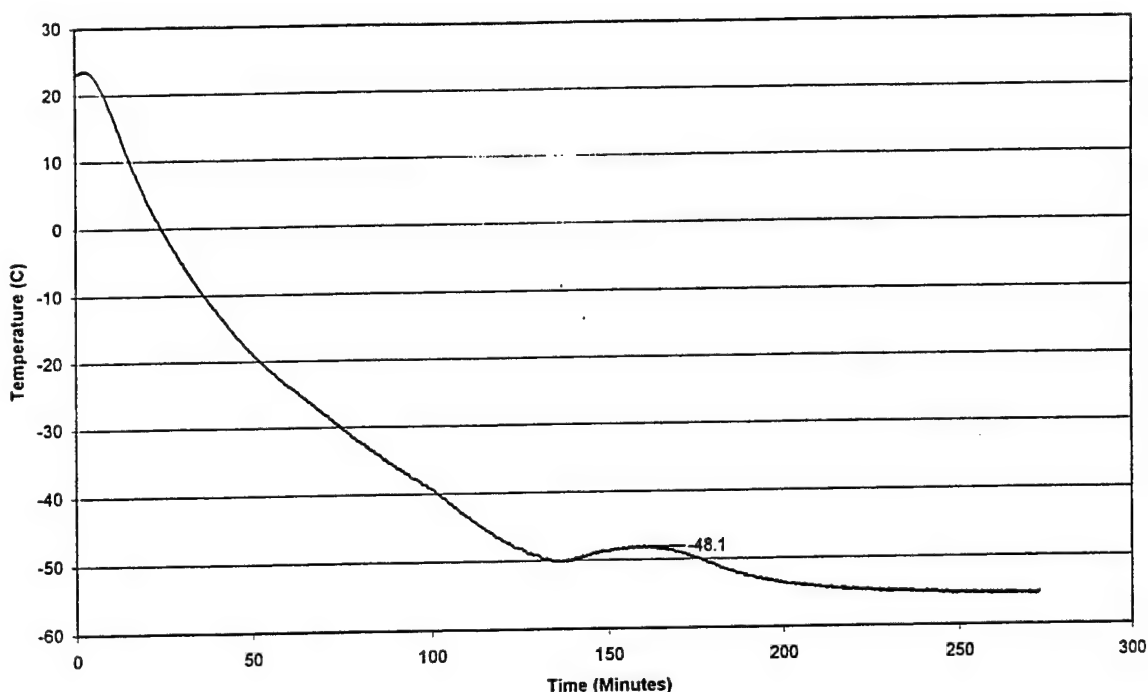


Figure 17. Melting Point Determination of EC/DMC/EMC 1M LiPF₆ using Environmental Chamber.

To confirm the freezing points, a further experiment was conducted. All nine electrolytes were placed into an environmental chamber and the temperature was set to -10°C. The chamber was then given 2 hours to reach temperature and all the samples were examined. The chamber was then set to -20 °C and the same procedure followed. These steps were repeated in 10 °C intervals until -60 °C. From this experiment a 10 °C freezing range was obtained for all of the samples except the ones which did not freeze at -60 °C. In all cases except one the results of these two experiments were in 100% agreement. Inconsistent data was obtained for the EC/EMC/EA 1M LiPF₆ electrolyte.

Examination of the tabulated data suggests that six of the electrolytes will be in the liquid phase at -40 °C. However, below -50 °C only EC/EMC 1:3 1M LiPF₆ is still totally in solution while the other two samples which are not solid have a precipitate present.

During all freezing/melting point tests, careful observations were made. In some cases a precipitate was always noted and in others, a precipitate was never observed. An intermediate case was the group of electrolytes where a precipitate was noted occasionally. In all cases where a precipitate was present, the solid would re-dissolve after warming to room temperature and sitting overnight. Therefore, even though no precipitation is most advantageous, it appears that even if a precipitate is formed, the solid will re-dissolve.

As with all materials when subjected to wide variations in temperatures, particularly those

involving phase change, electrolytes will expand or contract as a function of temperature. Almost universally, materials expand during heating and contract as temperature decreases. All electrolytes volume expanded when heated to 50 °C and contracted when frozen.

The experimental procedure for the determination of low temperature contraction was as follows. A measured amount of electrolyte was added to a calibrated measuring cylinder and the volume recorded. The cylinder was then slowly cooled in liquid nitrogen until the electrolyte was solid. The volume of the electrolyte was then measured and the amount of contraction was calculated. In a similar fashion, expansion was determined with the same apparatus only the samples were heated to 50 °C. The results of these experiments are given in Table 5.

Table 5. Thermal expansion and contraction of electrolytes heated to 50 °C or frozen in liquid nitrogen.

Electrolyte	% Contraction of liquid to solid phase transition*	% Expansion of sample heated from 25 °C to 50 °C*
EC/EMC 1:3 1M LiPF ₆	20.6	2.5
EC/DEC 1M LiPF ₆	18.3	2.6
EC/DEC/DMC 1M LiPF ₆	29.4	1.7
EC/DMC/EMC 1M LiPF ₆	25.6	2.2
EC/DEC/EMC 1M LiPF ₆	21.9	1.9
EC/DMC/MA 1M LiPF ₆ 40:45:15	10.5	1.6
EC/DMC/EA 1M LiPF ₆ 40:45:15	9.5	2.1
EC/EMC/MA 1M LiPF ₆ 40:45:15	16.6	2.9
EC/EMC/EA 1M LiPF ₆ 40:45:15	15.2	1.6

* Carried out in duplicate

The contraction due to freezing is far greater (9.5% to 29.4%) than the expansion due to heating (1.6% to 2.9%). The results suggest a major concern with respect to electrolyte expansion and contraction lies with the potential damaging effects on the electrodes caused by freezing. This will be addressed empirically in a separate section.

Once the physical characteristics of the electrolytes were determined, three sets of five C cells with 1M LiPF₆ EC/DEC 1:1, or 1M LiPF₆ EC/DEC/DMC 1:1:1, or 1M LiPF₆ EC/EMC 1:3 were assembled and cell resistance and capacity were determined at various temperatures. The resistance was determined by polarization techniques for all five C cells in each group and averaged. The resistance was measured between room temperature and -50 °C. The results from these tests are shown in Figure 18. The resistance of the three electrolytes are quite similar at

room temperature and 0 °C but as temperature decreases the resistance of the cells containing 1M LiPF₆ EC/DEC 1:1 increases very rapidly compared to the other two electrolytes. The resistance of the cells containing 1M LiPF₆ EC/EMC 1:3 or 1M LiPF₆ EC/DMC/DEC 1:1:1 remains almost identical from room temperature to -30 °C.

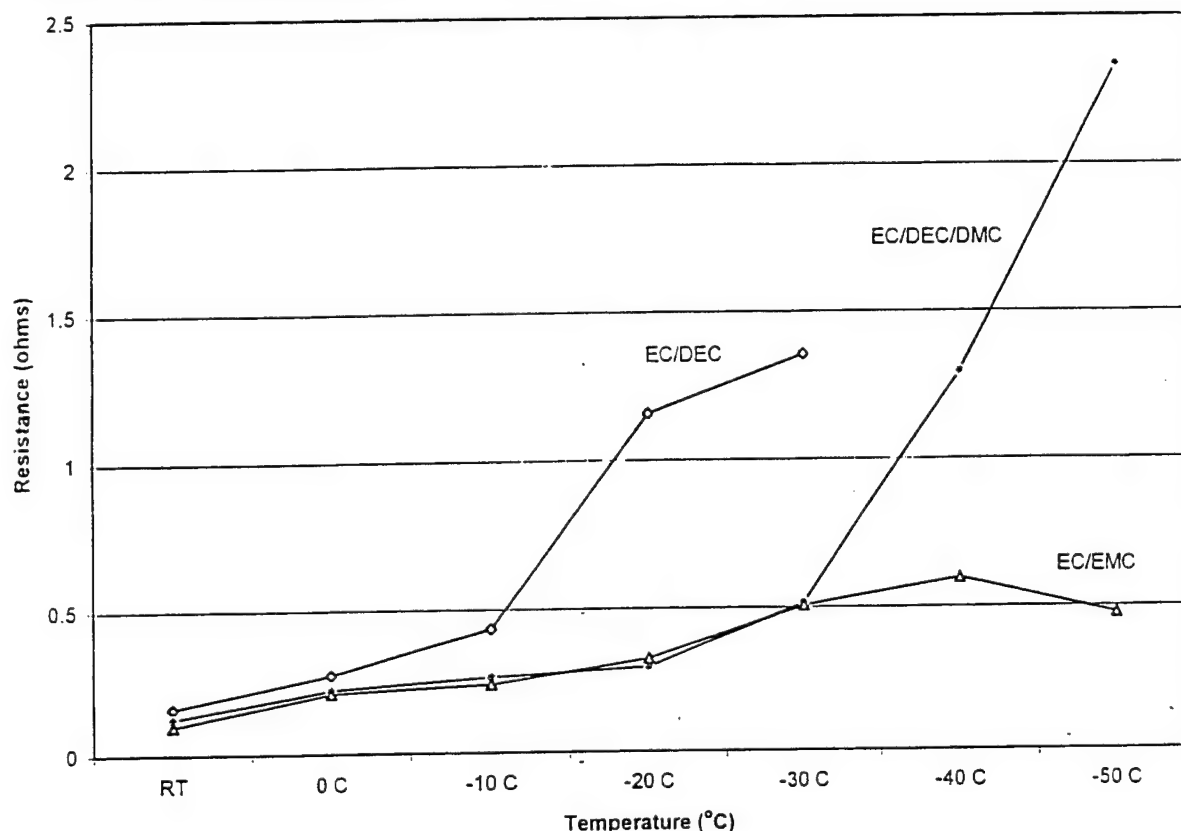


Figure 18. Pulse discharge resistance for C cells using three different electrolytes.

At temperatures below -30 °C, the resistance of the cells filled with 1M LiPF₆ EC/DMC/DEC 1:1:1 increases dramatically while the resistance of the cells filled with 1M LiPF₆ EC/EMC 1:3 goes up only slightly at -40 °C and decreases at -50 °C. The reason for the reduction of cell resistance at the lowest temperature could be due to the electrolyte undergoing supercooling.

Cell resistance will have an influence on cell capacity because charge is terminated based on voltage. But the cell performance is based on capacity and not cell resistance. Therefore, the cell performance for the three electrolytes tested at the C/5 charge and discharge rates at various temperatures is shown in Figure 19. These test results represent the most severe conditions since bare cells were suspended in the environmental chamber. Also, the cells were charged and discharged at the test temperature to realistically model the true conditions of a spacecraft. After every discharge and charge the cells were held for 4 hours at open-circuit to allow the cells to re-equilibrate to temperature. The cells were charged to 4.1V and held at constant voltage for 2.5 hours. At room temperature the capacity of the cells is almost identical for all three electrolytes. However, at 0 °C the cells using the EC/DEC electrolyte have only 80% of the room temperature capacity while the cells using EC/EMC 1:3 or EC/DEC/DMC 1:1:1 have greater than 90% of the room temperature capacity.

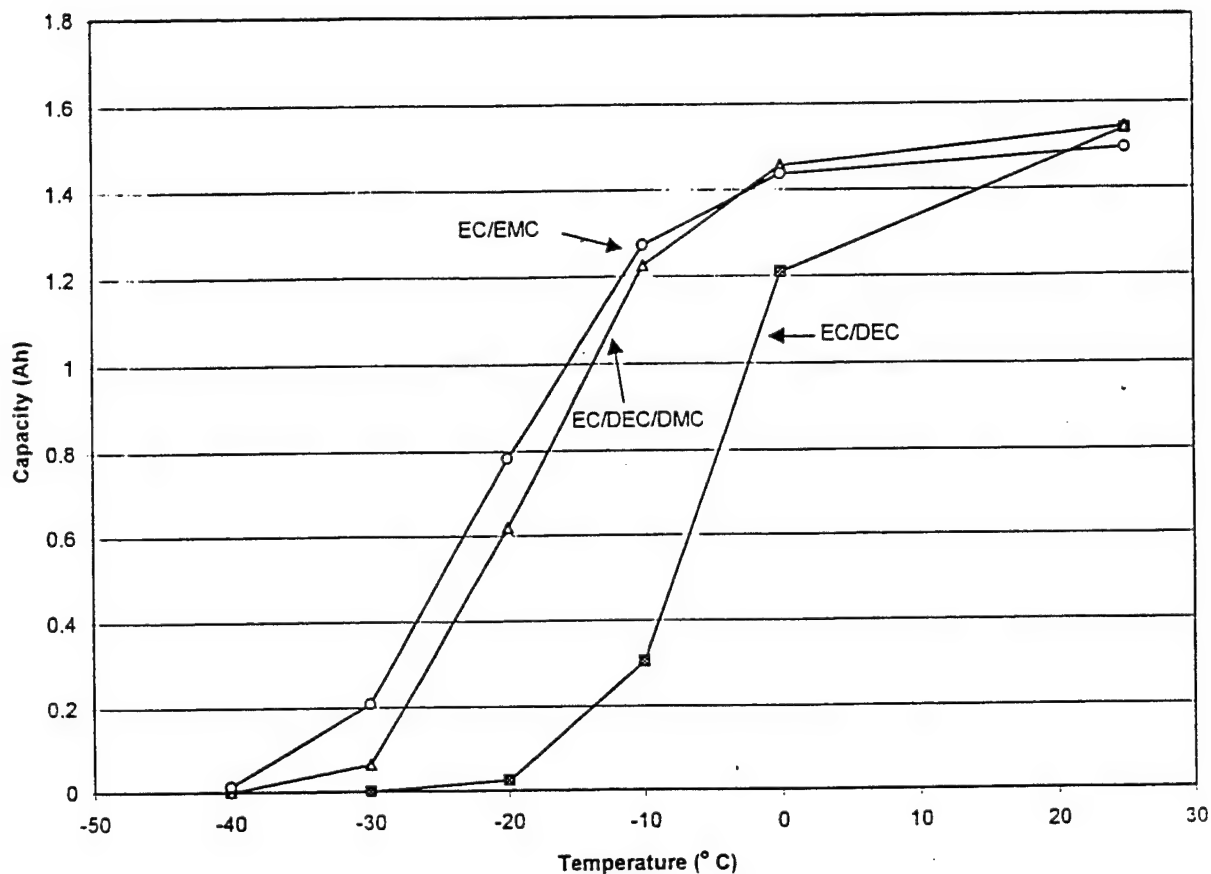


Figure 19. Capacity versus temperature for C cells using three different electrolytes.

At temperatures lower than 0 °C the advantage of the two low temperature electrolytes, 1M LiPF₆ EC/DMC/DEC 1:1:1 and 1M LiPF₆ EC/EMC 1:3 is striking. While the standard BATC electrolyte has zero capacity at -20 °C the 1M LiPF₆ EC/EMC 1:3 electrolyte exhibits 53% at C/5. The capacity under the same conditions for the same electrolyte at the C/2 rate is 38%.

When the cells are used in an application they can be insulated. This will result in improved low temperature performance due to self-heating. The effect of battery packaging is illustrated by tests on an insulated three-cell pack tested at -30 °C with 1M LiPF₆ EC/DMC/DEC 1:1:1 and 1M LiPF₆ EC/EMC 1:3. The graphical representation is shown in Figure 20.

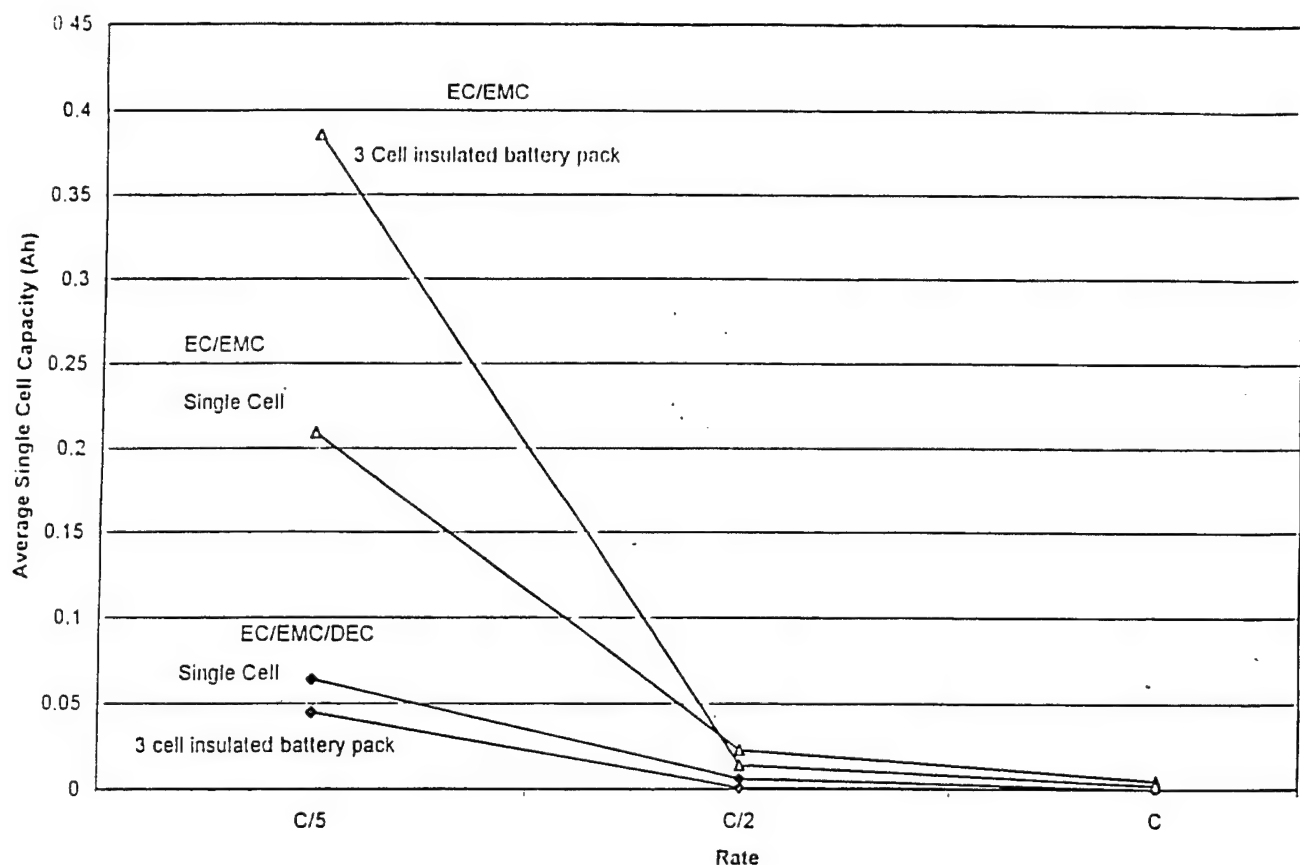


Figure 20. Capacity at -30 °C for three C cell battery packs using two different low temperature electrolytes.

For the cells/battery with the EC/DEC/DMC electrolyte the capacity at was greater for the single cell than the three-cell pack -30 °C, but the capacity in both cases was quite small and so the result is not significant. For the cells with 1M LiPF₆ EC/EMC 1:3, the three-cell pack had almost twice the capacity as the single cell. Even though the capacity is only 25% of the room temperature capacity at the C/5 rate, the test temperature was -30 °C. Test results were more dramatic when DD cells were tested instead of C cells. The capacity of a bare DD cell at C/5 and C/2 is basically

the same as a bare C cell at -30 °C. When three DD cells were placed into an insulated pack, the capacity at -30 °C at the C/5 rate was 40% of the room temperature capacity. At the C/2 rate the effect of self-heating or "boot strapping" is illustrated by the capacity being greater than 50% of the room temperature capacity. The results from the DD pack tests are shown in Figure 21.

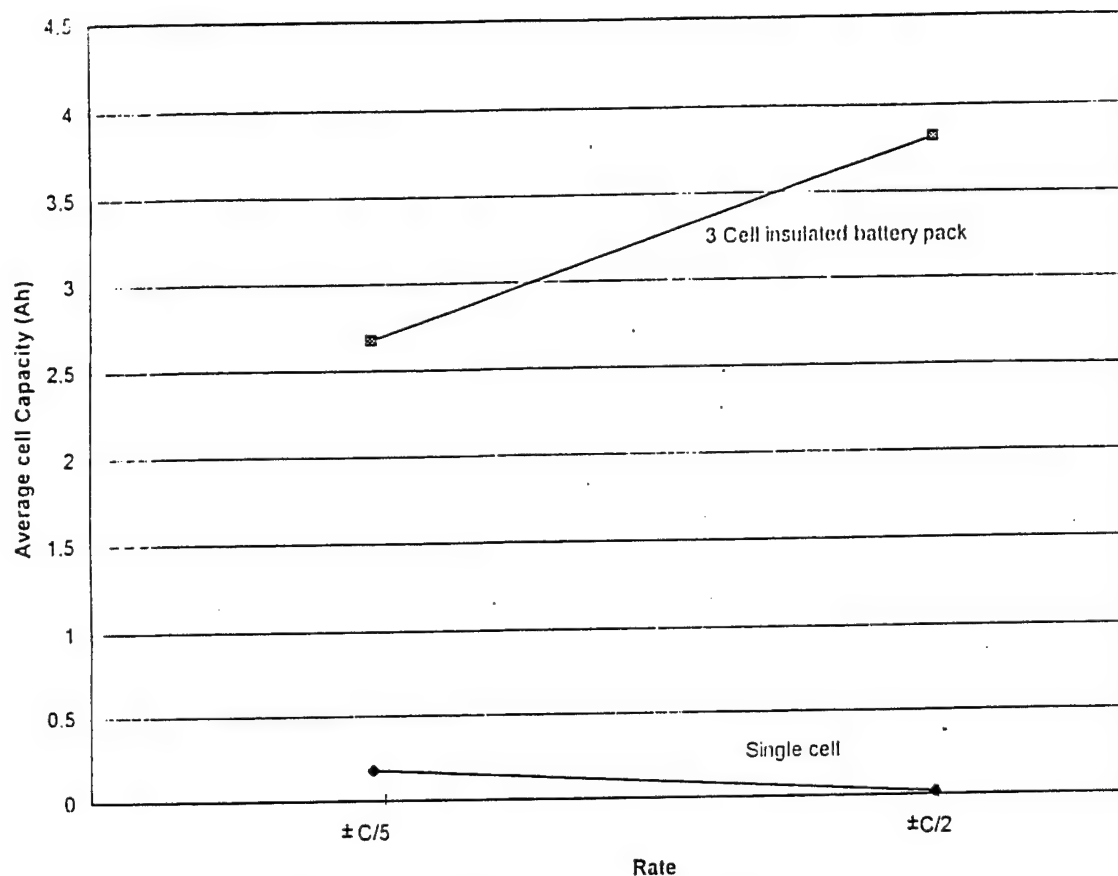


Figure 21. Capacity of three DD cell battery packs at -30 °C.

Cell survivability at ultra-low temperatures is of interest for planetary exploration. For example the temperature specifications for the Lunar Polar Rover is 50 K (-223 °C). The cells do not have to operate at this temperature but the hardware must be able to survive with no rupture of the cell casing or glass to metal seal (GTM). Initially, three C cells with different electrolytes (EC/DEC 1:1 1M LiPF₆, EC/DEC/DMC 1:1:1 1M LiPF₆ and EC/EMC 1:3 1M LiPF₆) were selected for survivability tests. All the cells were weighed before and after each experiment to determine if any loss of electrolyte had occurred. In the first test the cells were immersed in liquid nitrogen (77 K) for 1.25 hours. The cells were then allowed to equilibrate to room temperature (48 hours). All welds, vent and the GTM's were examined and no evidence of leaking or any cracks were observed. The structural integrity of the cells was confirmed by the cell weights being consistent before and after the test. As a further test, the cells were again frozen in liquid nitrogen for 16 hours and the same equilibration and examination procedure were carried out with identical results.

Liquid helium was used as a coolant in the third test. In this case four C cells were selected: three used previously and one control cell for destructive physical analysis (DPA). Liquid helium was chosen because it is readily available and has a boiling point below 50 K. The four C cells were cooled in liquid nitrogen before being placed into a Dewar with a K type thermocouple. Liquid helium was then layered over the cells for 20 minutes. The temperature was monitored by a thermocouple showing the temperature stabilized at -250 °C (23 K). The Dewar was then covered and placed into an insulated tub. The apparatus kept the temperature at 23 K for 6 hours.

The cells were then allowed to equilibrate to room temperature for 90 hours and examined as previously outlined. No evidence of cell structural failure was observed.

One cell in the group frozen at 23 K was then examined via DPA and the electrodes compared to a cell which had not been treated at ultra-low temperature. In both cases the positive electrode was in excellent condition showing no signs of delamination. However, the material on the negative electrodes was delaminating from the current collector. The negative electrode of the cell exposed to liquid helium appeared to be in worse shape than the cell not exposed to ultra-low temperatures. However, this was a subjective examination and the differences could easily be associated with cell to cell variation.

Survivability of cell hardware is important but the cells must also be able to perform after extreme conditions. For all the ultra-low temperature tests the cells were fully charged before and during ultra-low temperature exposure. After the cells equilibrated to room temperature, the cells were discharged. The results of these tests are tabulated in Table 6.

Table 6. Discharge performance of C cells after ultra-low temperature tests.

Electrolyte	Capacity After 1.25h at -196 °C	Capacity Retention After Freezing	Discharge Capacity After 16h at -196 °C	Capacity Retention After Freezing	Capacity After 6h at -250 °C	Capacity Retention After Freezing
EC/EMC 1M LiPF ₆	1.109 Ah	96.4%	1.126 Ah	99.2%	1.068 Ah	97.4%
EC/DEC 1M LiPF ₆	1.278 Ah	94.1%	1.289 Ah	98.9%	1.232 Ah	98.0%
EC/DEC/ DMC 1M LiPF ₆	1.083 Ah	95.7%	1.097 Ah	98.8%	1.050 Ah	99.3%

In all cases the cells retained their capacity. There does not appear to be any detrimental effects on cell performance after the ultra-low temperature tests.

After the ultra-low temperature tests the cells were returned to cycle life testing. The results of one of these cells is shown in Figure 22. As can be seen the cells are still capable of cycling.

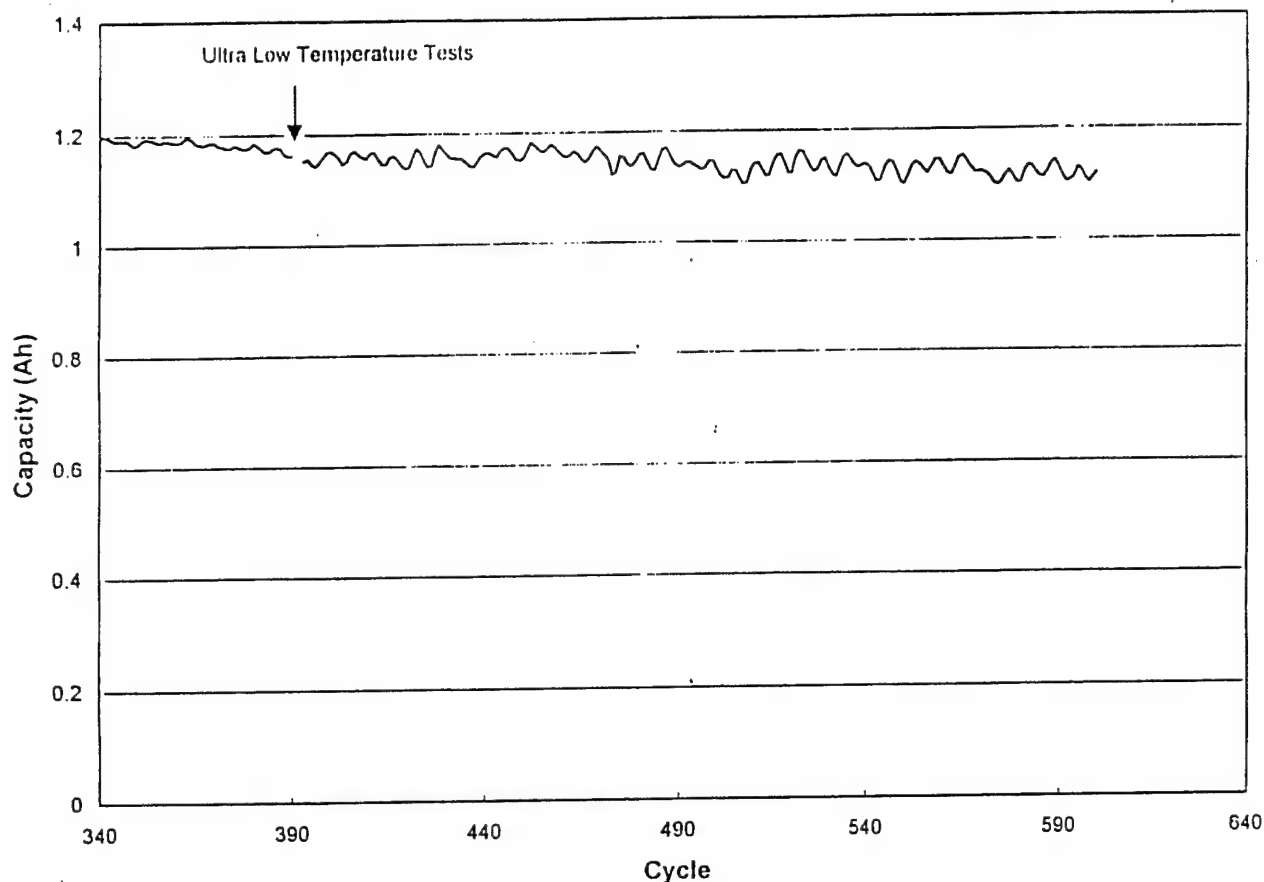


Figure 22. Cell capacity after exposure to ultra-low temperatures 1M LiPF₆ EC/EMC 1:3.

2.1.5 Task 1.5. Status Cells

It is necessary to periodically establish performance benchmarks to determine the present state of the technology and to ensure that the technology is moving forward. To establish bench marks a series of Status Cells were prepared. Over the course of the program five sets of cells were prepared. Initially, 30 C cells were prepared for the Generation I, II and III with current processes and materials. The first set of cells, designated Generation I, was initiated August 1996. A test matrix in which both charge rate and depth of discharge were varied. After the formation cycles, 5 cells in each group were cycled according to the following conditions:

- o C/5 charge, C/2 discharge to 60%, 75% and 90% depth of discharge
- o C/2 charge, C/2 discharge to 60%, 75% and 90% depth of discharge

After the first three generations of cells it was observed that there was no difference between the cells charged at C/5 and C/2 rate; therefore, the next two sets of Status Cells consisted of 15 C cells tested at C/2 for both charge and discharge. The materials and processes used in the fabrication of the electrodes are outlined in Table 7.

Table 7. Status Cells general characteristics.

Generation	Positive Electrode	Negative Electrode	Date Initiated	Comments
1	Honjo LiCoO ₂ Manual methods	SFG 15 Graphite Manual methods	30 July 1996	Completed
2	Honjo LiCoO ₂ Semi-automated methods	LK-702 Graphite Semi-automated methods	15 January 1997	Positive electrodes dried at 200°C for 6 weeks - poor efficiencies, low capacities, terminated.
3	Honjo LiCoO ₂ Semi-automated methods	LK-702 Graphite Semi-automated methods	30 January 1997	Completed
4	Honjo LiCoO ₂ Semi-automated methods	LK-702 Graphite Semi-automated methods	15 August 1997	Test in progress
5	Honjo LiCoO ₂ Semi-automated methods	MCMB Semi-automated methods	20 August 1997	Test in progress

Status Cells were evaluated by two different measures. Since the cells were not tested at 100%, the first measure of performance was the onset of capacity loss. The second performance criterion was end of life, defined as the cycle number where the capacity of the cell fell below 75% of initial capacity. The performance of the Generation I Status Cells is shown in Table 8. There does not appear to be any difference in performance at the two different charge rates. The electrodes for the Generation II Status cells were prepared before Christmas 1996 and placed into the 200 °C drying ovens over the holidays. The performance of the cells was very poor. This was attributed to binder decomposition at elevated temperature. The next set of Status cells were prepared as a replacement of the Generation II cells. The results from the Generation III Status Cells are shown in Table 9.

Table 8. Performance characteristics of Generation I Status Cell.

Charge Rate	Discharge Rate	Depth of Discharge	Onset of Capacity Loss (cycle #)	End of Life 75% _{init} (cycle#)
C/5	C/2	90	150	247
		75	425	425
		60	600	N/A
C/2	C/2	90	160	245
		75	425	425
		60	550	N/A

Table 9. Performance characteristics of Generation III Status Cells.

Charge Rate	Discharge Rate	Depth of Discharge	Onset of Capacity Loss (cycle#)	End of Life 75% _{init} (cycle#)
C/5	C/2	90	40	259
		75	420	420
		60	1375	N/A
C/2	C/2	90	65	343
		75	415	415
		60	1400	N/A

A comparison of Generation I to III shows a sooner onset of capacity loss observed for the 90% dod of Generation III. However, the end of life for both sets of Status Cells at 90% dod is identical. Therefore, Generation III Status Cells have a steeper initial capacity fade which then fades at a slower rate from 90% to the end of life. The cells tested at 75% dod for both

Generation I and III showed identical results. And finally, the cells tested at 60% dod continued the trend with the Generation III Status Cells performing better than the Generation I Status Cells. The onset of capacity loss for Generation III occurred near 1400 cycles as opposed to 600 cycles for Generation I. The results for the Generation III Status Cells are shown in Figure 23.

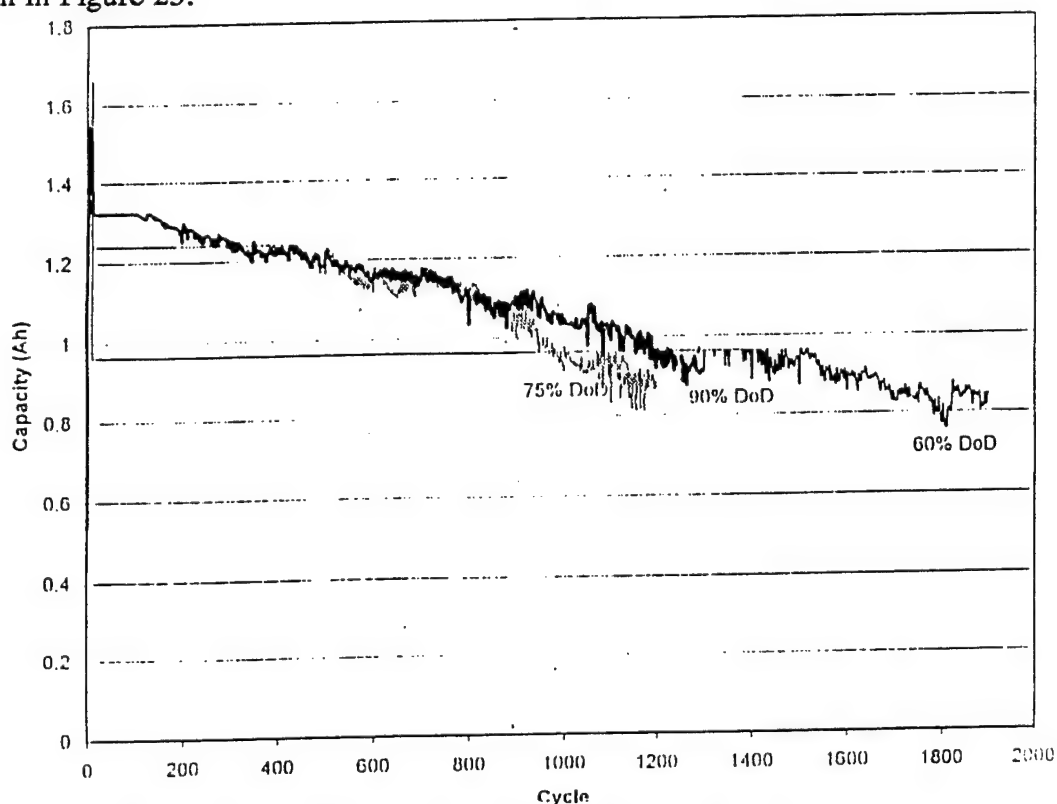


Figure 23. Generation III Status Cells cycle life data, C/2 rate.

The next two sets of Status Cells, Generation IV and V, were made in identical fashion to Generation III. The only difference between these sets of cells was that the negative electrodes were made from LK-702 for Generation IV and from MCMB for Generation V. The test summary for Generation I through V for the C/2 rates are shown in Table 10. The most important observation from these data is the change from manual methods to automated methods and a change in the active carbon material. The comparison between Generation I and III and IV is the most. Generation IV shows superior performance over Generation I and III in both onset of capacity loss and end of life for all depths of discharge. This demonstrates that even with changes in processes, materials and time, performance is improving. The Generation V cells, which used an MCMB negative electrode, exhibited inferior performance to the Generation IV cells which were assembled simultaneously. However, the MCMB cells are performing almost identically to the Generation III cells which used an LK-702 negative electrode. This suggests that more process refinement with MCMB may result in similar performance compared to LK-702. The performance of a typical Generation IV cell at the three dods are shown in Figure 24. These graphs show that dod does not seem to influence

Table 10. Performance data for Generation I to V Status Cells.

Generation	Charge Rate	Discharge Rate	Depth of Discharge	Onset of Capacity Loss (cycle#)	End of Life 75% _{Init} (cycle#)
I	C/2	C/2	90	160	245
			75	425	425
			60	550	N/A
III	C/2	C/2	90	65	343
			75	415	415
			60	1400	N/A
IV	C/2	C/2	90	210	485
			75	633	633
			60	not observed after 1340	N/A
V	C/2	C/2	90	59	359
			75	485	485
			60	1375	N/A

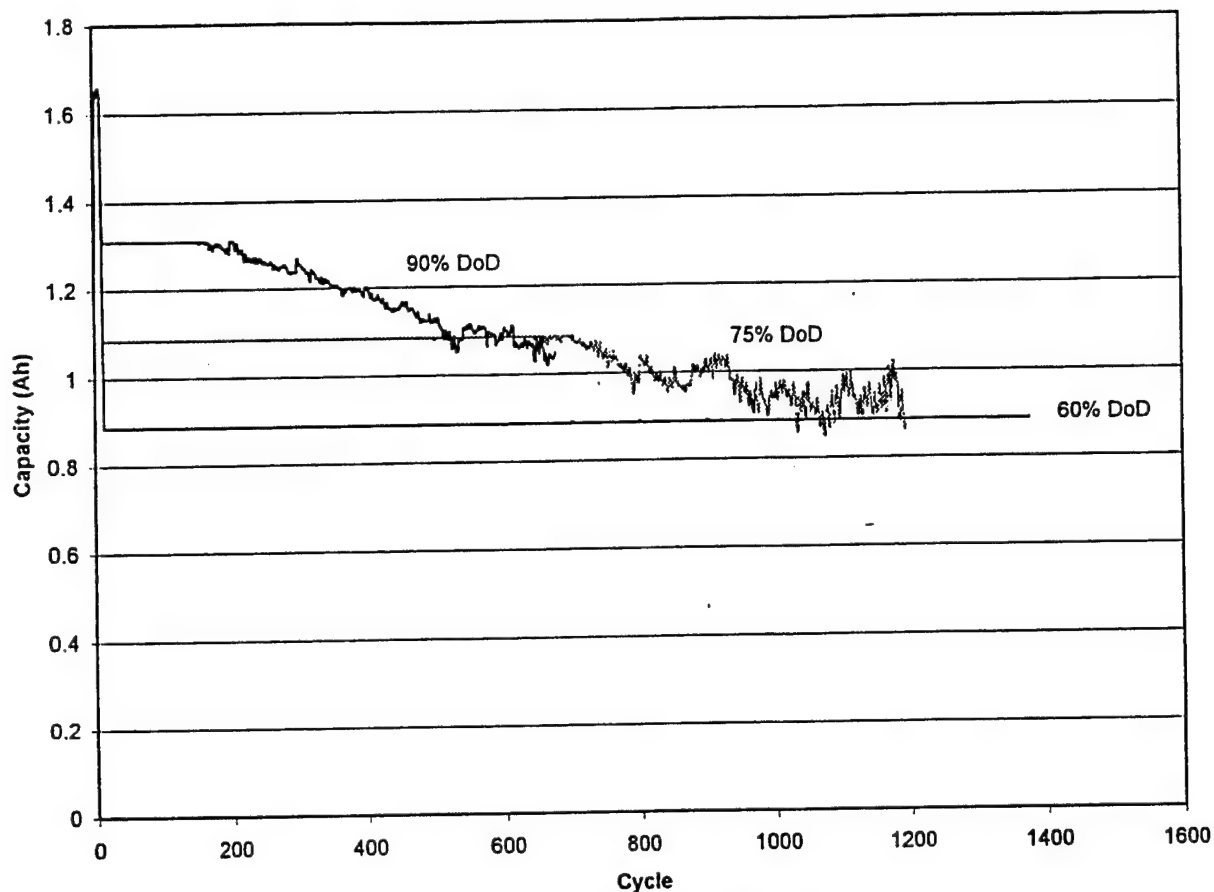


Figure 24. Generation IV Status Cells cycle life data, C/2 rate.

the end of life since the 90% dod data almost overlays the 75% dod data. The 60% dod lasts longer than expected but the 75% has a very slow fade in capacity after 1000 cycles as well. A graph which compares the 90% dod for Generation III, IV and V is shown in Figure 25. The earlier onset of fade in capacity for generation III and V is quite evident. However, the rate of capacity fade does not differ much between the three generations of cells. Therefore, the key is to delay the onset of capacity loss as long as possible.

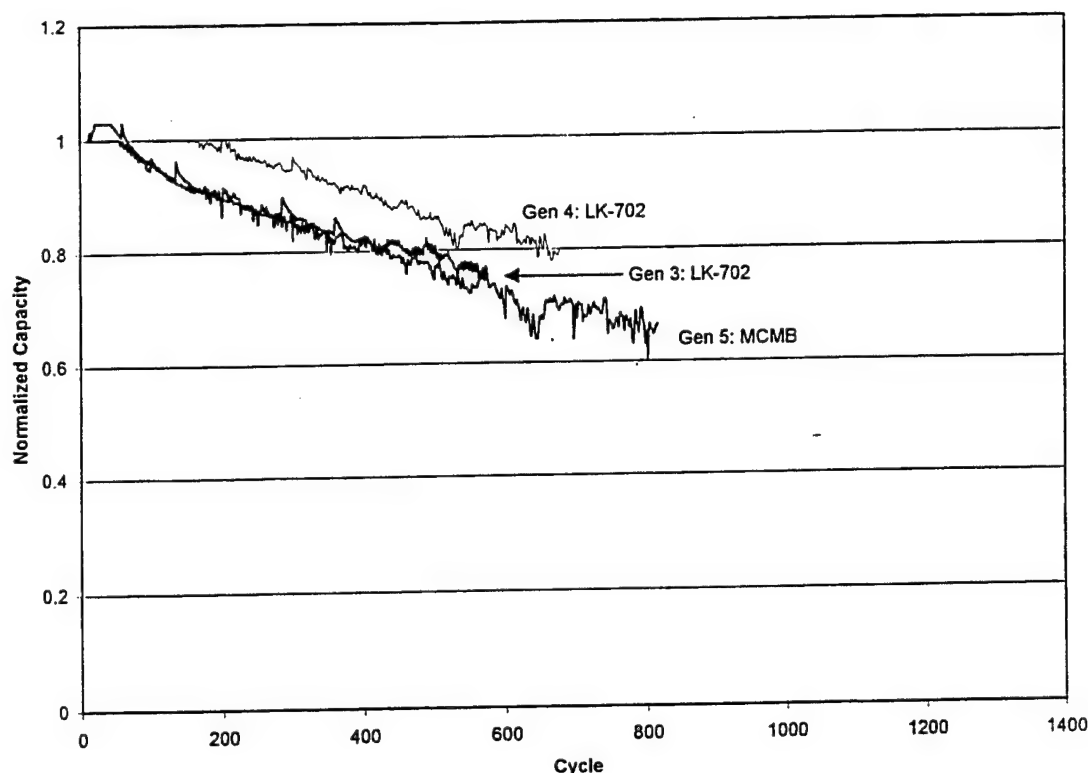


Figure 25. Generations III, IV and V at 90% dod.

2.2 Task 2.0. Evaluate Cell Fabrication Techniques

Cell and component fabrication techniques are quite important in lithium ion chemistry as cell performance is strongly dependent on the electrode processing. It is also necessary to process significant quantities of electrode material for a single cell due to the very thin nature of the positive and negative electrode material coatings. The loading of typical electrodes is of the order of 4 mAh/cm², implying that a 20-Ah cell will require 5000 cm² of both positive and negative electrode material. A second aspect of this peculiarity of lithium ion cells is the electrode pack. The design is complicated by the large areas of electrode material required which requires that particular attention be given to the actual design of the active element. Tab design and design for manufacturability are obvious areas of concern. The most efficient design of large cells may well be a prismatic design in which case alternatives to conventional wound design must be developed. These aspects of cell design are addressed as part of this task.

2.2.1 Task 2.1 Improve Electrode Fabrication Processes

Improvements for both positive and negative electrode showed a large increase when the new processing equipment was purchased in the fall of 1996. Since then, refinement in processing and variability have occurred, as discussed in the following sections on cell performance.

2.2.2 Task 2.2. Evaluate Alternative Electrode Configurations

The large electrode areas required by lithium ion cells, as they are presently designed, complicates the design of the cell pack. The most straightforward approach for electrodes of this type is simply scaling up the wound cylindrical approach to cell design used for the small cells used in portable electronics. The deficiencies of this approach are: packaging inefficiency (only 78.55% of a given rectangular volume is used by an inscribed cylinder); thermal management concerns in larger cell sizes; and current collection, which relies on a single tab and a current collection path which traverses the entire length of the rather long foil electrode. Activities during the program focussed the pseudo-elliptical approach.

The conventional approach to the design of prismatic electrochemical cells is based on the stacking of multiple, independently tabbed, rectangular electrode plates. Such an approach, although possible for the thinly coated foil electrodes typical of Li ion technology, is complicated by the need to collect a large number of very thin tabs for contact to the external feed-through. An alternative is to employ continuous electrode creases resulting in non-uniform stack pressure which leads to poor electrical performance. BATC explored various folded configurations and found them to be feasible but undesirable, particularly from the standpoints of performance and manufacturability. As a potential solution of this problem, BlueStar explored a wound elliptical approach, which offers packaging efficiencies approaching those of a true prismatic cell but which also offer the simple tab design and manufacturability of the cylindrical wound approach. BATC analyzed this concept and found that packing efficiencies of 90% or greater may be achieved, the design to be readily manufacturable, and the product to offer the predicted performance.

The theoretical limits of this approach may be readily established by consideration of Figure 26 which shows a pseudo-elliptical wound element enclosed in a rectangular package of dimensions $a \times b \times c$ where $a > b > c$. The volume of the pseudo-elliptical element is the sum of the rectangular elements $([\alpha \times c]b)$, where $\alpha = a - c$ minus its center void $(\alpha \times \beta \times b)$ plus the volume of this cylindrical element $(\pi c^2 b / 4)$. The packing efficiency (fp) may be expressed as the ratio of their cross-sectional areas. Symbolically then

$$fp = \{(\alpha c - \alpha \beta) + (c/2)^2 \pi\} / ac \quad (1)$$

which when simplified results in

$$fp = 1 - 0.22(c/a) - \beta(1/c - 1/a) \quad (2)$$

For the cases in which $a \gg c$ this may be further simplified to

$$fp = 1 - 0.22(c/a) - \beta/c \quad (3)$$

In this simplified approximated form, these are useful parameters as (c/a) represents the cross-sectional aspect ratio of the cell and β/c represents a fractional expression for the center void volume as shown in Figure 26. Packing efficiency calculated according to (3) as a function of these parameters is shown in Figure 27. Several interesting observations are possible based on equations (1) and (2) and the results shown in Figure 27. These are:

- i) It is comforting to note that as β/c goes to 0 and as a/c goes to infinity, f_p approaches 1 and that as c goes to a and β to 0, f_p goes to $\pi/4$; both of which are the intuitive limits.
- ii) Packing efficiency begins to approach an asymptotic limit as the length-to-width ratio reaches values of 3 - 4.
- iii) The asymptotic limit is established by the value of the void volume
- iv) Packing efficiencies > 90% are achieved when $a/c > 5.0$ and $\beta/c < 0.05$

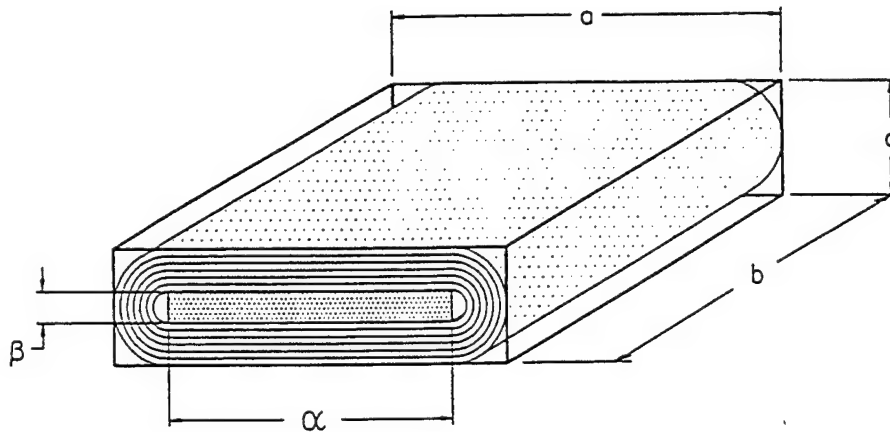


Figure 26. Model of pseudo-elliptical wound element.

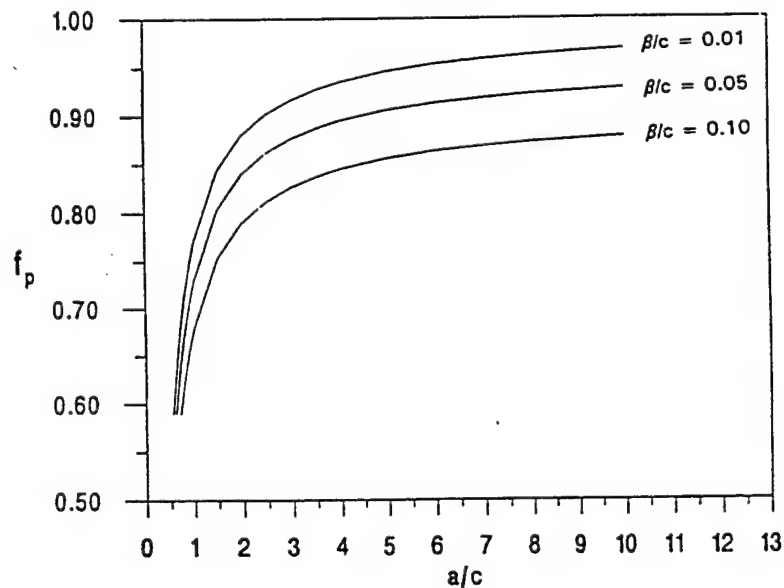
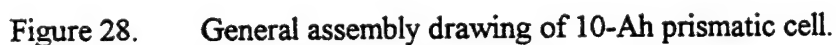


Figure 27. Packing efficiency as a function of the geometry of the pseudo-elliptical wound element.

- o Standard GTM seals, fill tube and 235 psi rupture disc, 0.3125" ϕ welded into cap
- o Electrode dimensions
 - Positive electrode 6.5 x 416 x 0.017 cm
 - Negative electrode 6.8 x 422 x 0.011 cm
- o Performance
 - 10.75 Ah, 75.6 Wh/kg, 177 Wh/l
 - 639 cycles, 100% dod at C/2 to 75% of initial capacity
 - 1000 cycles to 61% of initial capacity, terminated after 1100 cycles



The cell was formed for 10 cycles as with the Status Cells and then a capacity test was used to determine performance. The cell was then placed on test. The test regime was C/2 charge to 4.1V followed by a 1.5 hour constant voltage charge (CVC) hold at 4.1V and then discharged to 3.0V at a rate of C/2. The history for the cell tested the most extensively is shown in Figure 29.

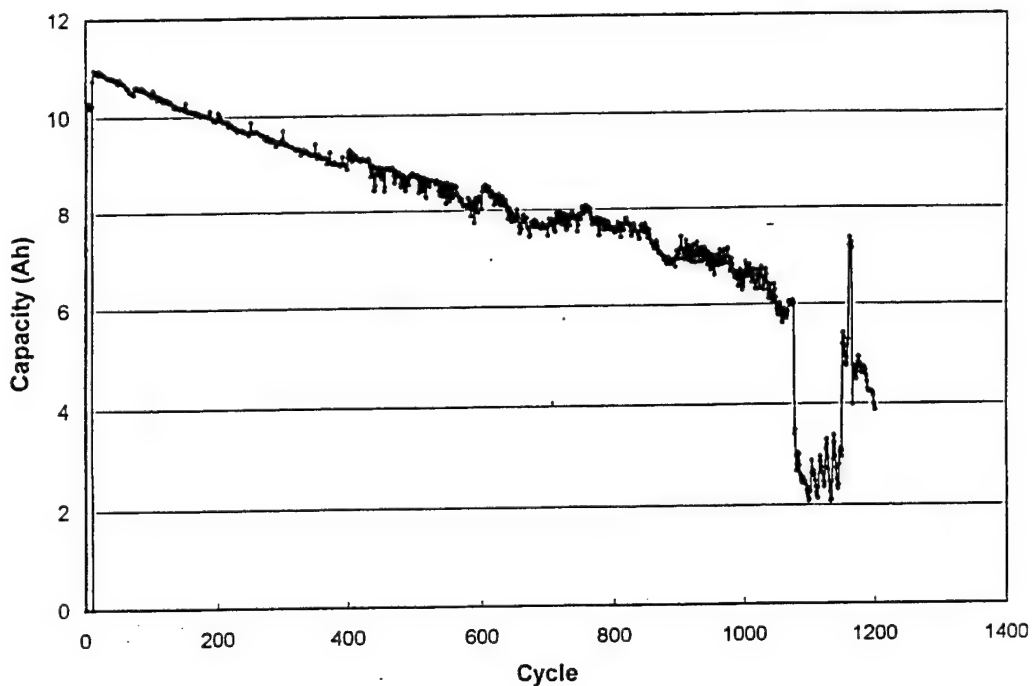


Figure 29. Cycle life of 10-Ah prismatic cell.

As seen in Figure 29, the fade in capacity is very linear until cycle approximately 1050, after which the cell capacity dropped dramatically and any attempt to rejuvenate the cell failed. The resistance of the cell was also measured by dc polarization techniques for the life time of the cell. These results are shown in Table 11. The resistance results are illustrated in Figure 30. As seen from the data, the resistance increases by 70% from cycle 20 to 1000 while the capacity has diminishes by 40%. Therefore, the decrease in capacity is partially due to the increase in resistance but there are other irreversible capacity losses. The importance of the constant voltage charge regime used for lithium ion cells is illustrated in Figure 31. Figure 31 shows that as the cell cycled the amount of charge the cell took during the constant current segment of the charge regime gradually decreased from 92% to 75% from cycle 11 to cycle 400. This is mostly a result of the increase in resistance, which will result in the cell reaching the voltage cut-off earlier. The consequence of the increase in resistance is that the end of charge voltage limit is reached before the cell is totally charged. This is partially compensated by the constant voltage charge portion of the charge cycle since the contribution increases from 8% to 25%.

Table 11. Cell cycling history for 10-Ah wound prismatic cell.

Cycle #	Capacity (Ah)	Capacity as % of Initial	Resistance (ohm)
20	10.75	100	0.0415
100	10.43	97.0	0.0508
200	9.93	92.4	0.0611
300	9.54	88.7	0.0655
400	9.14	85.0	0.0655
500	8.73	81.2	0.0687
600	8.03	74.7	0.0656
700	7.58	70.5	0.0696
800	7.50	69.8	0.0656
900	7.18	66.8	0.0627
1000	6.53	60.7	0.0705

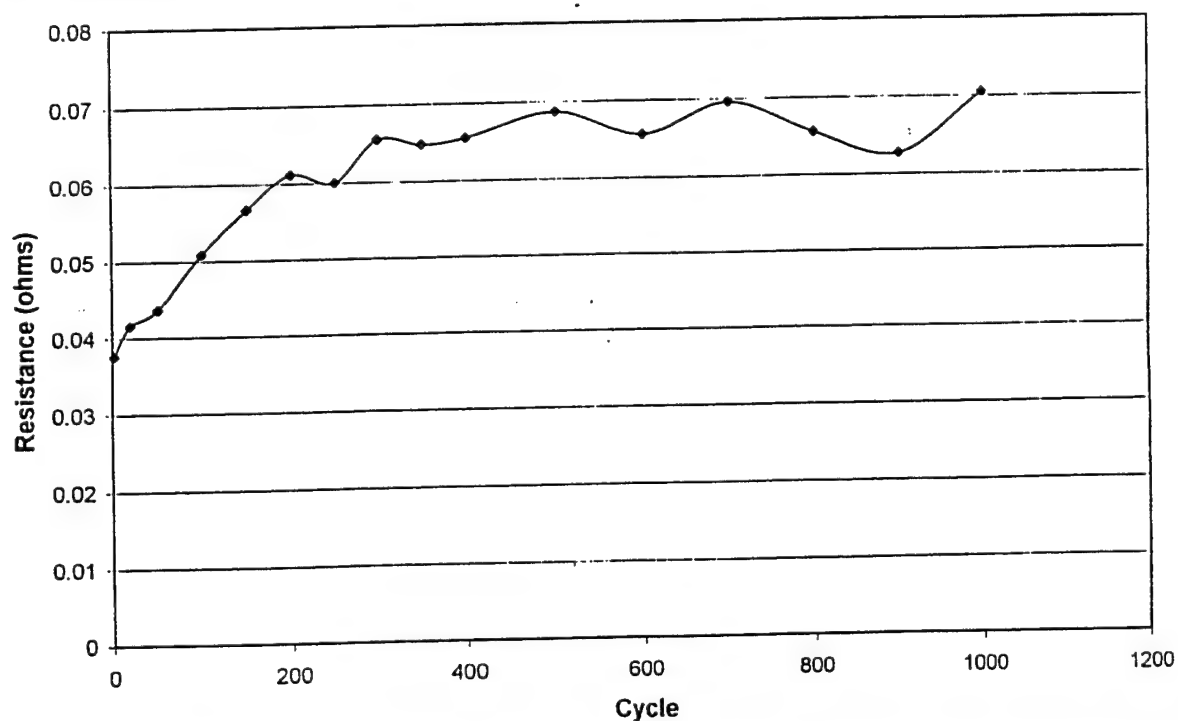


Figure 30. Pulse discharge resistance as a function of cycle number for the 10-Ah prismatic cell.

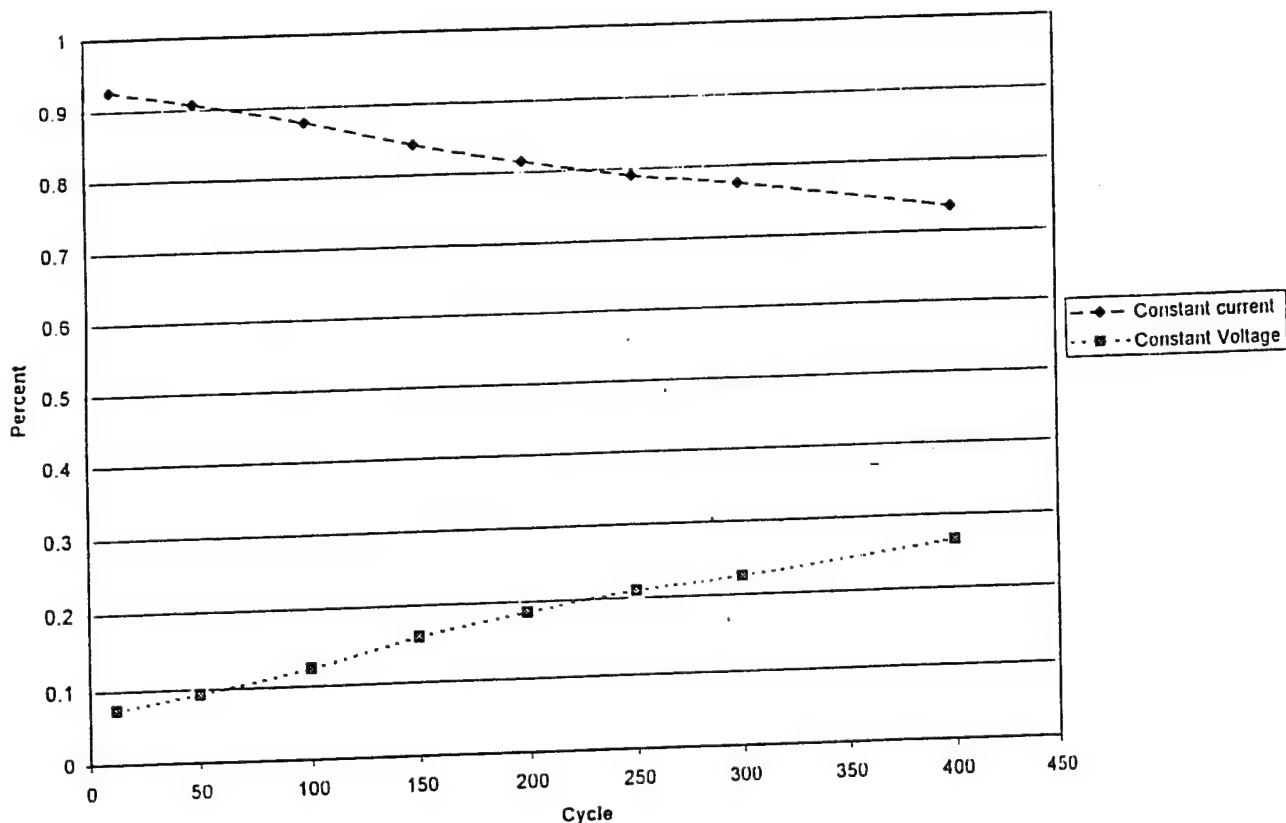


Figure 31. Contribution to total charge capacity of the constant current and constant charge portions of the charge half-cycle.

One advantage of a cell design which uses two feed-throughs is that the cell case can be used as a reference electrode. In the case of the 10-Ah prismatic cell the negative electrode and positive electrode were working electrodes. The reference electrode was measured against the negative electrode and the reference electrode versus positive electrode was calculated. Figure 32 shows the discharge curves of cycles 12, 25, 50, 100, 150, 199, 250, 300 and 400 of the two working electrodes. In Figure 32 the gradual fade in capacity is readily observed. As cycle number increases the time to reach the charge voltage limit diminishes and therefore the discharge capacity slowly decreases. However, this does not tell the complete story since the capacity of the cell is determined by the charge which is comprised of two parts, the first being constant current and the second constant voltage. Figure 33 shows the potential of the reference electrode versus the negative electrode and Figure 34 uses calculation to give the curves of reference versus the positive electrode. In contrast no trend is apparent in the graphs of the negative electrode versus reference. This implies that the negative electrode is not decaying in any dramatic fashion due the similar voltage profiles of the cycles. Figure 34 which is positive electrode versus reference electrode, shows similar profiles as discussed for Figure 33. One explanation for the gradual loss in cell capacity is the slow increase in cell resistance as outlined previously. Even though the increase in resistance is a factor in capacity fade it is not the only factor. This accompanied with the three electrode data suggests that the gradual fade in capacity must be at least partially due to the loss of lithium.

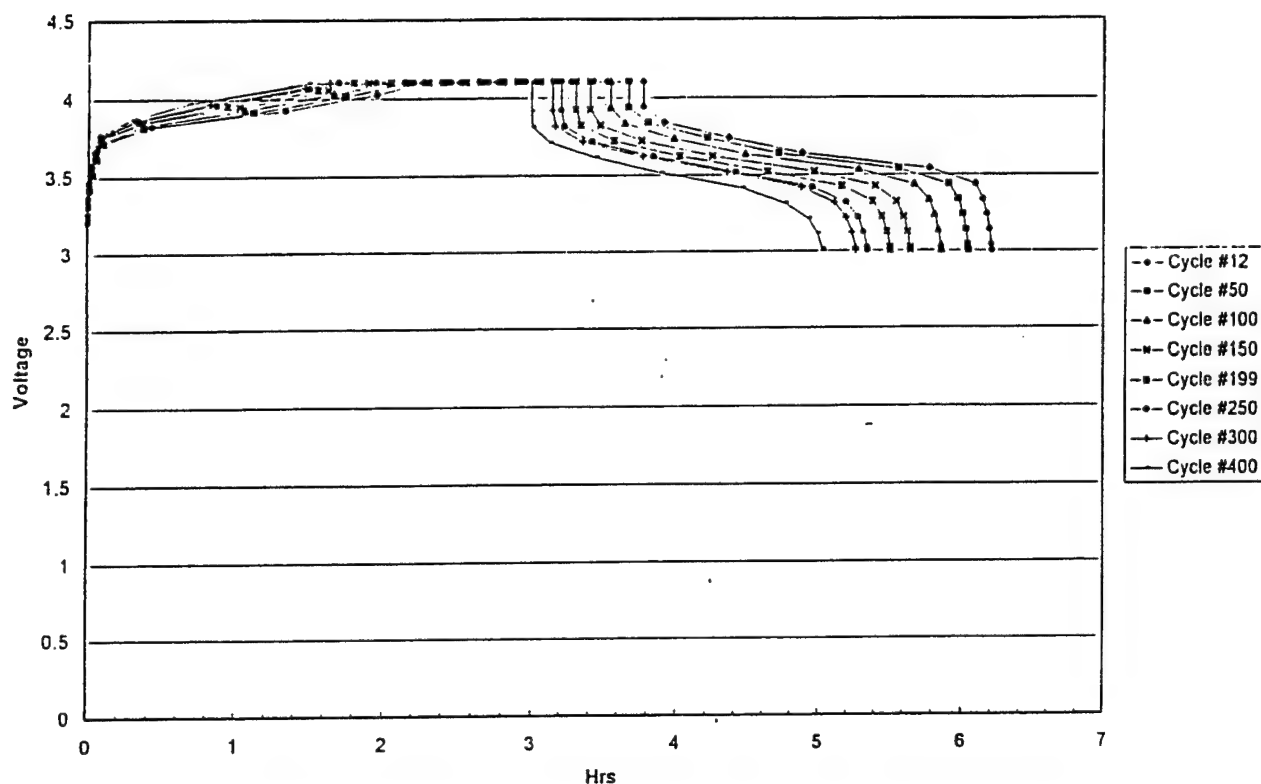


Figure 32. Charge-discharge for 10-Ah prismatic cell LiCoO₂ versus graphite.

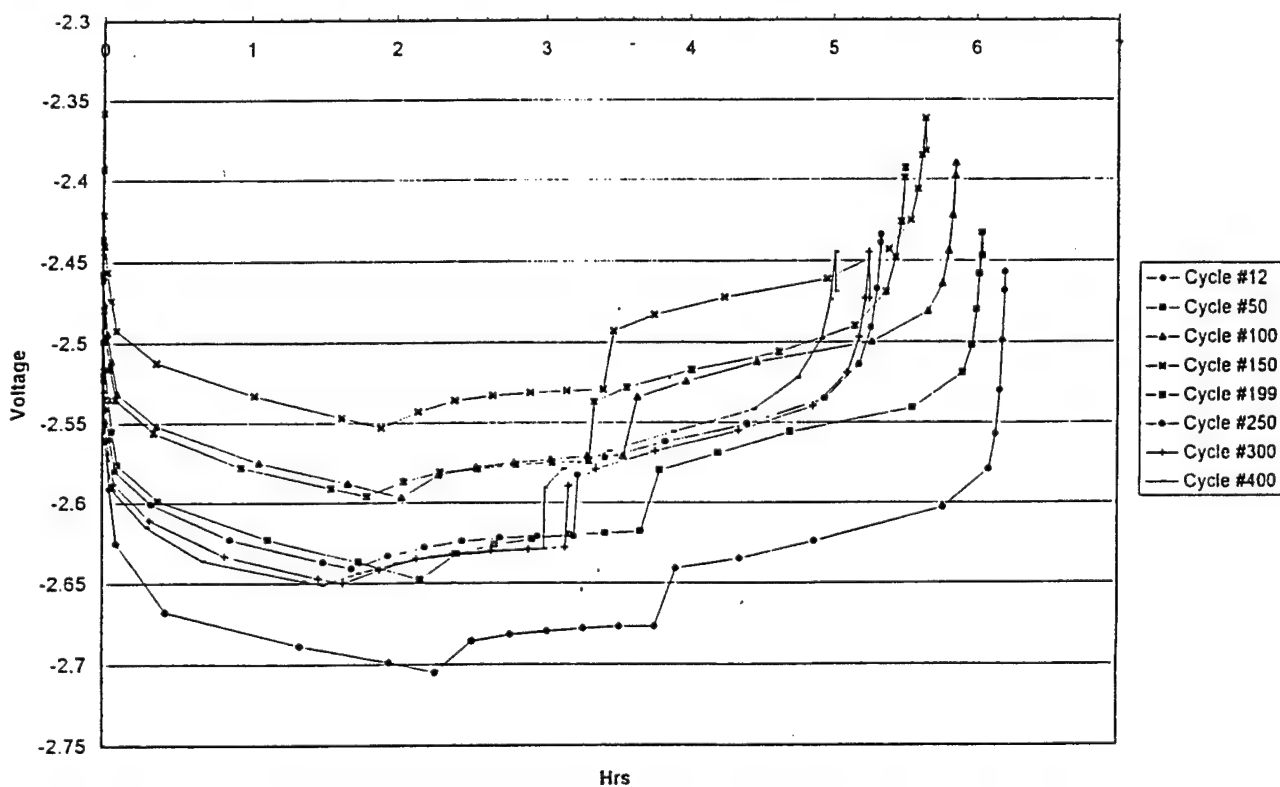


Figure 33. Charge-discharge voltage for 10-Ah prismatic cell negative electrode versus case.

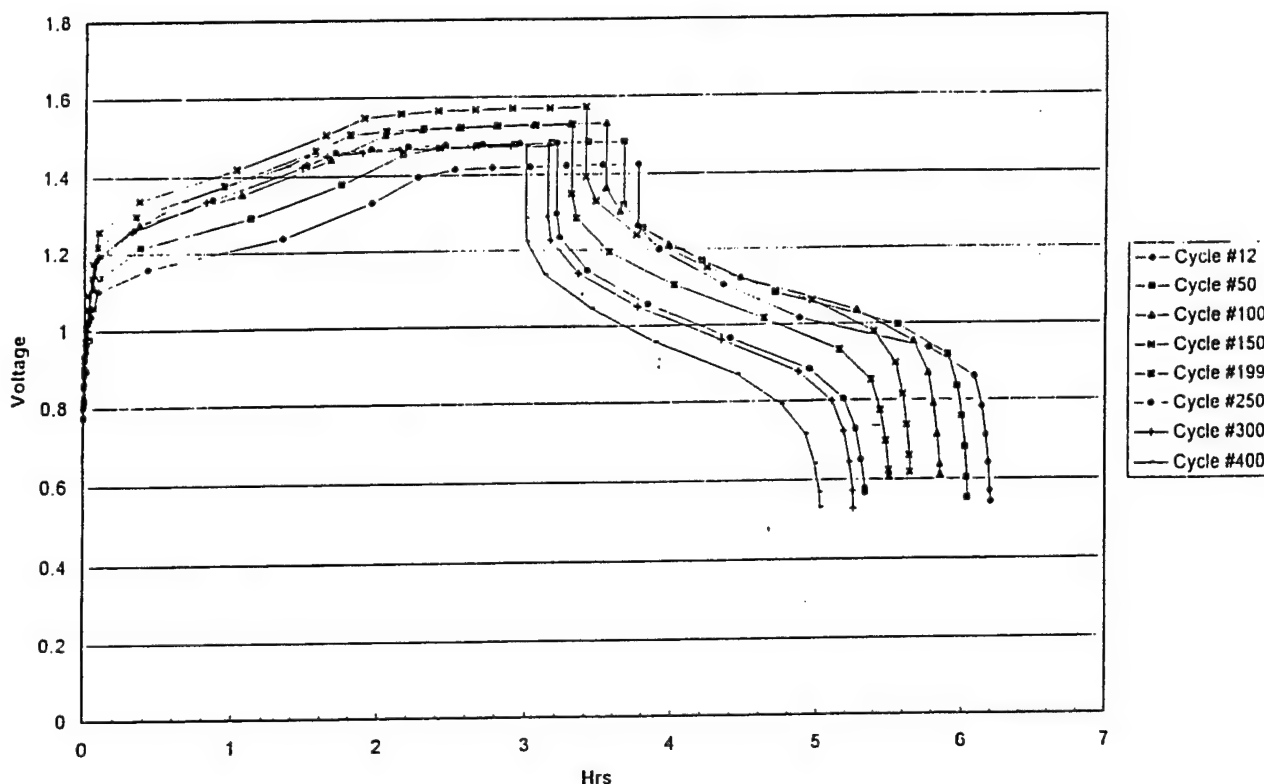


Figure 34. Charge-discharge voltage for 10-Ah prismatic cell positive electrode versus case.

2.3 Task 3.0. 20-Ah Prismatic Cell Development

The objective of this task was to accomplish the first stage of cell scale-up and compare the design to a 20-Ah cylindrical cell. The design for the prismatic cell was based on calculations of the packing efficiency outlined in the previous section. In order to achieve a packing efficiency greater than 90% the a/c ratio was set equal to 5. In order to have maximum freedom in size and shape, a welded case was designed instead of a drawn case. The characteristics of the first iteration of this design are shown below:

- o GTM pins were 0.090" ϕ Mo, standard SO₂ hardware
- o Fill tube standard SO₂ hardware, rupture disc 0.3125", ϕ opening at 235 psi
- o Case 0.030" welded enclosure
- o 2.69 x 12.9 x 10.9 cm
- o Electrode dimensions
 - Positive electrode 600 x 8.80 x 0.017cm
 - Negative electrode 630 x 9.10 x 0.011 cm
- o Performance
 - 82.2 Wh/kg, 197 Wh/l

The general assembly drawing for the first design iteration is shown in Figure 35.

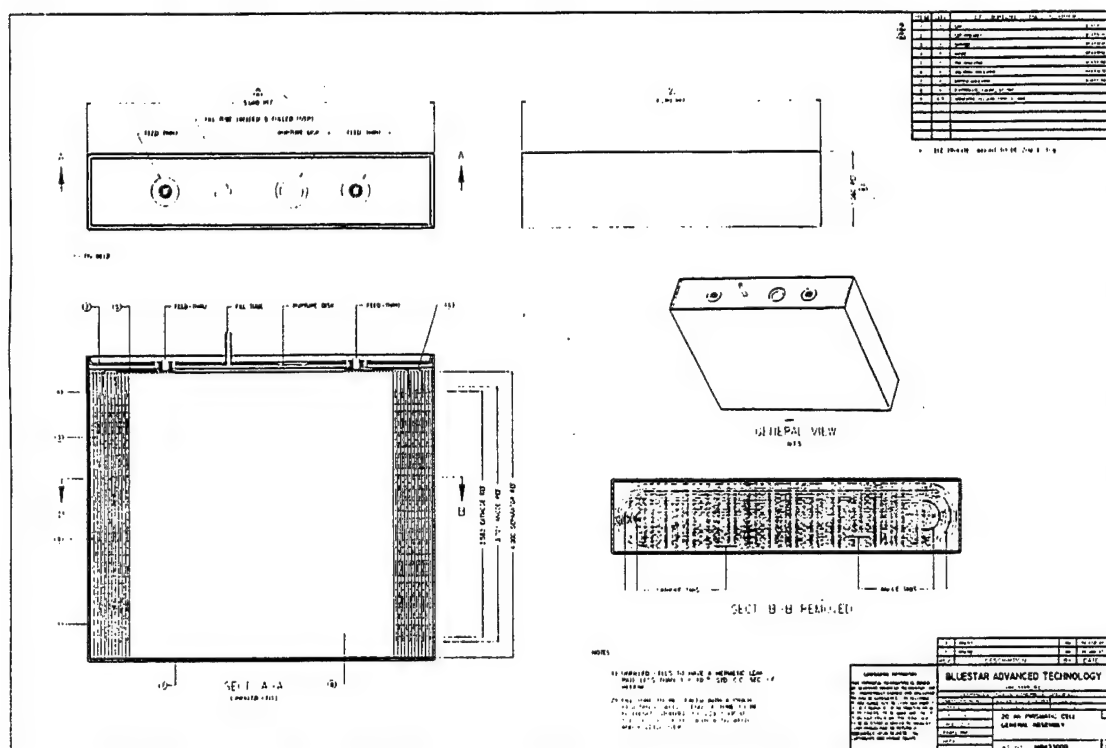


Figure 35. General assembly drawing of 20-Ah prismatic cell.

The first build of this design consisted of five cells with manually slit electrodes. A tuning fork mandrel was used to facilitate the construction of the elliptical wrap. The performance data of the first cells is outlined in Table 12.

Table 12. Performance characteristics of first iteration of 20-Ah prismatic cell.

Cell ID.	Cell Mass, g	Capacity, Ah	Specific Energy, Wh/kg	Energy Density, Wh/l
B880A1	952	22.0	83.2	215
B880A2	862	20.1	84.0	196
B880A3	888	21.1	85.5	206
B880A4	869	18.8	77.9	184
B880A5	836	18.7	80.5	182

Variation between cells was very large. There were two parameters that contributed significantly to the large degree of variation. The first parameter was the mass of electrolyte in each cell, which varied from 184 to 248 g. This huge difference was partially due to inexperience in filling large cells and to the design of the fill station. A new fill station was designed to help reduce the

variation. This plus further experience filling large cells reduced variability. The second parameter was the mass of the electrodes, the mass of the positive electrode varied from 258 to 296 g. These cells were some of the first with electrodes made using the automated coater and press roller. Experience again reduced these variations.

A mass analysis was carried out to further understand the role each component contributes to a cell. Table 13 is an example of mass analysis. To increase specific energy we must maximize the mass of active materials and minimize the mass of the inactive components. Three inactive components were targeted for mass reduction. These were cap/can, electrolyte and copper foil. As seen from the table the cap/can contributes 25.8% of the total mass while the electrolyte contributes 24.3%. Copper foil contributes 7.2% of the total mass but constitutes 45% of the negative electrode.

The first parameter tested to improve specific energy was electrolyte mass. Eight cells were manufactured with 2 cells each filled to 160g, 180g, 210g and greater than 230g. The results are shown in Figure 36.

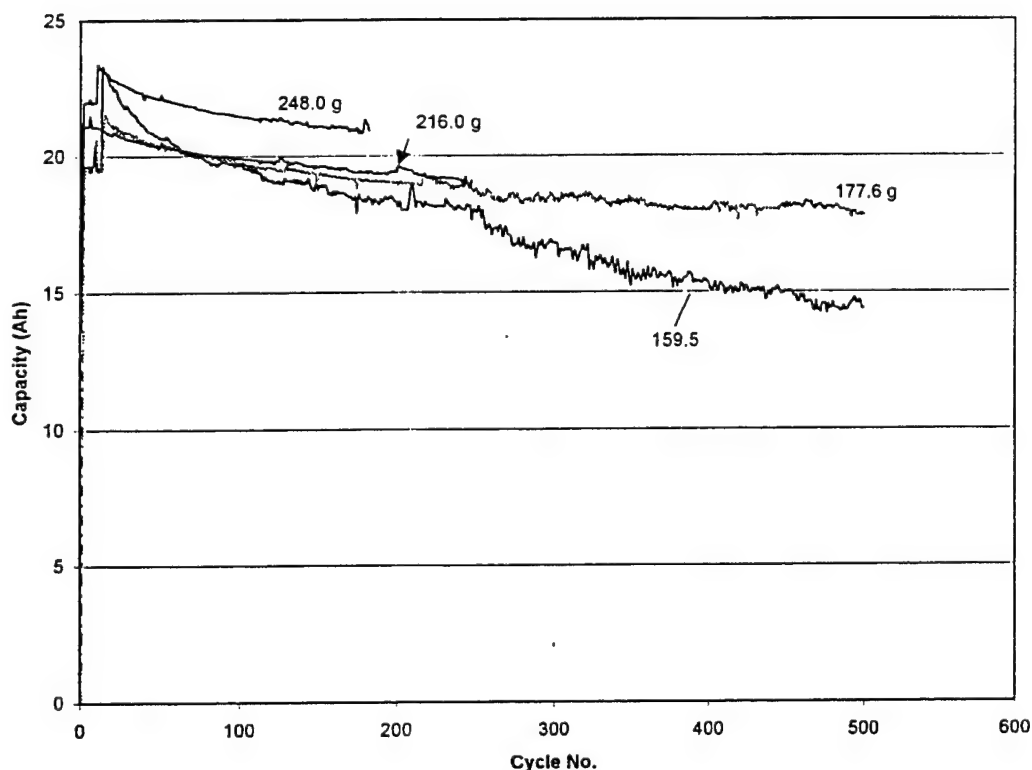


Figure 36. Capacity versus cycle number for 20-Ah prismatic cells filled with different electrolyte mass.

Table 13. Cell mass analysis of 20-Ah prismatic cell.

Component	Mass, g	%
Can	207.4	23.4
Cap assembly		
- Cap blank	19.2	2.2
- GTM seals, rupture disk, Fill tube	2.2	0.2
Total	21.4	2.4
Electrolyte		
- DEC	81	9.1
- EC	110	12.4
- LiPF ₆	25	2.8
Total	216	24.3
Positive electrode		
- LiCoO ₂	203.2	22.9
- 0.001" Al Foil	36.9	4.2
- Binder	6.7	0.8
- Conducting	13.4	1.5
Total	260.2	29.3
Negative electrode		
- Graphite	67.0	7.5
- 0.0005" Cu foil	63.8	7.2
- Binder	7.9	0.9
- Conducting	3.9	0.4
Total	142.6	16.1
Fiddley bits		
- Positive tabs	3.5	0.4
- Negative tabs	6.9	0.8
- Insulators	4.5	0.5
- Positive tape	2.0	0.2
- Negative tape	4.0	0.5
- Separator	19.2	2.2
Total	40.1	4.5
Total	888	100

The results show that all cells filled with more than 175g of electrolyte have almost identical rate of capacity fade. Cells filled with 160g of electrolyte had a greater capacity fade, therefore 180g was selected as the optimal electrolyte mass.

The next component change to enhance specific energy was cap/can wall thickness. The first set of cells were made with 0.030" thick SS. The second set of manufactured cases had a wall thickness of 0.017". This resulted in a cap/can weight of 143g instead of 229g, a weight savings of 86g. The third set of prismatic cells were built with thin wall cases and used an electrolyte mass of 180g to improve specific energy. To determine the maximum specific energy with the present techniques the negative electrode was made from MCMB. As shown with the Status Cells, the MCMB cells did not have the cycle life of the LK-702 cells. To finally determine which design to deliver, prismatic or cylindrical, the highest specific energy prismatic cells were made. The results from these cells are shown in Table 14.

Table 14. Cell capacity, mass and cell performance data for 20-Ah prismatic cells.

Cell ID	Capacity (Ah)	Cell Weight (g)	Specific Energy (Wh/kg)	Energy Density (Wh/l)
20AhP018	24.8	843	105.9	236
20AhP019	24.6	843	105.0	234
20AhP023	23.7	815	104.7	226
20AhP024	22.3	861	92.2	210
20AhP025	24.2	837	103.5	229
20AhP027	24.8	842	103.8	231
20AhP029	24.8	843	102.1	228
20AhP030	24.2	829	104.2	228
20AhP031	24.3	828	103.3	226
Average	24.2	838	102.7	228

The results in Table 14 show a marked improvement in specific energy from the first iteration. These performance data will be compared to the cylindrical design performance data in the following section, resulting in the selection of the deliverable design for the cells sent to the USAF.

The electrical performance of 20-Ah prismatic cells was tested along with rate performance. The performance of the cells still under test is shown in Table 15. The cells not included in this table are listed underneath.

Table 15. Cell mass, performance and cycle life of 20-Ah prismatic cells still under test.

Cell Id.	Cell Mass, g	Capacity, Ah	Specific Energy, Wh/kg	Energy Density, Wh/l	Cycle Life			
					Rate	Cycle No.	do/dc	ECL
P002	862	23.4	97.9	223	C/5	1000	n/a	905
P005	836	20.2	87	192	C/3, C/2	687	n/a	325
P009	848	22.8	97	217	C/5	601	n/a	253*
P010	858	21.4	89.8	204	C/5	700	0.008	1168*
P017	781	21.9	101	209	C/2	1050	n/a	335
P022	805	23.4	105	223	C/10	300	0.013	481*
P023	815	23.7	105	226	C/5	266	0.0102	561*

* Projected

+ 163g electrolyte

19 Cells MCMB, 2 cells abuse, 7 cells shorted on cycling, 3 cells shorted before filling

Cells of this design suffer a very high rate of mortality after extended cell cycling of the first generation of cells. This was attributed to the hand-slitting of the first set of cells versus the mechanical slitting of all subsequent sets of cells. The cells using MCMB as the active component in the negative electrode had a faster capacity fade than the LK-702 cells as discussed previously. The cycle life history of cell P010 is shown in Figure 37. The large increase in capacity at cycle 500 was due to changing the voltage leads. Now voltage is monitored directly at the pin instead of at a banana jack that is also used to carry the current. The latter method resulted in a voltage drop and in the cell not charging completely.

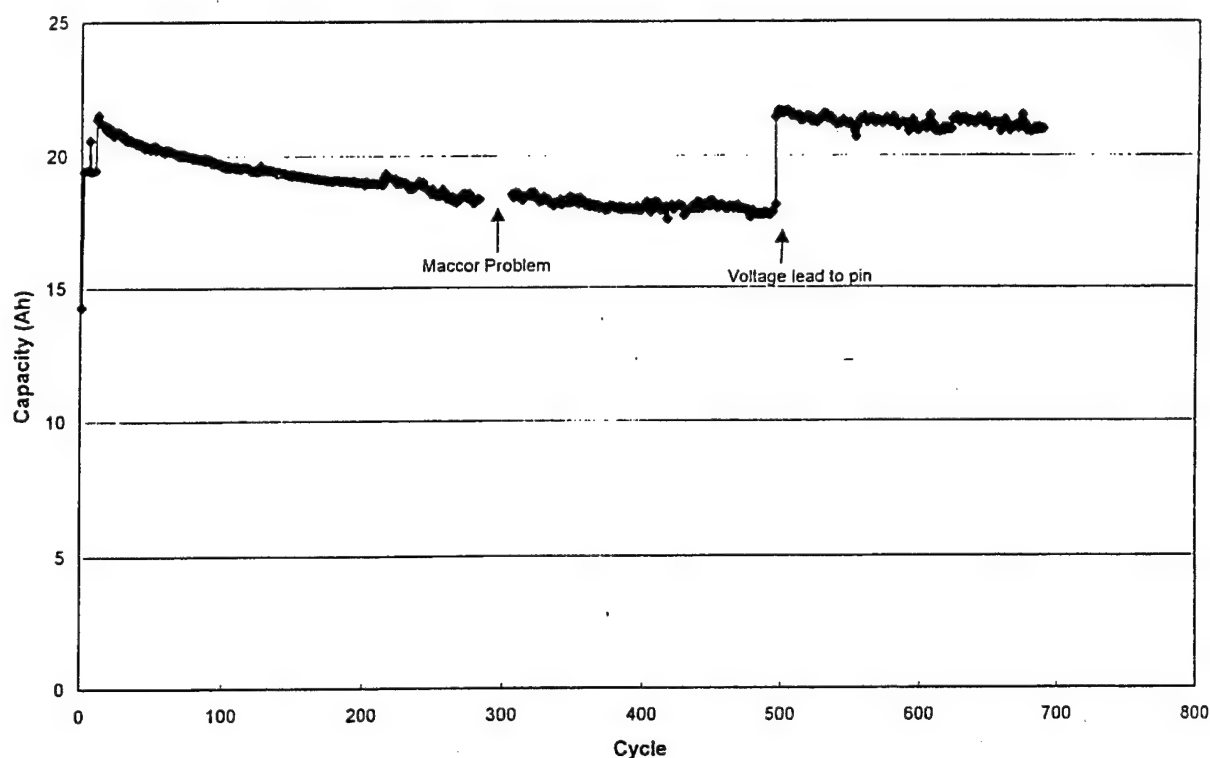


Figure 37. Cycle life for cell P010 at C5 to 100% dod.

The rate capability of the prismatic cell design was tested and the results are shown in Figures 38 and 39. The cells used in these tests were charged and discharged at the same rate. The voltage versus capacity profiles for the 20-Ah prismatic cell explicitly show the effect of IR drop during operation. The voltage for the higher discharge rates is lower, with the exception of the C/2 rate which has approximately the same voltage as the C/5 rate. This anomaly could be due to self-heating, resulting in lower cell resistance. The capacity at the C/10, C/5 and C/2 rates is very similar while the capacity starts to fall off at the C rate. This is shown in the log C-discharge graph. Overall the rate capability of the cell is quite good for applications which require less than C rate.

In conclusion the manufacture and testing of the prismatic design was extremely profitable. These cells were the first to use electrodes made with the automated equipment. The high cell mortality rate after extended cell testing highlighted the need for a mechanical slitter. The better a/c ratio of the design over the 10-Ah prismatic cell improved packing efficiency as shown by the improved specific energy of the 20-Ah cell. The optimization of the specific energy with the reduction in electrolyte and the case weight gave the expected results as shown in Table 16. The cells using the 0.017" light-weight cell cases bulged slightly after the first charge, most likely due to gas evolution, but after the first discharge and subsequent cycles the cases no longer bulged. The cycle life of some of the cells was quite good but a comparison with the cylindrical cells discussed in the next section led to the latter being selected for USAF deliverables.

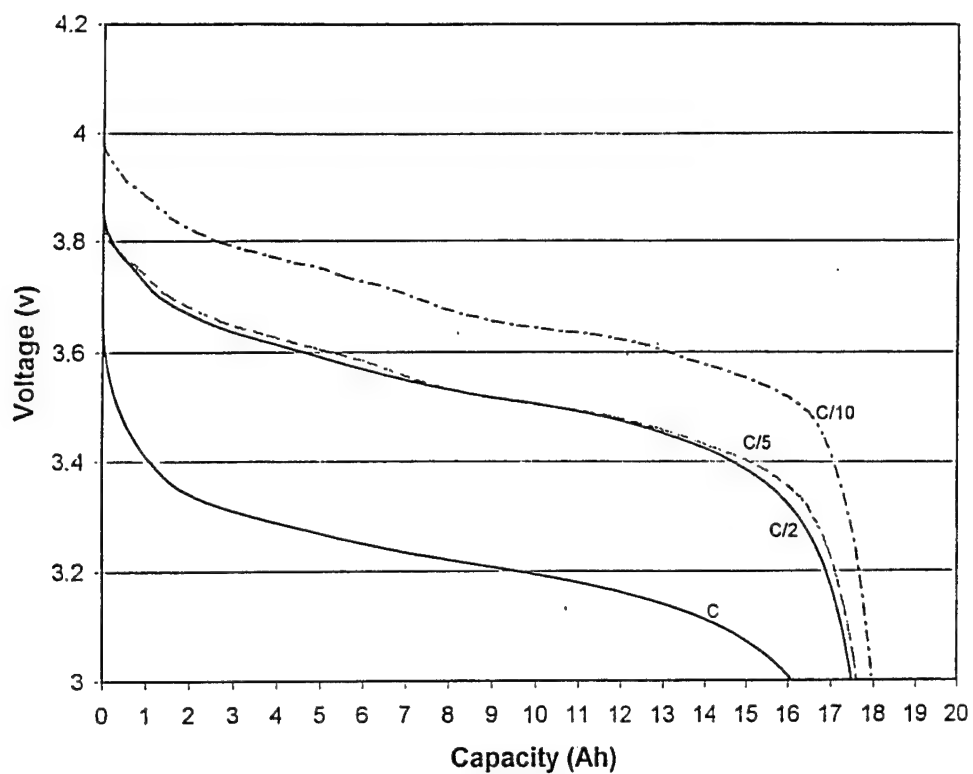


Figure 38. Rate capability of 20-Ah prismatic cell at room temperature and 100% dod.

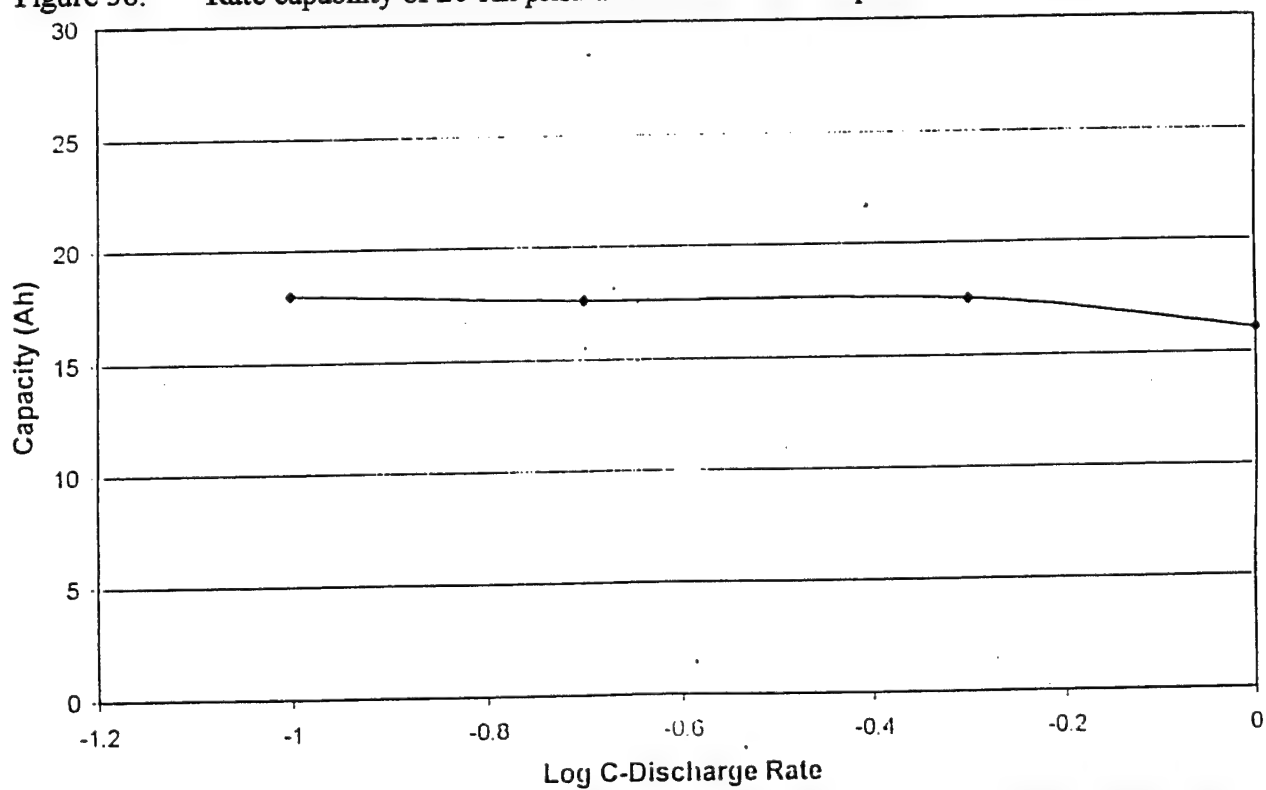


Figure 39. Capacity versus log rate for 20-Ah prismatic cell at room temperature and 100% dod.

Table 16. Projected performance versus measured performance for design changes to 20-Ah prismatic cell.

Design Change	Projected	Actual
Change Carbon from LK-702 to MCMB	101 Wh/kg	99 Wh/kg
Change to Lighter Case (LK-702)	98.7 Wh/kg	98.5 Wh/kg
Reduce Electrolyte Volume to 175g (LK-702)	105 Wh/kg	101 Wh/kg

2.4 Task 4.0. 20-Ah Cylindrical Cell Development

One design approach for a wound cell is the elliptical wrap as discussed above for the 10 and 20-Ah cell designs. Another approach, with which BATC has years of experience, is the cylindrically wound or jellyroll cell. This design is the same type used in C cells for material evaluation. During the Design Review held at Phillips Laboratory on 19 February 1997 it was decided that the first deliverable cells would be 10, 20-Ah cylindrical cells based on the designs presented and the trade-offs outlined. By careful calculation of cell mass distribution it was found that the cylindrical design would offer specific energy advantages over the prismatic design. The data presented in Albuquerque showed that the specific energy of the prismatic design was 85 Wh/kg while the projected performance of the cylindrical design was 97 Wh/kg. When the cells were manufactured for the deliverables, the performance was better than projected at 110 Wh/kg. The general assembly for the 20-Ah cylindrical cells Design I is shown in Figure 40. The performance and design characteristics of the cells are as follows:

- o GTM pins were 0.125" ϕ versus standard hardware at 0.090" ϕ .
- o Fill tube was standard SO₂ hardware and the rupture disc was 0.3125" ϕ opening at 235 psi
- o Electrode dimensions
 - Positive electrode 4.4 x 1300 x 0.017 cm
 - Negative electrode 4.7 x 1330 x 0.011 cm
- o Performance
 - 24.0 Ah, 110 Wh/kg, 219 Wh/l

The performance data of the 10 cells delivered to the USAF is shown in Table 17.

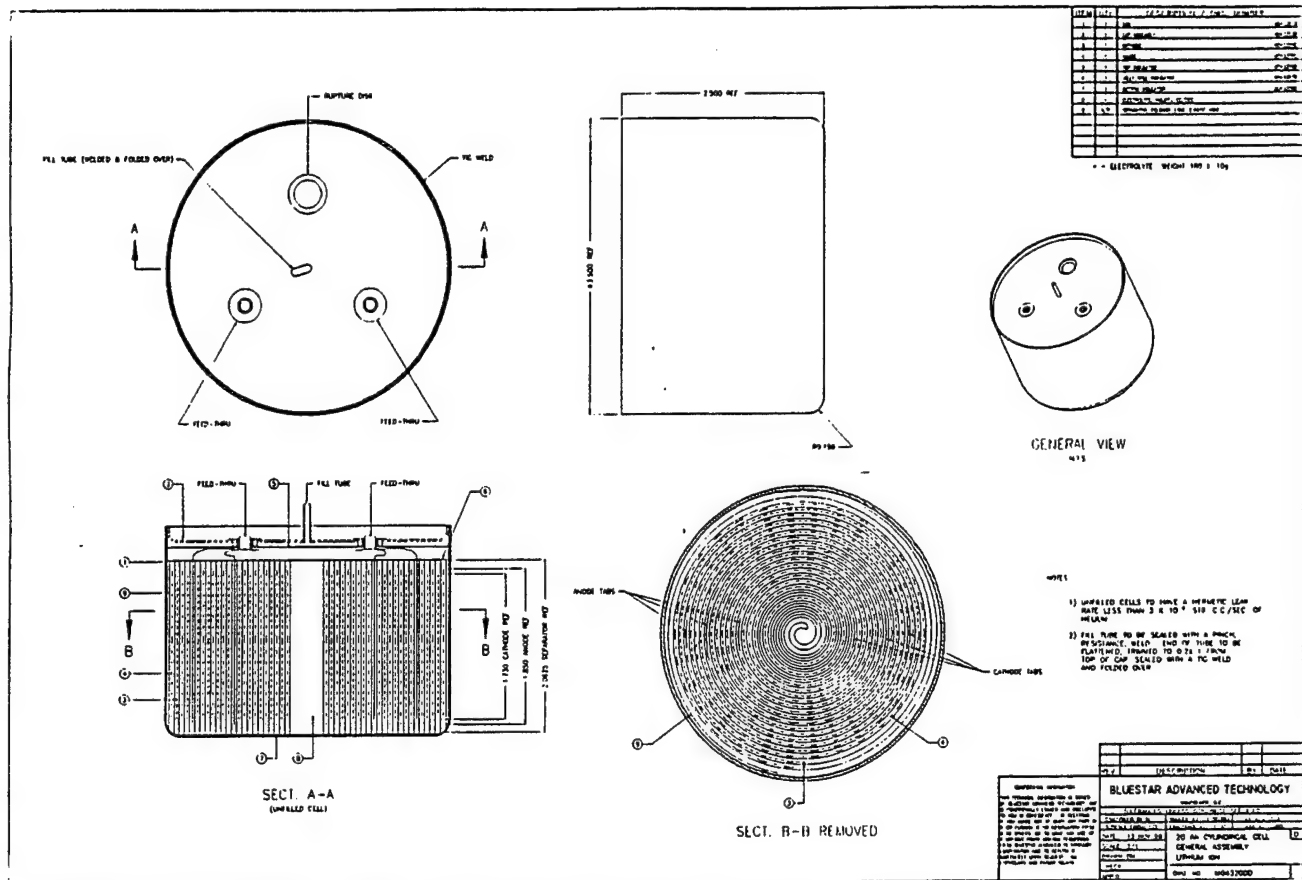


Figure 40. General assembly of 20-Ah cylindrical cell Design I.

The variation between cells of this design was quite large, however these were the first large cylindrical cells built at BATC and the performance of the cells was quite good. During the construction of the Design I cylindrical cells a very high incidence of infant mortality, close to 50%, was observed. These losses were attributed to the very long electrodes used in the manufacture. The 20-Ah cells for delivery to the USAF were the first cells which used electrodes slit with the equipment at BlueStar Battery. Even though there was a large number of cells with infant mortality it was believed that mechanically slit electrodes would prevent cell failures after extended cycling. The tabulated results for the cell mass distribution is shown below.

Table 17. Cell mass, capacity and performance of 20-Ah Design I delivered cells.

Cell Id.	Cell Mass, g	Capacity, Ah	Specific Energy, Wh/kg	Energy Density, Wh/l
C006	811	25.4	113	232
C008	782	24.4	112	223
C009	783	24.3	112	222
C014	762	23.1	109	211
C015	792	24.3	110	222
C018	766	23.0	108	210
C019	772	23.8	111	217
C021	781	24.0	111	219
C023	810	24.0	107	219
C024	768	23.9	109	218
Average	783	24.0	110	219
Std. Dev.	$\sigma = 17$	$\sigma = 0.7$	$\sigma = 2$	$\sigma = 6$

Table 18. Cell mass analysis of 20-Ah Design I cylindrical cell.

Component	Mass, g	%
Can	89.4	11.4
Cap assembly		
- Cap blank	33.9	4.3
- GTM seals, rupture disk, Fill tube	2.2	0.3
Total	36.1	4.6
Electrolyte		
- DEC	64.3	8.2
- EC	87.1	11.1
- LiPF ₆	20.0	2.6
Total	171.4	21.9
Positive electrode		
- LiCoO ₂	228.4	29.2
- 0.001" Al Foil	37.6	4.8
- Binder	7.5	1.0
- Conducting	15.0	1.9
Total	288.5	36.9
Negative electrode		
- Graphite	77.9	10.0
- 0.0005" Cu foil	65.8	8.4
- Binder	9.2	1.2
- Conducting	4.6	0.6
Total	157.5	36.9
Fiddley bits		
- Positive tabs	3.5	0.4
- Negative tabs	6.9	0.9
- Insulators	4.5	0.6
- Positive tape	2.0	0.3
- Negative tape	4.0	0.5
- Separator	19.2	2.4
Total	40.1	5.1
Total	783	100

The mass analysis reveals some interesting facts about the composition of the cell. The mass contribution of the can and cap for the cylindrical cell is 16% compared to 25.8% for the prismatic cell. This is a major reason for the superior specific energy of the former. As with the prismatic cell, the mass contribution of the positive electrode is acceptable, with active materials contributing close to 89% of the total mass of the electrode. In contrast the negative electrode is less than 50% active. The largest contributor to the inactive components is the copper foil, which makes up 42% of the total weight of the electrode, so other sources of copper were sought and used in the cell designs discussed later. The amount of electrolyte is probably optimal and no study was undertaken to reduce the mass of electrolyte. Instead the results from the 20-Ah prismatic study were used.

The performance of these cells was investigated after the deliverables were sent to the USAF. The cell cycling performance is shown in Table 19.

Table 19. Cell capacity, mass and cycle life of 20-Ah Design I cylindrical cell.

Cell ID.	Cell Mass, g	Capacity, Ah	Specific Energy, Wh/kg	Energy Density, Wh/l	Cycle Life			
					Rate	Cycle No.	dq/dc	ECL
C002 (MCMB)	837	26.1	112	238	C/5	800	n/a	657
C004	799	24	108	219	C/5	600	n/a	435
C033	791	24.1	110	220	C/3, C/2	1000	n/a	459 ¹
C034	787	23.8	109	218	C/3, C2	1500	n/a	250 ¹
C036	781	23.6	109	217	C/10	350	0.006	970*
C037	802	24.7	111	225	C/10	300	0.009	614*
C038	801	25.0	112	229	C/5	500	n/a	500
C039	806	25.6	114	234	C/5	700	0.004	1400*
C045	882 ⁺	22.4	92	205	C/2	240	0.024	339*

* Projected, ⁺ Pressure transducer test

¹ Voltage sensor changed

5 MCMB, 10 deliverables, 2 samples, 2 LEO, 10 short on formation, 2 tab disconnect, 5 abuse tests, 1 pressure transducer on hold

The capacity of the cells using LK-702 as the negative electrode are quite uniform as are the specific energy and energy density. The one cell that has a very low specific energy and energy density was designed for pressure experiments and was equipped with additional hardware. From the table the cycle life, whether projected or experimental, was better at the C/5 and C/10 rates than the C/3 or C/2 rates. The cycle life of the C/10 and C/5 rates is excellent ranging from 435 cycles to over 1000 cycles. Part of the reason why the C/2 and C/3 charge rates are not performing as well as the lower charge rates is due to the testing method. The capacity test carried out on cycle #11 uses a C/10 charge to 4.1V and then trickle charged at 4.1V for 1.5 hours. The cell is then discharged at a C/2 rate to 3.0V. Since the cell is charged at C/10 for the capacity test the cell is totally charged. However, since the test set up used a two lead system where the voltage sensors and the current went through the same banana jack, the voltage drop due to the banana jack, banana plug and nickel tab would result in the cell not being completely charged at the higher rates even though it was completely charged for the capacity test. The results of the two voltage sensor system at the C/2 rate is shown in Figure 41.

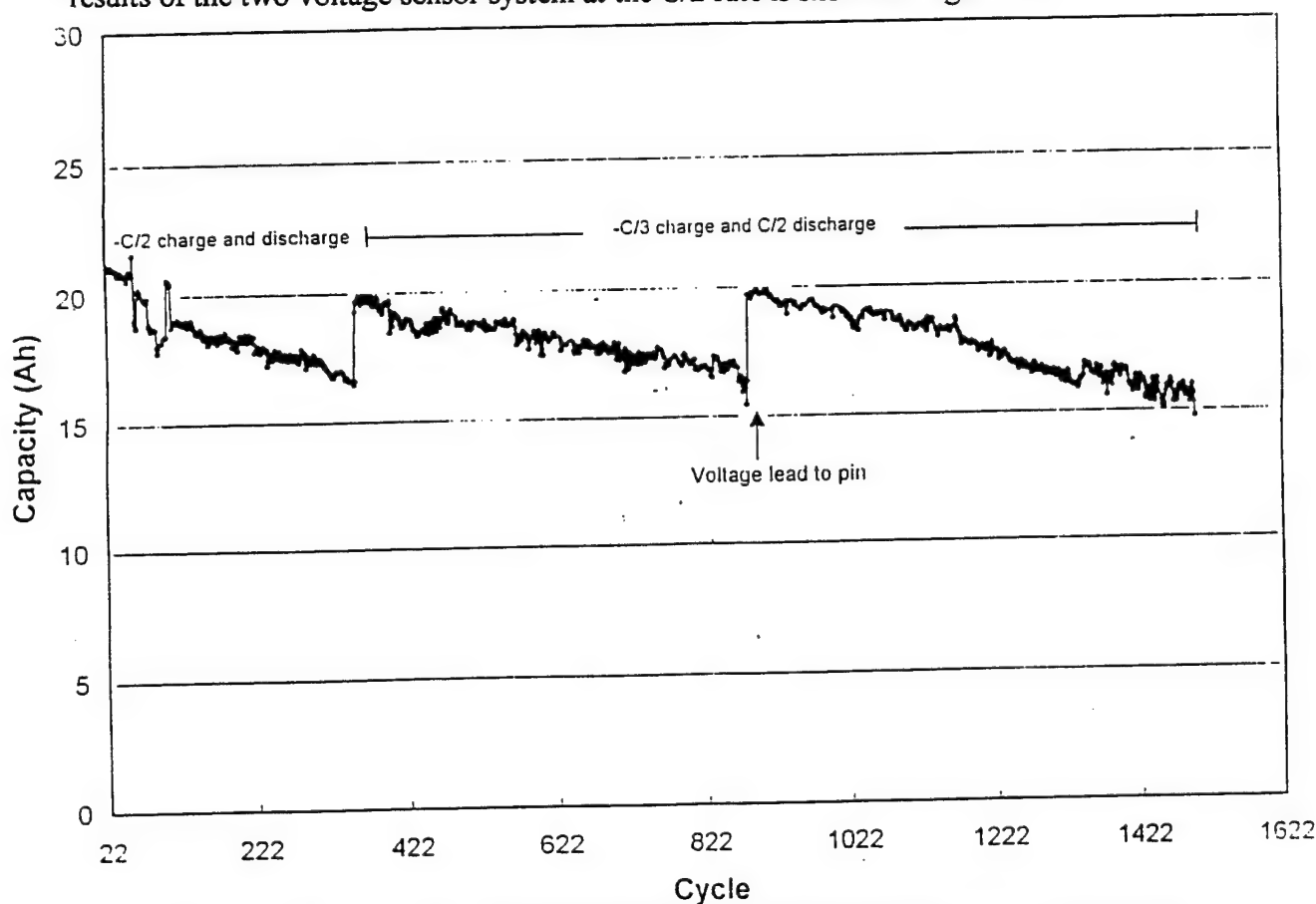


Figure 41. Capacity versus cycle number for cell C034 at the C/2 rate to 100% dod.

Figure 41 shows the impact of not charging the cell completely. After 350 cycles the charge regime was changed from 12 A to 8 A. By changing the charge rate by 4 A the capacity increased 25%, from 16 Ah to 20 Ah. As the cell testing continued the slope of the capacity fade is the same whether the charge rate was 8 A or 12 A. At cycle 900 the voltage connections were changed so that the voltage sensors were directly connected to the pins and therefore all voltage drop associated with IR was removed. When the cell was charged based on the correct voltage

the cell capacity increased by 25%. These results suggest that the performance at the C/2 rates is better than shown in Table 19. When the charge rate was changed to C/2 the cell was not completely charged due to the incorrect voltage readings. Since end of life is calculated at 75% of capacity the values are very poor for the C/2 rates. A better measure of end of life would be 75% based on a capacity which uses a C/2 charge rate instead of a C/10 rate.

A representative cell tested at the C/5 charge and discharge rate is shown in Figure 42. The change from a two lead system to a four lead system is also noted on the graph. The change in capacity is only 1-Ah, which is less than at the C/2 rate, as expected, when the change is due to IR. The exact same observation can be made at the C/10 rate shown in Figure 43. The voltage leads were changed at cycle 250 and is barely noticeable.

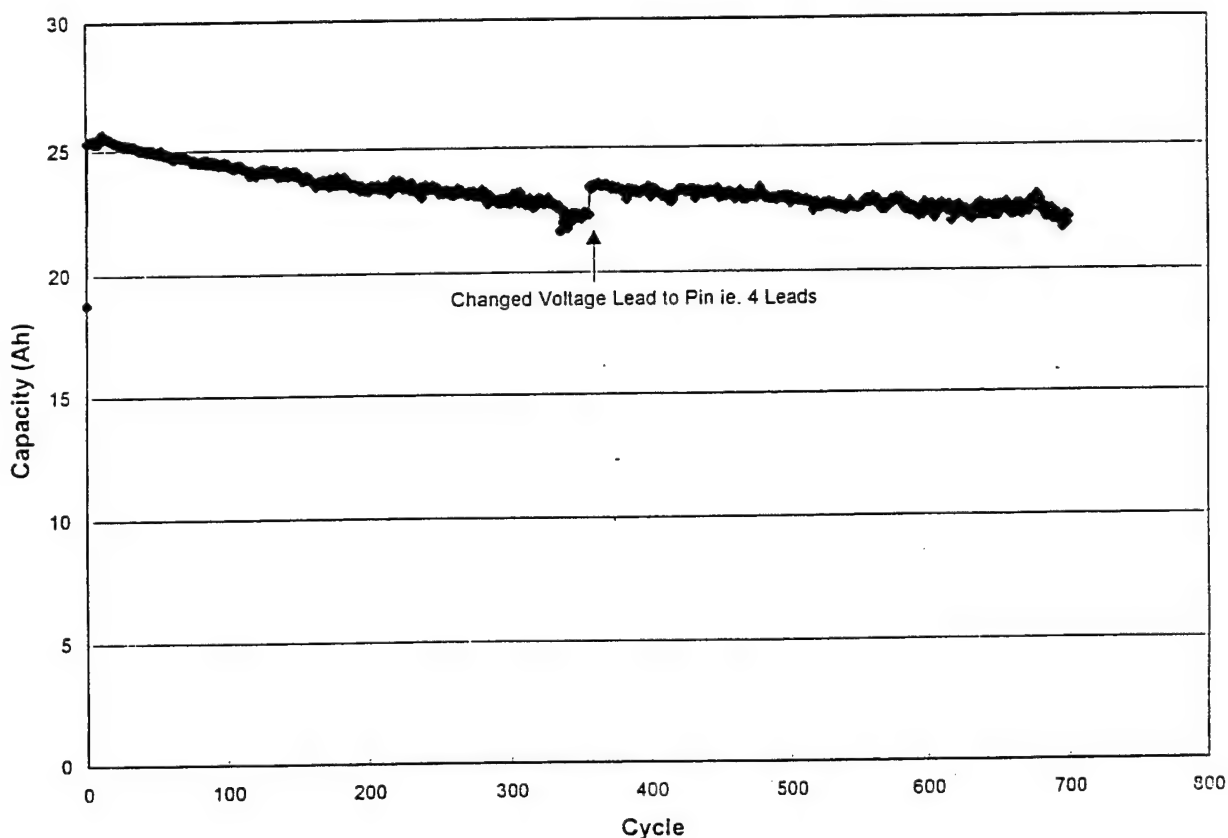


Figure 42. Capacity versus cycle number for cell C039 at the C/5 rate to 100% dod.

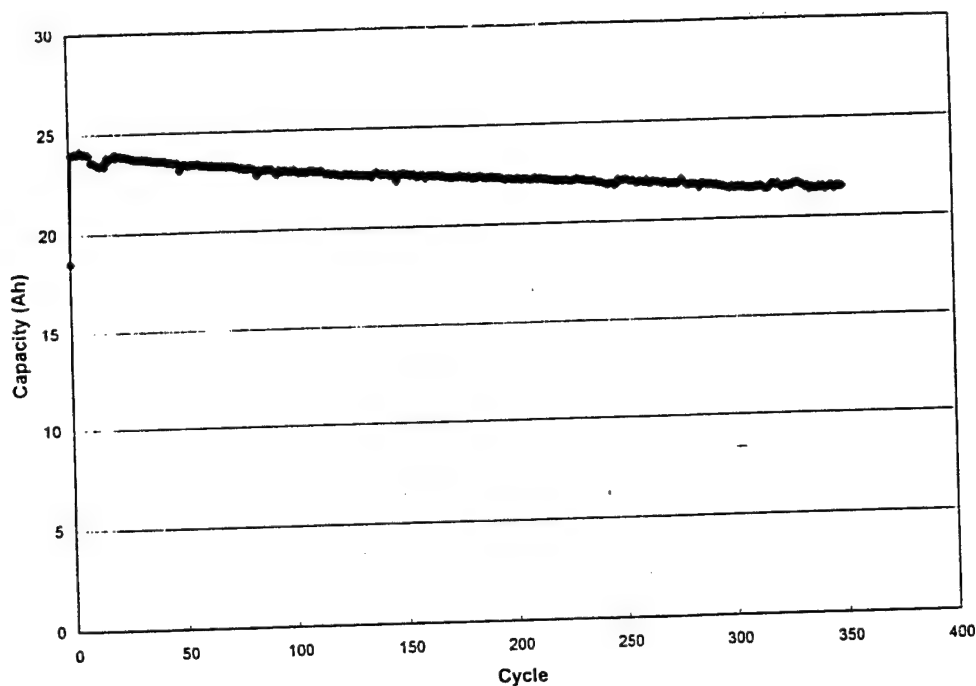


Figure 43. Capacity versus cycle number for cell C036 at the C/10 rate to 100% dod.

A comparison of negative electrode materials, LK-702 versus MCMB, was carried out in this cell format. Again a large problem with the MCMB electrodes was slitting. The cells were also harder to wind and had a high incidence of internal short circuits. The results of a comparison between LK-702 and MCMB is shown below.

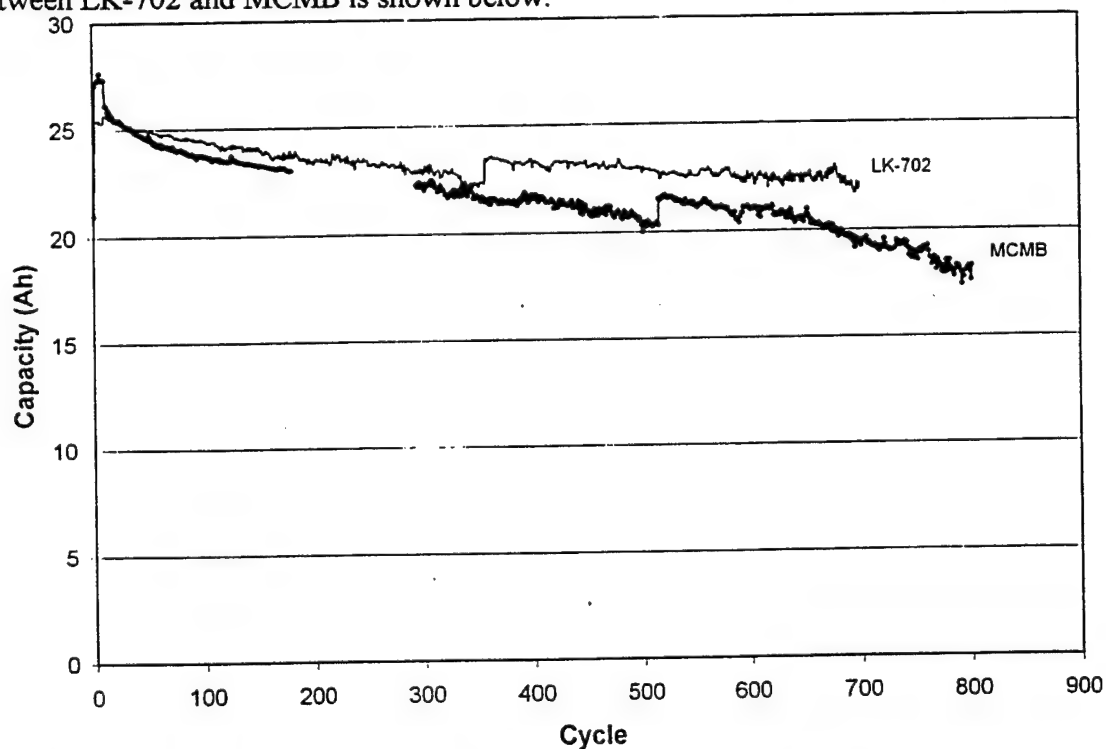


Figure 44. Cycle life performance of MCMB and LK-702 to 100% dod.

As with the Generation IV and V Status Cells, the capacity of the MCMB cells is higher but only briefly. Due to difficulties in cell manufacture using the MCMB negative electrode, LK-702 electrodes were used for the deliverables.

One performance parameter tested for this design was high rate/low temperature. Before these tests were initiated, the author suspected that the cell would have poor rate capability since there were only three tabs per electrode and the electrodes were very long. The low temperature performance was unknown at the time. Since the cells used 1M LiPF₆ EC/DEC as the electrolyte we cannot expect good performance as shown with the electrolyte studies. The tests at different rates and low temperature used symmetrical charge and discharge rates (i.e., C/10 charge and discharge). All tests used a constant current charge regime to 4.1V followed by a constant voltage charge at 4.1V. At room temperature the constant voltage step was 1.5 hours long while at low temperature this step was 2.5 hours long. Both the charge and discharge were carried out at low temperature. The cells were not insulated, so after each charge and discharge the cells were held for 4 hours at open circuit to ensure temperature equilibration. The tests at room temperature are shown in Figures 45 and 46 and the tests at 0 °C are shown in Figure 47.

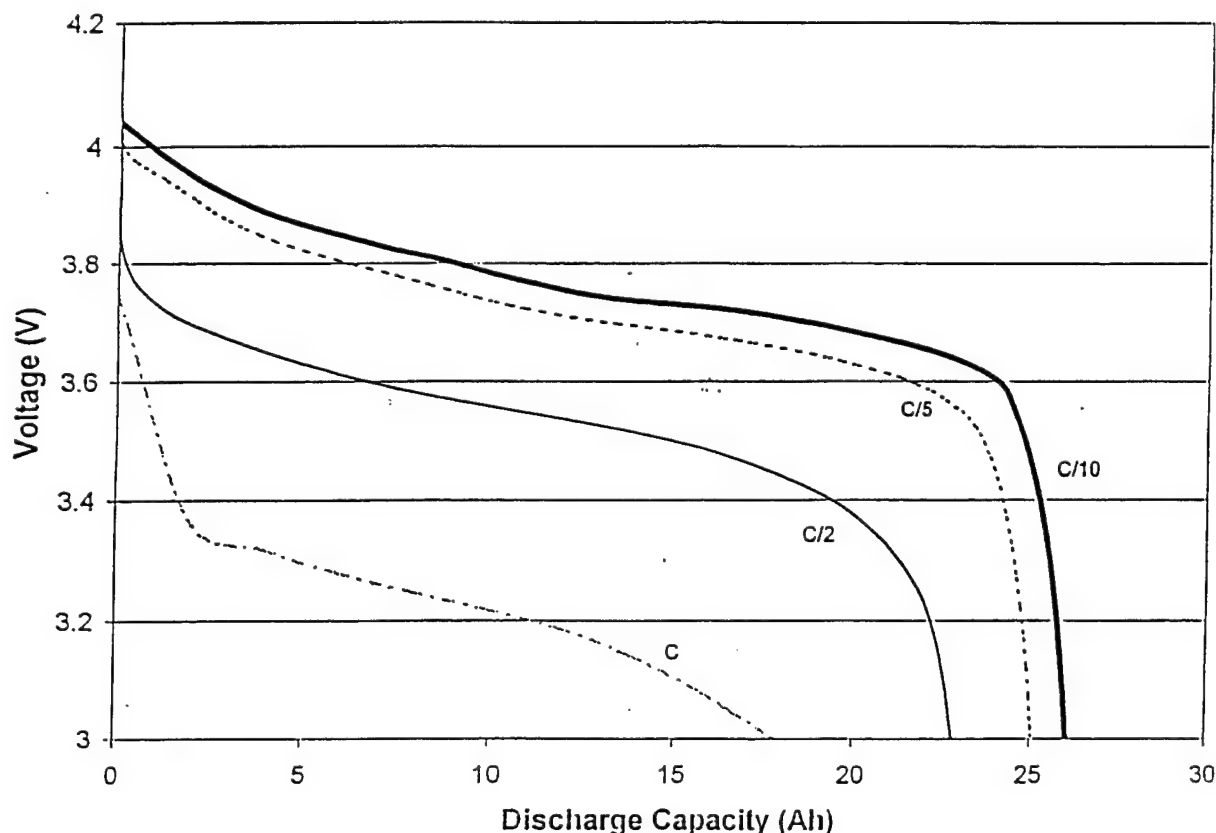


Figure 45. Rate performance of 20-Ah at room temperature at 100% dod.

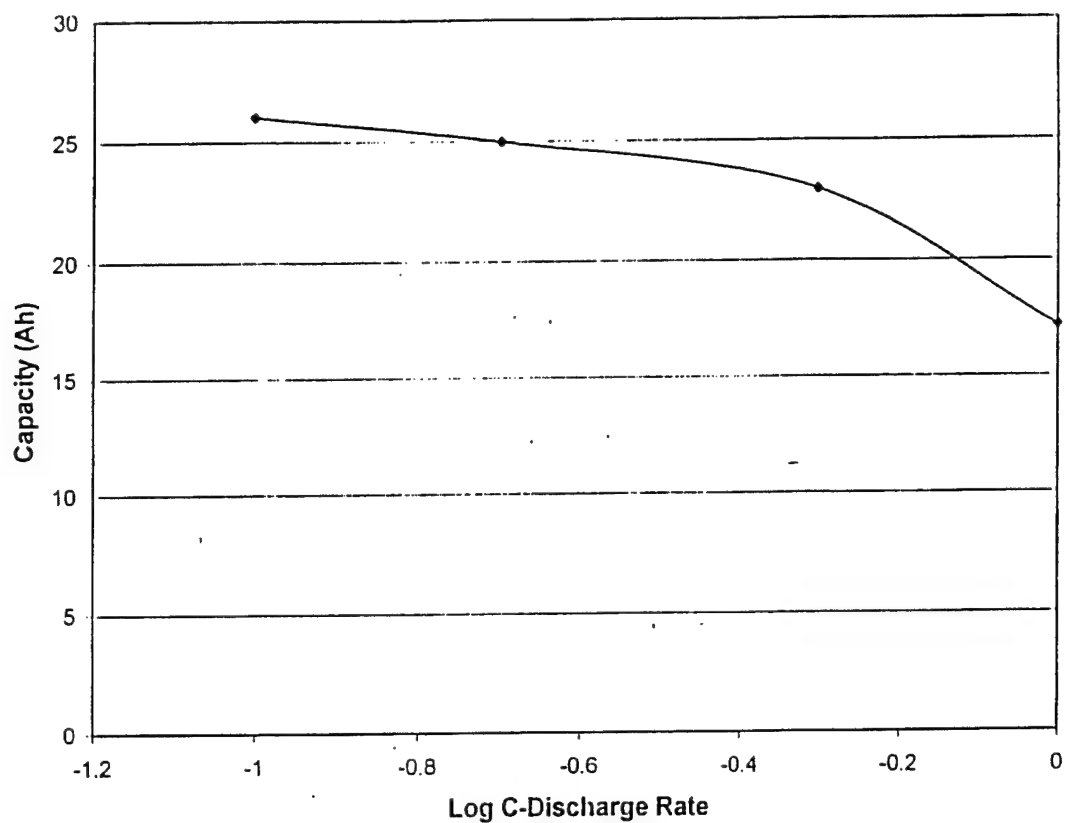


Figure 46. Rate capability at room temperature, 100% dod, capacity versus log rate.

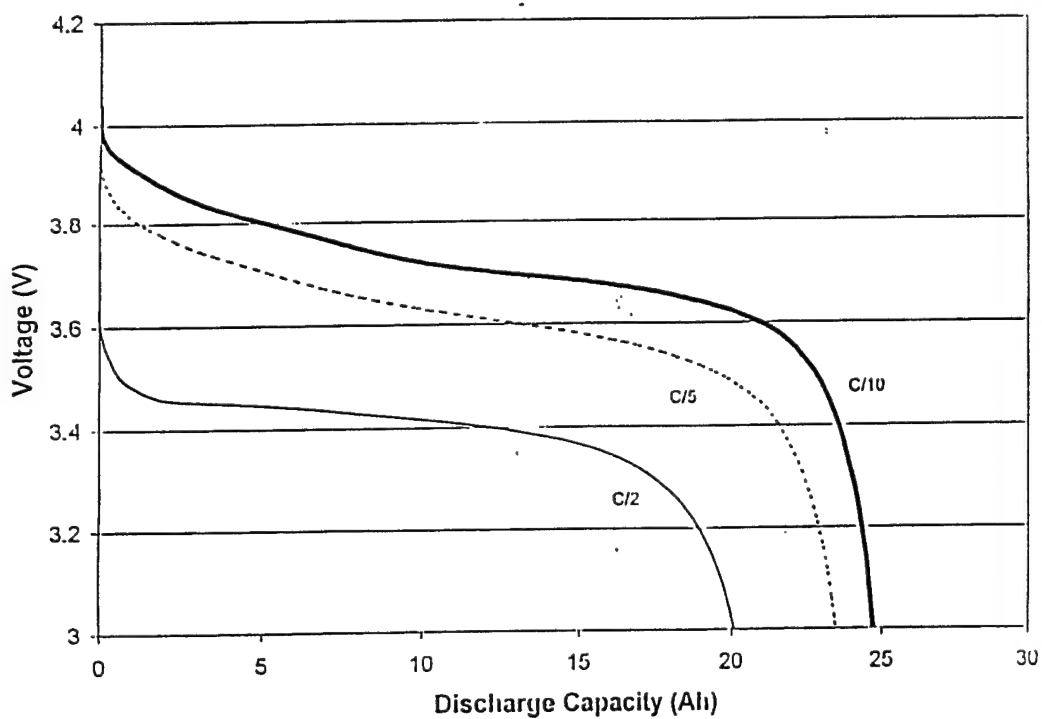


Figure 47. Rate capability at 0 °C, 100% dod.

The graph of room temperature performance, Figure 45, shows that the capacity differs only slightly at the C/10 and C/5 rates but starts to fade at the C/2 rate, and is only 70% of the C/10 capacity at the C rate. This is shown more clearly in Figure 46 where the slope of the graph changes dramatically from C/2 to the C rate. The 0 °C rate studies show very similar results with poor performance. When the cells were tested at -20 °C the only data obtained were at the C/5 rate. The cells tested at C/10, C/2 and C rates had no capacity due to the voltage dropping below 3.0V. At C/5 a total capacity of 5.5-Ah was realized. For the discharge at C/5 the voltage gradually increased with time as would occur with self-heating. A comparison between the prismatic and cylindrical 20-Ah cells at room temperature along with the cylindrical cell performance at 0 °C is shown in Figure 48.

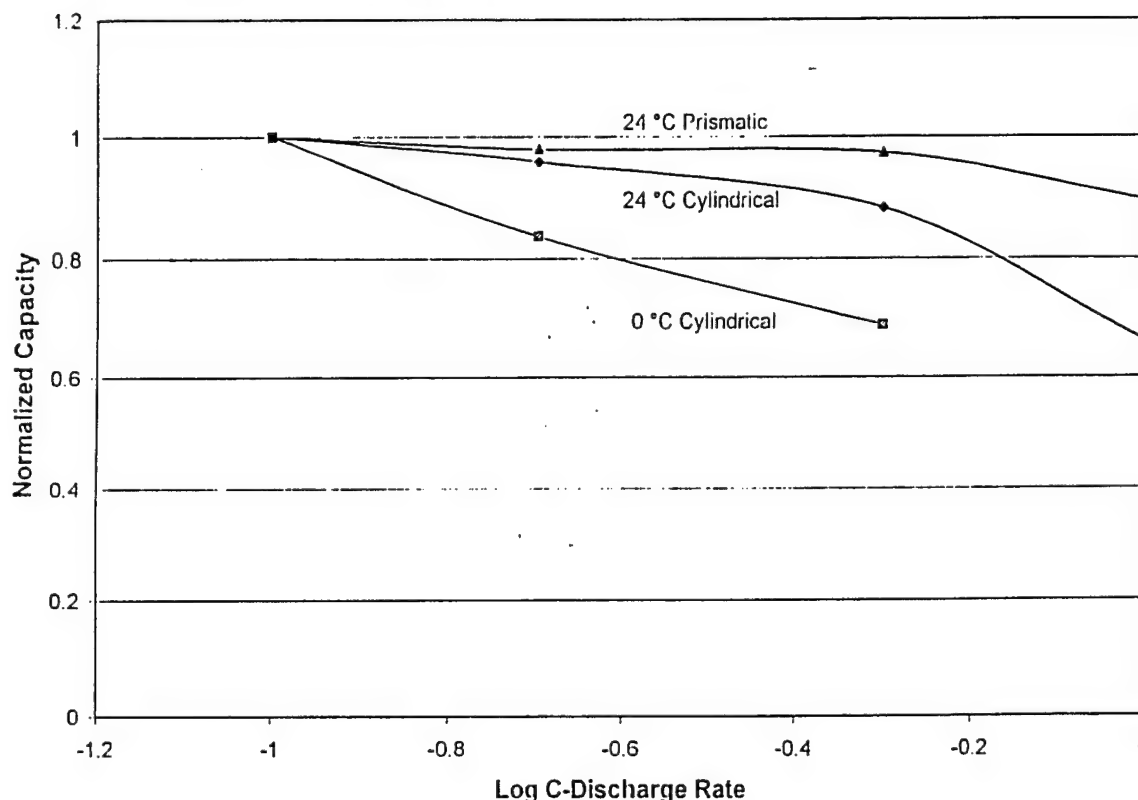


Figure 48. Rate comparison between 20-Ah prismatic and 20-Ah Design I cylindrical cell.

The superior rate capability of the prismatic cell at room temperature is immediately noted. The explanation postulated at BATC is the differing length of the electrodes. Both cells use three tabs for each electrode but the cylindrical cell electrodes are twice as long. Therefore, the distance between tabs is far greater for the cylindrical cell. This leads to a larger voltage drop along the electrodes and since the charge is based on a voltage end point the capacity is lower. To enhance the rate capability the Design II cylindrical cell used similar width and length of electrodes to the prismatic design.

Studies were conducted with the 20-Ah cylindrical cells to better understand the thermal characteristics of the cells. Thermocouples were placed on the side and top of the cell and the cell was cycled at the C/10, C/5 or C/2 rates. A representation of one of these tests at the C/5 rate is shown in Figure 49. The temperature profiles for the two thermocouples, voltage and power

graphs are also shown in the figure. Once the cell has equilibrated the cell temperature lies between 24 °C and 29 °C. Temperature follows a pattern: increasing slightly or remaining constant during the constant current charge and then decreasing during the constant voltage charge. The temperature decreases because the power diminishes quite rapidly. Also the temperature increases quite substantially during discharge. This implies that the discharge is an exothermic reaction as expected.

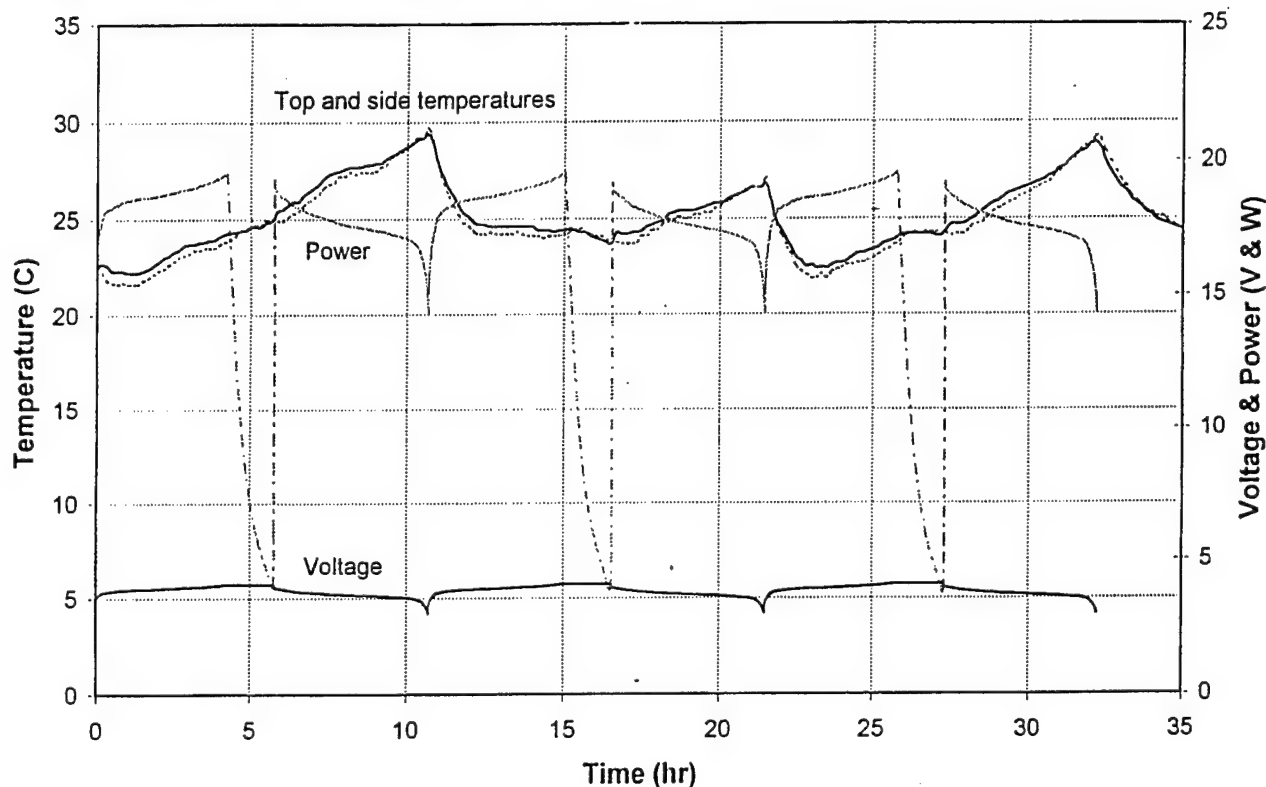


Figure 49. Temperature and power plot versus cycle number for 20-Ah Design I cylindrical cell.

A related experiment monitoring temperature and pressure during the first charge or formation cycle was done with the 20-Ah cylindrical cell. Li ion cells are assembled in the discharged state and the first charge is extremely important. During the initial charge the solid electrolyte interface (SEI) is formed and this loss of lithium due causes irreversible capacity loss. The formation of the SEI layer results in the production of Li_2CO_3 and ethylene, due to the presence of ethylene carbonate in the electrolyte. Another reaction which must occur during the first formation cycle is the reaction of water with the newly formed Li_xC_6 negative electrode.

To better understand these processes a 20-Ah cylindrical cell was equipped with a pressure transducer to measure the pressure during formation and subsequent cycles. The experiment also followed the temperature at the top of the cell and inside the test chamber. These results are presented in Figure 50.

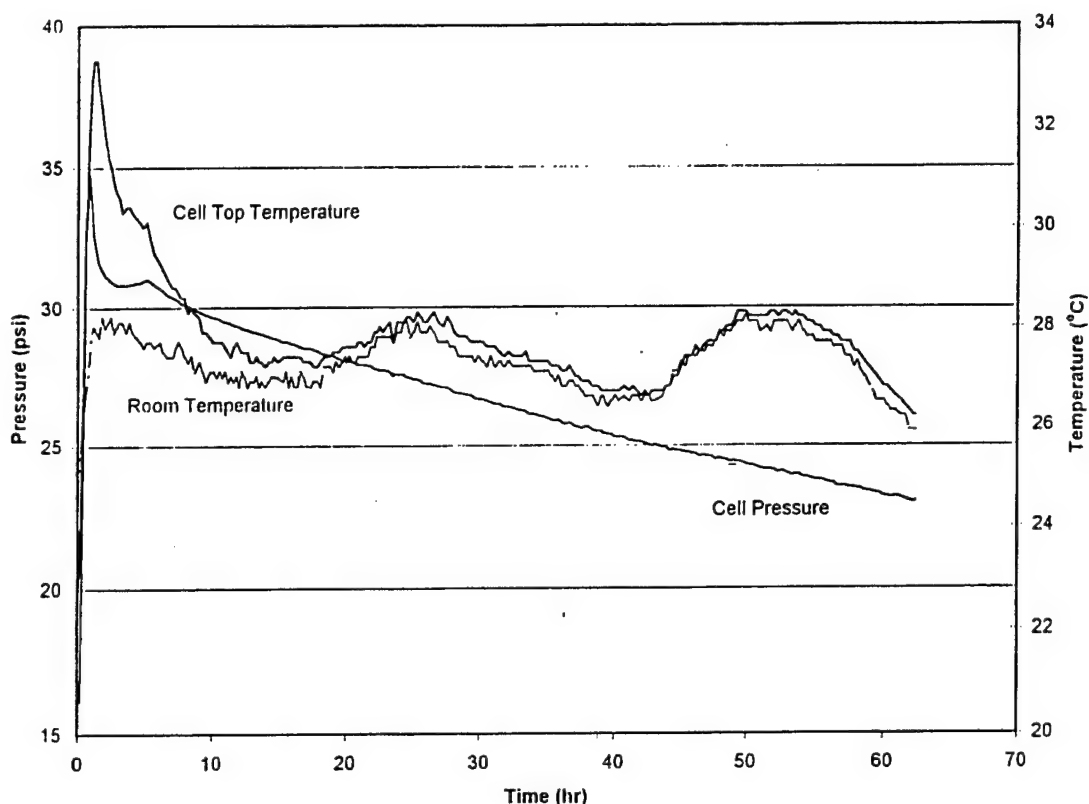


Figure 50. Pressure and temperature profiles of 20-Ah cylindrical cell during first charge half-cycle.

As shown in the figure, the cell temperature and cell pressure rise very dramatically in the first hour. The pressure increases from 17 psi to 35 psi in 30 minutes. The pressure then rapidly decreases to 31 psi and slowly increases again until the charge is stopped after 5 hours. Once the charge step is ended and the cell held at open circuit the decrease in pressure is linear. The shape of the curve during the first 5 hours indicates two processes. The first process is very fast while the second process seems to speed up as the cell reaches maximum potential. Perhaps the first step is the reaction between water and the lithiated graphite and the second process is the reaction between the lithiated graphite and EC to form the SEI layer. The rapid increase in cell temperature in the first half hour supports this hypothesis since the reaction of water with lithiated graphite is more exothermic than the reaction of solvent and Li_xC_6 . After the 5 hour charge the cell temperature matches the temperature of the chamber. After the initial charge cycle the cell was held at open circuit for 72 hours and then cell testing started. The pressure was followed periodically from the initial cycles to almost 200 cycles. These results are shown in Figure 51. After the first formation cycle the cell pressure was 18 psi, which is marginally above an ambient pressure of 16 psi. The pressure varied very slightly with cell cycling and any variations were due to temperature changes during charge and discharge. The pressure for cycles 12-21 is almost identical to that for cycles 1-5, so any pressure increase is slow. The pressure for cycles 189-194 is also shown in Figure 51. The cell pressure is now 18.5 psi versus 17 psi for the earlier cycles. It appears that pressure increases over time but the increase is slow and not substantial.

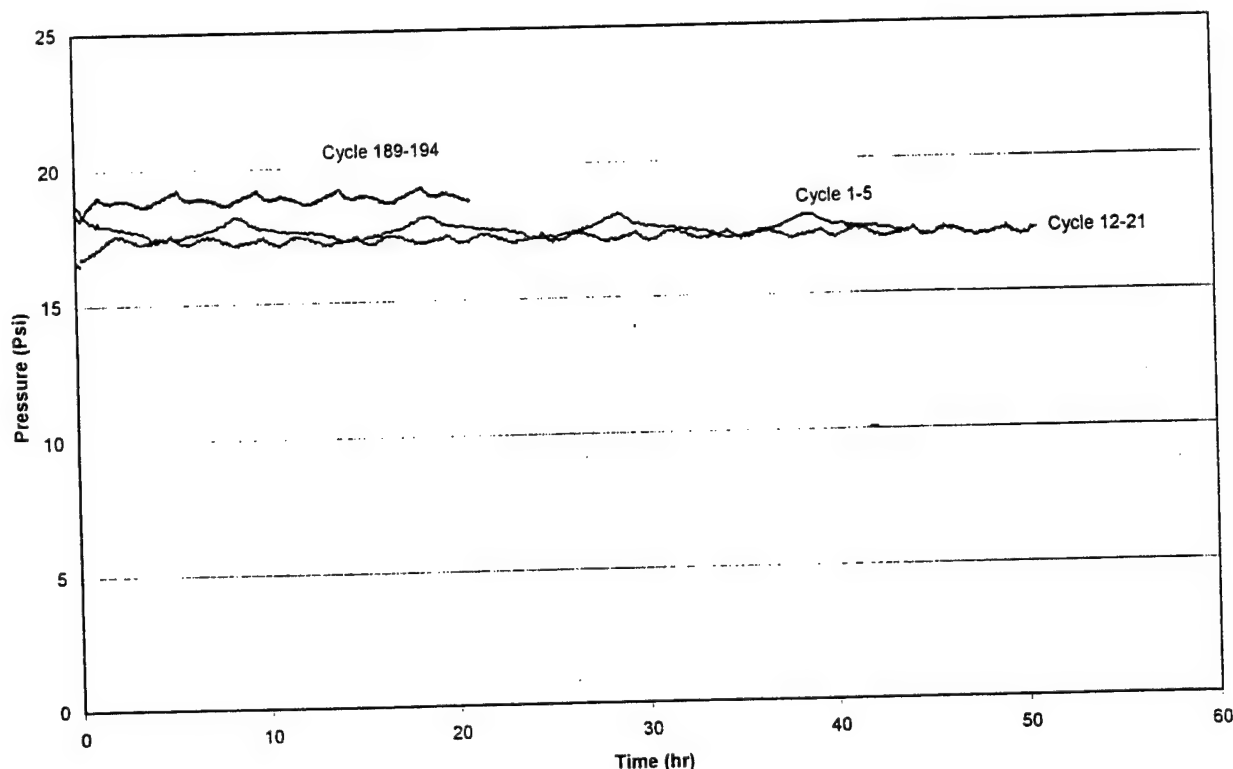


Figure 51. Cell pressure of 20-Ah Design I cylindrical cell during cell testing.

One of the projected uses for lithium ion batteries in the near future is satellite applications. The most demanding application would be for a low earth orbit (LEO) satellite which presently requires a battery cycle life of 30,000 cycles. As satellites evolve the power requirements and cycle life demands increase. To determine how close the technology at BATC is to meeting the requirements of the application, two 20-Ah cylindrical cells were tested using an accelerated LEO test sequence. The tester charged the cells at 10 A to 4.05V and then charged at constant voltage for a total time of 36 minutes. The cells were discharged at 20 A for a total of 12 minutes or 4-Ah (20% dod). The results for capacity versus cycle number and for end of discharge voltage versus cycle number are shown in Figures 52 and 53.

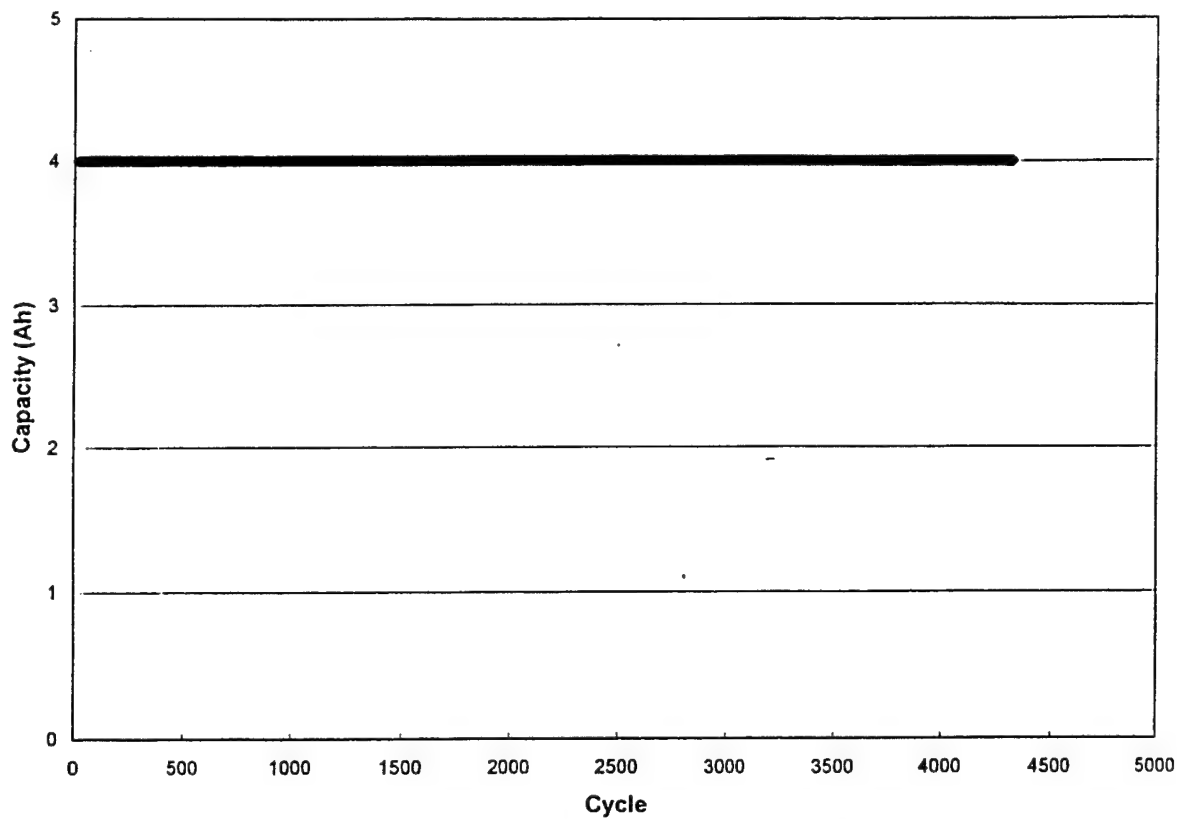


Figure 52. Accelerated LEO testing with 20-Ah cylindrical Design I cell, capacity versus cycle number.

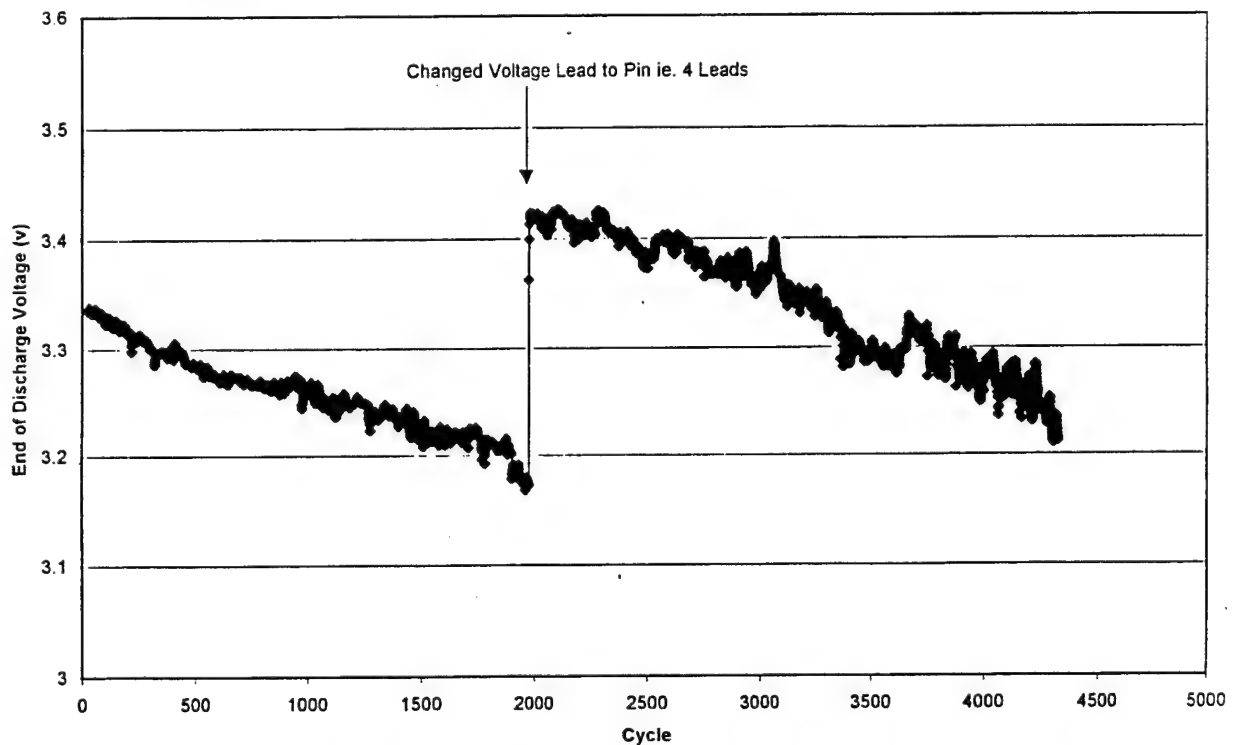


Figure 53. Accelerated LEO testing with 20-Ah cylindrical Design I cell, end of discharge voltage versus cycle number.

Figure 52 shows that after more than 5000 cycles the cell capacity has not started to fade. This should not be surprising since the Generation III Status cells showed no capacity fade until 1400 cycles at 60% dod, and these cells were made in a comparable time frame. The next figure shows the end of discharge voltage as a function of cycle number. End of discharge voltage is the true measure of cycle life at less than 100% dod. At cycle 2000 the voltage leads were changed from a two lead to a four lead system which resulted in an end of discharge voltage increase from 3.2 to 3.4V. This was due to an IR drop across the cell connectors resulting in the cell not being fully charged. The cell has now completed 5400 cycles with an end of discharge voltage of 3.1V. The cell may last 6000 cycles before the capacity starts to fade, but the test is very promising.

In conclusion, the overall performance of the Design I 20-Ah cell has been shown to be very good. Both the BATC results and USAF testing verify that the overall cycle life is exceptional. The performance in terms of specific energy and energy density at 110 Wh/kg and 219 Wh/l is acceptable for a first attempt at scale-up but this will be improved with the subsequent generations of cells. However, the low temperature performance and rate capability of the cell design is poor. As outlined in the section on electrolytes a change to the EC/EMC or EC/DMC/DEC solvent will enhance the performance for the next set of deliverable cells. The poor rate capability will be addressed in Task 4.0 where the Design II 25-Ah cell is discussed.

2.5 Task 5.0. 25-Ah Design II Cell Development

The performance of the 20-Ah cylindrical cell was as projected and showed superior specific energy over the prismatic cell and had cycle life equivalent to industry standards. However, there were two limitations of the cell design: low temperature performance and rate capability. The low temperature performance of the Design II 25-Ah cell is an improvement over the 20-Ah Design I cylindrical cell with an electrolyte change from 1M LiPF₆ EC/DEC 1:1 to 1M LiPF₆ EC/EMC 1:3. The Design II cylindrical cells use the same width of electrodes as the prismatic cell and therefore have good rate capability as discussed below. The general assembly drawing of this cell is given in Figure 54. The design characteristics of this design are as follows:

- o GTM seals are larger (0.187"φ) and made of Ta which is flattened, drilled and threaded (4-40)
- o Lower pressure (150 psi) and larger opening (0.500"φ versus 0.3125"φ) rupture disc
- o Electrode dimensions
 - Positive electrode 639 x 8.80 x 0.017 cm
 - Negative electrode 656 x 9.10 x 0.011 cm
- o Performance
 - 27.3 Ah, 122 Wh/kg, 253 Wh/l

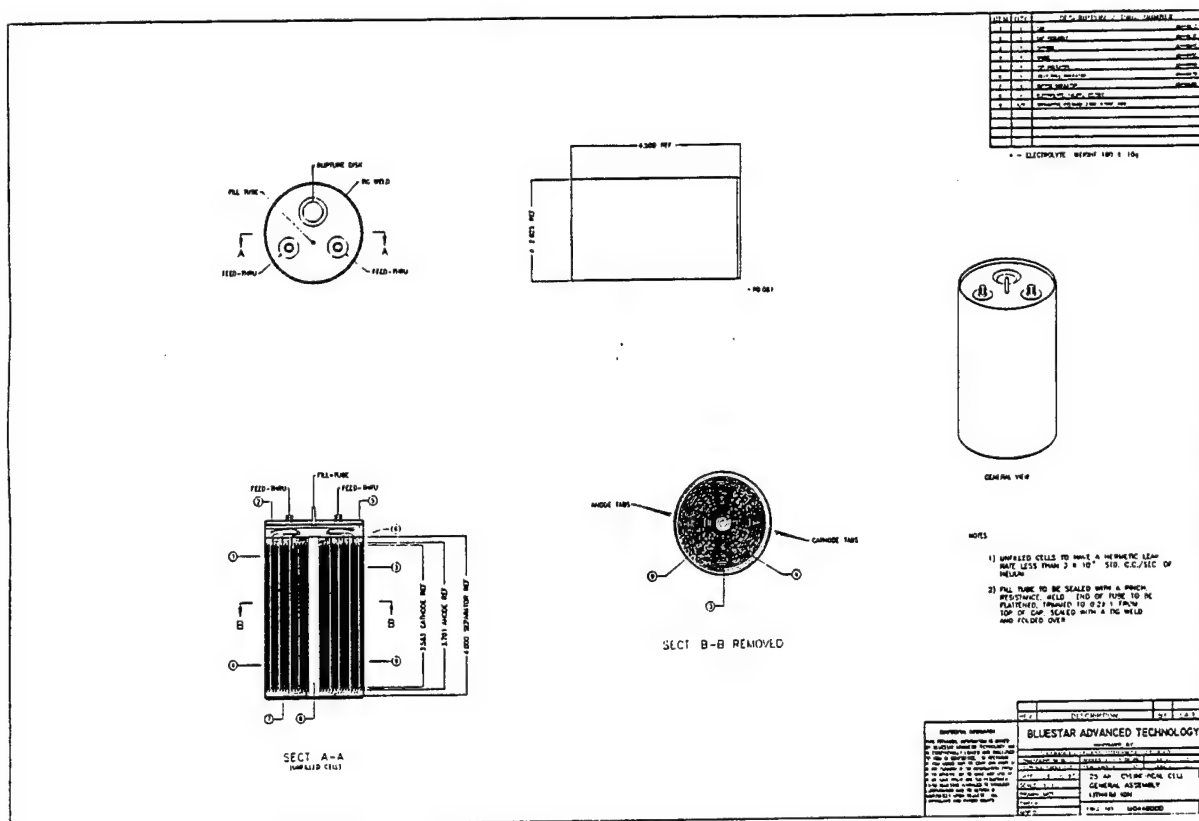


Figure 54. General assembly drawing of 25-Ah Design II cylindrical cell.

The performance data of the 10 cells delivered to the USAF in May 1998 are shown in Table 20.

When Design II 25-Ah cells delivered in May 1998 were compared to the Design I cells delivered in May 1997, a large improvement in the standard deviation of cell mass (17 to 8), capacity (0.7 to 0.4) and energy density (6 to 4) was achieved. The standard deviation for specific energy was unchanged. This indicates that the processing of the electrodes has been tightened considerably.

The 25-Ah Design II was developed to enhance rate capability. The poor rate capability of Design I was due to the presence of only three tabs for each very long electrode. To enhance the rate capability the width of the electrodes was increased two-fold, but the number of tabs was kept the same. The maximum distance between the tabs is halved, as shown in Table 21.

Table 20. Cell mass, capacity and performance of 25-Ah Design II cylindrical deliverable cells.

Cell ID.	Cell Mass, g	Capacity, Ah	Specific Energy, Wh/kg	Energy Density, Wh/l
25AhC016	832	27.6	122	255
25AhC019	823	26.9	121	249
25AhC022	837	26.9	118	248
25AhC024	824	26.5	119	246
25AhC025	828	27.3	122	253
25AhC027	813	27.2	124	253
25AhC028	828	27.4	123	254
25AhC029	838	28.0	123	258
25AhC031	817	27.5	125	256
25AhC033	827	27.5	123	254
Average	827	27.3	122	253
Std. Dev.	$\sigma = 8$	$\sigma = 0.4$	$\sigma = 2$	$\sigma = 4$

Table 21. Comparison of electrode characteristics of Design I and Design II cells.

Design Characteristic	First Generation Design I	Second Generation Design II
Cathode length, cm	1300	639
Cathode width, cm	4.4	8.8
Max. distance to tab, cm	217	107
Anode length, cm	1330	656
Anode width, cm	4.7	9.1
Max distance to tab, cm	222	110

Due to the importance of rate capability associated with the Design II 25-Ah cell, the first test was to compare the rate capability of this design to that of the Design I cylindrical cells. The rate capability of the Design II cells was superior to the Design I cells especially at the C rate. The comparison of rate capability is shown in Figure 55.

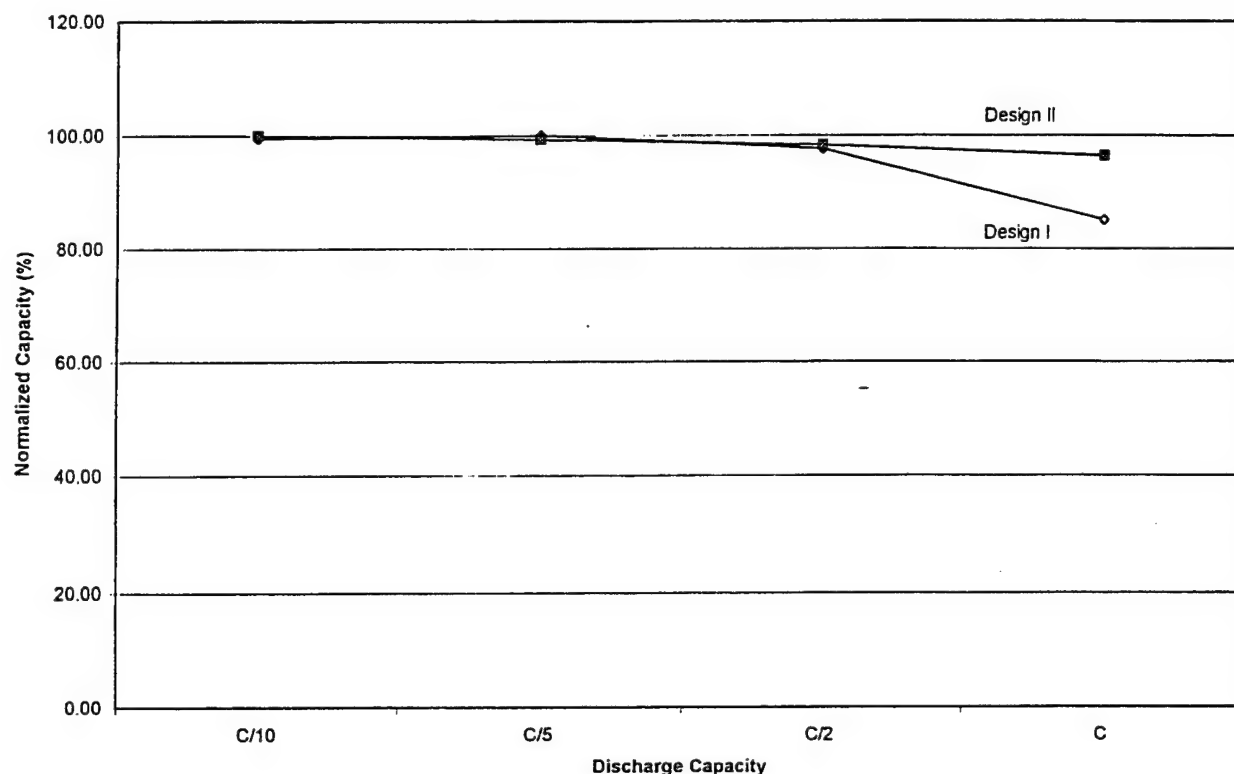


Figure 55. Comparison of rate performance between Design I and Design II cylindrical cells.

The mass analysis of the Design II 25-Ah cylindrical is shown in Table 22. When compared to the Design I cell most of the components contribute very similar amounts to the overall mass. The positive electrode contributes 37.9% of the total mass compared to 36.9% for the Design I cell. The largest difference between the two cell designs can be found in the negative electrode. The graphite contributes 10.0% to the cell mass for both Design I and II. However, the copper foil contributes 6.7% of the total mass for Design II but 8.4% for Design I, because thinner copper foil was used: 0.0004" for Design II 0.0005" for Design I.

Table 22. Cell mass analysis of 25-Ah Design II cell.

Component	Mass, g	%
Can	109	13.2
Cap assembly		
- Cap blank	13.7	1.7
- GTM seals, rupture disk, Fill tube	6.8	0.8
Total	20.5	2.5
Electrolyte		
- EMC	116.9	14.2
- EC	51.4	6.2
- LiPF ₆	23.6	2.9
Total	191.9	23.3
Positive electrode		
- LiCoO ₂	246.9	30.0
- 0.001" Al Foil	40.5	4.9
- Binder	8.1	1.0
- Conducting	16.3	2.0
Total	311.8	37.9
Negative electrode		
- Graphite	82.8	10.0
- 0.0004" Cu foil	55.3	6.7
- Binder	9.7	1.2
- Conducting	4.9	0.6
Total	152.7	18.5
Fiddley bits		
- Positive tabs	1.7	0.2
- Negative tabs	3.4	0.4
- Insulators	4.6	0.6
- Positive tape	1.9	0.2
- Negative tape	3.5	0.4
- Separator	23.4	2.8
Total	38.5	4.6
Total	824.4	100

The first cells of this design have been tested at the C/5 and the C/2 rates. The results for cycle life is shown in Figure 56 and 57.

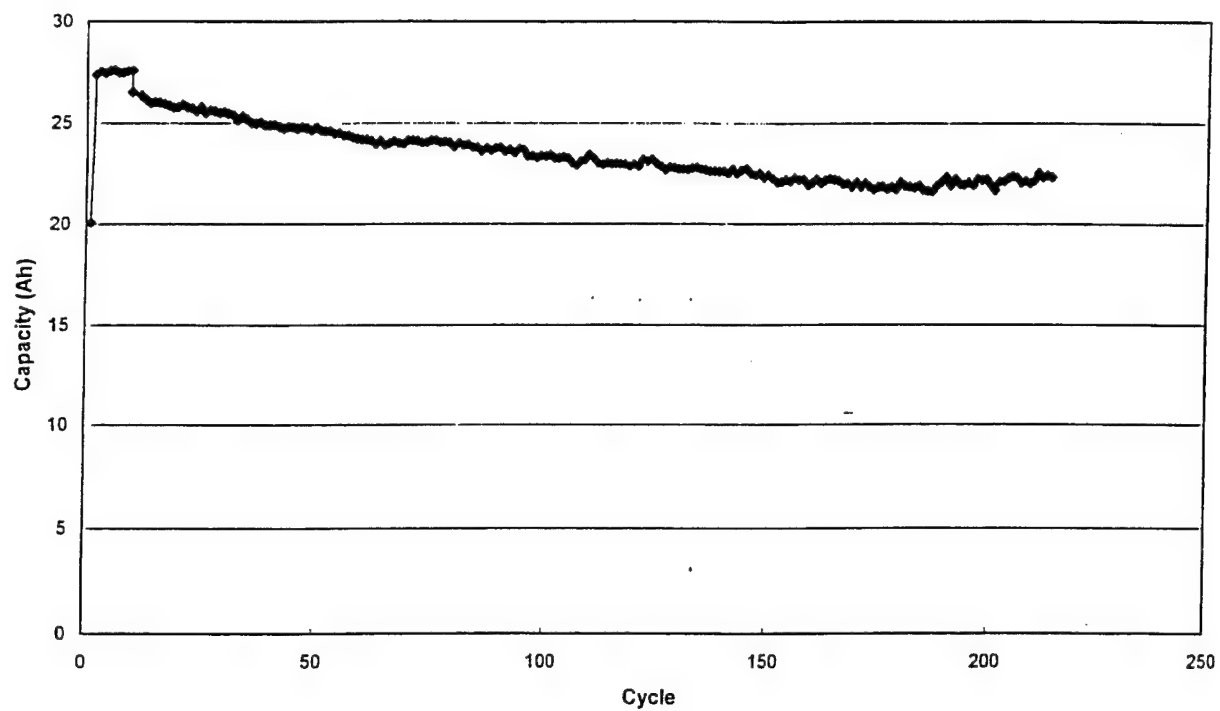


Figure 56. Cycle life testing, 25-Ah cell at C/5 to 100% dod.

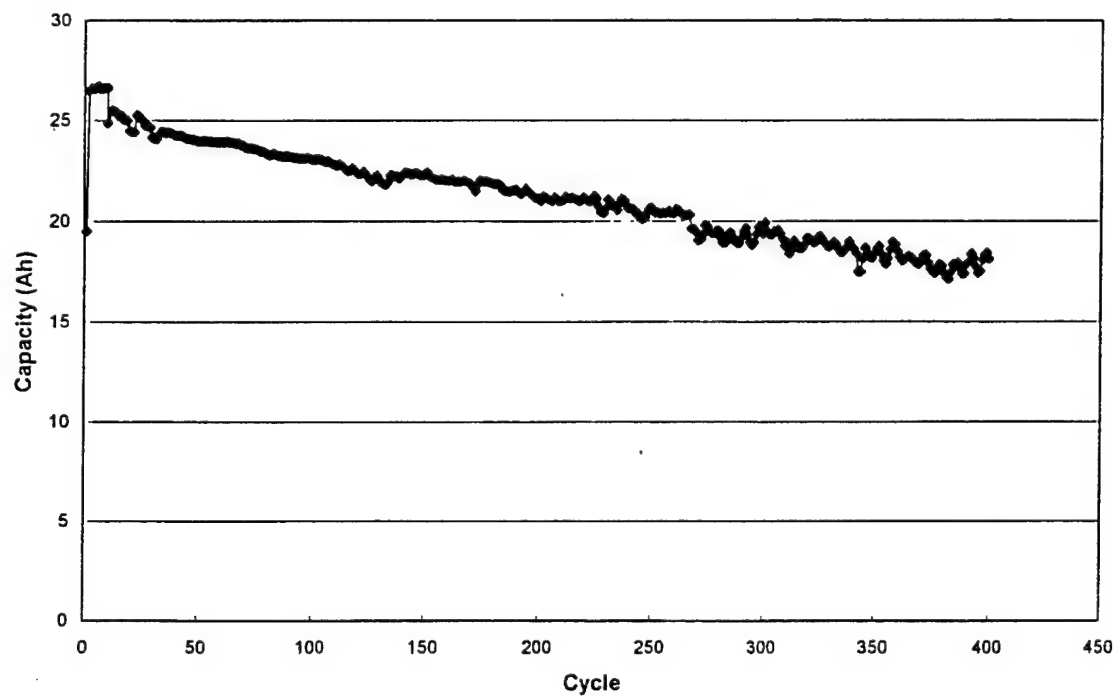


Figure 57. Cycle life testing, 25-Ah cell at C/2 to 100% dod.

The cycle life performance of Design II cells does not appear to be as good as the Design I cells.

Several design and processing changes were made to enhance both rate capability and specific energy. Previously, both positive and negative electrodes were dried at 110 °C. However, when BATC started manufacturing larger cells it was discovered that the negative electrodes were expanding substantially (20%) after drying at 110 °C which was effecting capacity. If the temperature was changed to 65 °C the negative electrode would expand only 8%. If the negative electrodes were dried at room temperature no expansion was noted. To determine the effect of negative electrode drying temperature on performance, a series of C cells were prepared with the negative electrodes dried at room temperature, 65 °C or 110 °C. Initial testing showed that the cells with the negative electrodes dried at 65 °C showed the best coulombic efficiency. To increase specific energy the Design II 25-Ah, 45-Ah and DD negative electrodes were dried at 65 °C. After the deliverables were sent the test results have shown no difference in capacity fade for the three drying temperatures. Therefore, it is assumed that the testing at JPL will show that the Design II 25-Ah cells have equivalent cycle life to the first cells delivered.

The Design II 25-Ah cells replaced the 0.0005" copper foil with 0.0004" copper foil as the negative electrode current collector which reduced the contribution of that component to the cell mass. This change was partially responsible for the higher specific energy of Design II: 122 Wh/kg versus 110 Wh/kg for the Design I cell. The electrodeposited copper is also cleaner than the copper which is calendered to desired thickness.

To increase the current collection the tabs were changed from nickel to copper and the thickness doubled. Changing the current collector and negative electrode tabbing is not thought to affect capacity fade.

Another change from the Design I 20-Ah cell was the 1M LiPF₆ EC/DEC 1:1 electrolyte was replaced with 1M LiPF₆ EC/EMC 1:3. There is no information at the moment to suggest that the new electrolyte will result in a premature end of life. Another area that must be addressed is the weight of electrolyte. Further studies into negative electrode drying temperature and electrolyte fill weight will be evaluated.

Design II has better rate capability than Design I as projected. Also, as illustrated by the reduced cell to cell weight variation of the deliverable cells, BATC has made progress in controlling manufacturing parameters. The enhanced manufacturing control is partially responsible for the higher specific energy and energy density of these cells over the Design I cells. A taller design is also responsible for improved performance since the amount of head space in the Design II cells is less than the Design I cells due to the smaller diameter of Design II. Finally the use of low temperature electrolyte improved the low temperature performance of the Design II cells.

2.6 Task 6.0. 45-Ah Cylindrical Cell Development

The objective of this task was to complete the secondary stage of scale-up of the technology. The successful completion of the task was demonstrated by the delivery of 10 cells to the USAF in May 1998. Due to the success of the first scale-up no de-mountable cells of this format were attempted. The general assembly drawing for the cell is shown in Figure 58. The design characteristics of the cell are very similar to the 25-Ah cell with the following components.

- o GTM seals (0.187"φ) are Ta which is flattened, drilled and threaded (4-40)
- o Low pressure (150 psi) rupture disc 0.500"φ opening
- o Electrode dimensions
 - Positive electrode 526 x 16.1 x 0.017 cm
 - Negative electrode 540 x 16.4 x 0.011 cm
- o Performance
 - 37.6Ah, 117 Wh/kg, 244 Wh/l, LK-702, LiCoO_2
 - 49.5 Ah, 141 Wh/kg, 321 Wh/l, LK-702, $\text{LiCo}_x\text{Ni}_{1-x}\text{O}_2$

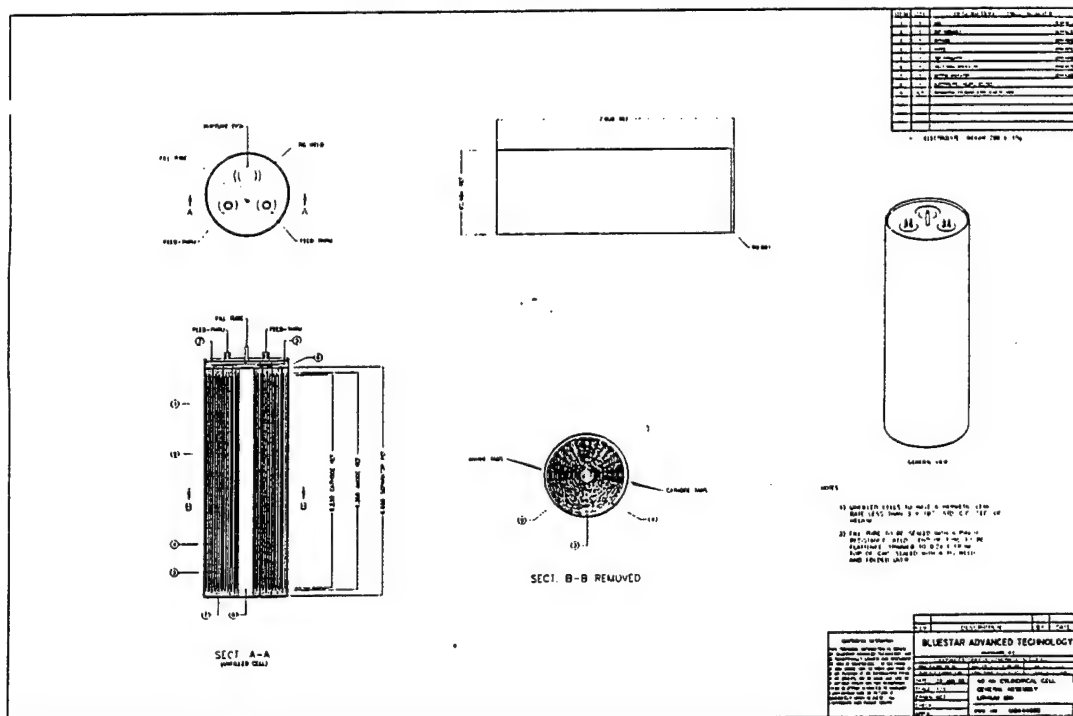


Figure 58. General assembly drawing for 45-Ah cylindrical cell.

The performance characteristics of the 10 cells delivered to the USAF are outlined in Table 23. Several comments concerning this cell format are appropriate at this point. Due to the success of the 10-Ah and 20-Ah prismatic cells and the specific energy and rate capability improvement from the Design I to Design II cells, it was decided to quickly move to the 45-Ah cell size. In retrospect the jump to the larger format was too rapid and more testing and improvements were required. However, BATC now has a greater understanding of the problems with the design and

is actively seeking ways to enhance performance. Several problems were encountered during the construction of the cells. One of the problems was associated with electrode processing, which was mentioned briefly in the section concerning the Design II cylindrical cell. A second was due to formation techniques and a third due to testing. These will be dealt with in the order in which they were noted.

Table 23. Cell performance for 45-Ah cylindrical cells.

Cell Id.	Cell Mass, g	Capacity, Ah	Specific Energy, Wh/kg	Energy Density, Wh/l	Cycle Life			
					Rate	Cycle No.	dq/dc	EOL
45AhC003 ¹	1164	34.6	101	224	C/2	350	0.019	493*
45AhC004 ¹	1220	38.5	108	250	C/2	300	0.025	413*
45AhC005 ¹	1192	36.2	103	235	C/5	311	0.014	657*
45AhC006 ¹	1169	34.1	99	221	C/5	319	0.016	493*
45AhC010 ¹	1197	37.5	105	243	C/2	701	n/a	531
45AhC012 ²	1318	42.9	121	278	C/2	100	0.037	304*
45AhC015 ²	1322	46.4	129	301	C/2	150	n/a	150
45AhC016 ²	1320	43.5	122	282	C/2	500	n/a	288
45AhC017 ²	1305	44.4	126	288	C/2	132	0.031	354*
45AhC024 ²	1245	40.9	120	266	C/2	200	0.029	381*
45AhC025 ²	1209	35.8	108	232	C/2	155	0.040	249*
45AhC026 ²	1220	39.4	117	256	C/2	120	0.009	723*
45AhC028 ² LiNi _x Co _{1-x} O ₂	1233	49.5	141	321	C/2	50	0.078	176*
45AhC029 ² LiNi _x Co _{1-x} O ₂	1235	48.4	136	314	C/2	50	0.064	178*

¹ Dried negative electrode at 110°C under vacuum

² Dried negative electrode at room temperature under vacuum

* Projected

The first 45-Ah cells built at BATC exhibited poor specific energy and energy density. The key to energy density in any battery is to maximize the amount of active components in the cell. For lithium ion cells the maximum amount of active components is determined by the density of the electrodes. Since thickness of both electrodes is measured before and after drying, any changes in density are noted. The drying procedure previously used for both electrodes involved heating the electrodes under vacuum at 110 °C for 72 hours. The vacuum is monitored with a vacuum gauge and the pressure routinely drops below 100 microns. The thickness of the positive electrode does not change during drying. However, the negative electrode relaxes during drying

and increases in thickness. Therefore, one method to increase specific energy and energy density is to arrest the expansion of the negative electrode. To better understand the effect of temperature on the relaxation of the negative electrode, negative electrodes were dried at three different temperatures: 110 °C, 52 °C and 23 °C, under vacuum for 72 hours and the thickness was measured before and after. The results are shown in Table 24

Table 24. Drying temperature and negative electrode expansion.

Negative Electrode	Drying Temperature (°C)	Thickness Before (mm)	Thickness After (mm)	% Increase
LK-702, 0.0004" Cu	110	0.16	0.195	21.9
LK-702, 0.0004" Cu	110	0.135	0.165	22.2
LK-702, 0.0004" Cu	110	0.16	0.195	21.9
LK-702, 0.0004" Cu	110	0.13	0.155	19.2
LK-702, 0.0004" Cu	110	0.17	0.215	26.5
LK-702, 0.0004" Cu	52	0.155	0.17	9.7
LK-702, 0.0004" Cu	52	0.165	0.175	6.1
LK-702, 0.0004" Cu	52	0.165	0.175	6.1
LK-702, 0.0004" Cu	23	0.13	0.13	0.0
LK-702, 0.0004" Cu	23	0.125	0.135	8.0
LK-702, 0.0004" Cu	23	0.17	0.17	0.0

The data from the negative electrode drying experiment highlights the effect of drying temperature on electrode relaxation. However, an even greater concern is the variation in electrode thickness between the electrodes before drying. The reason for the variation is probably due to the press roller. The manufacturing process followed at BATC is to slit the electrodes to width and then compress the electrodes. A drawback of this method is that any warping or curving of the electrodes will make winding difficult. The electrodes are slit before compression because of equipment limitations. The press roller has a maximum load pressure of one metric ton over the width of the roller (250 mm). If the full width of the roller is used the pressure will be 220 pounds per linear inch (pli). For the 25-Ah design II cell the pressure

exerted on the negative electrode is 615 pli while for the 45-Ah negative electrode the pressure exerted is 335 pli. With the wider electrodes for the 45-Ah, the required compression is greater than the equipment can deliver. With the present press roller it is impossible to press the material more than once since the material will fold on itself and crease.

Because the negative electrodes dried at room temperature did not expand it was decided that the next set of 45-Ah cells would use negative electrodes dried at room temperature. The cell capacity and therefore specific energy and energy density did increase substantially as shown in Table 23 which lists the cell performance and electrode drying conditions. When the cells with the negative electrodes dried at room temperature are compared to those dried at 110 °C, as shown in Table 25, the average capacity increases from 36.2-Ah to 41.9-Ah, with a corresponding increase in specific energy and energy density from 103 to 120 Wh/kg and 235 to 272 Wh/l respectively. The differences are quite staggering and the second set of 45-Ah cells would have been successful if all of the cells had not bulged substantially. Whether this was due to the larger amount of active material in the cell or due to incomplete drying at room temperature or because of the cell design itself was not known. However, as shown previously the pressure increase is restricted to the first half hour of the formation cycle. The gas evolution is probably associated with moisture reacting with the newly formed Li_xC_6 . Also, as observed with the 20-Ah Design I cell the temperature increase is very rapid and reaches a maximum in the first hour of the charge cycle. The bulging of the 45-Ah cells was noted almost immediately. One possible method to stop the bulging was to use a slower formation rate on the first charge step. To determine what effect formation rate would have on cell bulging and formation temperature two 45-Ah cells were charged at either the C/5 or C/10 rate. The temperature at the top of the cell was monitored and the results are shown in Figure 59.

Table 25. 45-Ah cell performance with different negative electrode drying temperatures.

Performance Parameter	Drying Temperature	
	110 °C	Room Temperature
Average Capacity (Ah)	36.2	41.9
Specific Energy (Wh/kg)	103	120
Energy Density (Wh/l)	235	272

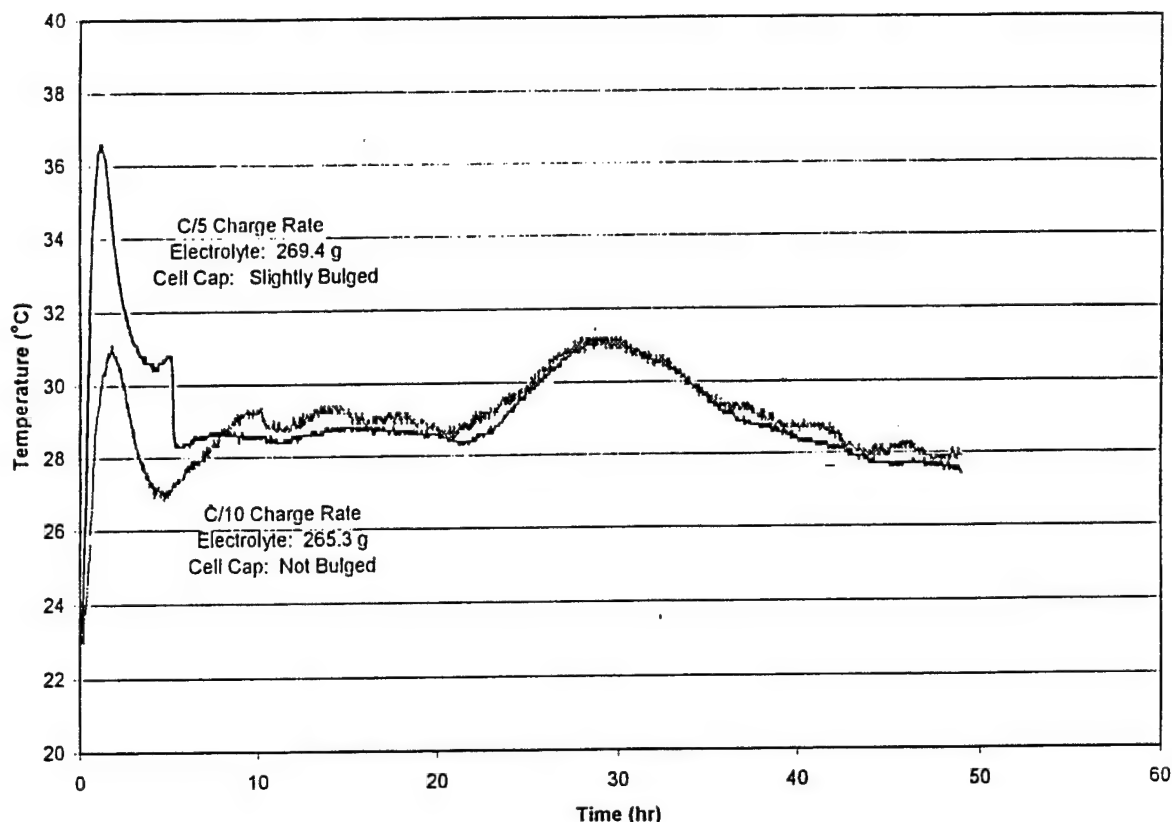


Figure 59. Cell temperature during the first charge cycle at two different rates for 45-Ah cylindrical cells.

The cell charged at the C/5 rate reached a maximum temperature of 37 °C while the cell charged at the C/10 rate reached a maximum of 31 °C. The cell charged at the C/5 rate reached its maximum temperature faster than the cell charged at the C/10 rate. As with the data previously discussed, the temperature trace shows the presence of a second process occurring as the potential approaches a maximum. The abrupt drop in temperature at the C/5 rate corresponds to when the formation step stops and the cell is allowed to rest at OCV. Another consequence of the slower charge rate was that the cap of the cell charged at C/5 bulged a small amount while the cap of the cell charged at C/10 did not bulge.

An unpredicted consideration regarding the larger format cells was cell resistance. If the average resistance of a C cell is 120 milli-ohms, the 45-Ah cells should have a resistance of about 4 milli-ohms since the capacity is close to 30 times greater. The resistance of all the cell sizes made at BATC is shown in Figure 60.

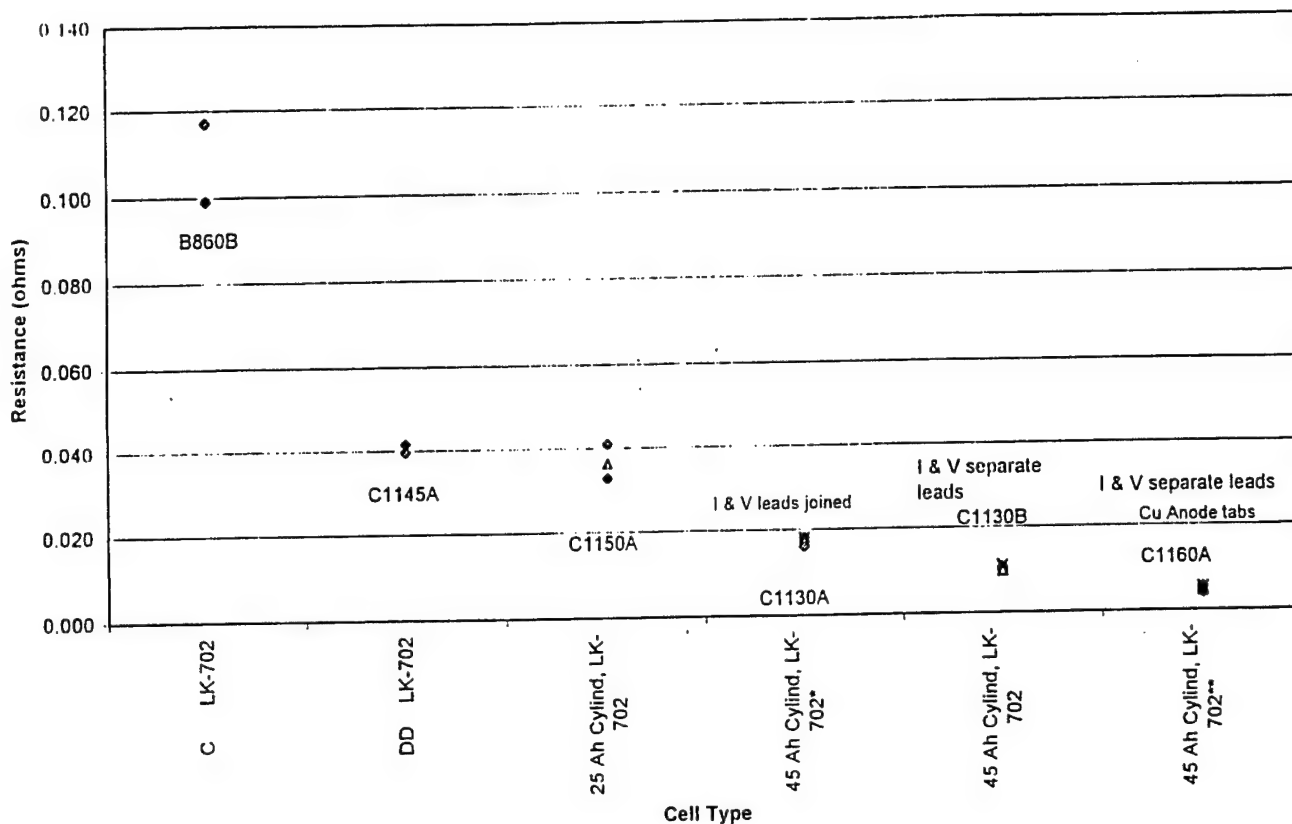


Figure 60. Pulse discharge resistance as a function of cell size.

When the first 45-Ah cells were tested the resistance was first measured at approximately 18 milli-ohms, which is high for cells of this size. The resistance of the cell was really lower since the voltage leads were not separated at the pin; therefore, the resistance of the tabs was included in the resistance. Even when the tab resistance was removed from the calculation the resistance was approximately 10 milli-ohms. While the resistance is decreasing, the value is still greater than desired. An examination of a resistance model suggests that a large amount of cell resistance is due to the tabs, more specifically the nickel tabs used for the negative electrode. In order to reduce the cell resistance the nickel tabs were replaced with copper tabs. The resistance of cells made with copper negative tabs was 4 to 5 milli-ohms which is in the range expected.

The effect of the voltage leads was extremely dramatic especially for the cells tested at high rates. When the first 45-Ah cells were tested at the C/2 rate the capacity of the cells was the same as the 25-Ah Design II cells. There was obviously something extremely wrong with the method of testing. By examination of the voltage versus time profiles in Figure 61 the cell with only two leads (one lead for both current and voltage) was not fully charged as shown by the voltage drop. The voltage profile for the same cell with separate current and voltage sensors is also shown in Figure 61. Figure 62 shows the effect on capacity.

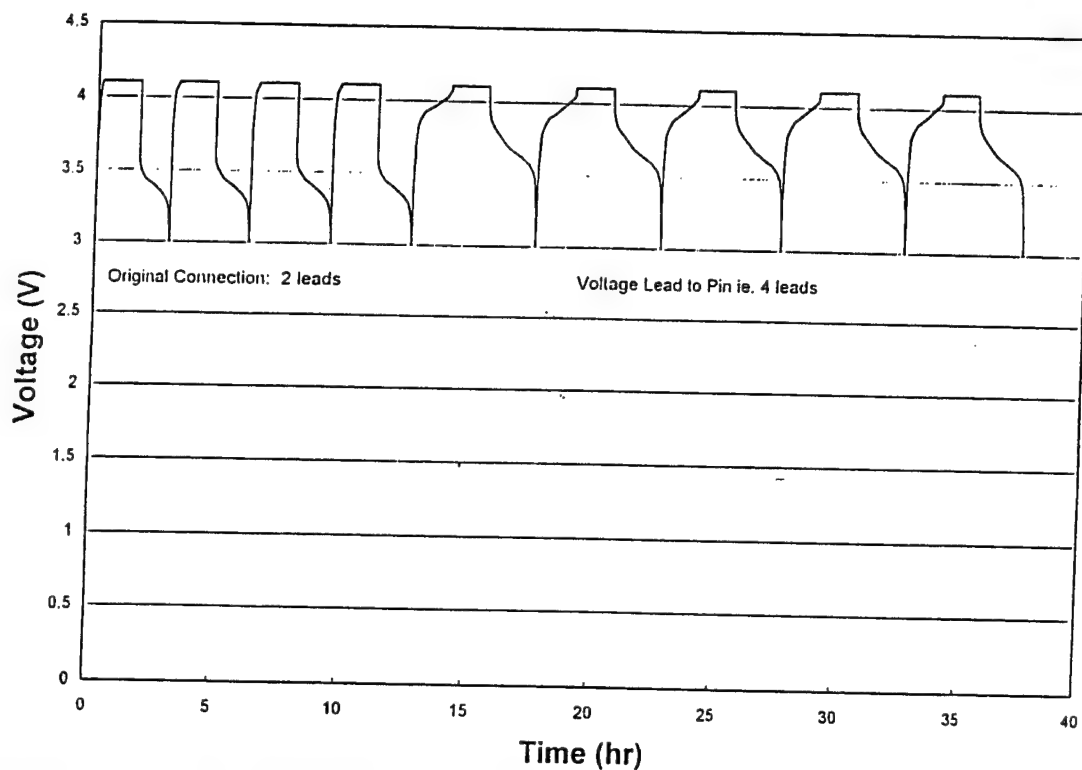


Figure 61. Effect of separate voltage leads on cell voltage during cycling for 45-Ah cylindrical cell.

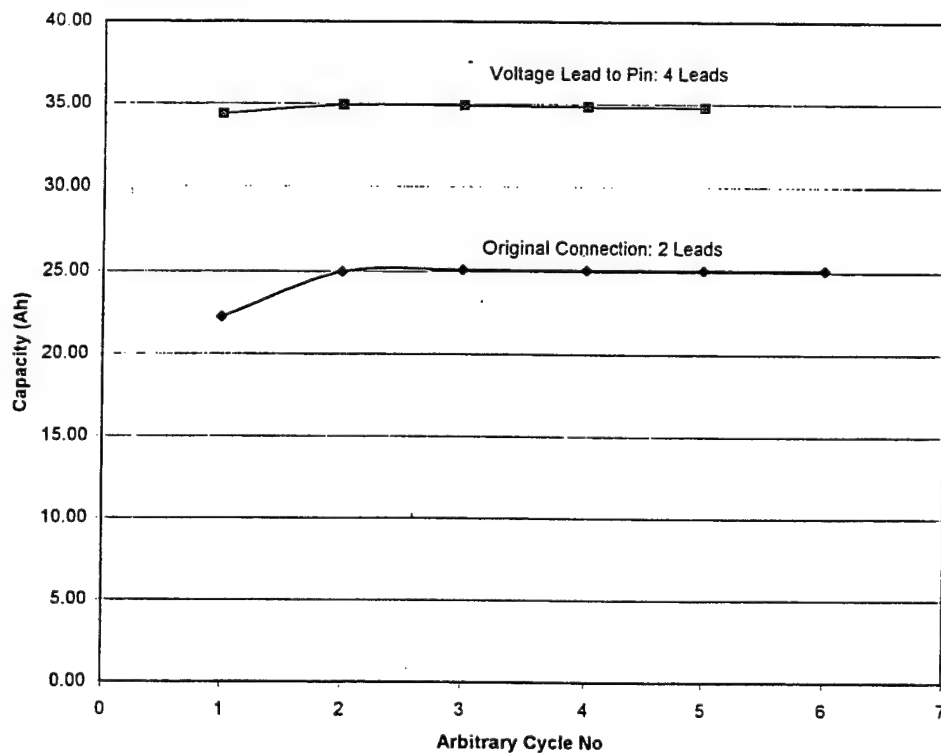


Figure 62. Effect of separate voltage leads on cell capacity during cycling for 45-Ah cylindrical cell.

By changing the voltage leads to separate wires the cell capacity increased from 25-Ah to 35-Ah. The effect of different voltage leads has the greatest effect at higher rates and hence was observed so dramatically with the 45-Ah cells. If the connectors have a resistance of 0.008 ohms and the current is 20A then the cell will only be charged to 3.94V and not 4.1V. Current versus time for the cell with connected current and voltage leads and separate voltage leads is shown in Figure 63. The cell was charged in identical manner with both types of voltage leads. As shown in Figure 63, the cell with connected and voltage leads charged at constant current for less than 30 minutes. After 1.5 hours at constant voltage, the cell was still charging at over 11A, indicating that the cell was not fully charged. In contrast, the cell with separate voltage leads charged at constant current for almost 2 hours; after 1.5 hours at constant voltage, the cell was charging at 1A, indicating that the cell was not fully charged.

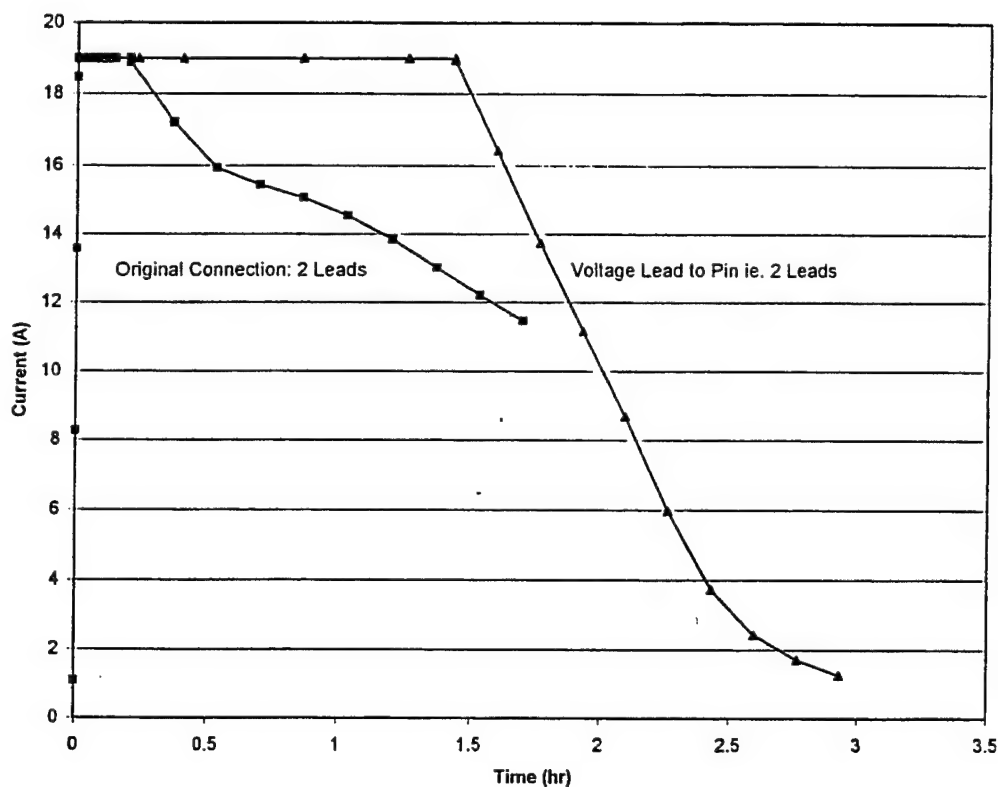


Figure 63. Current versus time during charging of 45-Ah cells with separate and combined voltage leads.

Once some of the processing and testing issues were addressed the deliverable cells could be constructed. The performance parameters of the deliverable cells is shown in Table 26. The standard deviation of the 45-Ah cells is better than the first deliverable cells (Design I) but not as good as the 25-Ah Design II cells or the DD cells discussed in the following section. However, cell performance was more disappointing than weight variability. The specific energy and energy density of the 45-Ah cells (117 Wh/kg and 244 Wh/l) was not as good as the Design II 25-Ah (122 Wh/kg and 253 Wh/l) and not much better than the DD cells (105 Wh/kg and 247 Wh/l). The common factor in the latter two cells is the width of the electrodes. As discussed above the wider electrodes of the 45-Ah cell cannot be compressed to the desired density with the

equipment available at BATC.

The mass analysis of the delivered cells is shown in Table 27. Again the advantage of the thinner copper current collector is noted. The enclosure contributes only 13.4% as opposed to 15.4% for the 25-Ah cell. The positive electrode and negative electrode are 31.7% and 10.5% active as opposed to 30.0% and 10.0% for the 25-Ah cell. So there is some minimal improvement, but more was expected for a cell that is 39% larger than any other cell made at BATC. A comparison of mass analysis for the various cell sizes is shown in Table 28.

Table 26. Cell mass, capacity and performance for delivered 45-Ah cylindrical cells.

Cell Id.	Cell Mass,g	Capacity, Ah	Specific Energy, Wh/kg	Energy Density, Wh/l
45AhC031	1174	36.9Ah	115	239
45AhC032	1181	37.8Ah	118	245
45AhC034	1164	36.4Ah	115	236
45AhC035	1168	37.4Ah	118	243
45AhC036	1219	39.0Ah	118	253
45AhC039	1168	36.9Ah	115	240
45AhC040	1163	38.4Ah	122	249
45AhC041	1187	38.7Ah	118	251
45AhC042	1161	36.6Ah	117	238
45AhC044	1181	37.5Ah	115	243
Average Standard Deviation	1177 $\delta = 17.3$	37.6 $\delta = 0.9$	117 $\delta = 2.2$	244 $\delta = 5.8$

Table 27. Mass analysis for 45-Ah cylindrical cell.

Component	Mass, g	%
Can	137.4	11.8
Cap assembly		
- Cap blank	11.7	1.0
- GTM seals, rupture disk, Fill tube	6.8	0.6
Total	18.5	1.6
Electrolyte		
- DEC	100.6	8.6
- EC	138.7	12.0
- LiPF ₆	32.6	2.8
Total	271.9	23.4
Positive electrode		
- LiCoO ₂	364.6	31.7
- 0.001" Al Foil	58.6	5.0
- Binder	12.0	1.0
- Conducting	24.0	2.1
Total	459.2	39.3
Negative electrode		
- Graphite	122.2	10.5
- 0.0004" Cu foil	79.4	6.8
- Binder	14.4	1.2
- Conducting	7.2	0.6
Total	223.2	19.1
Fiddley bits		
- Positive tabs	5.5	0.4
- Negative tabs	11.3	1.0
- Insulators	4.2	0.4
- Positive tape	3.5	0.3
- Negative tape	6.5	0.5
- Separator	25.6	2.2
Total	56.6	4.8
Total	1166.8	100

Table 28. Comparison of Mass Analysis for the various cell sizes.

Component	20-Ah Design I	25-Ah Design II	45-Ah Cell	DD Cell
Cap/can	16.0%	15.7%	13.4%	23.3%
Positive electrode	36.9%	37.9%	39.3%	33.0%
LiCoO ₂	29.2%	30.0%	31.7%	26.4%
Negative electrode	20.2%	18.5%	19.1%	16.4%
LK-702	10.0%	10.0%	10.5%	9.1%

The performance of the LK-702 cells is outlined in Table 29 with the cycle life projected near to 500 cycles, as with the previous cells. The performance at the C/2 rate is shown in Figure 64 and at the C/5 rate in Figure 65.

Table 29. Cell performance for 45-Ah cylindrical cells.

Cell Id.	Cell Mass, g	Capacity, Ah	Specific Energy, Wh/kg	Energy Density, Wh/l	Cycle Life			
					Rate	Cycle No.	dq/dc	EOL
45AhC003 ¹	1164	34.6	101	224	C/2	350	0.019	493*
45AhC004 ¹	1220	38.5	108	250	C/2	300	0.025	413*
45AhC005 ¹	1192	36.2	103	235	C/5	311	0.014	657*
45AhC006 ¹	1169	34.1	99	221	C/5	319	0.016	493*
45AhC010 ¹	1197	37.5	105	243	C/2	701	n/a	531
45AhC012 ²	1318	42.9	121	278	C/2	100	0.037	304*
45AhC015 ²	1322	46.4	129	301	C/2	150	n/a	150
45AhC016 ²	1320	43.5	122	282	C/2	500	n/a	288
45AhC017 ²	1305	44.4	126	288	C/2	132	0.031	354*
45AhC024 ²	1245	40.9	120	266	C/2	200	0.029	381*
45AhC025 ²	1209	35.8	108	232	C/2	155	0.040	249*
45AhC026 ²	1220	39.4	117	256	C/2	120	0.009	723*

¹ Dried negative electrode at 110°C under vacuum

² Dried negative electrode at room temperature under vacuum

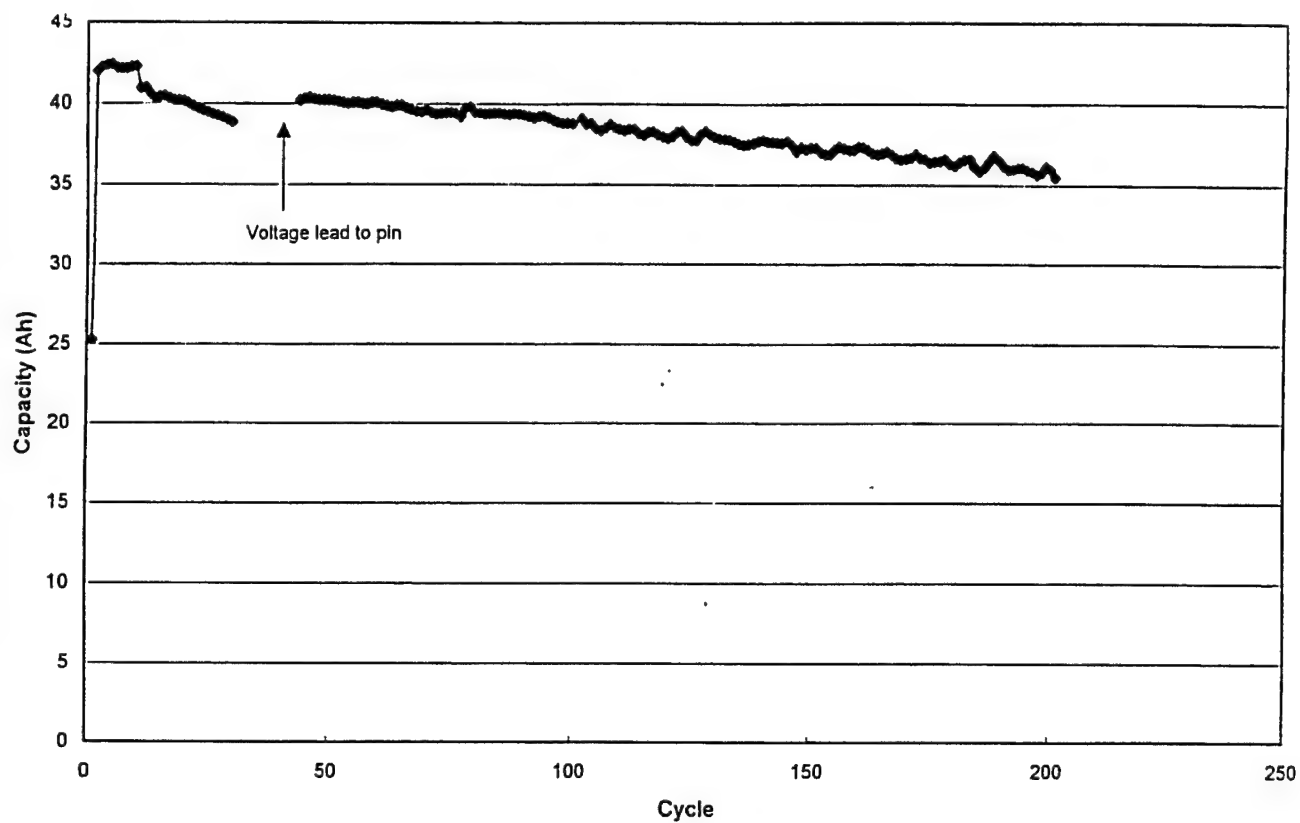


Figure 64. Cell cycling performance of 45-Ah cell at the C/2 rate to 100% dod.

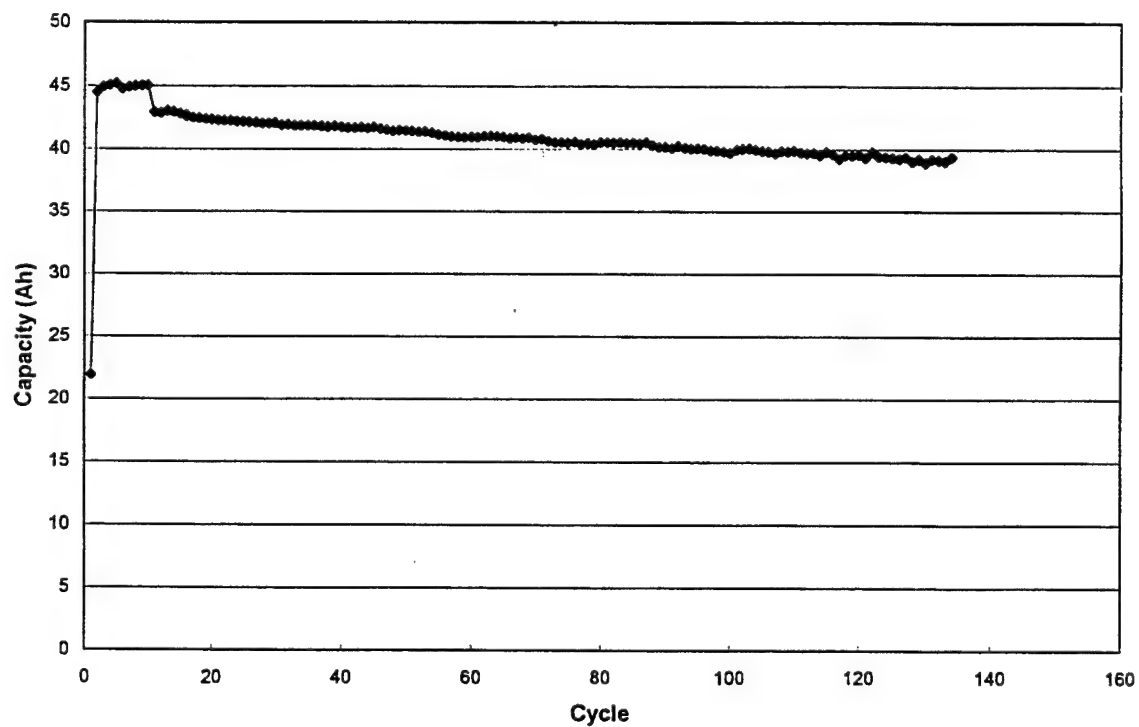


Figure 65. Cell cycling performance of 45-Ah cell at the C/5 rate to 100% dod.

Coulombic charging tests were conducted on this cell size. Coulombic charging was initiated after 200 cycles for one cell. The capacity of cycle 200 was 80% of initial capacity. The results for capacity versus cycle number are shown in Figure 66, and for charge time versus cycle number are shown in Figure 67. After 500 cycles, the cell capacity is still holding at 80% of capacity and the charge time has increased from 2 hours to 8 hours. The charge time is starting to increase exponentially and will soon become prohibitively long. Once the 45-Ah cell starts to fade in capacity the results must be compared to the Generation IV Status Cells at 75% dod.

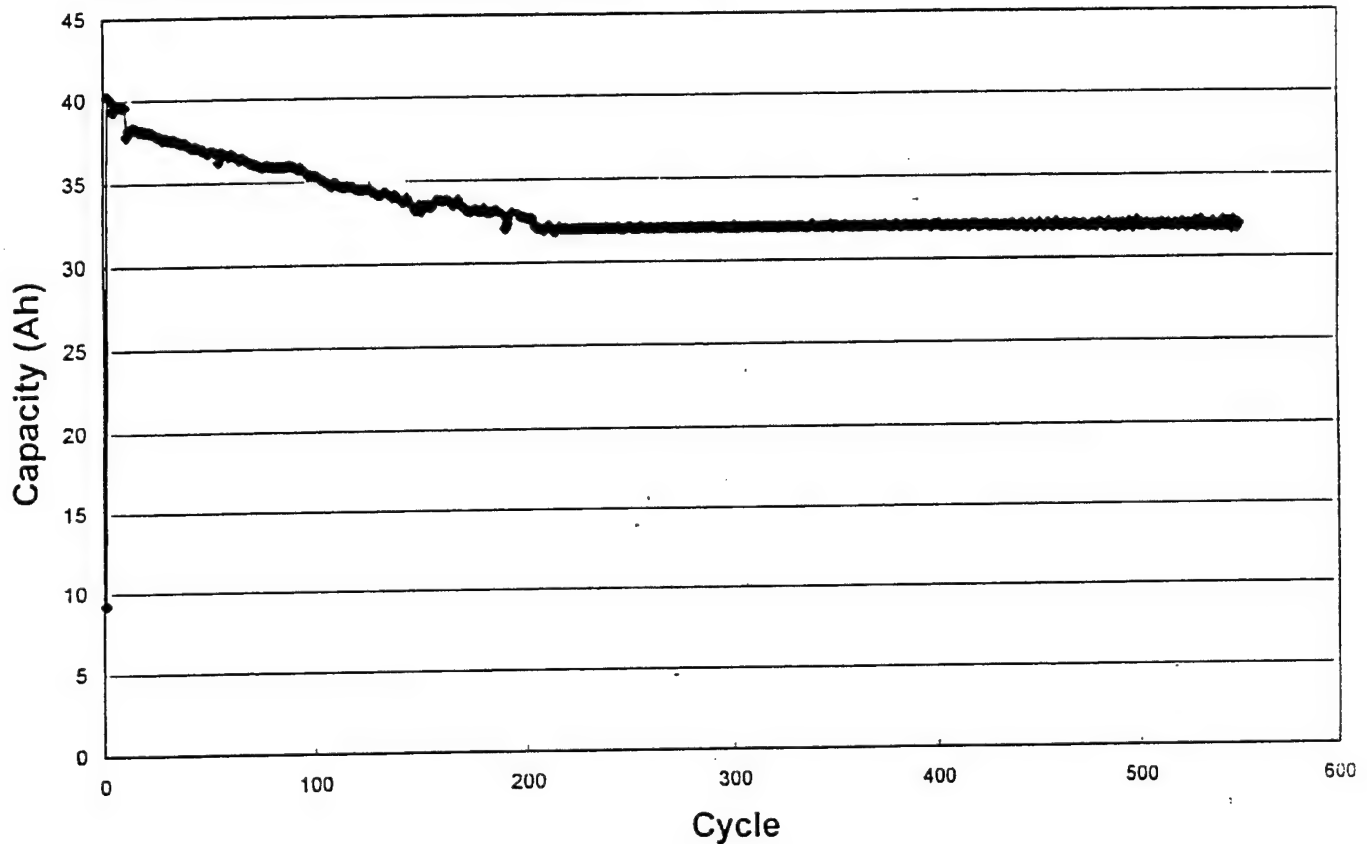


Figure 66. Coulombic charging of 45-Ah cell, capacity versus cycle number.

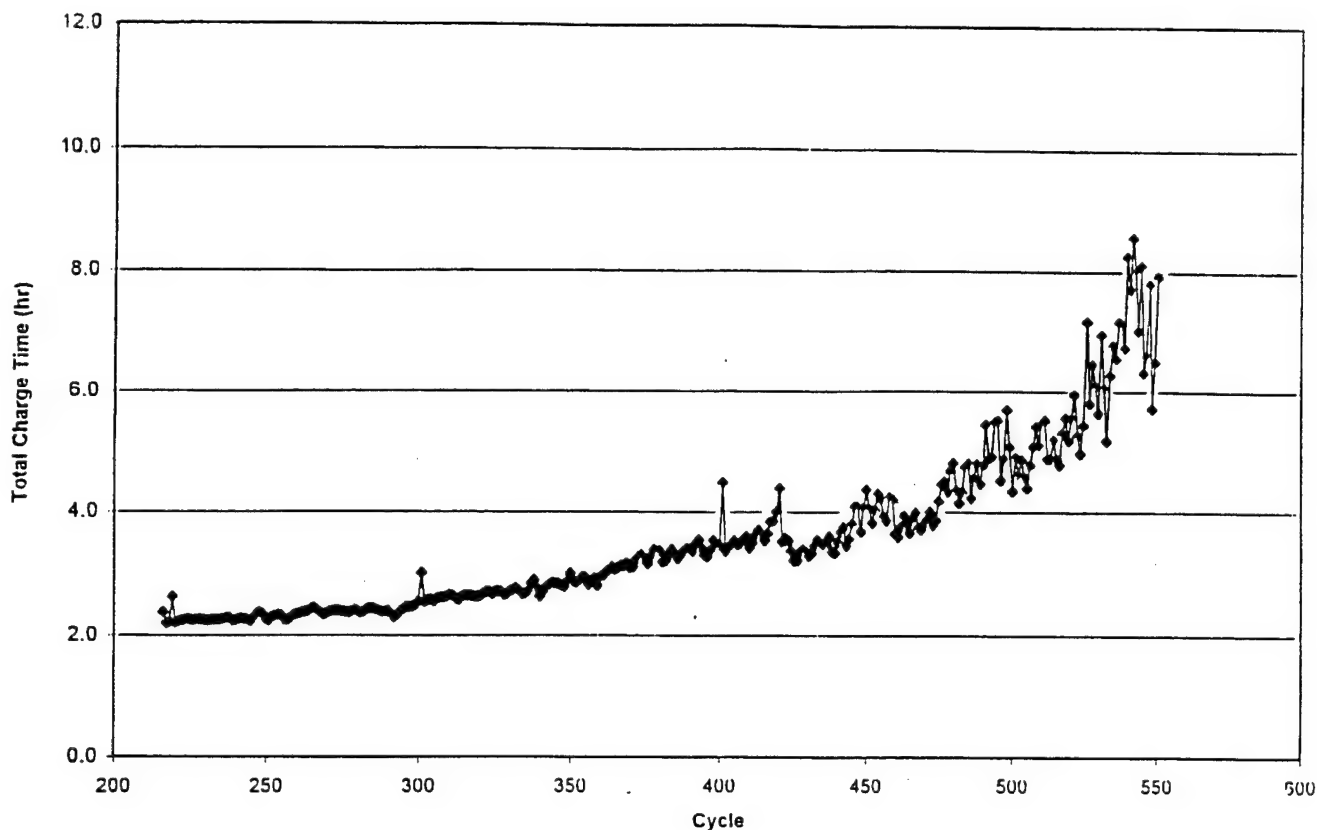


Figure 67. Coulombic charging of 45-Ah cell, charge time versus cycle number.

Coulombic charging was repeated with a 45-Ah cell at cycle 50 and was set up to cycle at 90% of capacity. The capacity graph is shown in Figure 68 and the charge time in Figure 69. To date the cell has completed 165 cycles and the charge time is five hours. If the cell cycles for another 100 cycles with a reasonable charge time this will represent an improvement over the 90% dod Status Cells, which are not charged coulombically

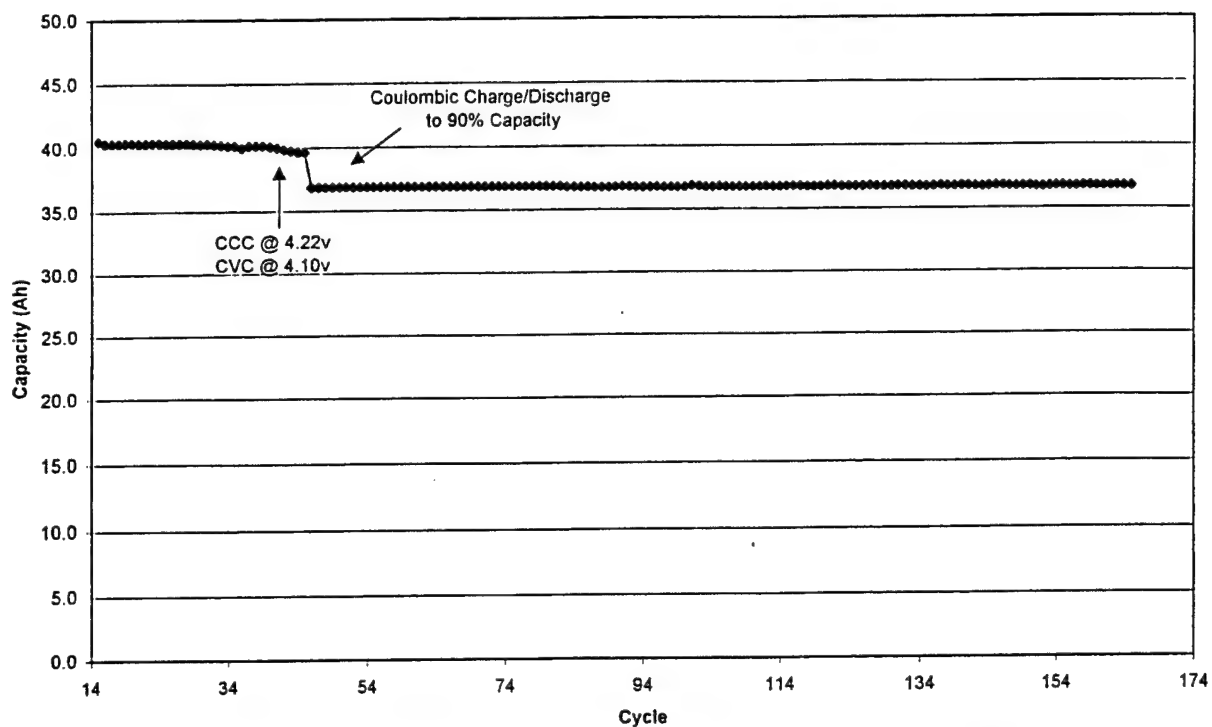


Figure 68. Coulombic charging of 45-Ah cell, capacity versus cycle number.

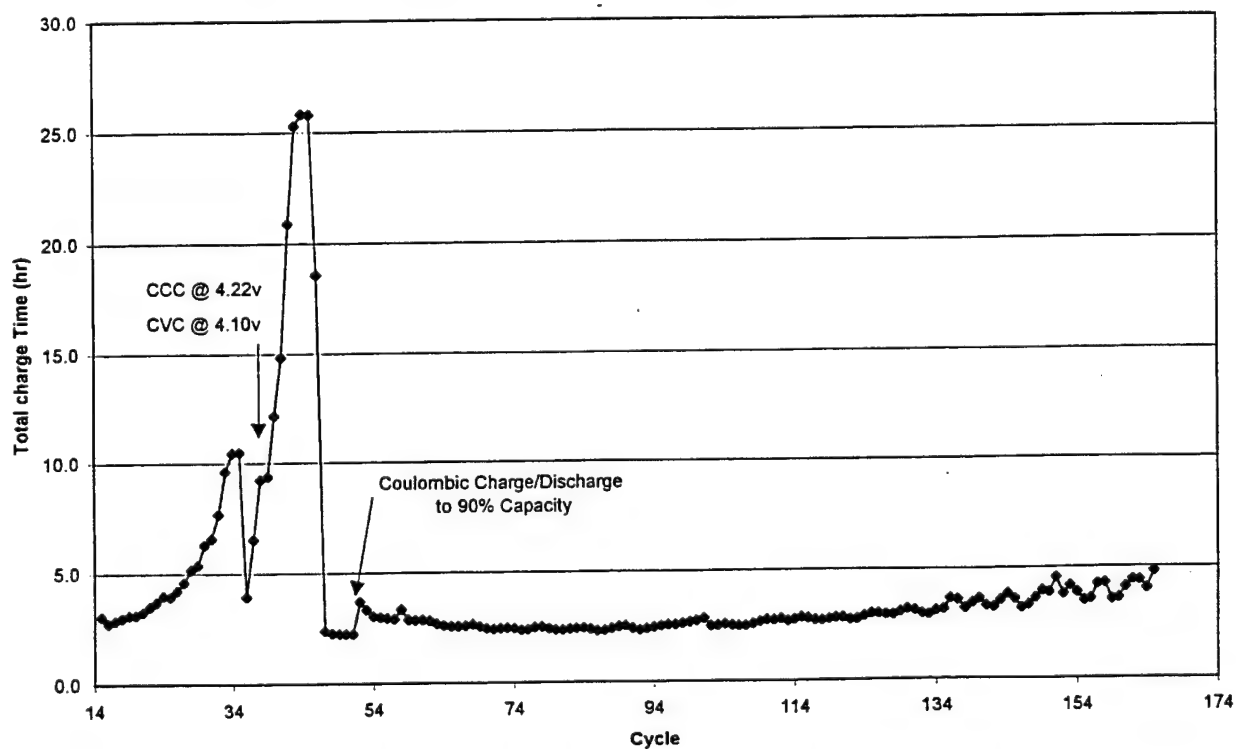


Figure 69. Coulombic charging of 45-Ah cell, charge time versus cycle number.

The Design I 20-Ah cell had poor rate capability. This led to the Design II 25-Ah cell. By extrapolation one expects that the rate capability of the 45-Ah design to be good due to the length and width of the electrodes. Also, the negative electrode tabs were changed to copper from nickel and both the negative tab and positive tabs were doubled up to allow for better current collection (see Design II 25-Ah cell). The results for the rate studies are shown in Figure 70. The rate capability of this design is very good, with the highest capacity achieved at the C/1.4 charge and discharge rate. The capacity of the Li ion technology is completely determined by the charge. Perhaps the highest capacity was achieved from the highest charge rate because the cell temperature was highest at the C/1.4 rate, and higher temperature enhances conductivity. However, the difference in capacity among all the rates is only 5%.

In a separate experiment the Design II 25-Ah cell and the 45-Ah cell were tested at high pulse discharge rates. Results for the tests are shown in Table 30. The cells were pulsed for 10 seconds and the voltage measured at 5 and 10 seconds. Then the cell was held at open circuit for 10 minutes. The specific power is also recorded in Table 30.

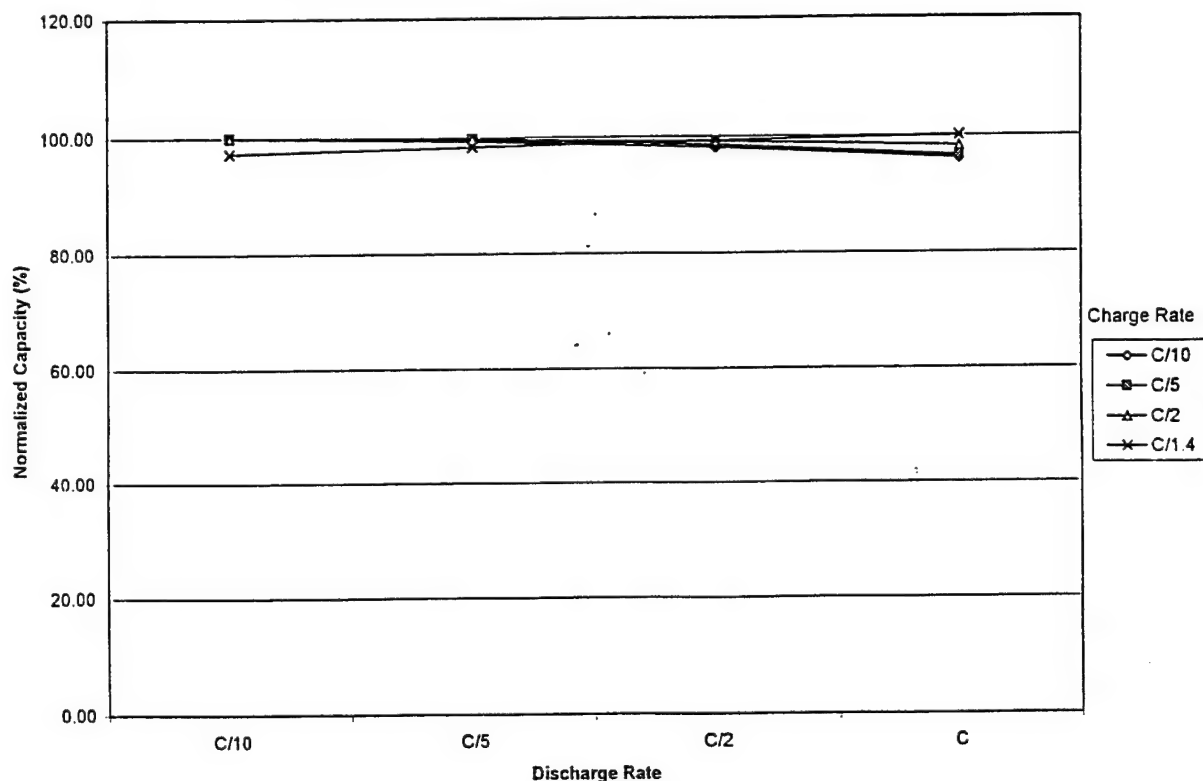


Figure 70. Rate performance of 45-Ah cylindrical cell.

Table 30. High rate pulse testing for Design II 25-Ah and 45-Ah cell.

Rate, C	Design II 25-Ah Cell				45-Ah Cell			
	5 Seconds		10 Seconds		5 Seconds		10 Seconds	
	Voltage, V	Spec. Power, W/kg	Voltage, V	Spec. Power, W/kg	Voltage, V	Spec. Power, W/kg	Voltage, V	Spec. Power, W/kg
1	3.473	104	3.454	104	3.661	127	3.646	126
2	2.963	178	2.809	168	3.294	228	3.265	226
3	1.917	173	1.481	124	2.918	303	2.837	295
4	---	---	---	---	2.459	340	2.403	332
5	---	---	---	---	2.095	363	1.999	345
6	---	---	---	---	1.752	364	---	---

As illustrated the 25-Ah cell can sustain 3C (75 A) before the voltage drops below 2.0V. The specific power is close to 170 W/kg at the 2C rate. The 45-Ah design shows excellent rate capability exhibiting 345 W/kg at the 5C rate at 2.0V after 10 seconds. The next pulse at 6C (270 A) was sustained for only 5 seconds and the cell voltage went to 0 V before the end of 10 seconds. Any attempt to repeat the test was unsuccessful. The temperature of the 45-Ah cell was monitored at the side and top of the cell. The temperature profiles are shown in Figure 71. As seen in the figure most of the heat generated during the discharge, which is quite substantial, travels out of the cell in the axial direction. The top of the cell reaches a maximum of 70 °C. During the test the cell temperature, as shown by the thermocouple on the side of the cell, gradually increases from 22 °C to 27 °C. The 45-Ah cell was then subjected to destructive physical analysis to determine why the cell could no longer support current. This revealed that the positive electrode tab, which is aluminium, had melted.

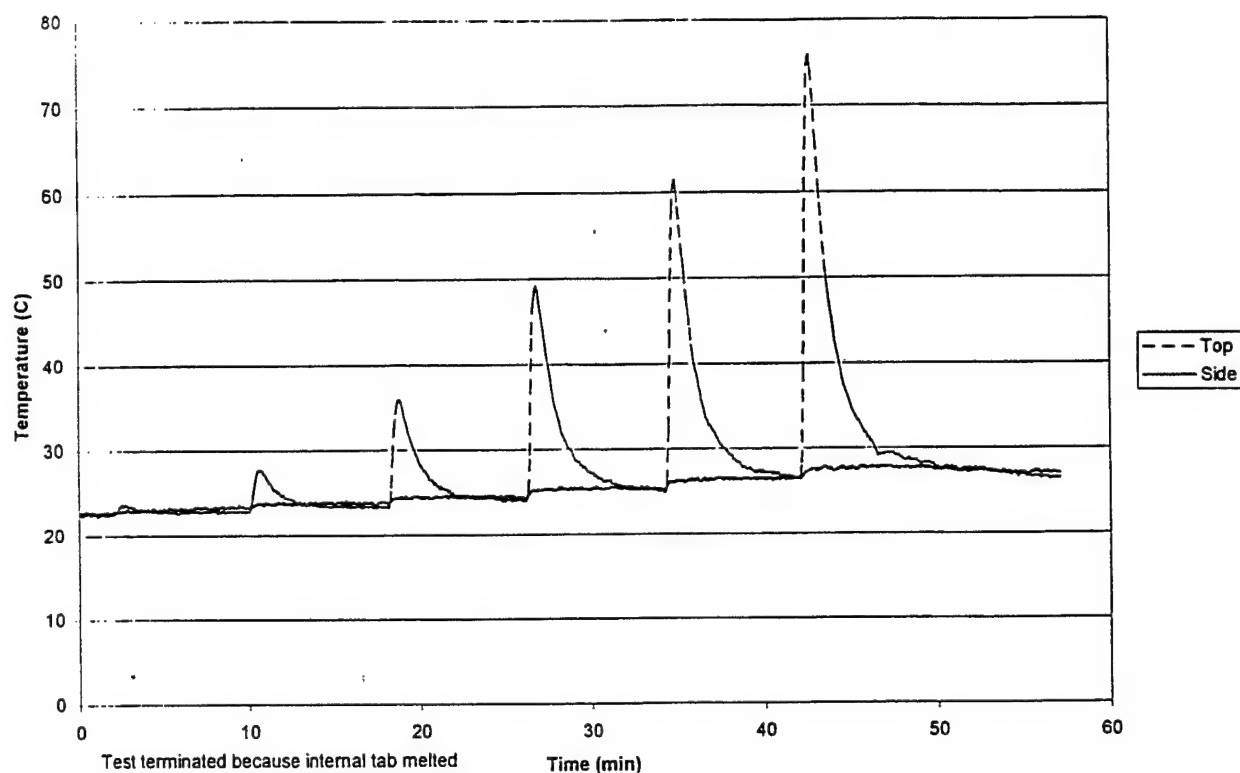


Figure 71. Cell temperature during high rate pulse testing.

With the desire for greater specific energy/energy density it was decided that the active component for the positive electrode would change to $\text{LiNi}_x\text{Co}_{1-x}\text{O}_2$ since this material is rated at 175 mAh/g. Two cells of this design were prepared: one tested at the C/5 rate and the other at the C/2 rate. The test results are shown in Figures 72 and 73. The cell capacity approaches 50-Ah at C/5 and has a specific energy of 139 Wh/kg and an energy density of 318 Wh/l. It appears that the capacity fade of these cells is greater than the fade of the LiCoO_2 system. But when the capacity of the $\text{LiNi}_x\text{Co}_{1-x}\text{O}_2$ battery is compared to a LiCoO_2 at the C/2 rate the capacity improvement of $\text{LiNi}_x\text{Co}_{1-x}\text{O}_2$ is apparent as shown in Figure 74.

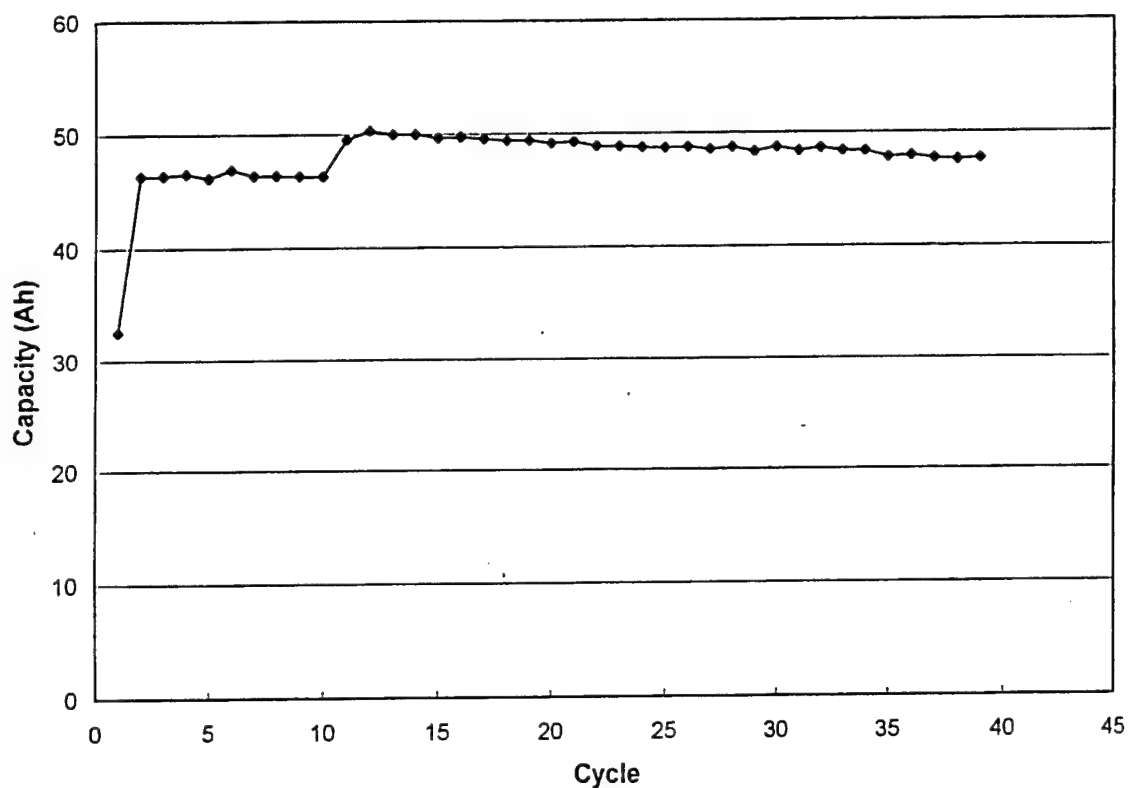


Figure 72. Cell cycling performance of $\text{LiNi}_x\text{Co}_{1-x}\text{O}_2$ 45-Ah cell at the C/5 rate to 100% dod.

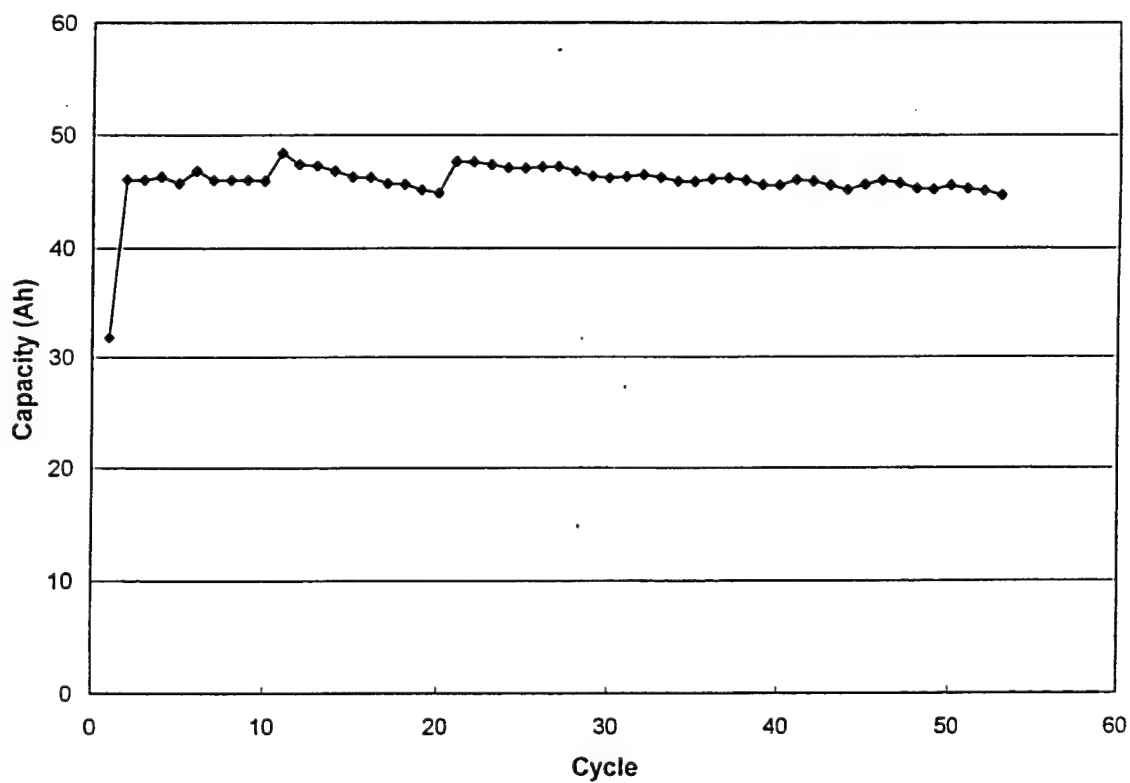


Figure 73. Cell cycling performance of $\text{LiNi}_x\text{Co}_{1-x}\text{O}_2$ 45-Ah cell at the C/2 rate to 100% dod.

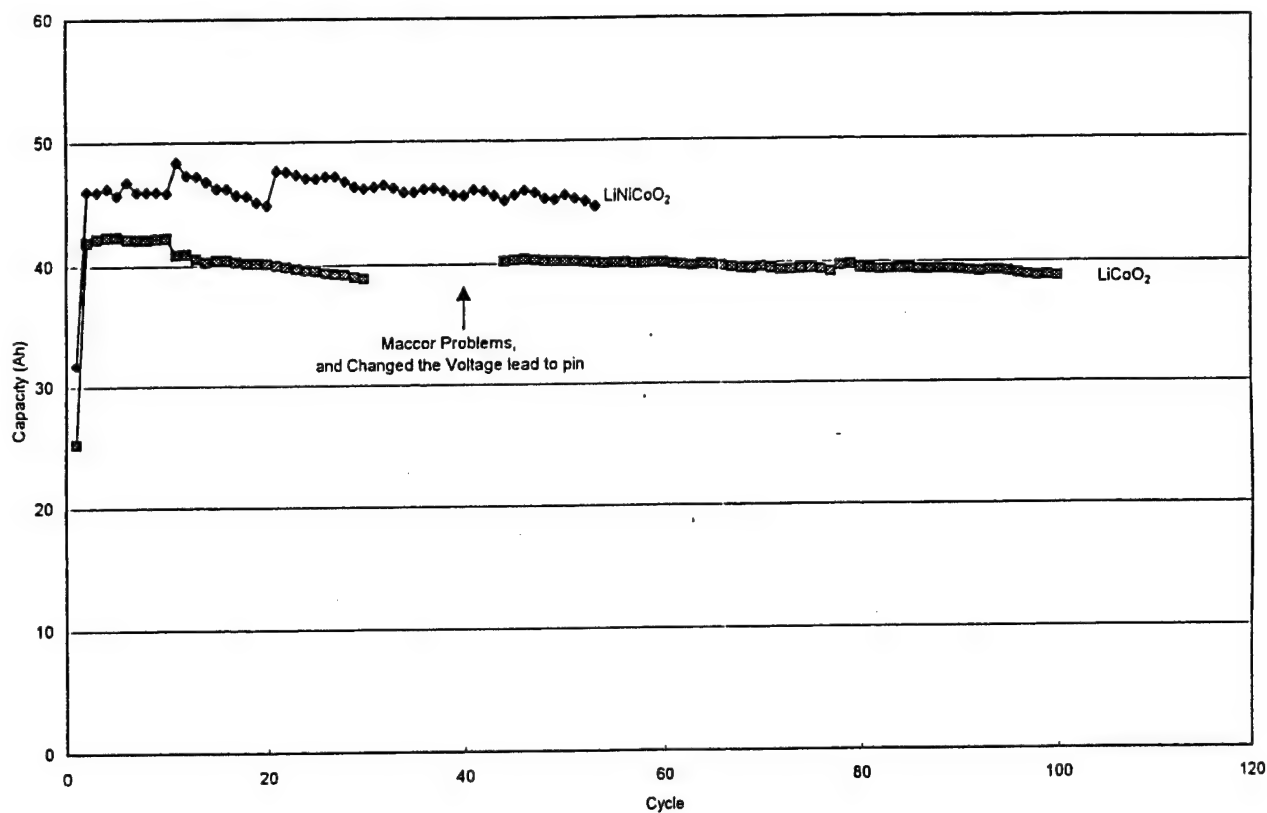


Figure 74. Cell cycling performance of LiCoO₂ and LiNi_xCo_{1-x}O₂ 45-Ah cells at 100% dod.

The work done with the 45-Ah cell was initiated close to the end of the contract and more work is required. More processing experience and refinement are required for electrodes wider than 4.0". One problem was solved when the formation cycle was changed to C/10 from C/5 to stop the bulging of the cells. In comparison with other large cells made at BATC the 45-Ah format has good rate capability and can be pulsed at up to 5C (225 A). The resistance of the 45-Ah cell was found to be quite high relative to smaller cells resulting. Therefore, copper replaced nickel as the negative tab material. As well, the tabs for both electrodes were doubled up to allow for better current collection. Future work will investigate better tabbing and further optimization of the LiNi_xCo_{1-x}O₂ positive electrode system.

2.7 Task 7.0. DD Cell Development

The drive to scale up the lithium ion technology was to support the applications for geo-synchronous or low earth orbiting spacecraft, along with aircraft applications which require, 50-Ah cells. Other applications for specialty lithium ion batteries are planetary exploration. One such application is the Mars Rover. The capacity required for the application is 6 to 7-Ah. Quite fortuitously the capacity and size is consistent with the size that BlueStar Battery Systems manufactures as a DD cell. The general assembly for this cell is shown in Figure 75. The important design characteristics of the cell are outlined below.

- o Two GTM seals, floating design. Standard SO₂ Mo pin 0.090" ϕ
- o Drawn can, SS304, 1.31" ϕ , 4.38" length, 0.019" thickness
- o Vent standard SO₂ style
- o Electrode dimensions
 - Positive electrode, 9.1 x 144 x 0.017 cm
 - Negative electrode, 9.4 x 153 x 0.011 cm
- o Performance
 - 6.4 Ah, 105 Wh/kg, 247 Wh/l

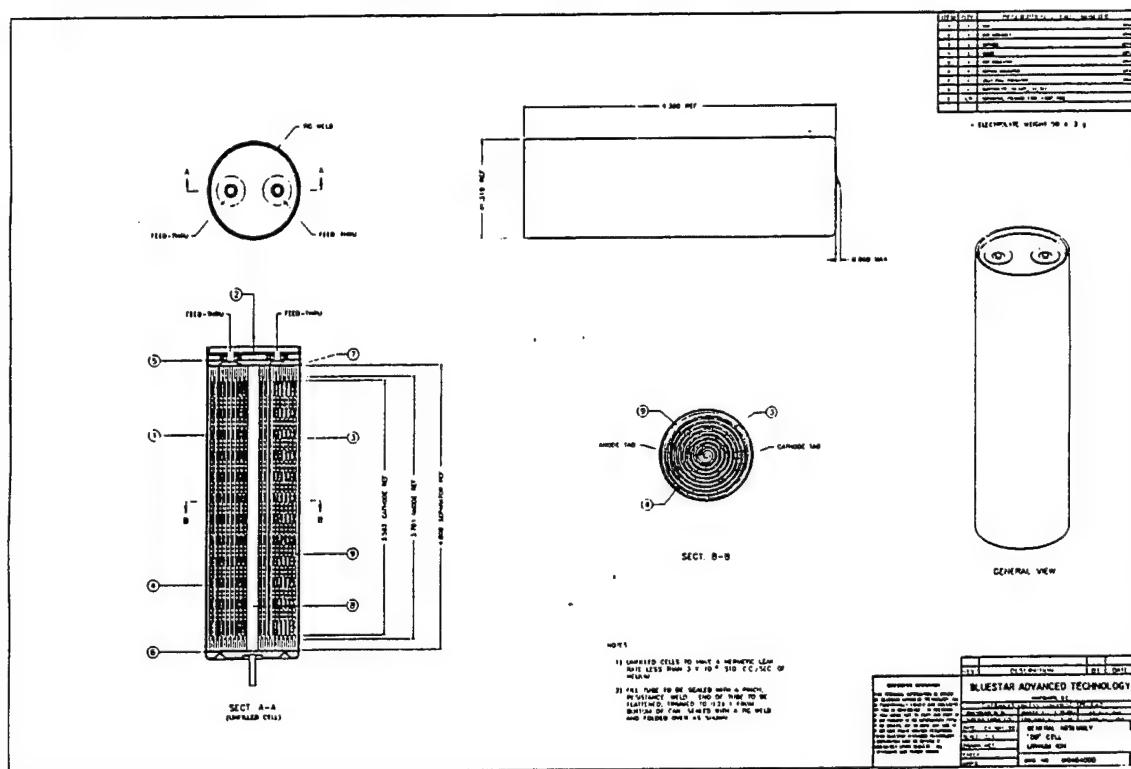


Figure 75. General assembly drawing of a DD cell.

In May 1998, 10 DD cells were delivered to the USAF for evaluation. Since the cells will be used in an environment requiring operation at low temperature the cells were activated with 1M LiPF₆ EC/EMC 1:3. The performance and weights of these cells are shown in Table 31.

The performance of the cells has been summarized; however, the difference in cell mass should be highlighted since the standard deviation is exactly as expected from the results for the 25-Ah Design II cell. The variation in the capacity, specific energy, and energy density is equivalent to the Design II cell as well. The cell to cell variability in the delivered cells again illustrates that BATC has reduced the variation in electrode processing. The cell mass distribution analysis is shown in Table 32. The most important feature to note is that the 0.0004" copper current collector increases the relative amount of active material in the negative electrode.

Table 31. Cell mass, capacity and performance of delivered DD cells.

Cell Id.	Cell Mass, g	Capacity, Ah	Specific Energy, Wh/kg	Energy Density, Wh/l
DD022	225	6.2	103	238
DD026	228	6.6	107	252
DD027	227	6.4	104	244
DD029	227	6.5	107	253
DD031	226	6.6	110	257
DD032	226	6.4	105	246
DD033	227	6.4	104	245
DD037	225	6.3	104	243
DD039	231	6.4	103	247
DD041	226	6.3	104	242
Average	227g $\sigma = 1.8$	6.4 $\sigma = 0.1$	105 $\sigma = 2.2$	247 $\sigma = 5.7$

Table 32. Cell mass analysis of DD cells.

Component	Mass, g	%
Can	46.7	21.0
Cap assembly		
- Cap blank	3.5	1.5
- GTM seals, rupture disk, Fill tube	1.8	0.8
Total	5.3	2.3
Electrolyte		
- EMC	31.3	13.8
- EC	13.8	6.1
- LiPF ₆	6.3	2.8
Total	51.4	22.7
Positive electrode		
- LiCoO ₂	60.0	26.4
- 0.001" Al Foil	9.2	4.0
- Binder	2.0	0.9
- Conducting	4.0	1.7
Total	75.2	33.0
Negative electrode		
- Graphite	20.5	9.1
- 0.0004" Cu foil	13.0	5.7
- Binder	2.4	1.1
- Conducting	1.2	0.5
Total	37.1	16.4
Fiddley bits		
- Positive tabs	0.6	0.2
- Negative tabs	1.1	0.5
- Insulators	1.0	0.5
- Positive tape	0.6	0.3
- Negative tape	0.5	0.2
- Separator	7.2	3.1
Total	11.0	4.8
Total	226.7	100

The contribution of the cell hardware is larger than the 25-Ah Design II cell or the 45-Ah. BATC has been manufacturing the DD cell for a short time and so the life testing is not extensive. Most of the testing at BATC for the DD cell was at the C/2 rates. The results for a DD cell tested at the C/2 rate is shown in Figure 76. Before the DD cells were built for the USAF several cells were sent to the US Army for evaluation. The US Army tested the cells at several different temperatures and at the C/2 rate. The results are shown in Figure 77. One cell tested by the US Army has completed 165 cycles at 100% dod and has a capacity retention of over 90%. Temperature studies conducted by the US Army are shown in Figures 78 and 79. Figure 78 shows the performance at 25 °C, 0 °C, -10 °C and -20 °C. The performance at 0 °C is 90% of ambient temperature performance while -10 °C is 78% of ambient temperature performance and -20 °C is 34% of the ambient temperature performance. The tests were done on bare cells, charged and discharged at the C/2 rate between the voltage limits of 4.1V and 3.0V. The low temperature performance under these conditions is good. As outlined in the section on low temperature electrolytes, performance in a battery pack or changing the charging limits or charge duration will enhance capacity. Figure 79 compares cell capacity at 55 °C to cell capacity at 25 °C.

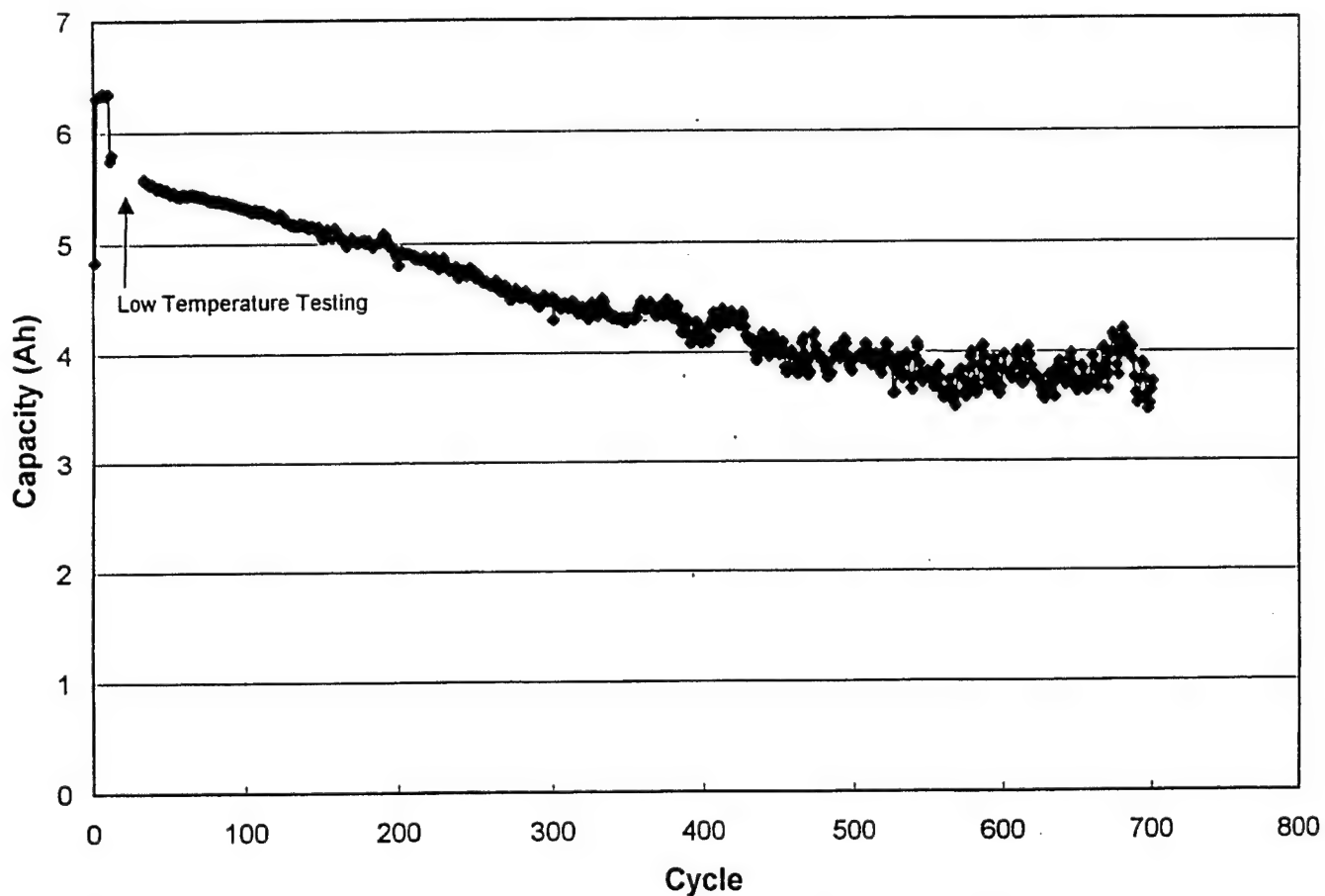


Figure 76. Cell cycling performance of DD cell at the C/2 rate to 100% dod

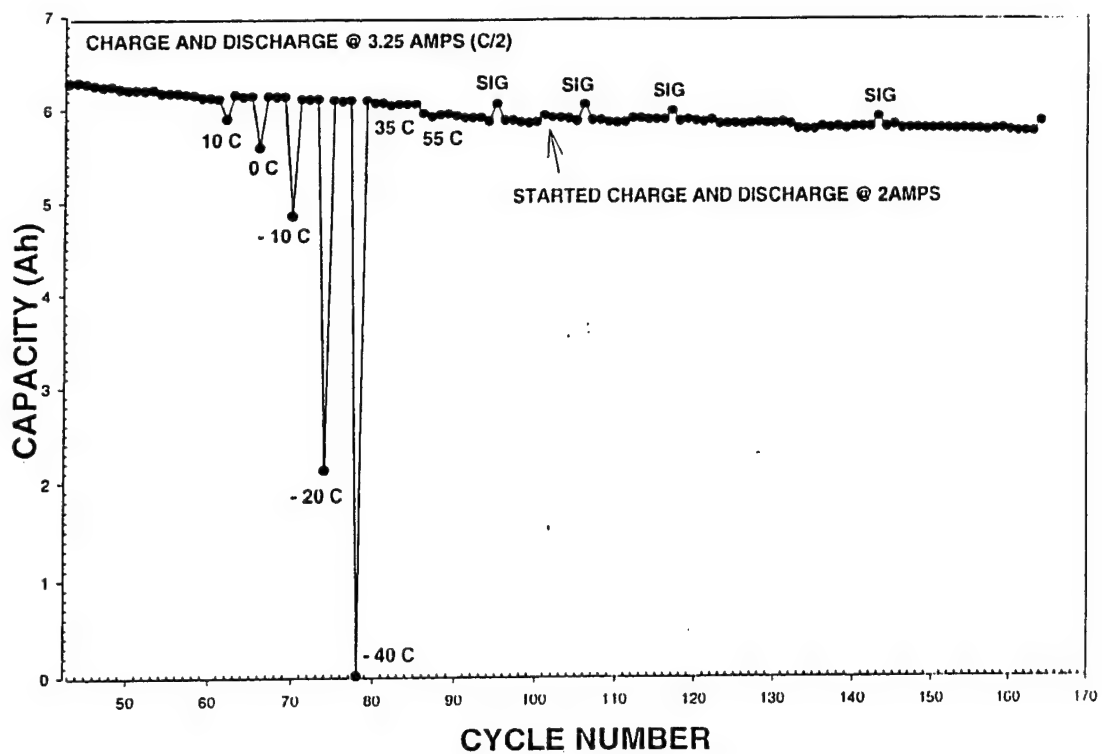


Figure 77. Cell cycling performance of a DD cell at the C/2 rate at 100% dod tested by the US Army.

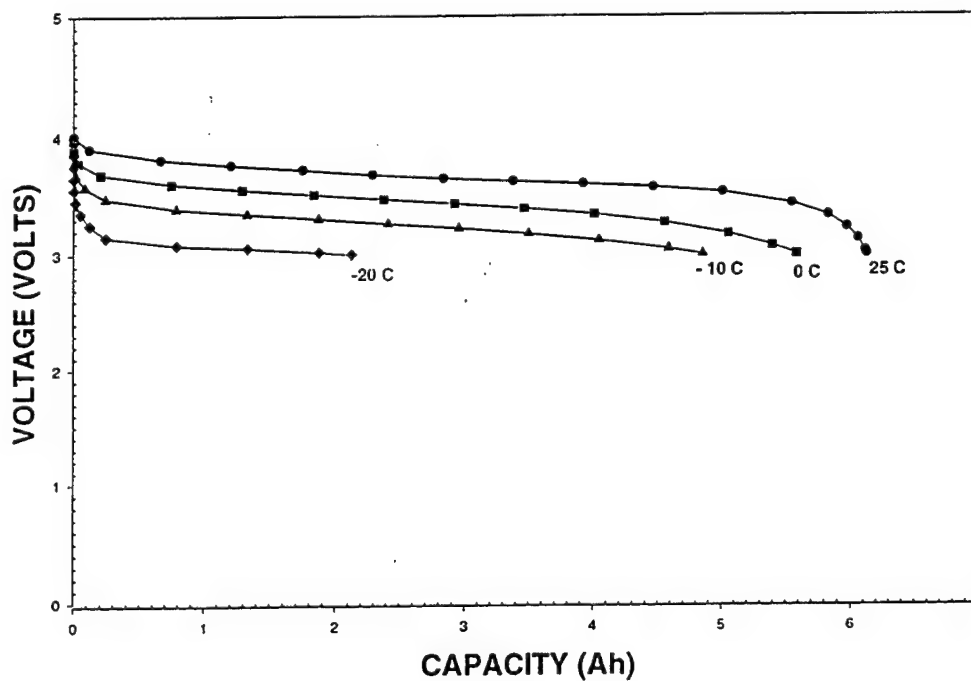


Figure 78. Low temperature testing of a DD cell by the US Army.

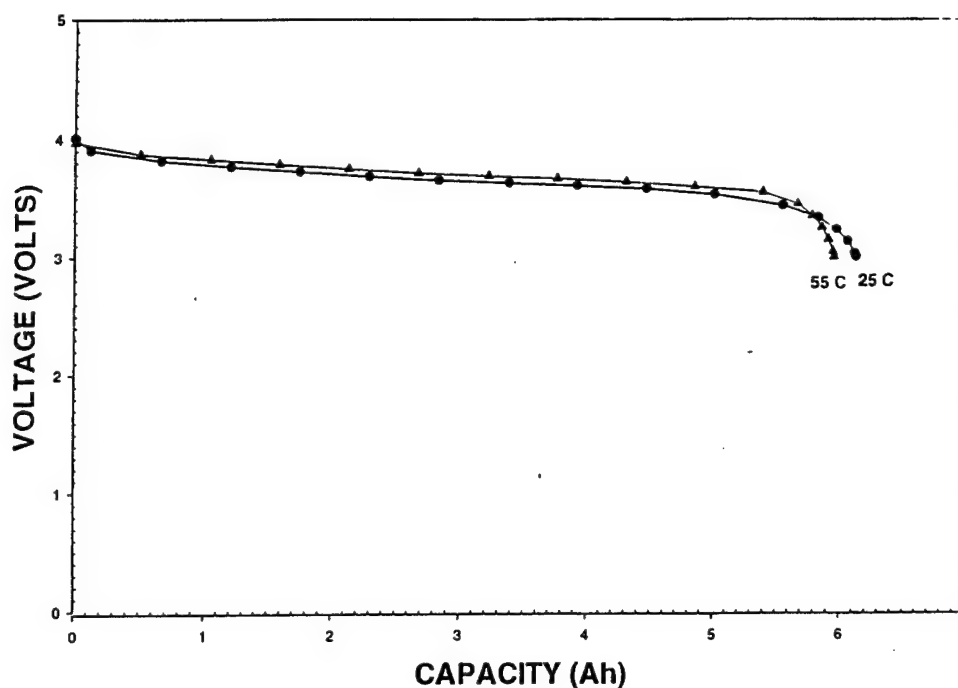


Figure 79. Testing of a DD cell at 55 °C and room temperature by the US Army.

Electrodes used in the DD cell are the same width as electrodes in the 25-Ah Design II cell, are 1.5 m long and have one tab, so the DD cell should have good rate capability. The rate performance of the DD cell presented in Figure 80 shows that the capacity follows the trend $C/10 > C/5 > C/2 > C$ but the differences are very small.

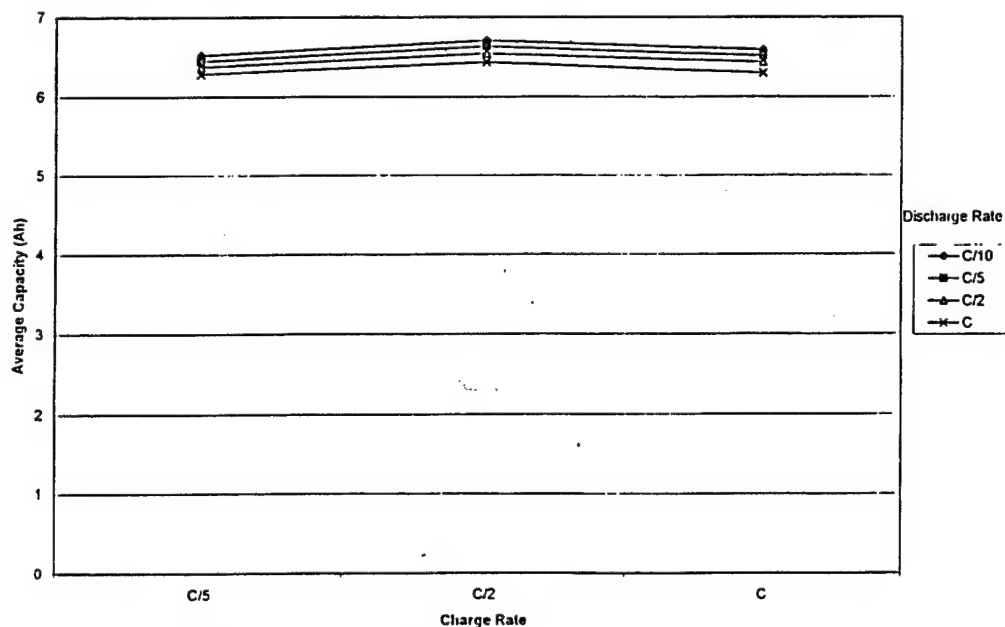


Figure 80. Rate performance of DD cell.

Due to the relatively small amounts of materials required for a DD cell, this cell size has recently been used for material evaluations. One of the materials tested in the DD format was $\text{LiNi}_x\text{Co}_{1-x}\text{O}_2$. The results for two DD cells using a $\text{LiNi}_x\text{Co}_{1-x}\text{O}_2$ positive electrode are shown in Figure 81. The capacity of the two cells is identical over almost 300 cycles. The capacity fade up to cycle 290 is quite large with only 72% of the capacity at cycle 11. However, the capacity of the $\text{LiNi}_x\text{Co}_{1-x}\text{O}_2$ cells are almost 20% higher than the corresponding cobalt cells as shown in Figure 82. There are still some issues to be addressed with the $\text{LiNi}_x\text{Co}_{1-x}\text{O}_2$ positive electrode.

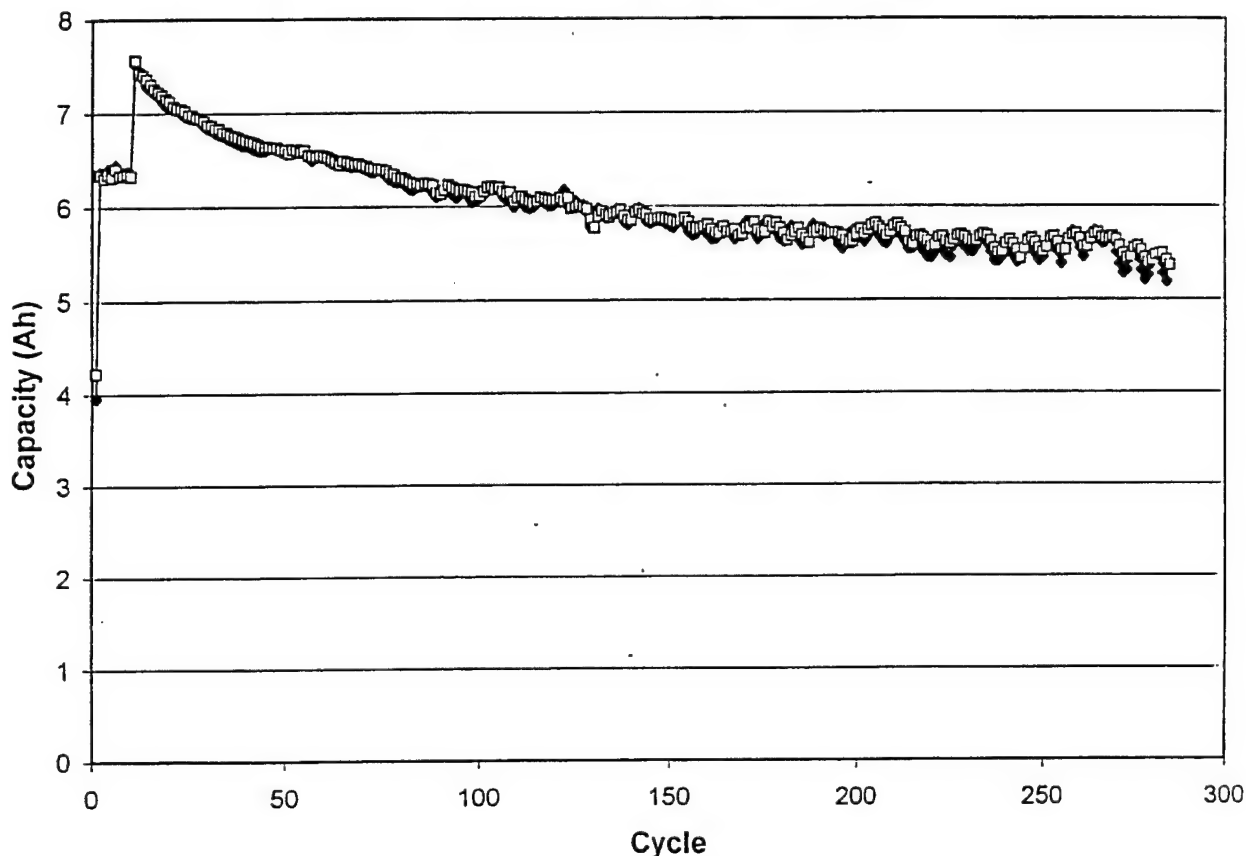


Figure 81. Cell cycling performance of a DD cell with a $\text{LiNi}_x\text{Co}_{1-x}\text{O}_2$ positive electrode at the C/2 rate at 100% dod.

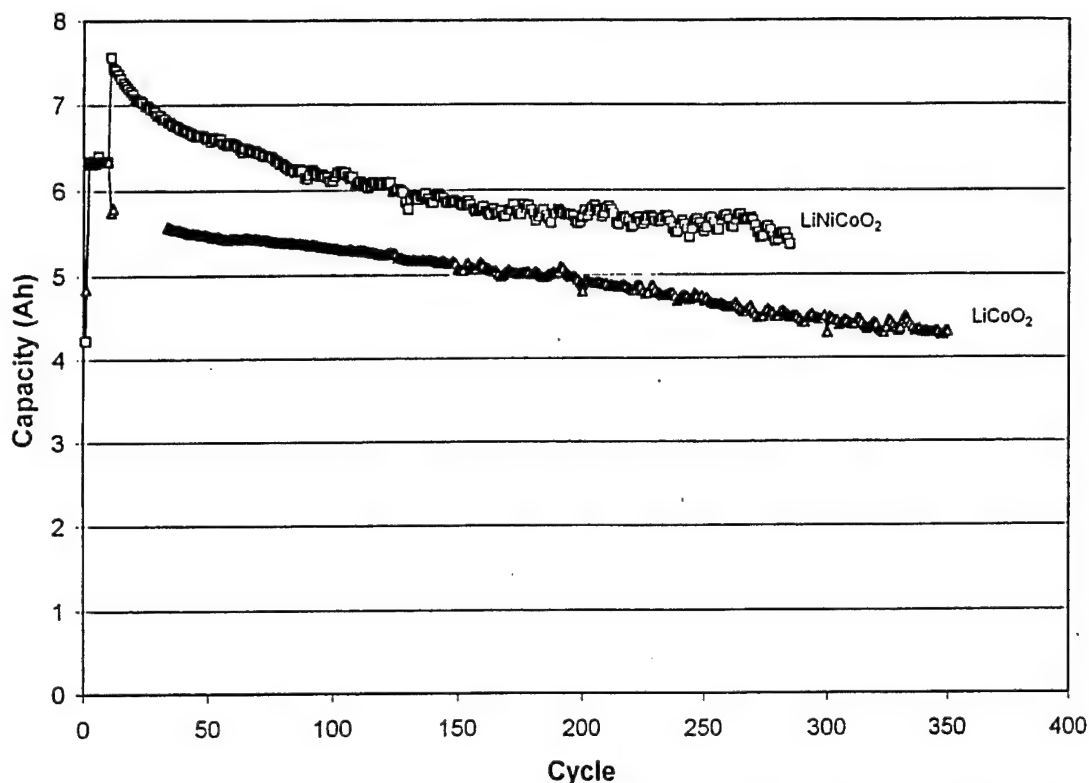


Figure 82. Cell cycling performance of a DD cell with a $\text{LiNi}_x\text{Co}_{1-x}\text{O}_2$ or a LiCoO_2 positive electrode at the C/2 rate at 100% dod.

Another positive electrode material evaluated in the DD cell format was LiMn_2O_4 supplied by MaxPower. One of the fundamental problems with the manganese oxide positive electrodes is the fade in capacity. As outlined in previous sections for the rate studies and for low temperature performance, it is the charge and not the discharge half cycle which is of great importance. One method would be to charge the cell at a lower rate to ensure that the cell is completely charged. Another method which is most useful in low temperature applications is to raise the charge voltage to compensate for any IR increase due to the electrolyte becoming less conductive. With the intention of fully charging the LiMn_2O_4 DD, cell the charge was stopped at a capacity limit and not a time limit (coulombic charging). The cell was charged at C/5 to 4.1V and then held at 4.1V until the capacity, as determined by cycle 11, had been delivered. As shown in Figure 83, the cell delivered 100% of capacity for 100 cycles. After 100 cycles, the capacity slowly decreased since a time limit of 25 hours was placed on the constant voltage step. The total charge time is shown in Figure 84. Even if the charge time was extended to 50 hours, the cell capacity would slowly decay since the current at the end of charge is only a few mill-amps.

Trying to retain 100% of the capacity as determined by cycle 11 may have been overambitious since the LiMn_2O_4 system has a faster rate of capacity fade than the oxides of cobalt and nickel. Another method would be to allow for the irreversible capacity loss in the initial cycles and set the charge to 90% of capacity. For this test a DD cell using LiCoO_2 was coulombically charged at the C/2 rate to 90% of capacity. The tests results for capacity are shown in Figure 85 and for charge time are shown in Figure 86. The results for capacity versus cycle number show that the

cell has completed almost 300 cycles and still is delivering 90% of the total capacity. The total charge time of the last cycle was less than three hours. Potentially this method may result in superior cycle life for lithium ion batteries. The DD cell at 90% dod has the best performance with coulombic charging due to superior current collection configuration.

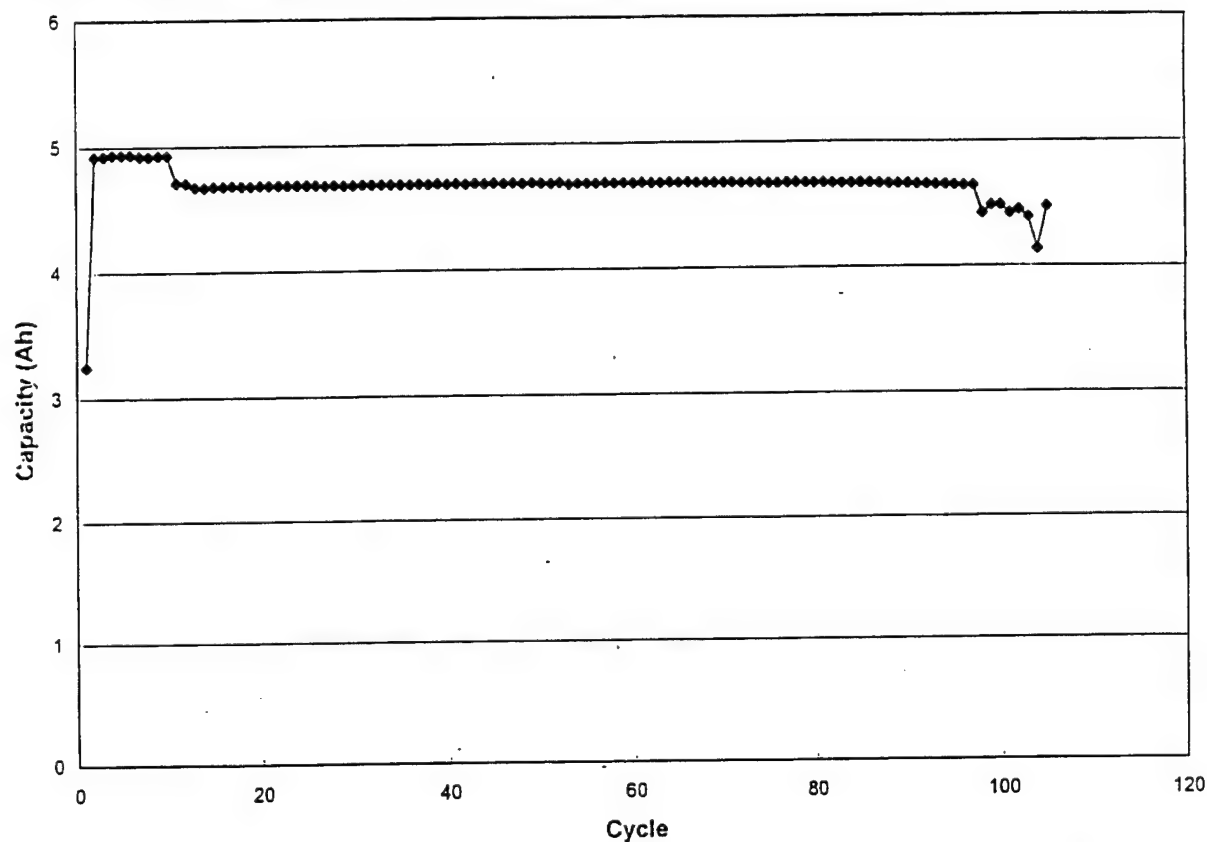


Figure 83. Coulombic charging of LiMn_2O_4 DD cell at the C/5 rate, capacity versus cycle number.

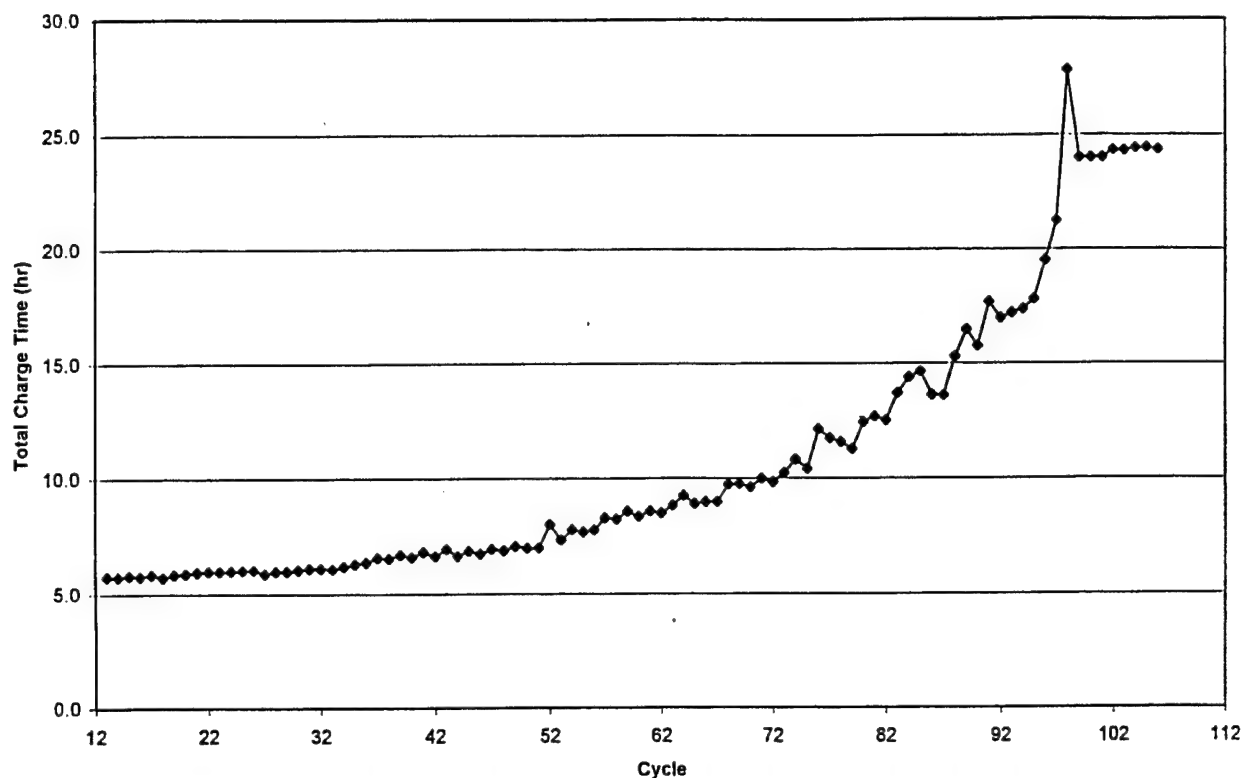


Figure 84. Coulombic charging of LiMn_2O_4 DD cell at the C/5 rate, total charge time.

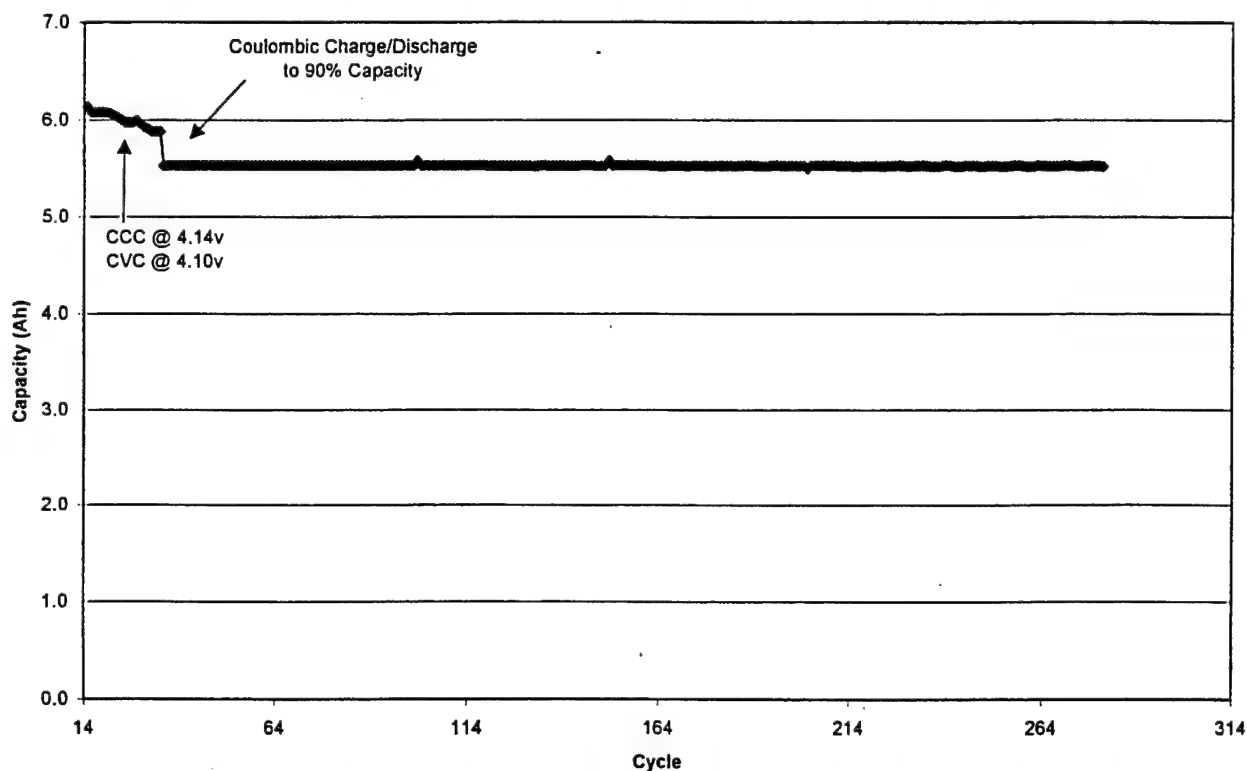


Figure 85. Coulombic charging of LiCoO_2 DD cell at the C/5 rate, capacity versus cycle number.

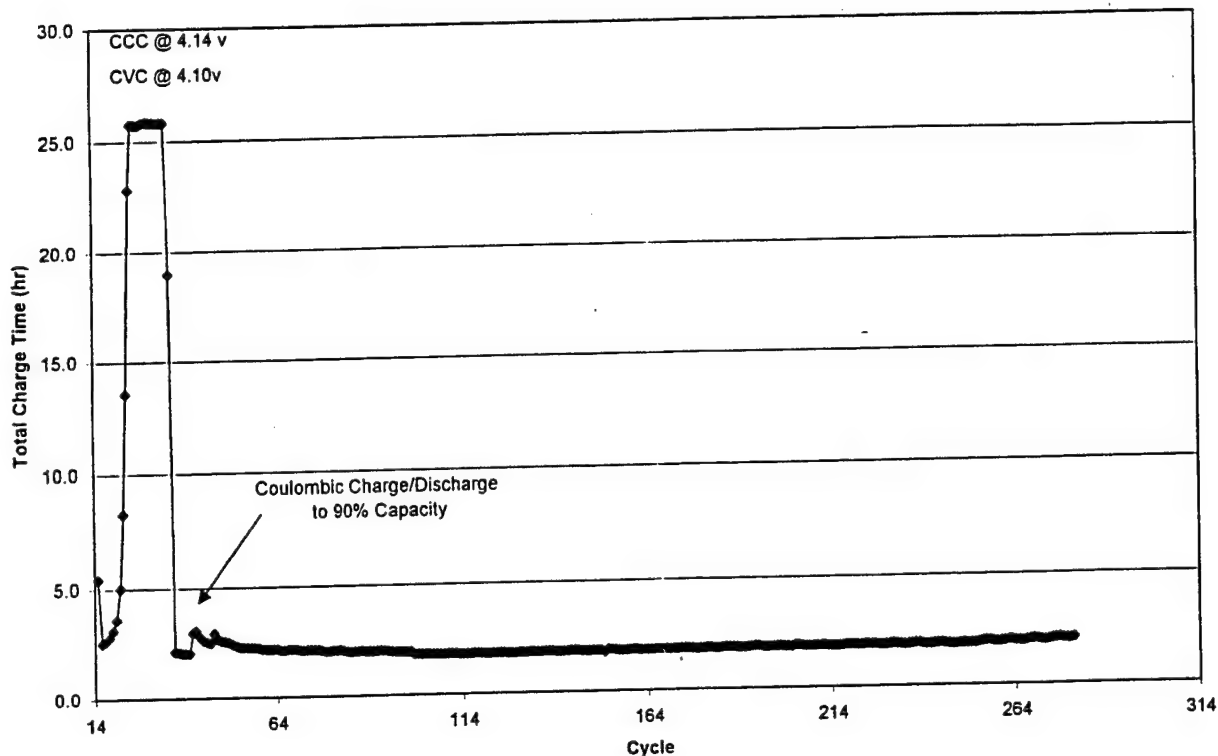


Figure 86. Coulombic charging of LiCoO_2 DD cell at the C/5 rate, total charge time.

The latest cell designed and manufactured by BATC, the DD cell, illustrates that the variability with the deliverables has been reduced in the last year. The rate capability of the cell design is very good. The low temperature performance is better than previous deliverables since the electrolyte was 1M LiPF_6 EC/EMC 1:3. For the next set of DD size deliverable cells, new hardware will be used so that a new vent, not a standard SO_2 style vent, can be used.

2.8 Task 8.0. Cell Safety

Safety is of extreme importance when manufacturing large hermetically sealed cells. With cells approaching 125 Wh/kg and 250 Wh/l , the energy is very high and safety becomes an issue. For the consumer market the safety requirement states that no amount of abuse will lead to cell rupture or fire, which is an issue with an organic electrolyte. However, safety is not viewed in the same light for spacecraft and military applications. Knowing the safety issues and ensuring that unsafe conditions do not arise is of more importance.

The first safety test was to determine what effect a short circuit would have on the 20-Ah Design I cylindrical cell. The cell was connected to an in-house short-circuit tester which would close the circuit with a resistance of less than 50 milli-ohms. Before the test began, the resistance of the tester was measured to be 40 milli-ohms. The temperature and current traces of the test are shown in Figure 87.

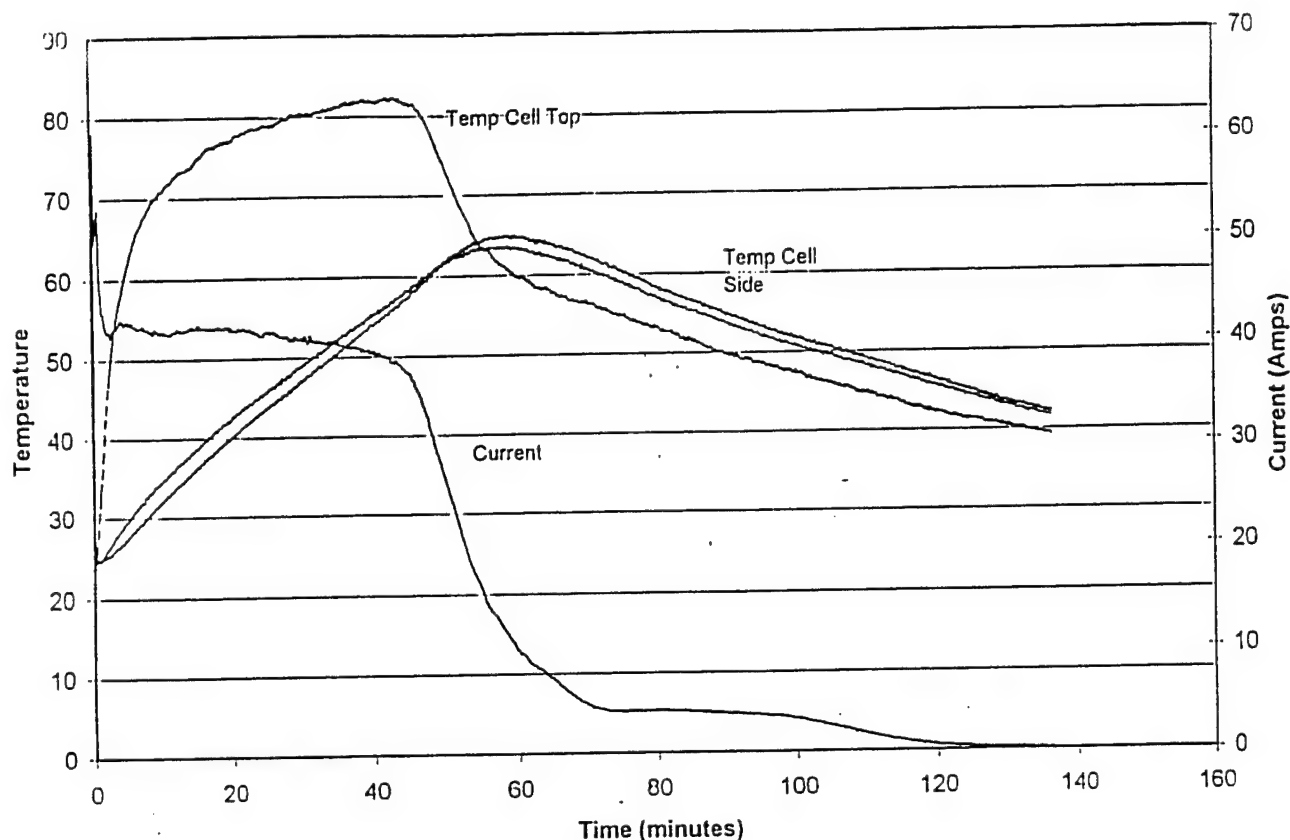


Figure 87. Short-circuit test of 20-Ah Design I cell.

The short-circuit did not result in any fire or explosion and the vent did not open. Also, the cell did not bulge. The current reached a maximum value of 60 A during the test then fell to a sustainable current of approximately 40 A for approximately 45 minutes, and then dropped to 5 amps for the remainder of the test. The temperature of the cell reached a maximum of 80 °C on the top of the cell and 50 °C on the side of the cell. From BATC's experience with primary Li/MnO₂ the temperatures reached were not sufficient to cause the shut-down separator to fuse. This is supported by the current trace which would have shown a decline in current far earlier than was observed. Also, if the current values were correct, the cell delivered over 35 Ah. This is far in excess of the 25-Ah that was charged into the cell initially even taking into consideration that the cell was discharged to 0 volts. The only explanation is that the current monitor must have become un-calibrated during the test since the calibration is checked before each test. However, the current was checked with an alkaline C cell and the current of the calibration is not as great as the current reached during the test.

The next cell tested under short-circuit condition was a 25-Ah Design II cell. In addition to temperature and current being monitored the voltage was also measured as shown in Figure 88.

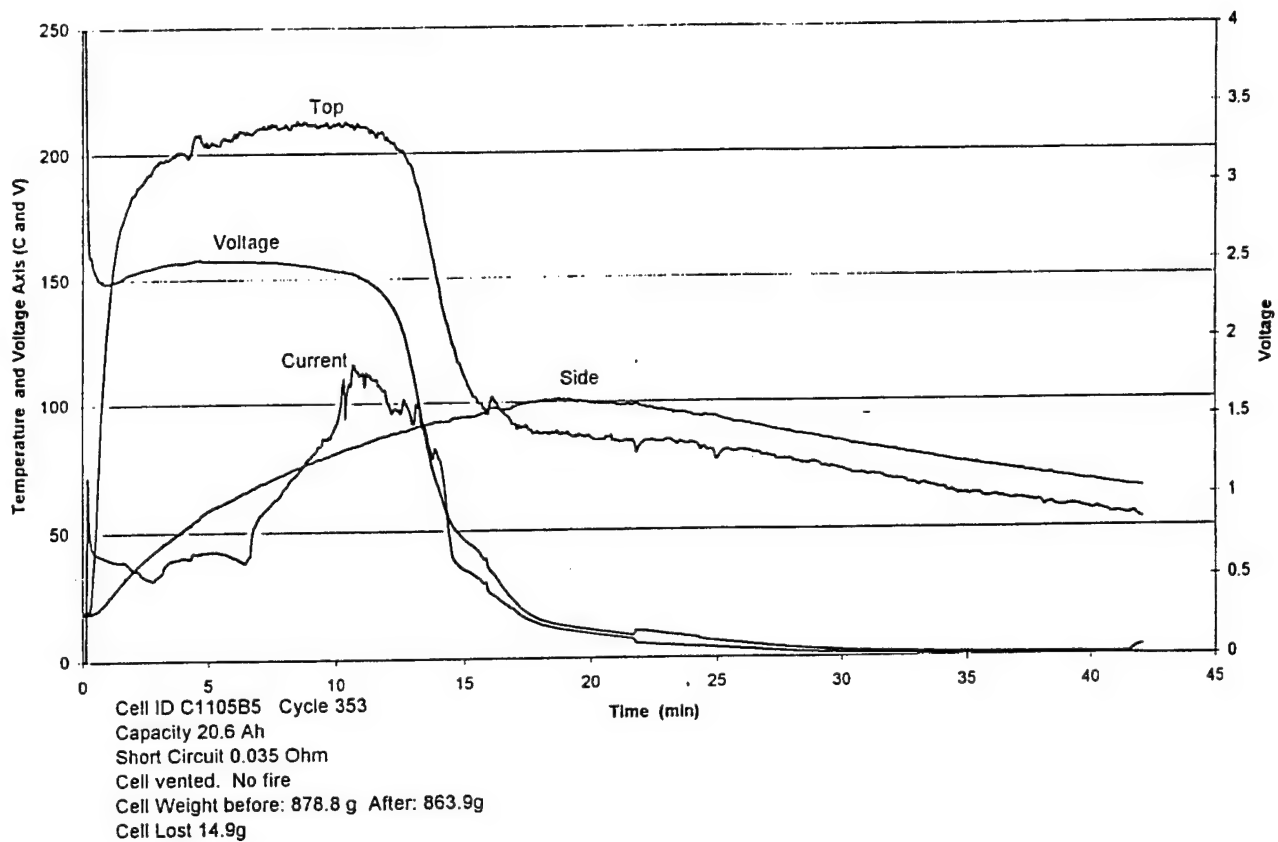


Figure 88. Short-circuit test of Design II 25-Ah cell

The resistance of the short circuit before the test was 35 milli-ohms. Before the test, the voltage, current and temperature sensors were all tested and calibrated. The result of the test was again safe with no fire or explosion. However, the cell did vent and 14.9 g of electrolyte was lost through the vent since the cell was weighed before and after the test. Also, the cell was severely bulged on the top and bottom. The temperature on the top of the cell was over 200 °C and reached 100 °C on the side of the cell. After the test was completed the thermocouples were checked and a calibration test indicated they were reading the correct values. The current monitor had lost calibration during the test so the values are inaccurate. Surprisingly the voltage of the cell was very constant at 2.5 V for the first 15 minutes of the test before it dropped close to zero. The voltage sensor was checked after the test and was found to be correct. Therefore, the test was through a 35 milli-ohm resistor as outlined above and was not a hard short.

To determine the safety of the DD cell under hard-short conditions the in-house tester was not used. Instead, heavy gauge wires were used to short the cell, and temperature and voltage were monitored. The resistance of the short-circuit was 2.2 milli-ohms. When these cables were used to short-circuit the cell the voltage immediately dropped to 0.065 V and the external nickel tabs connecting the cell melted. No thermal excursion was noted. New connectors were made and the cell was shorted once again. The voltage immediately went to zero but the temperature did not rise. Destructive physical analysis revealed that the internal negative tab (nickel) in the cell had melted through and the voltage was due to the thermal tape holding the tab together so that an

open circuit voltage reading was obtained but no current was drawn.

Over-discharge was the next test conducted on both the Design I and Design II cylindrical cells. For the Design I the cell was discharged at 2.5 A for 20 hours, which is equivalent to 100% over discharge. The results from this test are shown in Figure 89. After approximately 12 hours the cell voltage became negative. The lowest voltage the cell reached was -0.6V. The cell voltage remained at that voltage for 6 hours. The cell was then charged at 2.5 A to determine if the cell could recover. The subsequent charge is shown in Figure 90. The figure illustrates that the cell could not be charged after forced over-discharge, so the cell was essentially a large resistor. The Design II 25-Ah cell performed in an identical fashion when over-discharged. Once these tests were finished both cells were subjected to destructive physical analysis. When the cells were examined it became apparent that during over-discharge the copper foil, which acts as a current collector for the negative electrode, had been oxidized from the negative electrode and then reduced at the positive electrode. The copper foil had the appearance of copper leaf and had mostly decomposed. Copper was also plated onto the positive electrode and throughout the separator.

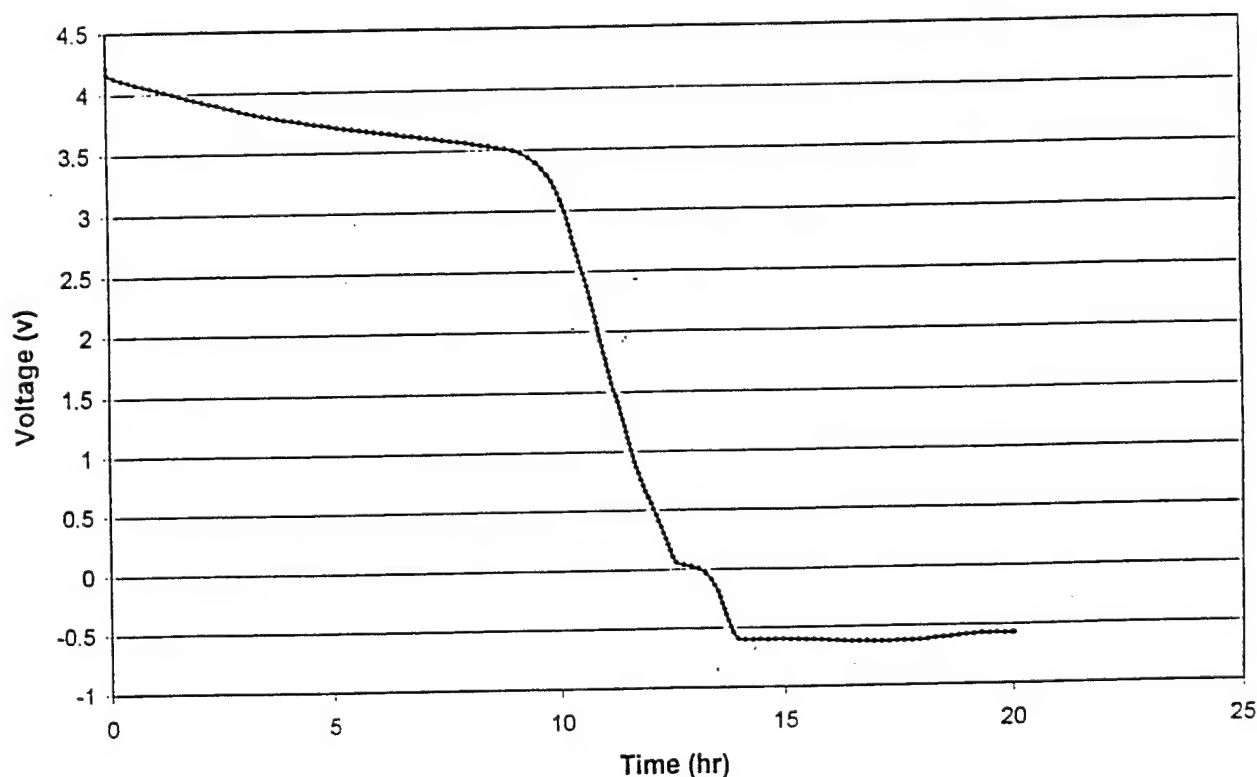


Figure 89. Over-discharge of Design I 20-Ah cylindrical cell.

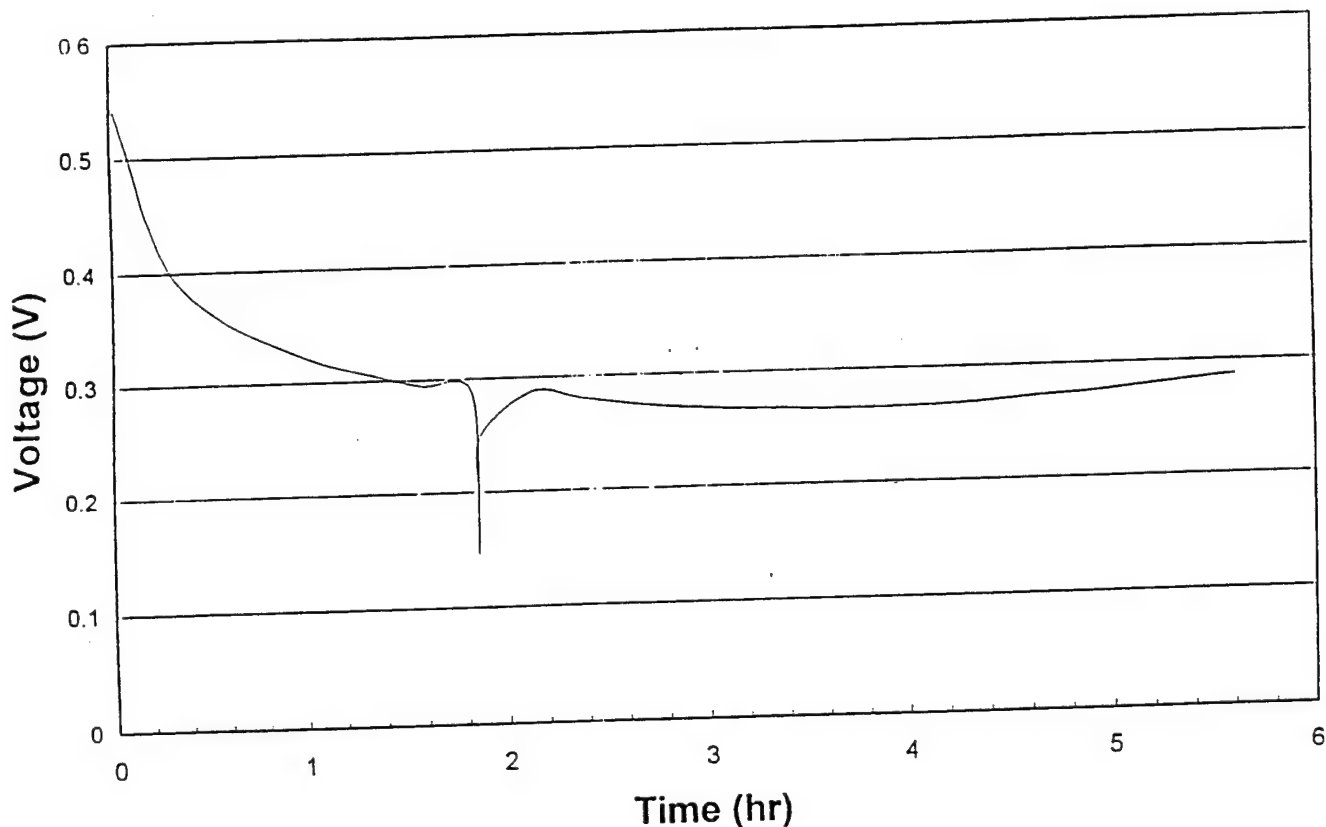


Figure 90. Subsequent charge of over-discharged Design I 20-Ah cell.

The next safety test was to determine how the cells would perform during overcharge. Design I 20-Ah cells were used. The first cell was 100% over-charged. The cell was charged at 2.5 A for a total of 20 hours, or 50-Ah. The over-charge results are shown in Figure 91. The graph shows that the cell continued to be charged for a total of 50-Ah and reached an upper voltage of 4.66 V. There was no fire, vent or bulging of the cell noted. The cell was then discharged to a 3.0V end-point for a total of 39.75-Ah. This corresponds to a specific energy of 176 Wh/kg and an energy capacity of 362 Wh/l. However, the coulombic efficiency was only 79.5%, so a large amount of lithium was lost. To determine whether this represented a reversible loss of capacity, the cell was returned to the original test procedure for five cycles. The results, shown in Figure 92, indicate that the cell can be charged and discharged and will function, but at approximately 80% of the capacity before the over-charge. Therefore, the capacity loss after over-charge is irreversible. Lithium has likely plated onto the surface of the negative electrode and reacted with the electrolyte.

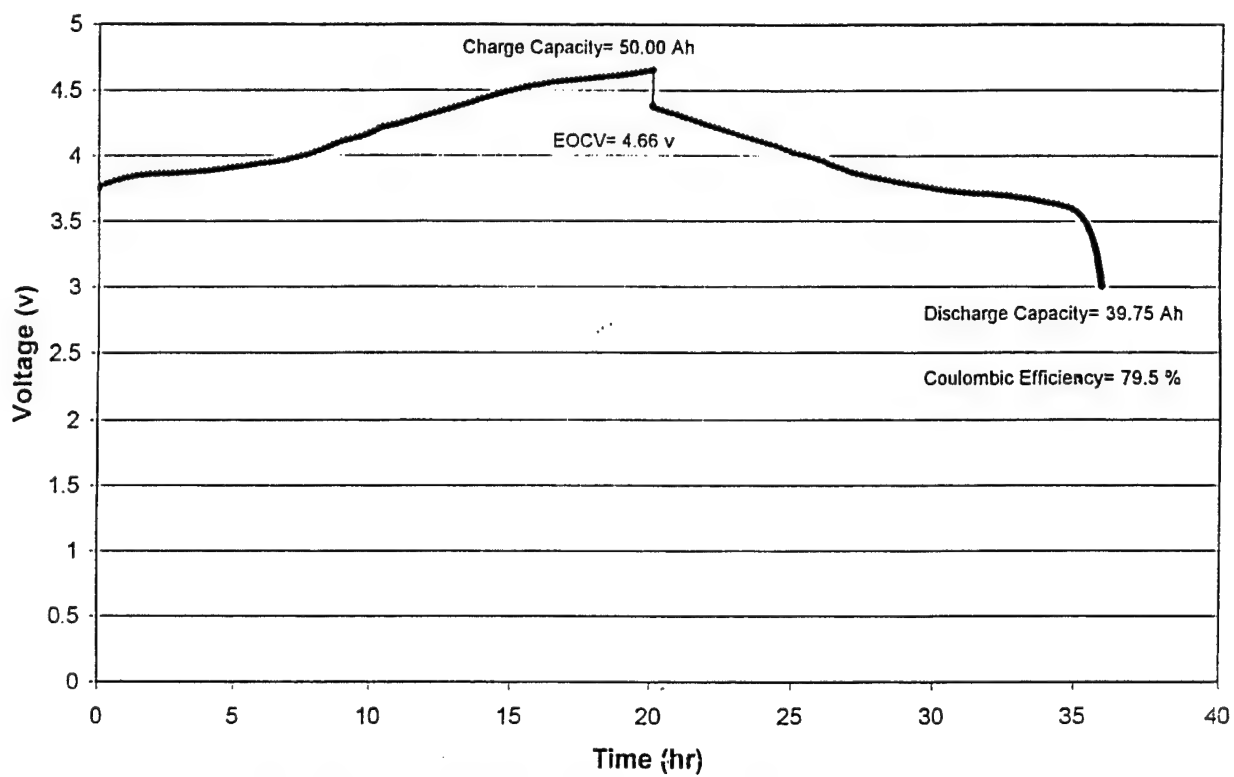


Figure 91. Overcharge to 100% of Design I 20-Ah cell.

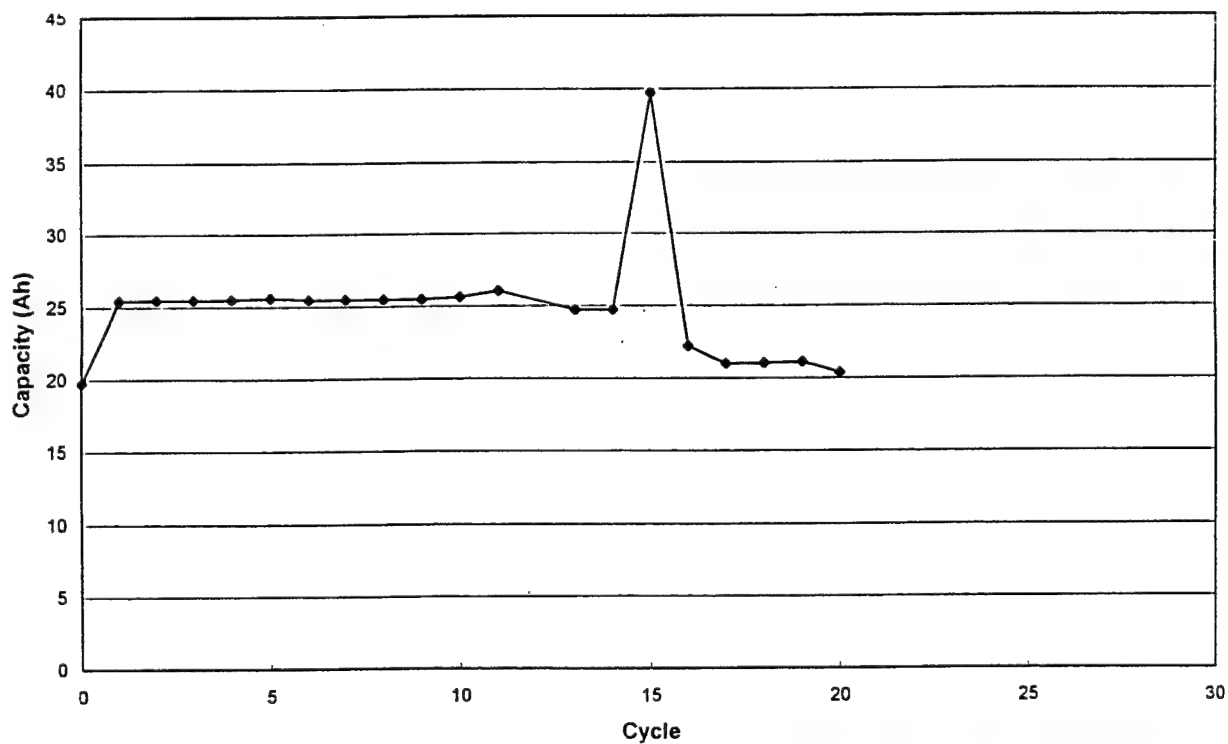


Figure 92. Cell cycling performance of Design I 20-Ah cell after 100% overcharge.

The next test would have an set the Ah limit of 75-Ah or 200% over-charge. The results from this test are shown in Figure 93. During the test the cell vented explosively with flames. The voltage profile shows that the cell charged to 56.16-Ah (125% over charge) and reached a maximum voltage of 4.68 V before the voltage started to slowly decrease until the vent occurred. The voltage trace may indicate that the cell charged a large amount of lithium onto the negative electrode surface and that an exothermic internal short-circuit caused the vent and fire.

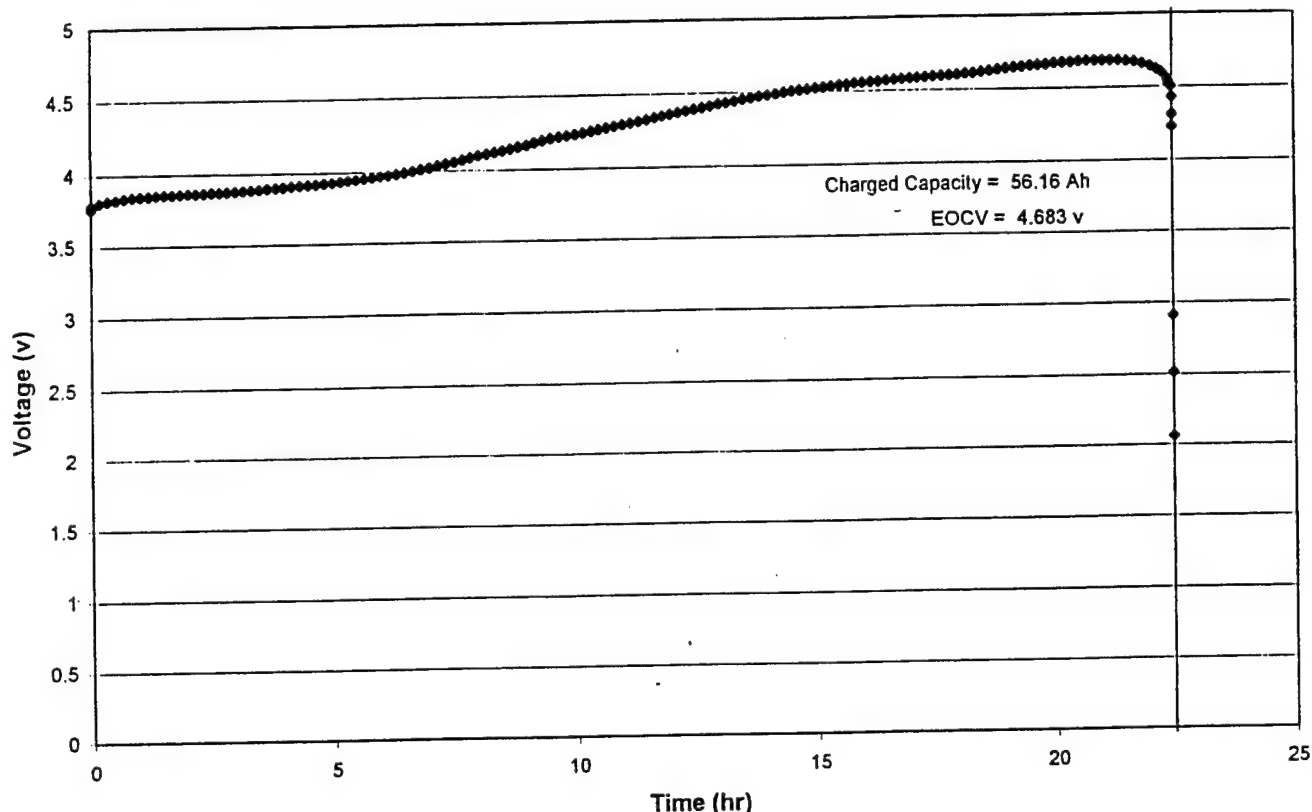


Figure 93. Overcharge to 200% of Design I 20-Ah cell.

Over the years at BATC much work involved in the commercialisation of primary lithium batteries. The first cell chemistry commercialized was Li/SO_2 and the second was Li/MnO_2 . In both cases a vent verification test, also called the oven test, was required. The cell is placed into a 90°C oven for 2 hours and then weighed to ensure that the vent has not been activated. Once the cell passes this initial test it is then placed into a 150°C oven and the cell must vent without flame or explosion within two hours. If the cell does vent before 2 hours it must stay in the oven for a total of 2 hours. The first cell tested under these conditions was the Design I 20-Ah cell. The results from the first oven test are shown in Figure 94. One thermocouple monitored the oven temperature while two other thermocouples followed the temperature of the cell at the top and side. The cell was placed into a 90°C oven for 2 hours and cell weights before and after showed no weight loss. The cell was then placed into the 150°C oven. The oven temperature was very stable at 150°C for the duration of the test. The cell temperature increased for approximately 1.25 hours to 140°C and then a very rapid increase in temperature was accompanied by a cell vent, fire and explosion. During the very rapid increase in temperature the cell vented with a large amount of electrolyte expulsion and the explosion immediately followed. The temperature on the

outside of the cell before explosion was above 140 °C. This is the temperature where the fusible separator fuses and is close to the temperature where the separator starts to shrink.

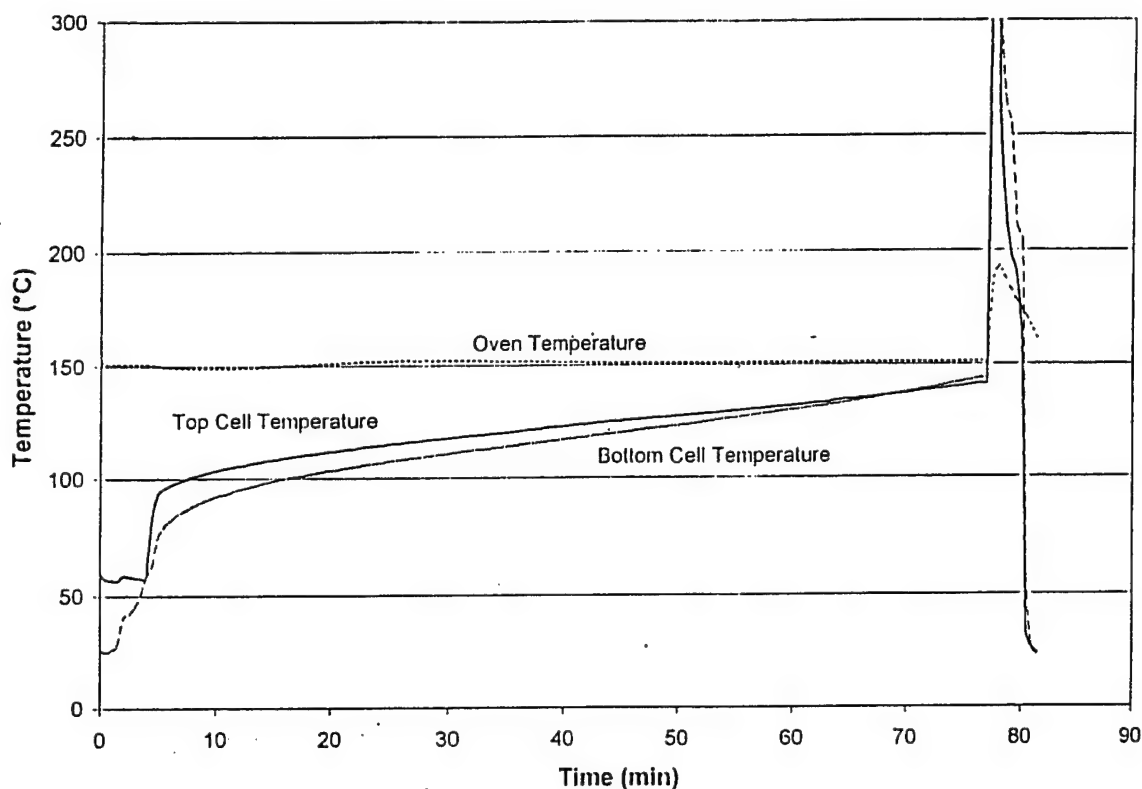


Figure 94. Oven test of Design I 20-Ah cylindrical cell.

To further understand the effect of the separator on the oven test, an identical experiment was conducted on a Design I 20-Ah with voltage and temperature monitored. This cell featured a rupture disc which vented at 125 psi and not 235 psi. The results from this test are shown in Figure 95. Again the cell did not leak at 90 °C. The results from the second test were identical to the first test with the cell venting violently with explosion. The test lasted approximately the same length of time. The voltage trace indicated that as the test progressed the voltage increased very slowly for close to an hour and then indicated of small internal short-circuits from 60 minutes to 85 minutes into the test. Near the 85 minute mark a large internal short-circuit was observed when the voltage dropped sharply to 2.5 V and then 1.6 V before reaching 0 V. The drop in voltage from 4.0 V to 1.6 V was accompanied by a cell temperature increase above the oven temperature indicating an exothermic reaction (i.e. discharge). The separator used in the Design I 20-Ah cell was Celgard® 2300 which is a tri-layer of polyethylene enclosed in two layers of polypropylene. The polyethylene fuses near 135 °C and the large increase in resistance effectively shuts down the cell during external short-circuit. The separator starts to shrink near 140 °C. The separator shrinking is the most likely cause of the internal short-circuit. Another separator used in lithium batteries is Celgard® 2500 which is a single layer of polypropylene. Celgard® 2500 fuses and shrinks at a higher temperature. This time a DD cell was constructed using Celgard® 2500 to determine the effect separator has on the oven test. The results of this test are shown in Figure 96.

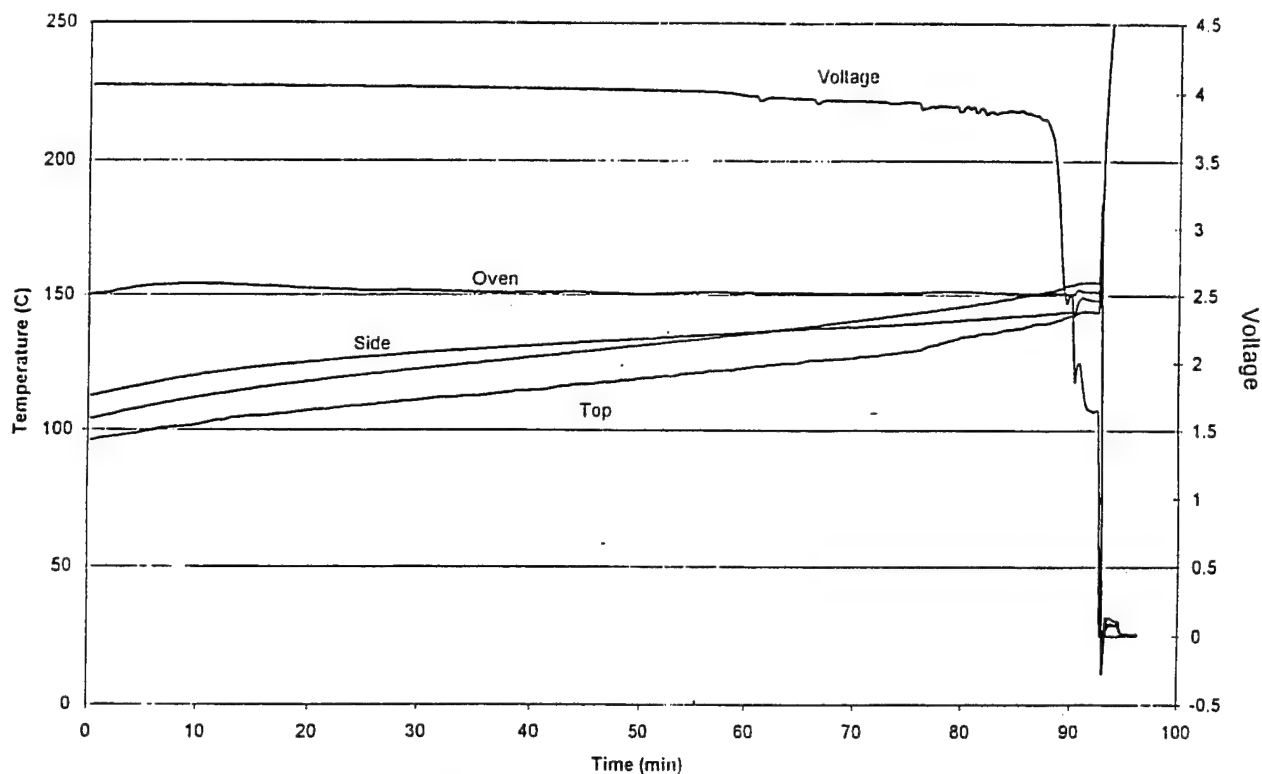


Figure 95. Oven test with Design I 20-Ah cell with voltage sensors.

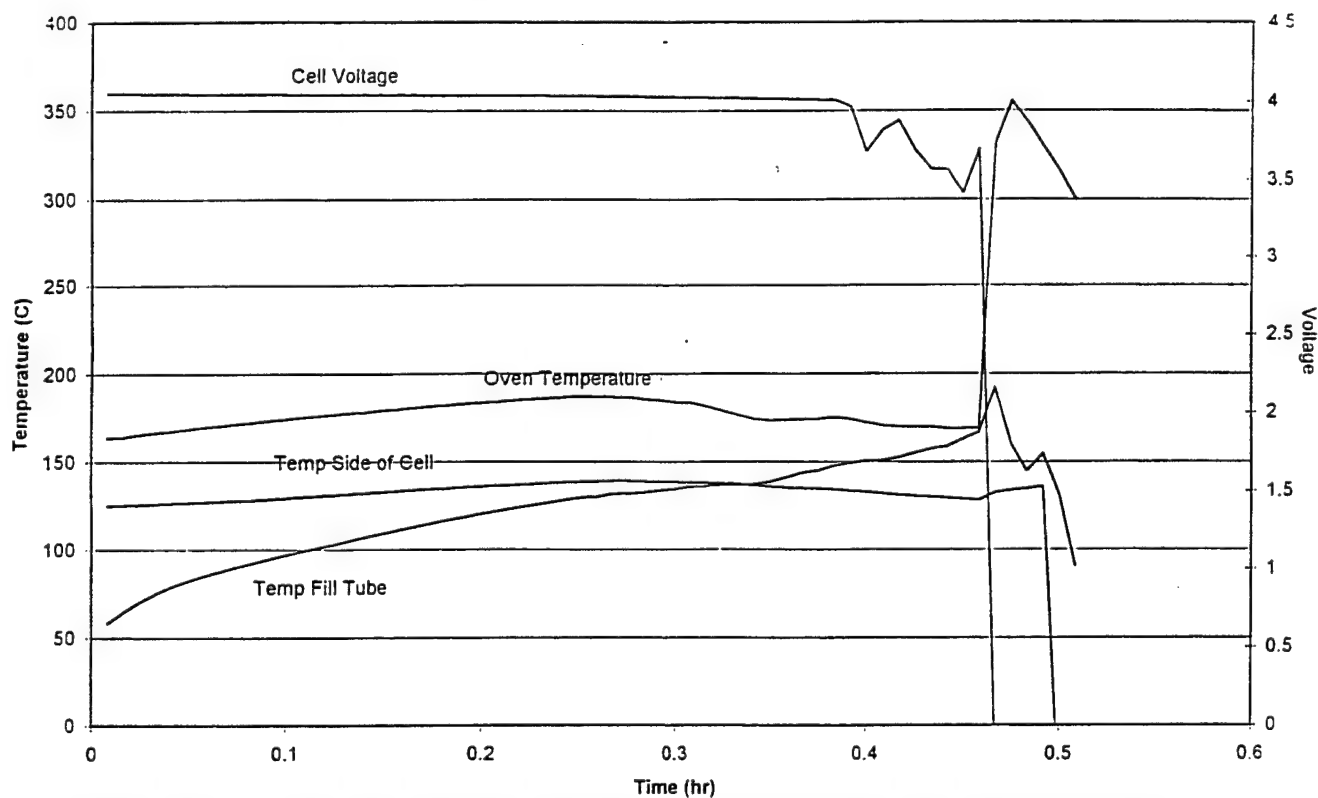


Figure 96. Oven test with DD cell using Celgard® 2500 and with voltage sensors.

The cell did not lose any weight during the 2 hours at 90 °C. Unfortunately, the oven temperature was not stable at 150 °C, and it reached 190 °C. As shown by the cell voltage, the separator shrank, resulting in a internal short-circuit followed by an explosion. Further testing in this area will investigate the use of a glass separator along with the polymeric separators to determine if this will stop short-circuits.

Another route to a safe vent test is to use a larger rupture disc. The rupture discs used previously had an active opening of 0.3125"φ while the Design II 25-Ah cells have an active opening of 0.5"φ, 2.5 times larger. One test was carried out on a Design I 20-Ah cell which had rupture disc pressure of 125 psi as shown in Figure 95. The results were again violent cell venting. To determine if the vent will open at 150 °C without flame, a discharged 20-Ah Design I cell was tested. The results from this test are shown in Figure 97. Three thermocouples were used to monitor cell temperature and oven temperature. As shown by the drop in oven and cell temperature after approximately 2 hours the discharged cell did vent with a 125 psi rupture disc. There was no fire and the cell lost 59.8 g of electrolyte.

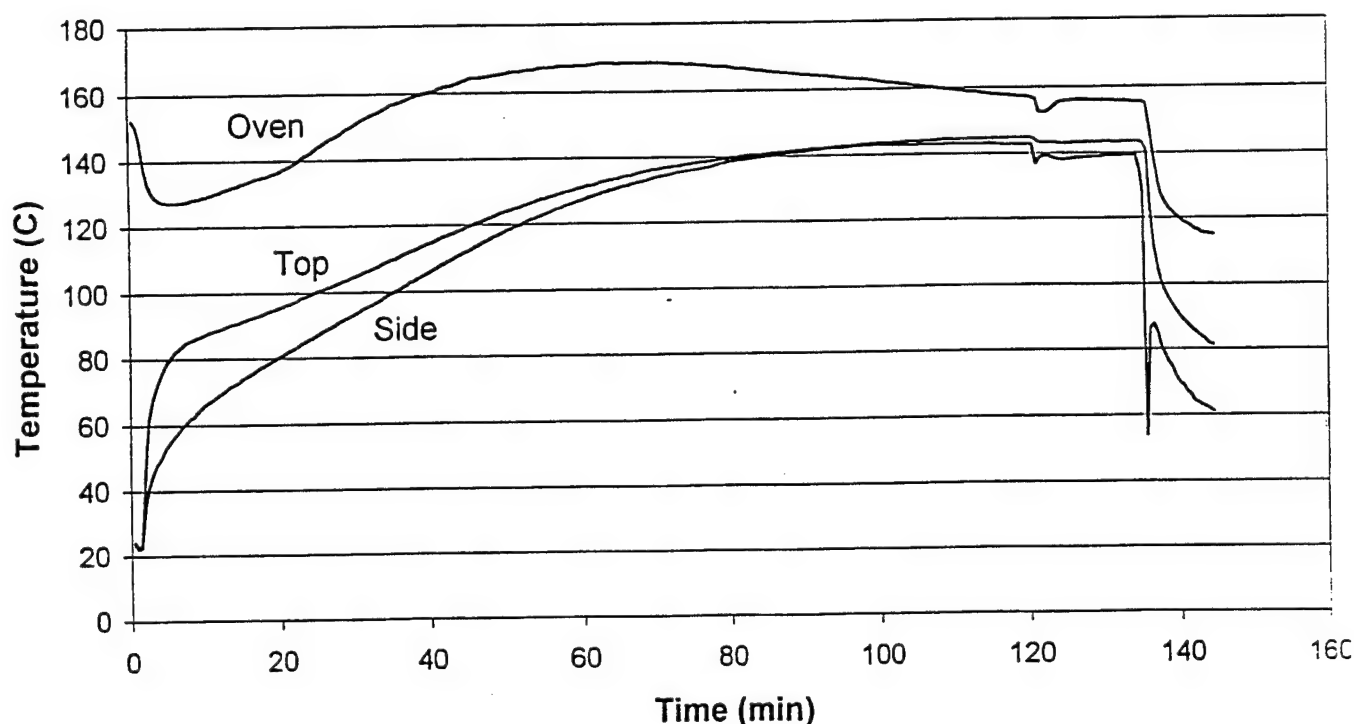


Figure 97. Oven test with discharged Design I 20-Ah cell.

The next abuse tests were crush tests. The cells were placed between the jaws of a remotely controlled vice, with a 6 mm steel rod located on one jaw. The cell was then crushed until the cell voltage reached 2/3 of the initial open circuit voltage. The voltage and cell temperature at the top and the side were monitored during the test. The first cell tested was a Design II 25-Ah cell. The test results are shown in Figure 98. Very surprisingly the cell voltage did not change until the cell voltage dropped to zero. The cell was crushed extensively before the cell voltage indicated an internal short. The test reduced the cell diameter from 2.625" to 1.72". At the moment that the

cell voltage dropped to 0 V the cell vented and the temperature rose to over 250 °C. This elevated temperature was sustained for 30 minutes. The temperature at the side of the cell increased immediately but dropped substantially after a short period of time. The cell contained only 180g of electrolyte, so the loss of 225 g during the test suggest that something other than just electrolyte was lost. The vent was accompanied by a large amount of smoke but no flames were observed.

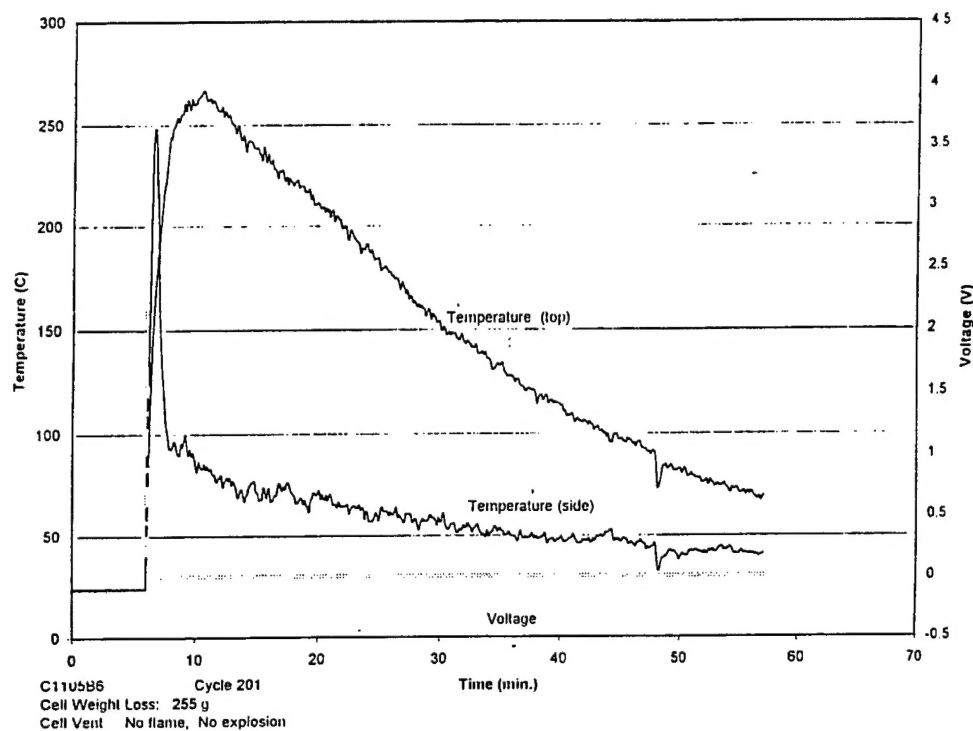


Figure 98. Crush test of Design II 25-Ah cell.

The next cell crushed was a 45-Ah cylindrical cell. The test was carried out in an identical fashion with temperature and voltage monitored. The results are shown in Figure 99. The figure is not very informative since when the cell was crushed to the point of internal short-circuit the shock wave stopped the data logger. Again the cell was crushed substantially before the cell failed. The crush test reduced the cell diameter from 2.484" to 1.42". The cell vented through both GTM's, the rupture disc and the cell cap was removed due to the force of the explosion. Flame was observed during the vent.

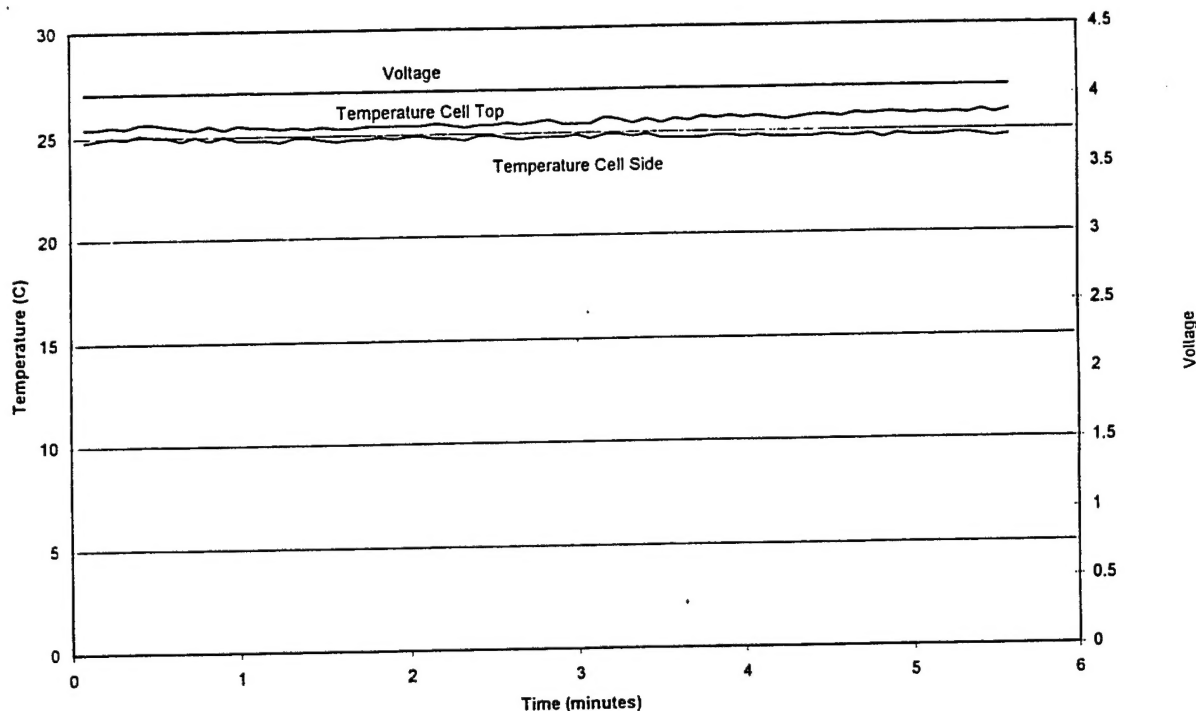


Figure 99. Crush test of 45-Ah cell.

The safety tests carried out to date have highlighted that the cells are safe during short-circuit and over-discharge. The tests on over-charge show once the cells are over-charged in excess of 100% the cells will vent violently, probably due to an internal short-circuit. Internal short-circuit is also the cause for the failure of the cells during the oven test. Finally, the crush test results in a violent cell vent, but the cell has to be crushed about 30% for this to occur.

3.0 Conclusion

When the program was redirected from the Minute Man Missile Silo application to Spacecraft and Aircraft applications a set of goals and targets were established. The Target is what the USAF wanted to achieve while the Goal is what the USAF and BATC should strive for. At the time the targets and goals seemed very ambitious. However, some of the targets were met and most of the achievements were at least close to the targets. The targets, goals and achievements as of April 1998 are shown in Table 33. With the baseline technology of $\text{LiCoO}_2/\text{graphite}$, the highest specific energy value was 122 Wh/kg for the 25-Ah Design II cells. The 45-Ah cells should have been higher but problems were encountered with the compression of the electrodes. Even so a 45-Ah cell using a $\text{LiNi}_x\text{Co}_{1-x}\text{O}_2$ positive electrode met the goal with a specific energy of 139 Wh/kg. At the time the targets and goals were established the end of discharge voltage was 2.5 V while all the tests at BATC used an end of discharge voltage of 3.0 V. This will result in the specific energy and energy density values at BATC to be lower than could have been achieved at the lower end of discharge voltage by approximately 5%. The energy density values came close to but did not meet the targets.

Cycle life targets have been met quite consistently while the goal is still rather elusive. Cycle life at 60% dod has not met the target but the Generation IV Status cells will probably reach 1500-1600 cycles instead of the desired 2000. But when the targets and goals were established it was believed that enhanced cycle life would be achieved at the lower dod values. However, it appears that the dod has a far smaller impact on cell cycle life than originally believed.

The low temperature performance goals were achieved. At the C/2 rate the bare cell showed 38% of capacity compared to a target of 50%. However, the 38% was realised with an end of discharge voltage of 3.0 V while the goal was established with an end point of 2.5 V. If the voltage of the cell was changed to 2.5 V, the target would have been met. The end of charge voltage was not set for the goal. If the end of charge voltage was established compensating for the increase in resistance due to the lower conductivity of the electrolyte, these targets and goals would most certainly be met.

Table 33. Program goals and achievements.

Performance Characteristics	Target	Goal	April 1998
Specific Energy, Wh/kg, (Cycle 10, 25 °C to 2.5V)	135	150	105 DD cell 110 Design I 20-Ah 122 Design II 25-Ah 117 45-Ah cell 139 45-Ah Cell $\text{LiNi}_x\text{Co}_{1-x}\text{O}_2$
Energy Density, Wh/l, (Cycle 10, 25 °C to 2.5V)	325	360	247 DD cell 219 Design I 20-Ah 253 Design II 25-Ah 244 45-Ah cell 318 45-Ah Cell $\text{LiNi}_x\text{Co}_{1-x}\text{O}_2$
Cycle Life - 100% dod, (Cycle 10, 25 °C C/2 75% Capacity)	500	1000	639 10-Ah 800-1100 Design I 20-Ah 531 45-Ah
Cycle Life - 60% dod (25 °C to 2.5V, C/2)	2000	5000	> 1400 Average EODV 3.19
Capacity @ -20 °C, %(Bare cell, Cycle 10, 2.5V, C/2)	50	75	38% 3.0V 53% at C/5 to 3.0V
Capacity @ -40 °C, %(Bare cell, Cycle 10, 2.5V, C/2)	---	50	